7 HYDROCHEMISTRY

7.1 INTRODUCTION

The hydrochemical data were collected during the pre-investigation phase of the Äspö site characterization as described in */Wikberg et al, 1991,* and *Smellie and Laaksoharju, 1992/.* During the course of the tunnel excavation more data has been obtained from the underground tunnel probe holes. Monitoring of the hydrochemistry in the packed off boreholes at Äspö, of the Baltic sea and in the 1700 m deep borehole at Laxemar have provided additional data and knowledge, which is used to present and update the model of the hydrochemistry of the Äspö area. The description is made for the natural conditions on Äspö and its surroundings. The situation caused by the inflow to and pumping from the tunnel is described in *Rhén et al /1997/* where the predictions made prior to construction are assessed by the data collected during the construction phase. These data obtained from the tunnel are of course useful both for evaluating the natural conditions as well as the disturbed conditions. The situation after tunnel construction is also presented.

During the entire Äspö project, starting with the site investigations in 1987 and finishing with the end of the tunnel construction work in 1995, hydrochemical data have been evaluated in many different aspects and with many different purposes:

- The hydrochemistry of wells drilled in Kalmar County was compiled and statistically evaluated by *Liedholm /1987/.*

- Chemical sampling and analyses of water from percussion drilled holes at Ävrö, Äspö and Laxemar was reported by *Laaksoharju /1988/.*

- *Laaksoharju and Nilsson /1989/* made the description of the hydrochemistry of the Äspö island based on the first deep drill holes at Äspö and Laxemar. Data from the next deep drilling programme was reported by *Nilsson /1989/.*

- Fracture filling minerals and their relation to the hydrochemistry was investigated and evaluated by *Tullborg /1989/* and *Tullborg et al /1991/.* A systematic evaluation of carbon, oxygen and sulphur isotope data was made as a pilot test of the KLX01 borehole at Laxemar */Wallin, 1990/.* These methods were later used for careful examination of fracture mineralogy in the tunnel */Wallin, 1992, Landström and Tullborg, 1993/.*

- Monitoring of the hydrochemistry in borehole sections permanently isolated by packers was started as soon as the boreholes had been drilled

and investigated. The first compilation of these data was made by Nilsson */1991/.*

- During the tunnel construction phase the monitoring data were reported together with the data from groundwater flow measurements in the same sections isolated by packers */Ittner et al, 1991, Andersson, et al, 1992, Ittner, 1992* and *Ittner 1994/. Ittner and Gustafsson /1994/* compiled all the data from groundwater flow measurements and hydrochemical sampling in the surface boreholes.

- Data from all tunnel boreholes were reported by *Nilsson /1995/.* Successively during the tunnel construction phase the data were evaluated for tunnel sections 700-1475 m, 1475-2265 m, 2265- 2874 m */Wikberg and Gustafsson, 1993, Wikberg et al, 1993, Wikberg et al, 1994/.* Tunnel section 0-700 m was reported together with the hydrogeological and geological data */Stanfors et al, 1992/.* An evaluation of the hydrochemistry during the entire tunnel construction phase was made by *Laaksoharju and Skårman /1995/.*

- Integrated reporting of the investigations and modelling of Äspö was made by the principal investigators in 1988, 1989 and 1991 */Gustafson et al, 1988, 1989, Wikberg et al, 1991/.* A final conceptual modelling of the hydrochemistry of the pre-investigation phase in relation to the existing hydrological and geological conditions was made by *Smellie and Laaksoharju /1992/.*

- The prediction of detailed conditions to be found in the tunnel was reported in advance of the tunnel construction work */Gustafson et al, 1991/.* Methods to be used as tools for the prediction work were assessed by *Laaksoharju /1990/.* A further more comprehensive assessment was made during the tunnel construction phase */Wikberg et al, 1993 and 1994/.*

- USDOE scientists carried out a joint project together with SKB scientists to combine stable and radiogenic isotopes of both the groundwater and fracture fillings to evaluate the origin and residence time of the groundwater */Wallin and Peterman, 1994/.* The most useful combination of methods was carbon-13, oxygen-18 and strontium-87 of calcites and groundwater.

- Hydrochemical modelling in general was an issue of particular interest to many of the foreign organizations taking part in the Äspö HRL project. Modelling tasks were discussed at a workshop in 1994 */Banwart, 1994/* and the results presented at a second workshop one year later */Laaksoharju and Wallin, 1997/.* The hydrochemical investigations in the deep KLX02 borehole at Laxemar */Laaksoharju et al, 1995/* have provided an important complement to the Äspö data.

- During a three year period from March 1991 to February 1994 a block scale redox experiment was conducted in a minor fracture zone in the entrance tunnel to Äspö. The project which took place at a vertical depth of 70 metres gave much information about the shallow groundwater hydrochemistry in addition to the planned examination of redox properties. The project has been summarized by *Banwart (ed), /1995/.* The results of the investigations were compiled by *Banwart et al /1995/.*

- Microbial sulphate reduction was observed in the tunnel section between Hålö and Äspö. Since this process is important for copper canister stability, the evaluation of the observations were organized as a separate project */Laaksoharju (ed), 1995/.*

7.2 TOOLS FOR EVALUATING GROUNDWATER PROCESSES AND HISTORY

Traditional hydrochemical evaluation is carried out by experts in the disciplines of geochemistry and isotope hydrology. Correlation diagrams (cross plots) are the most commonly used method for the purpose of understanding the system. In a second stage thermodynamic equilibrium modelling is employed to describe the processes which have caused the observed conditions. The modelling work at Äspö was started along this line, but it was observed that a different approach was more relevant.

The hydrochemical evaluation of Äspö indicated at an early stage that mixing was the dominating process behind the observed conditions. There are two main causes for the mixing. One is the disturbance caused by the borehole by short-circuiting the different water conducting fracture systems, the other one is the mixing which has taken place in the past due to varying hydraulic driving forces which made the groundwater flow along different paths. In the evaluation work, the mixing caused by the borehole is considered a disturbance which is taken into account and corrected for. The remaining mixing proportions of different water types is then described as the result of varying groundwater flow conditions.

Simple two component mixing and mass balance calculations were made by */Laaksoharju, 1990, Banwart et al, 1992 and Smellie and Laaksoharju, 1992/.* The main aim was to differentiate between the influences of mixing and water/rock reactions by using a single variable such as chlorine as a conservative (non-reactive) tracer. These methods had limitations because the Äspö groundwater system involved several end-members, where e.g. the chloride could have different sources, see *Section 7.2.3.* The end-members were strictly defined during the tunnel construction phase, but they were identified already during the pre-investigations. Groundwaters which had a similar chloride concentration could have a quite different oxygen-18 signature and bromide concentration which implied that they contained proportions of at least four types with different origins */Wiberg et al, 1991, Smellie and Laaksoharju, 1992/.*

7.2.1 Multivariate Mixing and Mass balance calculations *(M3)*

The origin and evolution of the groundwater is described and the effect from mixing and reactions can be examined separately, using a new method named **M**ultivariate **M**ixing and **M**ass balance calculations (abbreviated to M3).

The full sequence starts with a univariate analyses with the purpose of describing the depth dependence of the main parameters, followed by the Principal Component Analyses, reference water and end-member identification and finally the mixing and mass balance calculations. The aim of the Principal Component Analyses is to sort the data into different classes or water types. The extreme points, see *Figure 7-1*, are selected as reference waters. All other waters are then described as a mixing of the selected reference waters. The mass balance calculations are used to define the magnitude of reactions which have shifted the groundwater composition.

The M3 calculations contain the following steps:

1 A standard multivariate technique, called Principal Component Analysis (PCA) is used for cluster analyses of the data by using the major components Cl, Ca, Na, Mg, K, SO_4 and HCO_3 in combination with the isotopes δD, $\delta^{18}O$ and ^3H. The PCA aims to describe as much of the information from the ten variables as possible. The Principal Components are calculated as linear combinations of all chemical components in a way to minimize the difference (error) between the model and the data.

The first principal component is applied to the initial data. The variation not accounted for by the first principal component is described by the second principal component and so on. For the Äspö hydrochemistry data the first three principal components were calculated and analysed. It turned out that the first two components did describe the system well enough, whereas the third component mainly described the disturbance caused by drilling and pumping in one single deep borehole at Laxemar, KLX02, see *Section 7.5.2*. For the first two principal components an x, y scatter plot can be drawn. The x is the equation for the first principal component and y the equation for the second principal component. The plot is named the *M3 plot* and is used to visualise the clustering of the data as well as to identify extreme waters.

2 Extreme waters are called *end-members* and *reference waters*. A reference water is a well-sampled groundwater which resembles an assumed or modelled end-member e.g. Glacial meltwater (see *Figure 7-1a* and *b*) Lines are drawn between the reference waters so a polygon is formed. If well selected the reference waters can describe the observations inside the polygon. All observations are compared to the chosen reference water compositions.

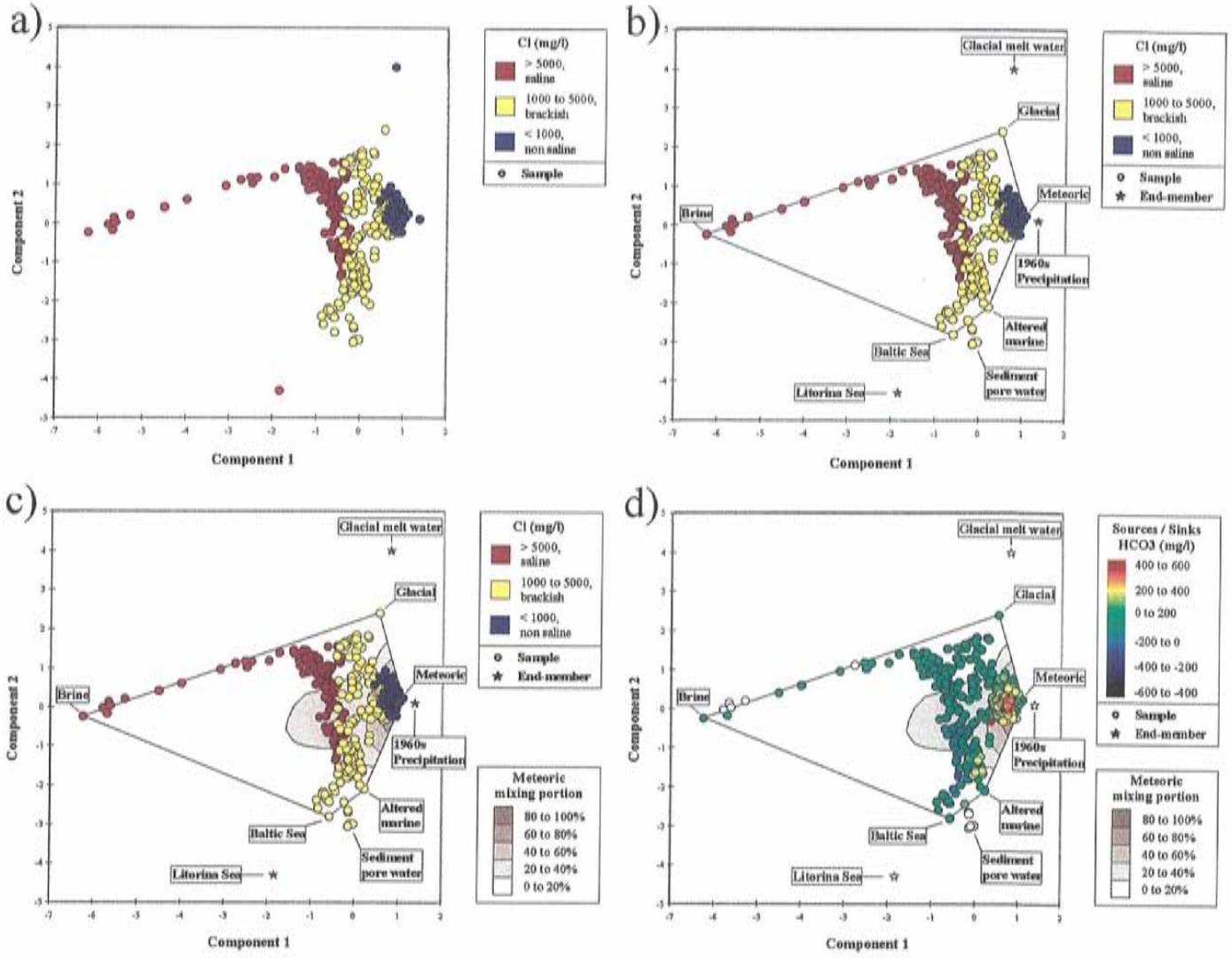

Figure 7-1. *Different steps in the M3 modelling; a) principal component analysis is used to obtain the maximum resolution of the data set, b) selection of end-members and reference waters - the other groundwaters are compared to these, c) mixing calculations - portions of meteoric water are shown in the figure, d) mass balance calculations - the sources and sinks of eg. Carbonate are shown which cannot be accounted for by mixing. The groundwater samples in Figure a, b and c have been colour coded based on the Cl-content into saline, brackish and non-saline groundwater.*

3 Mixing calculations are done to calculate the portions of the reference waters or the end-members in each observation. The calculated mixing portion can be used to evaluate the origin of the groundwater i.e. how large a proportion originates from the Baltic Sea etc. The mixing portions are proportional to the trigonometrical distance to the selected reference waters or end-members in the *M3 plot* (see *Figure 7-1c*).

4 Mass balance calculations are used to define the sources and sinks for different elements which deviate from the ideal mixing concentrations which are calculated from the known proportions and concentrations of the reference waters *(see Figure 7-1d).* No deviation between the

measured and calculated value indicates that mixing can explain the element behaviour. A source or sink is due to reactions. The evolution of the groundwater can be tracked and the effects of reactions are quantitatively described.

It is important to note that the M3 modelling is always relative to the selected reference waters or end-members. The boundary conditions of the modelling can be changed depending on the selection of reference waters or end-members. E.g. the now selected reference water "Glacial" is 50% glacial melt water (end-member) and 50% undefined meteoric water.

The advantage of using a reference water rather than an end-member in claculations is that the composition of the end-member is never as well known as for the reference water. Effects of reactions can therefore only be revealed for calculations that are based on reference waters.

7.2.2 Principal component analysis

The Principal Component Analysis (PCA) method */Pearson, 1901/* is generally used to classify and simplify data and to identify the most important variables in a data set */Chatfield and Collins, 1989/*. The technique, which is a linear mathematical transformation of the selected variables, is used to describe the water composition in an optimal way.

Factor analyses is precessor to the Principal Component Analyses. The correlation matrix of the factor analyses resembles the weighting factors of the constituent involved in the principal component analyses, cf. *Figure 7-2*.

In order to graphically represent the data, a two dimensional plane is oriented to obtain the largest possible resolution. The equations used to express the two dimensional plane are the Principal Components (first and second).

In *Figure 7-2*, as in all other figures where the PCA results are presented, the two components are normalized to the average weight point of all data. This means that the numerical values calculated for the two components are different from the values presented in the figure. All data points are nevertheless located at the same position relative to all the other points.

The weights of the different variables in the principal component equations are determined by the importance (variability) of each variable. The higher the information content the greater the weight. For the first principal component sodium, calcium, chloride and sulphate have the greatest weights. For the second principal component oxygen-18 and deuterium together with potassium and magnesium have the greatest weights. The reason is that chloride, calcium, sodium and sulphate are the major constituents which have no solubility limits and are congruent, i.e. increase and decrease simultaneously even if they are not linearly correlated. Oxygen-18 and deuterium are also totally conservative but do not correlate with the major constituents. Magnesium and potassium are

indicators of marine input and do not correlate with the major constituents either.

The advantage of the Principal Component Analyses is that all variables can be treated simultaneously and that no preconceptions need be made. All analyses are made on strictly mathematical bases.

7.2.3 Reference water and end-member identification

Groundwaters which are judged to be representative but have an extreme composition are called **reference waters**. Reference waters are the ones which constitute the corners in *Figure 7-2*. The reference waters have compositions which resemble specific end-member compositions. An **end-member** is a modelled water which is believed to be the original source of the reference water.

The reference waters and the identified end-members are labelled in *Figure 7-2*. They were selected so that most of the sampled Äspö site data can be described. The selected reference waters and end-members are:

- **Brine reference water** is found at the deepest location of the borehole KLX02, with a chloride concentration of 47000 mg/l. Characteristic of the brine, except for the high salinity (above sea water) is the non-meteoric values of deuterium and oxygen-18. No end-member is identified since the long-term groundwater/rock interaction can result in concentrated salt solutions with extreme isotopic composition */Blomqvist et al, 1995/*.

- **Glacial reference water** has been determined as a glacial water based on stable isotope values which indicate cold climate recharge ($\delta^{18}O$ = -15.8 ‰ and $\delta 2H$ = -124.8 ‰) in combination with an apparent ^{14}C age of 31 365 years */Smellie and Laaksoharju, 1992/*. This type of water is found in Äspö KAS03/depth 129-134 m. The water type is believed to have been injected into the basement during the melting and retreating of a continental ice sheet. The glacial reference water has a 50% proportion of the glacial end-member, and 50% of other meteoric and sea water, and 50% of other meteoric and sea water.

- The ***Glacial melt-water end-member*** is a modelled glacial meltwater composition where the stable isotope values ($\delta^{18}O$ = -21 ‰ and $\delta 2H$ = -158 ‰) were based on measured values ($\delta^{18}O$) in the calcite fracture fillings from different geological formations in Sweden. Some of the fracture fillings were assumed to be subglacial formations */Tullborg and Larson, 1984/*. Tests using many possible water compositions for the glacial water confirmed that the selected composition gave the best fit with the measured $\delta^{18}O$ content in the reference water. The chlorine content of this water was set to be zero although it may well be that the subglacial water can be enriched in salinity when the permafrost freezes the initially dilute subglacial water.

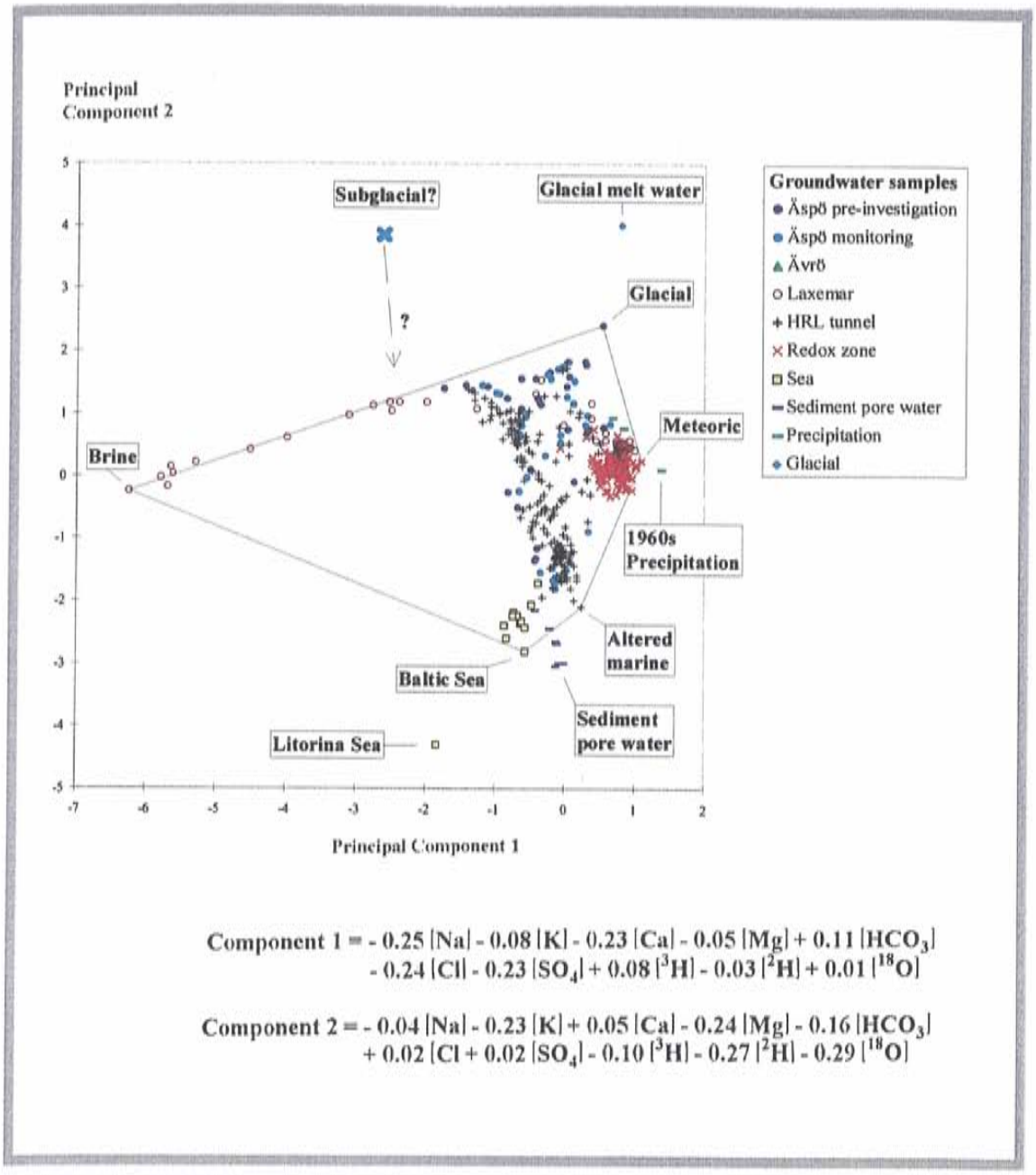

Figure 7-2. *Principal Component plot based on the major components and stable isotopes and tritium values from the Äspö and Laxemar groundwaters. The most extreme groundwaters which are well sampled and with an analytically established composition are called reference waters. A line is drawn between the reference waters so a pentagon is formed. The weight for the individual elements is given in the equations for the first and second principal component respectively. These two principal components together account for 72% of the variability, of the data. An end-member is a modelled water composition which is assumed to be the original groundwater composition of the reference water. The numerical values are normalized, see Section 7.2.2.*

- A possible ***Subglacial water end-member*** is shown in the PCA (*Figure 7-2*). The subglacial water composition probably changed with time during repeated freezing and melting of the continental ice sheet. The need for a *sub-glacial* end-member might also indicate that the groundwater system is more complex than the selected reference-waters/end-members are able to describe, see *Section 7.5.3*. Errors/uncertainties in the M3 calculations cannot either be totally ruled out.

- **Baltic Sea reference water** represents modern Baltic Sea water, sampled close to Äspö.

- The end-member is ***Litorina Sea water*** with a chlorine concentration of 6 100 mg/l which is based on analyses of micro fossils from the marine sediments in southern Finland */Kankainen, 1986/*. Similar determinations in the south part of Baltic Sea gave concentrations up to 14 000 mg/l Cl */Winn et al, 1988/*. Influx tests were performed in which different possible Litorina Sea water concentrations were tested. The former concentration of 6 100 mg/l gave the best fit with the measured chlorine and $\delta H^{18}O$ content in the groundwater. Thus the salinity of the Litorina Sea was higher (by a factor of almost two) than the selected sea reference water composition which is 3 760 mg/l. It should be pointed out that there is always a higher salinity in the south part of the Baltic Sea compared to the northern parts.

- **The Altered marine reference water** represents Baltic Sea water affected by bacterial sulphate reduction */Laaksoharju ed., 1995/*. This water type is obtained in the HRL tunnel below the marine sediments.

- The end-member of the Altered marine water is the extracted ***sediment pore water*** */Landström et al, 1994/*. The pore water composition resembled more modern Baltic sea water than Litorina sea water. In addition the groundwater flow calculations indicated that the modern sea can affect the sediments. Based on this knowledge the modern isotope values were retained in the modelling.

- **The Meteoric reference water** represents a dilute (Cl = 5 mg/l) non-saline water found in HBH02: 7.5 m, with a modern oxygen, deuterium and tritium isotopic signatures of -10‰, -77‰ and 20 TU respectively.

- ***1960 precipitation water end-member*** with a typical chemical composition of an infiltrating meteoric water and with a high tritium content, presently 100 TU after 5-6 halt litres.

The important characteristics of the reference waters and end-members are listed in *Table 7-1*.

Table 7-1. End-members identified in the Äspö groundwater system.

End-member/ Reference water	$\delta^{18}O$ ‰ SMOW	$\delta^{2}H$ ‰ SMOW	Cl mg/l	Tritium TU	SO_4 mg/l
Glacial melt-water	-21	-158	0	0	0
Sub-glacial water	-21	-158	11000	0	1500
Litorina Sea	-5	-35	6100	0	500
Sediment pore water	-7	-61	3400	0	53
1960 precipitate	-11	-80	0	100*	0
Glacial reference water	-15.8	-124.8	1120	0.1	31
Baltic Sea reference water	-5.9	-53.3	3760	42	325
Altered marine reference water	-7.3	-60.3	4490	17	112
Meteoric reference water	-10.2	-77.1	5	22	13

* the amount of tritium 1996 (after 4-5 halflife periods).

7.2.4 Accuracy of the multivariate mixing mass balance calculations

An extensive confidence-building exercise on the Äspö site data was performed with the Multivariate Mixing and Mass balance, M3, method. */Laaksoharju and Skårman, 1995, and Laaksoharju and Wallin, 1997/.*

Chloride and ^{18}O are the only truly conservative (non-reactive) constituents. A perfect model would therefore be able to describe their behaviour completely. A test was performed in which the ability of the M3 model to predict the chloride concentration and $\delta^{18}O$ of the Äspö site groundwaters was compared with more frequently used traditional linear regression. In the univariate model the chlorine content was used as a conservative tracer to predict the $\delta^{18}O$ values. The calculations were then repeated using $\delta^{18}O$ as a conservative tracer to predict the chloride content. The results show that the multivariate method is always better than the univariate methods by a factor of two. The only case in which the univariate methods gave a better result was for ^{18}O predictions in the non-saline groundwater */Laaksoharju and Wallin, 1997/*, which represent only the uppermost 100 m depth.

A back propagation test was also made to check the consistency of the mixing calculations. Preset proportions of the different reference waters, e.g. 10% Baltic Sea water, 18% altered marine water, 9% meteoric water, 47% glacial water and 16% brine water, were used to calculate a groundwater composition. The composition was then evaluated by the principal component analyses. No reactions were allowed to change the composition. The results gave a difference of 10.5% on an average. However, the largest difference was obtained for waters which are largely modified by reactions; meteoric water and altered marin water.

The standard code NETPATH */Plummer et al., 1991/* can be used to compute the mixing proportions of two or more end-members as well as net geochemical reactions that can account for the observed groundwater composition. M3 can be used for the same purpose except that M3 reports sinks and sources for different elements not accounted for by mixing. In the M3 approach the mixing is regarded as the dominating process which changes the water composition at site scale. In NETPATH, depending on the number of chosen phases, reactions are generally regarded as the dominating process.

7.3 GENERAL HYDROCHEMISTRY OF THE ÄSPÖ-LAXEMAR AREA

General trends of the analytical groundwater data, x y scatter plots for the Äspö site data (Äspö, Ävrö, Laxemar, Redox zone, HRL tunnel, Baltic Sea, precipitation and sea bed sediments) are shown in *Figures 7-3 to 7-6* for Cl, Na, Ca, HCO_3, Mg, K, SO_4, tritium, deuterium and ^{18}O plotted against Cl and depth. The locations of the sampled boreholes in the area are shown in *Figures 2-3* and *2-4* and the locations of sampling holes in the tunnel are shown in *Figures 7-40* and *7-41*. The data is also presented in *Appendix 3*.

Figures 7-3 to 7-6 show that the salinity described by chlorine increases with depth although non-saline waters occur at Laxemar down to a depth of 900 m. At Äspö, the saline water exists at shallow depths especially in the samples from the HRL tunnel. The other groundwater constituents such as Na, Ca, SO_4 and stable isotopes such as deuterium and oxygen-18 seem to increase with the salinity. K, Mg, HCO_3 and tritium seem to decrease with increasing salinity. The first impression is that the groundwater system is fairly simple and its evolution can be described by a non-saline and saline evolution path. Surprisingly the two known groundwater conservative tracers (Cl and ^{18}O) do not correlate when Cl <10 000 mg/L (*Figure 7-4*) which indicates a more complex system than first assumed. In addition a more complex system is depicted when plotting the Cl, Na, K, Ca, Mg, HCO_3 and SO_4 against depth (*Figures 7-3 to 7-6*). The distribution of groundwater chemistry is very heterogeneous when the Äspö site is considered as a whole. If only the conducting fracture zones are considered i.e. where the majority of water samples have been taken, then the groundwaters tend to have a more uniform composition because they obtain their character through mixing along fairly rapid conductive flow paths. Thus, knowing that most of the samples have been taken from water-conducting fractures, the undisturbed system may be even more complex, than the data imply.

Figure 7-3 represents the chloride concentration as a function of depths for groundwaters collected in the Äspö area. The upper part of the figure, a, represents the different locations where the samples were collected whereas the lower part of the figure, b, represents the same data divided into three classes of concentration, freshwater with a chloride concentration below 1000 mg/l, brackish water with a concentration between 1000 and 5000 mg/l, and saline water with a chloride concentration above 5000 mg/l. A careful comparison of

a and b in *Figure 7-3* reveals a distinct difference between the Äspö and the Laxemar data. The Laxemar data are classified as freshwater down to a depth of about 800 m whereas the Äspö groundwaters are brackish or saline from a depths of less than 100 m. This difference is thought to be result of recharge and discharge conditions at Laxemar and seawater intrusion at Äspö taking place after the latest glaciation, see *Section 7.4.*

Figure 7-4 and 7-5 presents the main constituents relative the chloride concentration and depth. Sodium and Calcium are almost linearly correlated to the chloride concentration, whereas Potassium, Magnesium, Bicarbonate and Sulphate are not correlated. Potassium, Magnesium and Bicarbonate have a maximum concentration in the boundary between brackish and saline water.

The reason is partly the effect of present day and ancient Baltic Sea water intrusion in combination with biological activity, see *Section 7.6.2.*

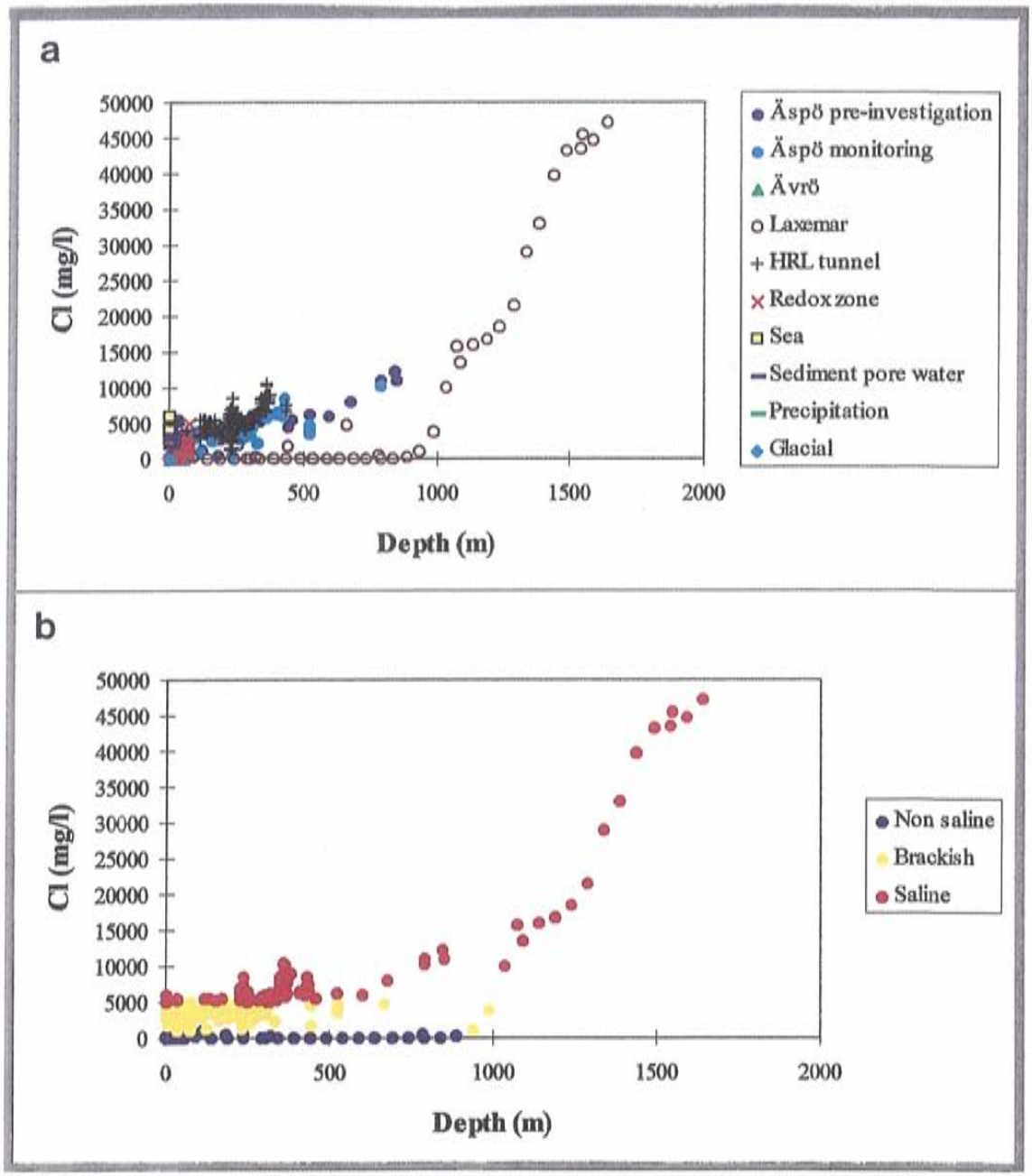

Figure 7-3. *Scatter plots for the Äspö site data shown for Cl versus depth. a) The samples from: Äspö (during the pre-investigation and monitoring phases of the HRL tunnel), Ävrö, Laxemar, Redox Zone, HRL tunnel, Baltic Sea, precipitation and sea bed sediments. b) The observations have been divided according to the groundwater classification: non-saline, brackish and saline.*

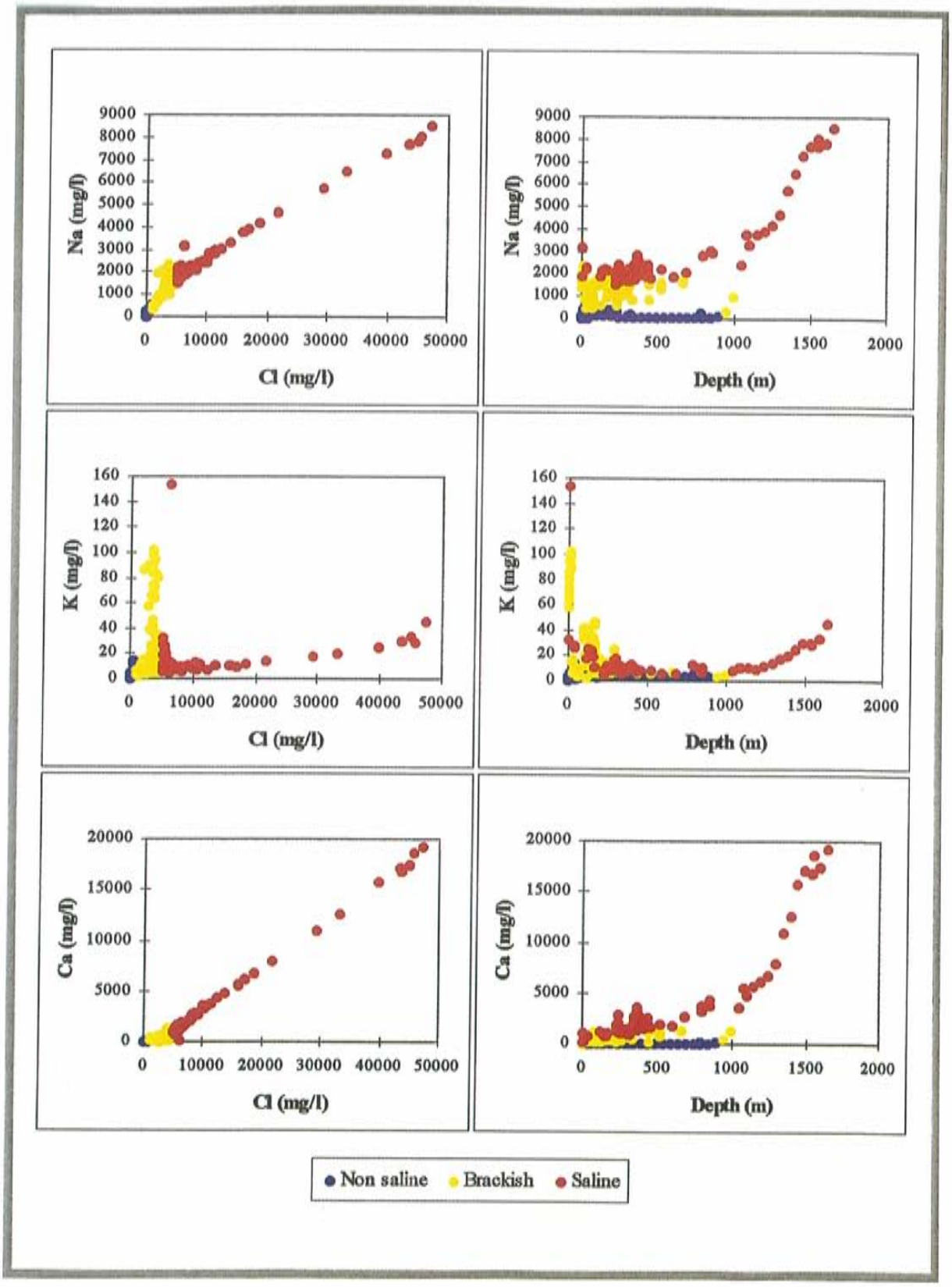

Figure 7-4. *Scatter plots for the Äspö site data for Na, K and Ca versus the Cl concentration and depth. The observations have been divided according to the groundwater classification: non-saline, brackish and saline.*

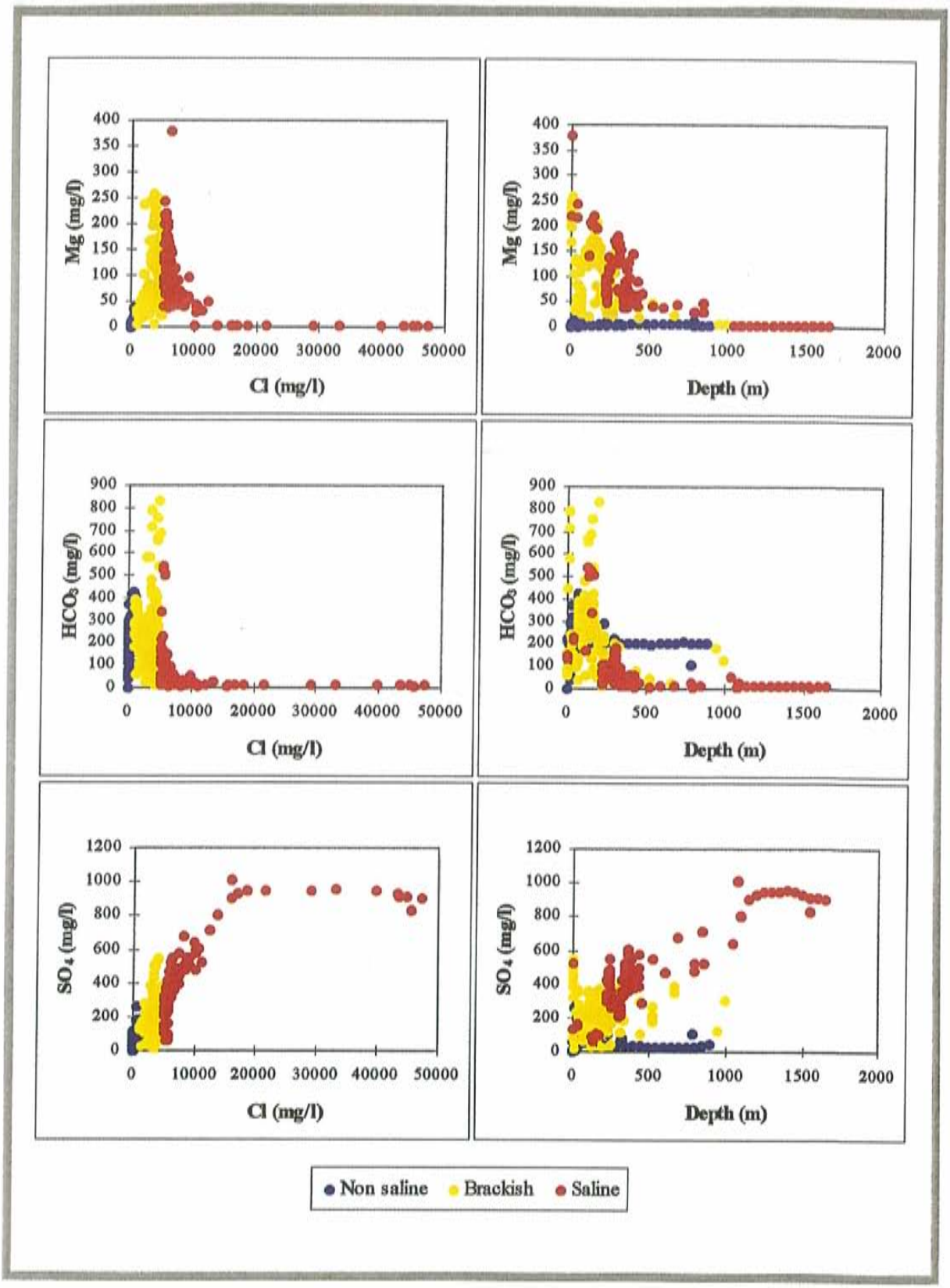

Figure 7-5. *Scatter plots for the Äspö site data for Mg, HCO_3 and SO_4 versus the Cl concentration and depth. The observations have been divided according to the groundwater classification; non-saline, brackish and saline.*

Figure 7-6 presents the tritium, deuterium and oxygen-18 isotope data relative the chloride concentration and depth. Non of these are linearly correlated with chloride and there is a wider spread in the brackish than in the fresh or saline water, which indicates that the brackish water is probably the most complex mixing system, see *Sections 7.5 and 7.6*.

There are remaining uncertainties to how representative the single borehole KLX02 is to the saline-fresh water interface at Laxemar. The long open borehole section in KLX02 makes it a fast path for near surface water to reach deep fracture systems, see *Section 7.6.2*.

Figure 7-7 shows the complex mixing system of the brackish water indicating that both seawater and glacial water can be dominating proportions in the brackish water type. As expected, the saline water can also be largely influenced by seawater, whereas the freshwater has a quite distinct meteoric origin.

The pH values vary in a relative narrow range, see *Figure 7-8*. There are only two observations with a value above 8.5. The vast majority lies between pH 7 and 8.5. pH values below 7 are mostly related to waters where biological processes have affected the composition. The relatively low pH values of the deep groundwaters is likely due to the high salinity */Toulhout, 1992/*.

Eh values were measured only during the pre-investigations. In *Figure 7-9* the Eh values are calculated for all data points where pH and ferrous iron concentrations are reliable. The calculations are made by the formula suggested by *Grenthe et al /1992/*, Eh = 835 mV - 57 mV (3 pH + log $[Fe^{2+}]$) at 15 °C.

In *Figure 7-10* the data points are coded as a function of depth. As expected the two deepest groups are lying on a mixing line between brine and glacial water. The implications of this fact are discussed in *Section 7.6.2*. There are reasons to believe that the simple two component mixing system is much more complex. It should also be noted that the 700 - 1000 m depth interval data plotting close to the meteoric reference water are from the KLX02 borehole.

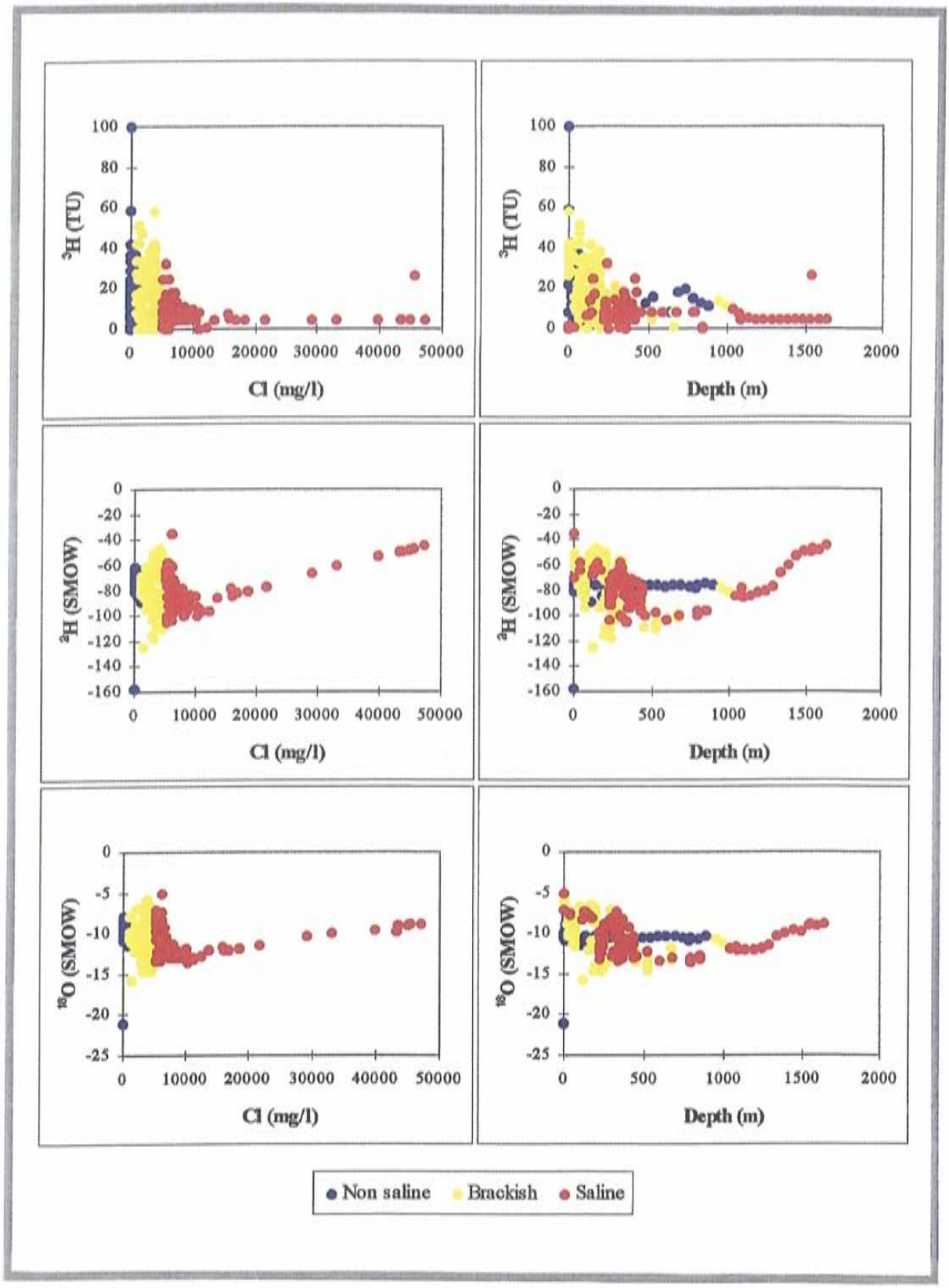

Figure 7-6. *Scatter plots for the Äspö site data for tritium, deuterium and oxygen-18 versus the Cl concentration and depth. The observations have been divided according to the groundwater classification; non-saline, brackish and saline.*

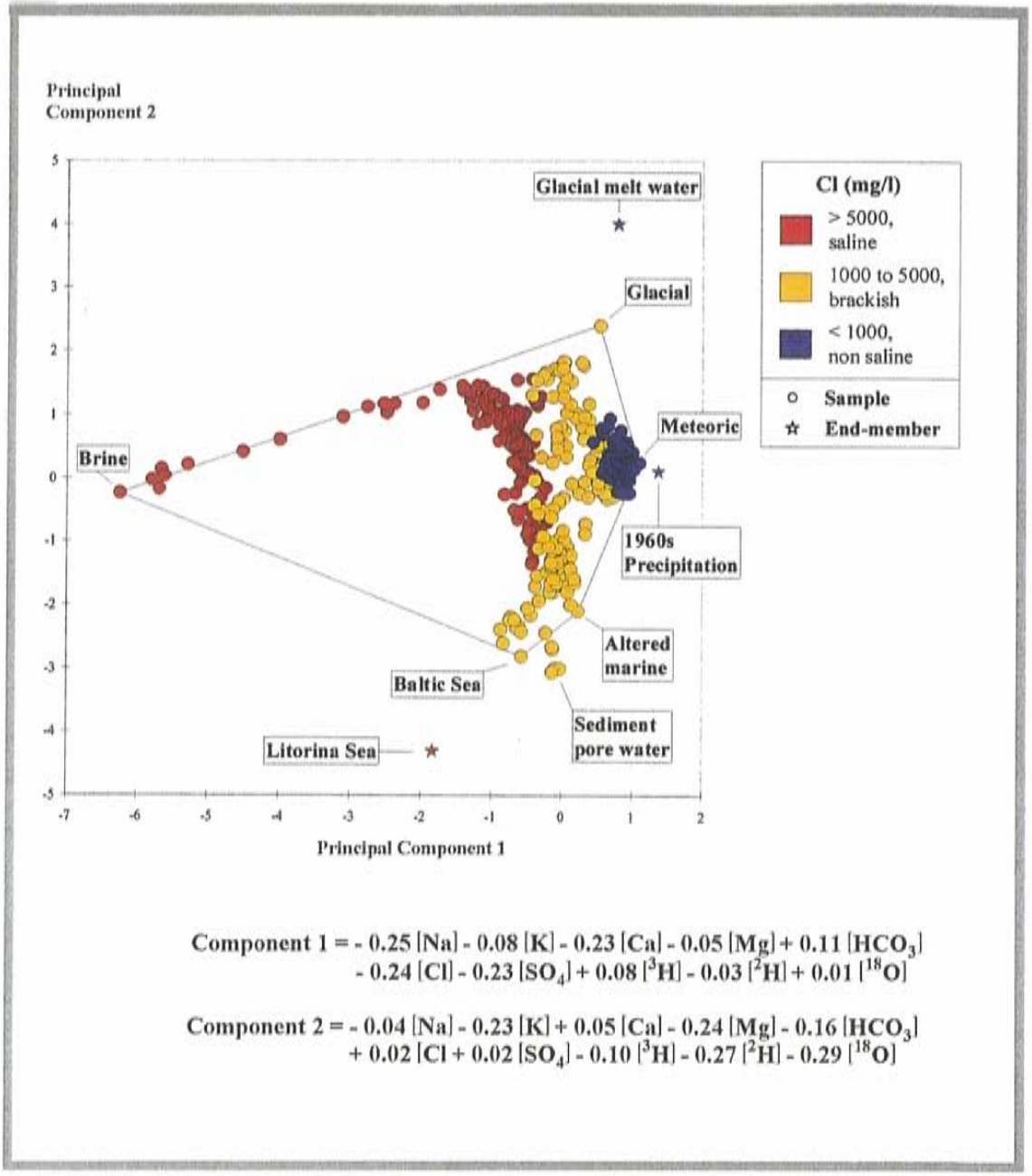

$$\text{Component 1} = -0.25\,[Na] - 0.08\,[K] - 0.23\,[Ca] - 0.05\,[Mg] + 0.11\,[HCO_3] - 0.24\,[Cl] - 0.23\,[SO_4] + 0.08\,[^3H] - 0.03\,[^2H] + 0.01\,[^{18}O]$$

$$\text{Component 2} = -0.04\,[Na] - 0.23\,[K] + 0.05\,[Ca] - 0.24\,[Mg] - 0.16\,[HCO_3] + 0.02\,[Cl] + 0.02\,[SO_4] - 0.10\,[^3H] - 0.27\,[^2H] - 0.29\,[^{18}O]$$

Figure 7-7. *Principal Component plot showing the subdivision of the groundwaters into non saline, brackish and saline groundwaters. The superimposed colour coding of the observations, i.e. the red colour, shows samples containing more than 5 000 mg/l Cl. The numerical values are normalized, see Section 7.2.2.*

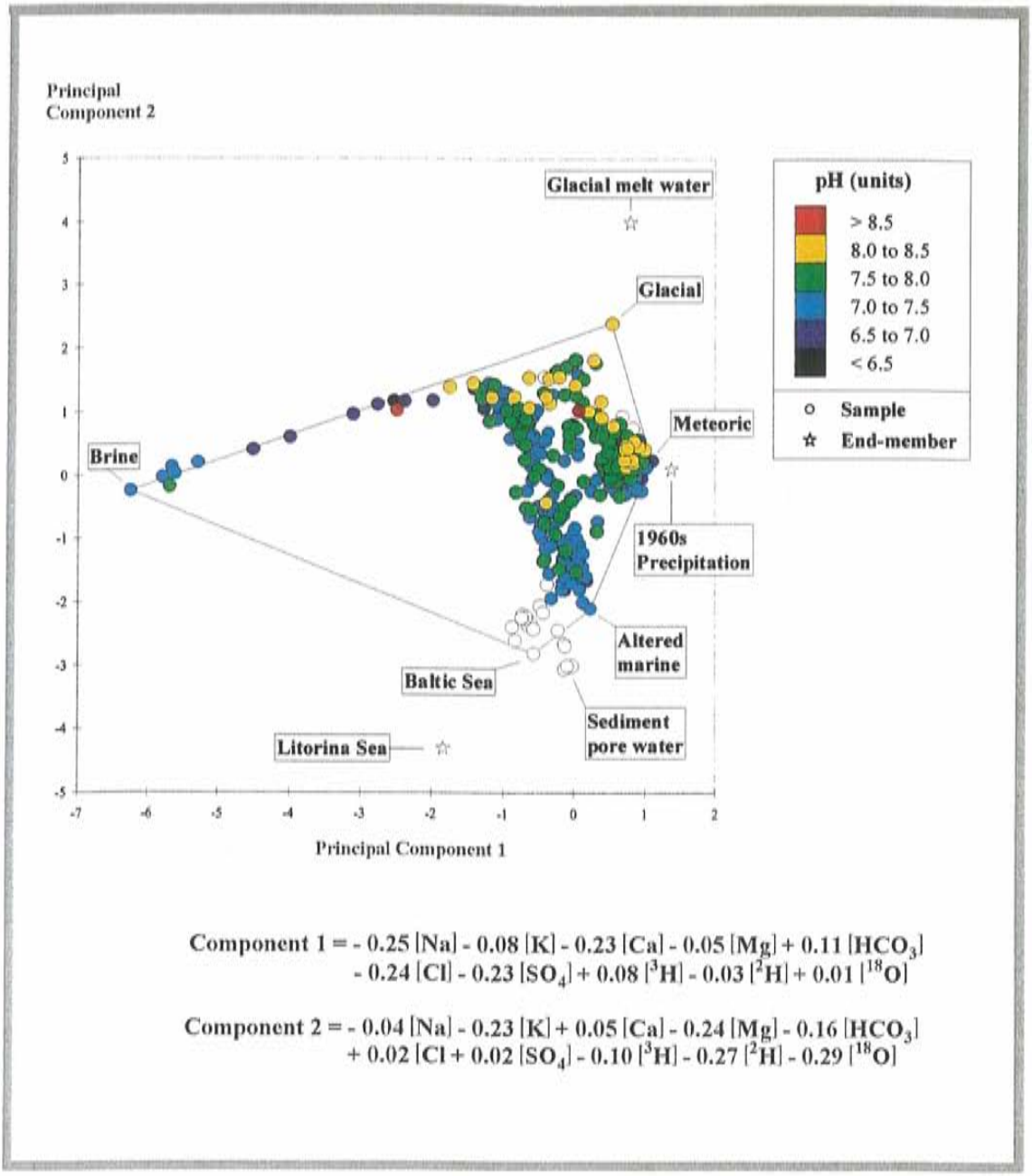

Figure 7-8. *Principal Component plot showing the distribution of measured pH values in the groundwaters. The superimposed colour coding of the observations, i.e. the red colour, shows a sample with a pH value above 8.5. The numerical values are normalized, see Section 7.2.2.*

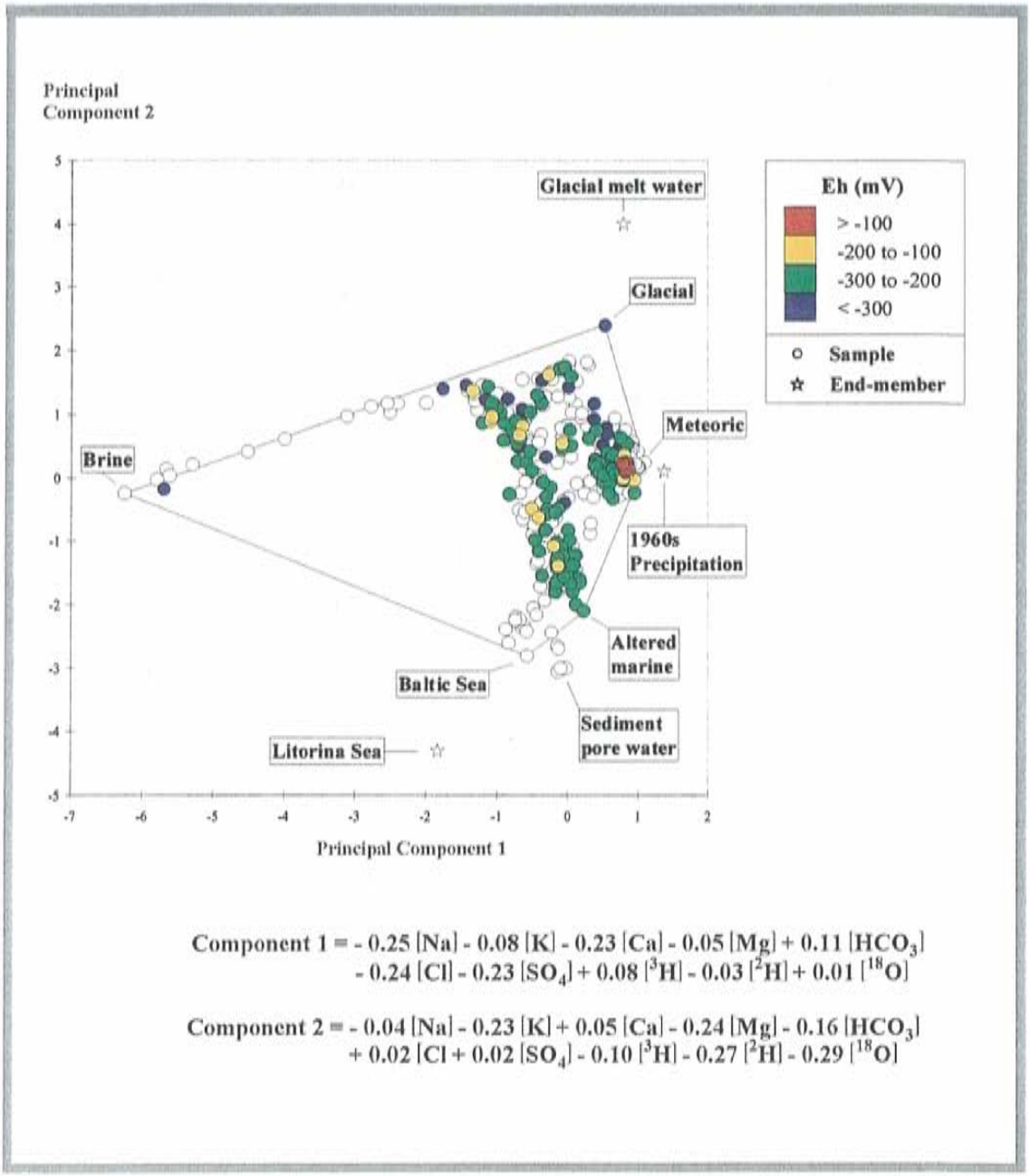

Figure 7-9. *Principal Component plot showing the distribution of calculated Eh values (according to Grenthe et al, 1992). The superimposed colour coding of the observations, i.e. the red colour, shows a sample with an Eh value above -100 mV. Open circles lack the necessary data for calculating the Eh values. The numerical values are normalized, see Section 7.2.2.*

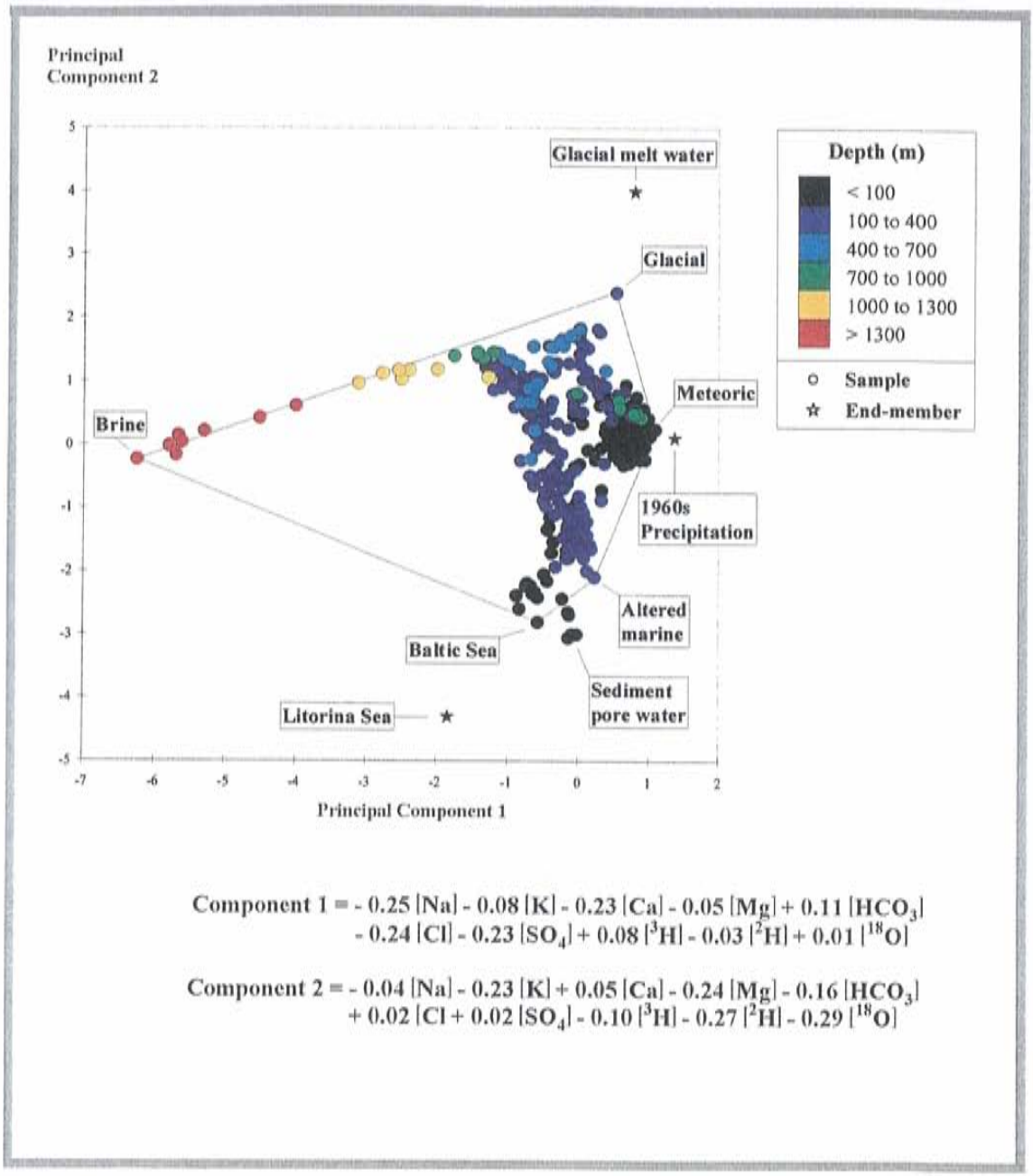

$$\text{Component 1} = -0.25\,[\text{Na}] - 0.08\,[\text{K}] - 0.23\,[\text{Ca}] - 0.05\,[\text{Mg}] + 0.11\,[\text{HCO}_3] - 0.24\,[\text{Cl}] - 0.23\,[\text{SO}_4] + 0.08\,[^3\text{H}] - 0.03\,[^2\text{H}] + 0.01\,[^{18}\text{O}]$$

$$\text{Component 2} = -0.04\,[\text{Na}] - 0.23\,[\text{K}] + 0.05\,[\text{Ca}] - 0.24\,[\text{Mg}] - 0.16\,[\text{HCO}_3] + 0.02\,[\text{Cl} + 0.02\,[\text{SO}_4] - 0.10\,[^3\text{H}] - 0.27\,[^2\text{H}] - 0.29\,[^{18}\text{O}]$$

Figure 7-10. *Principal Component plot showing the depth distribution of the groundwater samples. The superimposed colour coding of the observations, i.e. the red colour, shows observations collected from a depth greater than 1300 m. The numerical values are normalized, see Section 7.2.2.*

In the PCA plots the non-saline waters consist of a [Na-Ca-K:HCO_3-SO_4-Cl] or a [Ca-Na-K:HCO_3-SO_4-Cl] water and changing to a [Na-Ca-K:Cl-HCO_3-SO_4-] water near the surface (0-100 m). The brackish groundwater consists of a [Na-Ca-K:SO_4-HCO_3] water at a depth of 100-350 m. The saline groundwater found generally at a depth of 350-1700 m consists of a [Na-Ca-K:Cl-SO_4-HCO_3] or a [Ca-Na-K:Cl-SO_4-HCO_3] type of water. The groundwaters are moderately alkaline, pH values from 7.6-9, and reducing, with calculated Eh of -100 to -300 mV values. The measured Eh values showed readings similar to the calculated ones. These were only made during the pre-investigastions.

The way in which the flow and mixing affect the non-saline, brackish and saline groundwaters is illustrated using the results from the M3 mixing calculations *(Figures 7-11--7-15)*. The calculated influx portions of the different reference waters have been interpolated by Kriging */Henley, 1981, Fortner, 1992/*.

Figure 7-11 illustrates the proportions of brine reference water in the plane of the two first principal components. The saline water might contain less than 20% of brine due to the the high salinity of the brine reference water, 48,000 mg/l of chloride. Per definition therefore the proportion of brine in a brackish water must be less than 10%.

Figure 7-12 illustrates the proportion of glacial reference water in the plane of the first and second principal components. It should be noticed that there are many brackish and saline water points within the 60-80% proportion of glacial water. It is important to reallize that this does not imply that the proportion of glacial melt water is 60-80%. The proportion of real glacial melt water in the glacial reference water is roughly 50%, see *Section 7.2.2* and *Section 7.7.1*, and thus the proportion of glacial melt water in the 60-80% glacial reference water is 30-40%.

The influences of the Baltic Sea water, the altered marine water and the meteoric water affect a smaller part of the plane than the glacial and the brine waters. There is an important area formed between the Litorina sea and Galcial end members together with meteoric water, see *Section 7.7.1*, where the water is brackish, Cl = 1000 - 5000 mg/l, but where the mixing proportions can vary substantially.

The M3 model was used to calculate a possible ^{14}C age of the groundwater *(Figure 7-16)*. From a few measured ^{14}C ages the calculated mixing portions are used to predict values for observations lacking measurements. The results should only be used as an indication of a relative age rather than as a precise age determination. The reason for a high ^{14}C age (25 600 - 32 000 years) for the glacial water is that the age probably reflects the precipitation rather than the melting age.

Since the water is a mixture, different isotopes and elements give different histories of the water and also different ages. ^{36}Cl measurements give an age of several million years in a water where tritium measurements indicate

proportions of water which have penetrated from the surface in less than 40 years

/Laaksoharju and Wallin, 1997/. In the same way the ^{14}C age indicates only a possible age range for the carbon source.

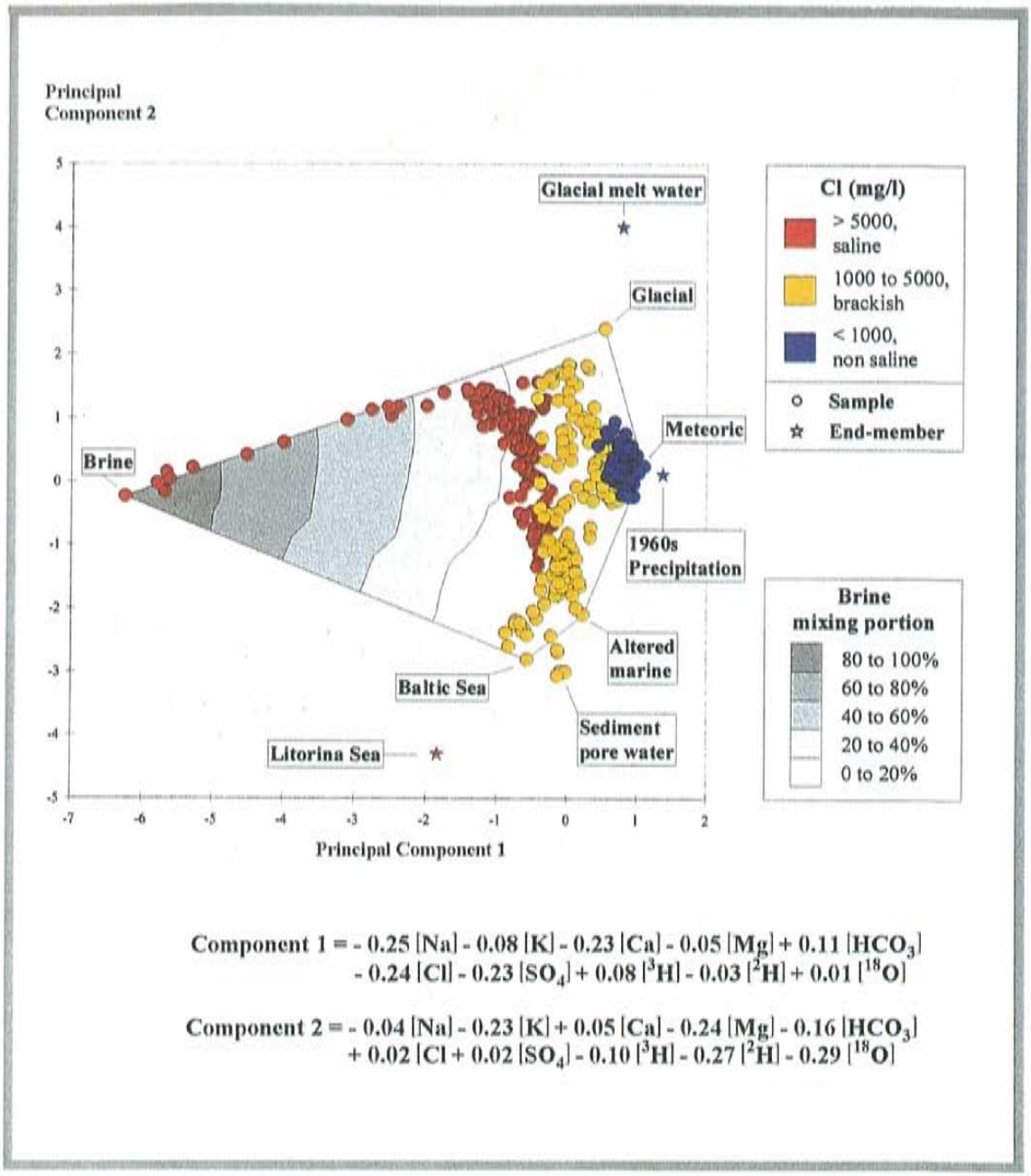

Figure 7-11. *Principal Component plot with a superimposed grey coding showing the mixing portions of brine reference water in relation to the non-saline, brackish and saline groundwater. The numerical values are normalized, see Section 7.2.2.*

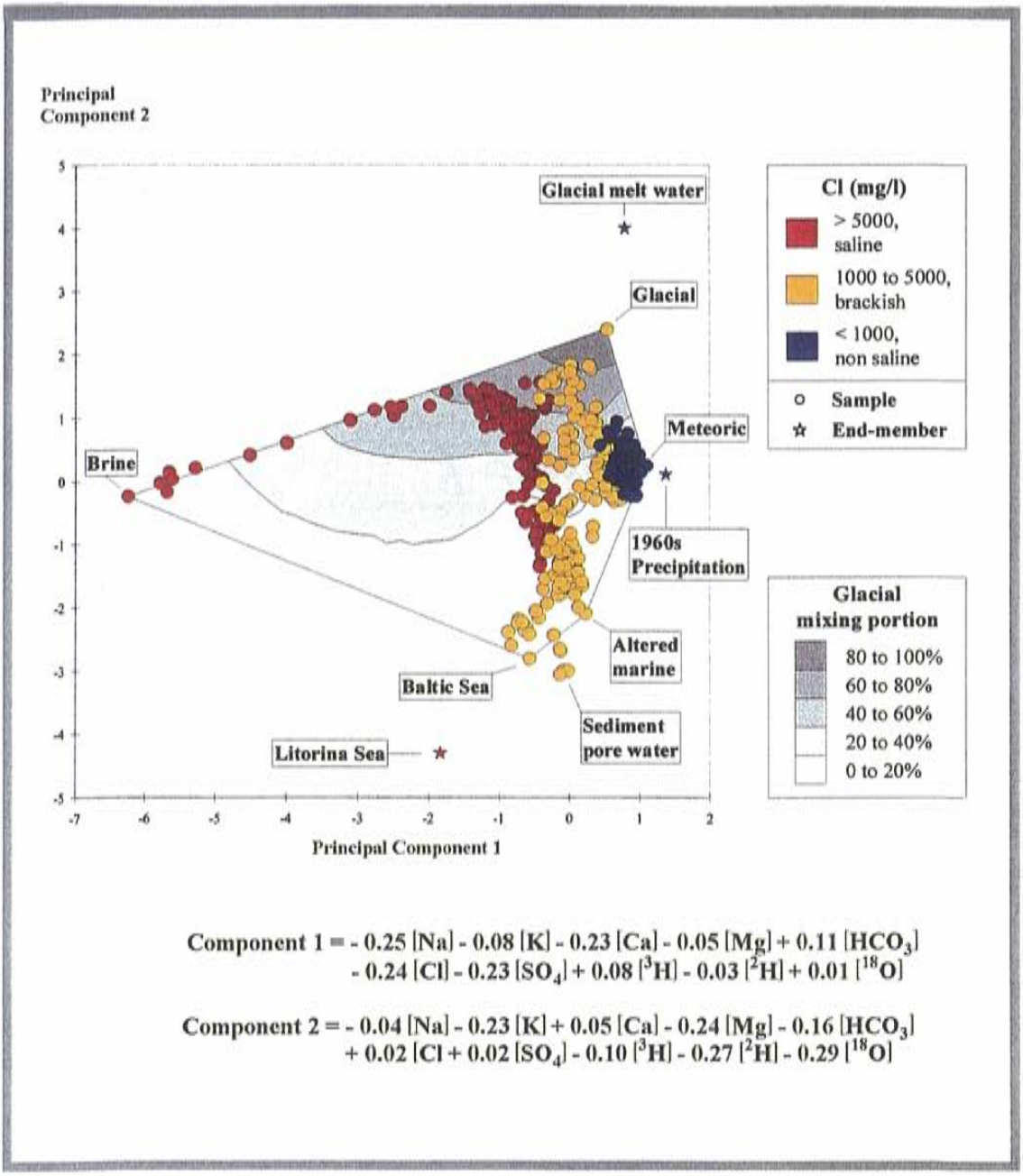

$$\text{Component 1} = -0.25\,[Na] - 0.08\,[K] - 0.23\,[Ca] - 0.05\,[Mg] + 0.11\,[HCO_3] - 0.24\,[Cl] - 0.23\,[SO_4] + 0.08\,[^3H] - 0.03\,[^2H] + 0.01\,[^{18}O]$$

$$\text{Component 2} = -0.04\,[Na] - 0.23\,[K] + 0.05\,[Ca] - 0.24\,[Mg] - 0.16\,[HCO_3] + 0.02\,[Cl + 0.02\,[SO_4] - 0.10\,[^3H] - 0.27\,[^2H] - 0.29\,[^{18}O]$$

Figure 7-12. *Principal Component plot with a superimposed grey coding showing the mixing portions of glacial reference water in relation to the non-saline, brackish and saline groundwater. The numerical values are normalized, see Section 7.2.2.*

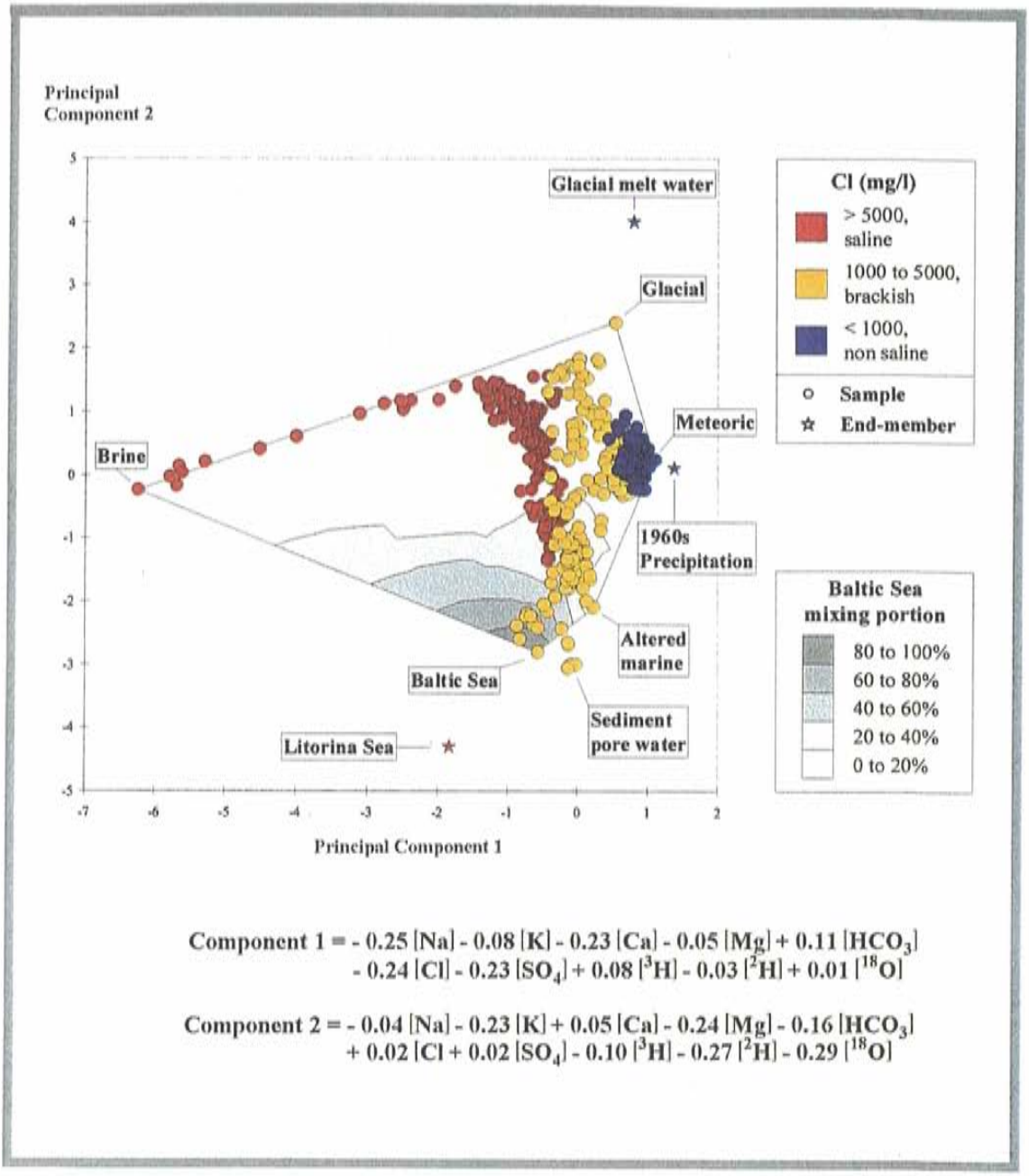

Figure 7-13. *Principal Component plot with a superimposed grey coding showing the mixing portions of Baltic Sea reference water in relation to the non-saline, brackish and saline groundwater. The numerical values are normalized, see Section 7.2.2.*

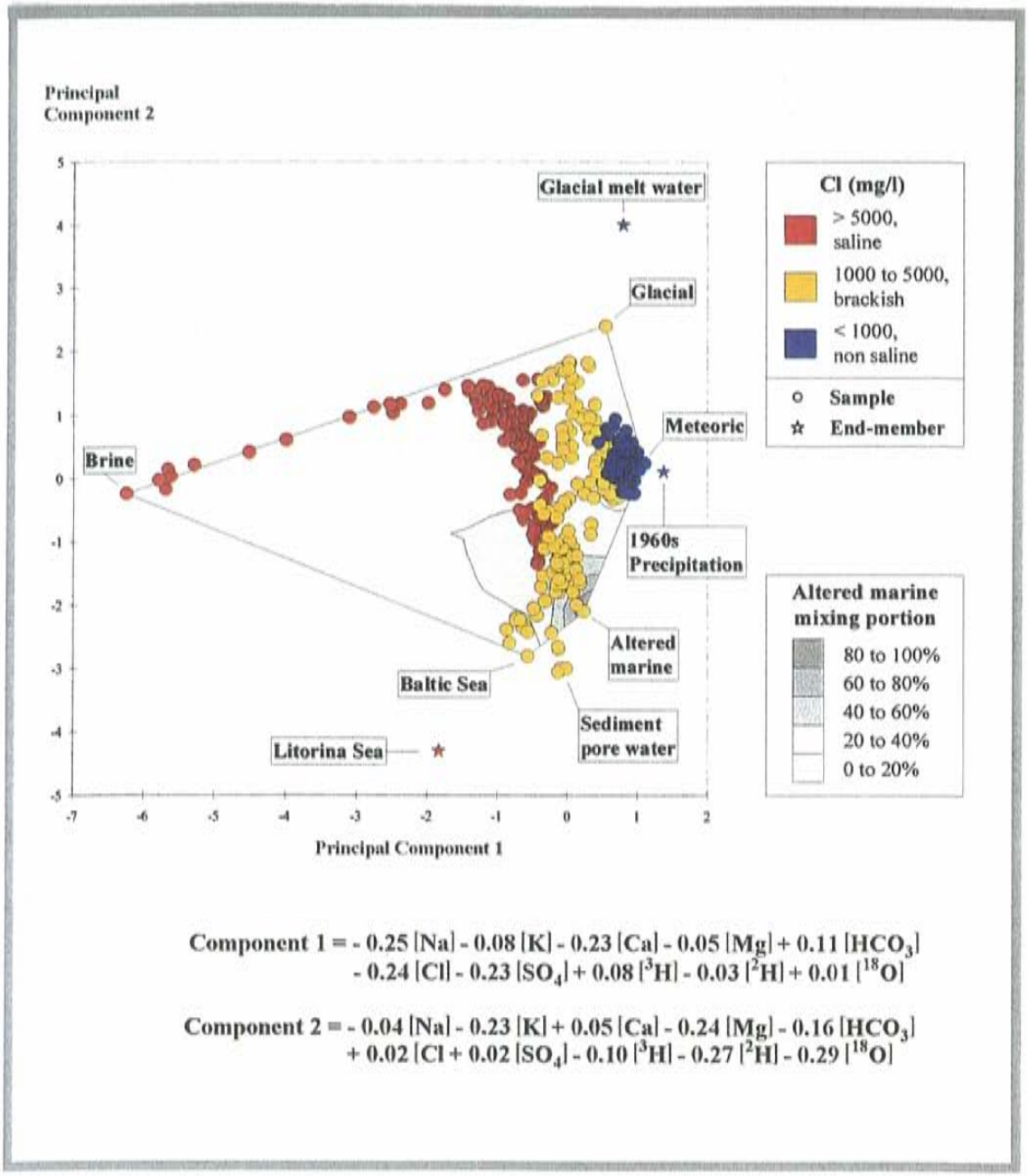

$$\text{Component 1} = -0.25[\text{Na}] - 0.08[\text{K}] - 0.23[\text{Ca}] - 0.05[\text{Mg}] + 0.11[\text{HCO}_3] - 0.24[\text{Cl}] - 0.23[\text{SO}_4] + 0.08[^3\text{H}] - 0.03[^2\text{H}] + 0.01[^{18}\text{O}]$$

$$\text{Component 2} = -0.04[\text{Na}] - 0.23[\text{K}] + 0.05[\text{Ca}] - 0.24[\text{Mg}] - 0.16[\text{HCO}_3] + 0.02[\text{Cl} + 0.02[\text{SO}_4] - 0.10[^3\text{H}] - 0.27[^2\text{H}] - 0.29[^{18}\text{O}]$$

Figure 7-14. *Principal Component plot with a superimposed grey coding showing the mixing portions of altered marine reference water in relation to the non-saline, brackish and saline groundwater. The numerical values are normalized, see Section 7.2.2.*

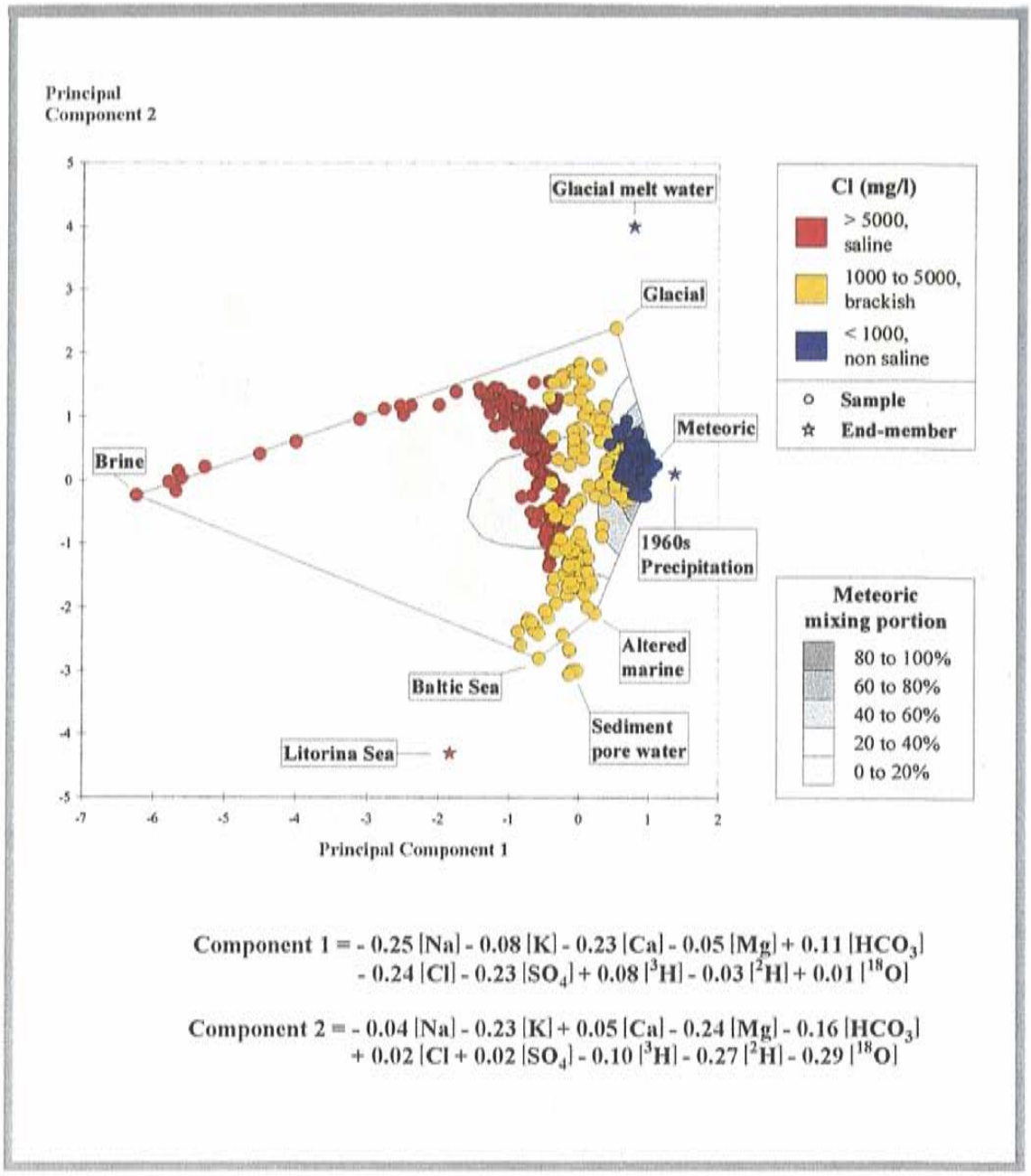

$$\text{Component 1} = -0.25\,[\text{Na}] - 0.08\,[\text{K}] - 0.23\,[\text{Ca}] - 0.05\,[\text{Mg}] + 0.11\,[\text{HCO}_3] - 0.24\,[\text{Cl}] - 0.23\,[\text{SO}_4] + 0.08\,[^3\text{H}] - 0.03\,[^2\text{H}] + 0.01\,[^{18}\text{O}]$$

$$\text{Component 2} = -0.04\,[\text{Na}] - 0.23\,[\text{K}] + 0.05\,[\text{Ca}] - 0.24\,[\text{Mg}] - 0.16\,[\text{HCO}_3] + 0.02\,[\text{Cl} + 0.02\,[\text{SO}_4] - 0.10\,[^3\text{H}] - 0.27\,[^2\text{H}] - 0.29\,[^{18}\text{O}]$$

Figure 7-15. *Principal Component plot with a superimposed grey coding showing the mixing portions of meteoric reference water in relation to the non-saline, brackish and saline groundwater. The numerical values are normalized, see Section 7.2.2.*

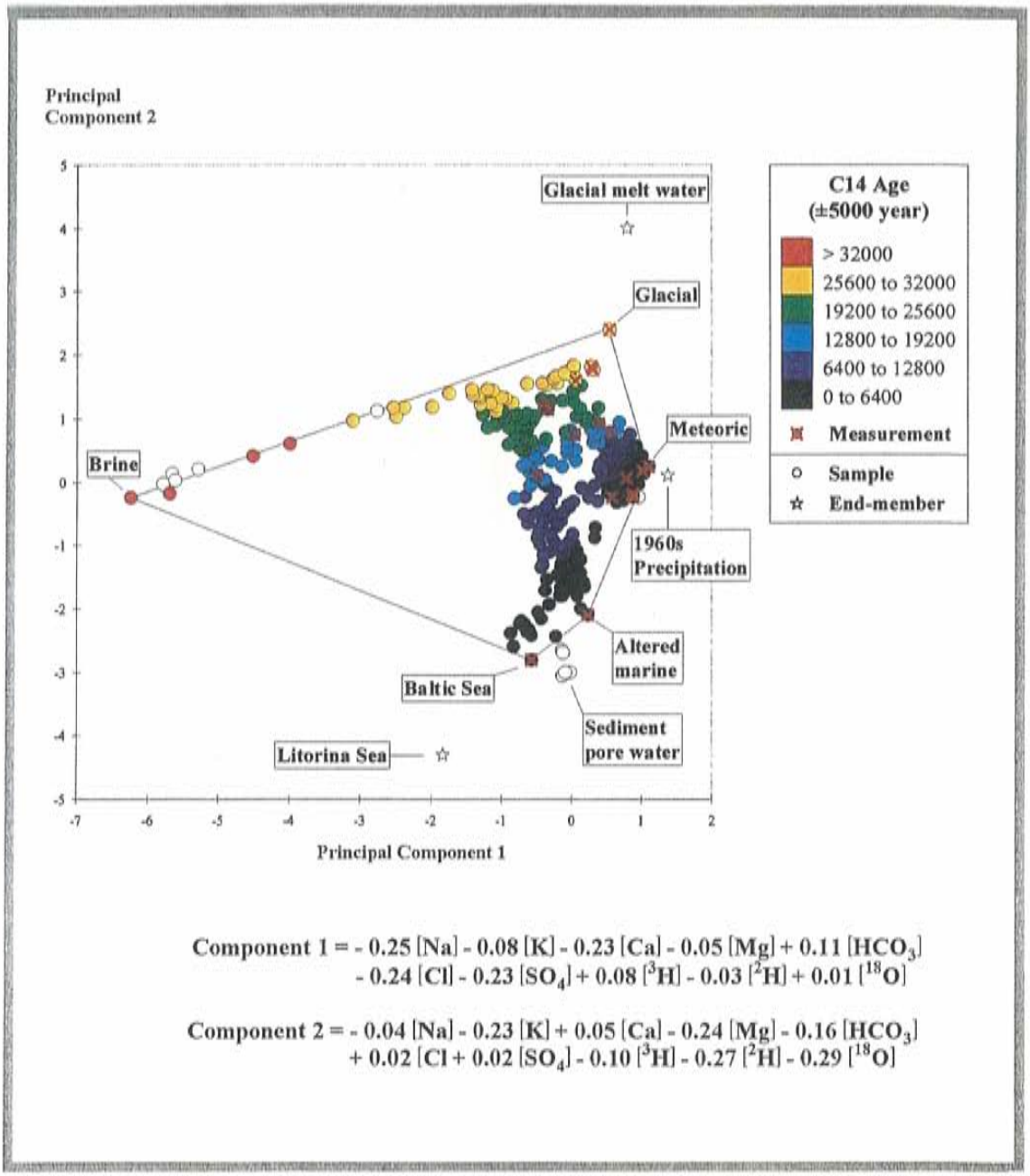

Figure 7-16. *Principal Component plot with a superimposed colour coding showing the predicted ^{14}C age for the groundwaters based on the values from the measured observations. The numerical values are normalized, see Section 7.2.2.*

7.4 THE GROUNDWATER HISTORY

The origin and sources of the different water types at the Äspö site reflect many events such as pre-glacial, glacial and postglacial in combination with water/rock interaction. The deglaciation and subsequent land rise are probably the most important recent events in the Äspö groundwater history.

The Baltic Shield as a part o Northern Europe has been affected by a number of glaciations during the Quaternary Period (2.4 Ma) */Ehlers, 1996/*. Geological evidence show that these glacial events had a great impact on the spatial distribution of soil types and erosion of the surface of the bedrock. The heavy ice load caused extensive isostatic movements of the basement, hence it also changed the hydrogeological system which had a large influence on the groundwater flow paths and groundwater chemistry.

The last three major glacial events during the Quaternary Period are Elster, Saale and Weichsel, where the Weichsel is the latest glacial event. It reached its maximum approximately at about 18 000 to 20 000 years ago */Ehlers, 1996/*. The cyclic behaviour in the climate during the Quaternary Period imply that different groundwaters in the basement must have been modified and even replaced several times. The extreme cold climate during the glacial events in the high latitudes form waters with typical low isotopic (^{2}H and ^{18}O) signatures, whereas the milder interglacials display a different isotopic pattern. Hence, the wide range in isotopic signatures give us a very useful tool in order to understand the meteoric water input, glacial meltwater and other end-members involved in the groundwater formation during this period. The different scale of the glacial events and different hydrogeological situations may have caused differences in penetration depth of for example glacial melt water, and hence there may be remnant waters still found in the basement from the early events as well. Most probably the events after the last glaciation is dominating. Bearing this in mind we present a working hypothesis and a conceptual model for the groundwater system at the Äspö site. This model mainly focus on the last glacial event and especially on the post-glacial development of the Baltic Shield and the Äspö area. *Figure 7-17* shows the coast line of Sweden at the different stages at the Baltic Sea during its shifting between fresh-water lakes and brackish seas since the last glaciation.

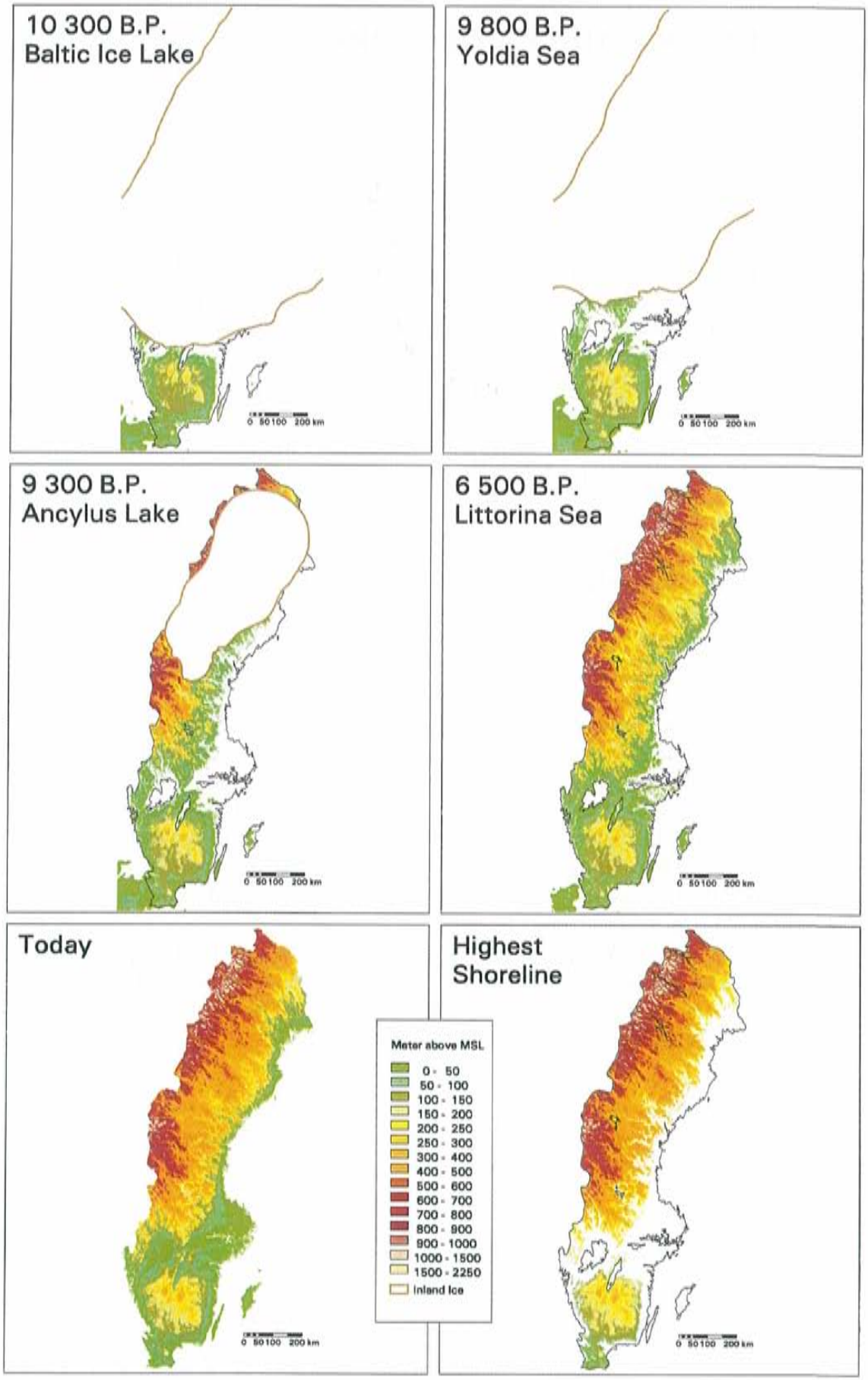

Figure 7-17. *The different evolutionary stages of the Baltic Sea after the most recent glaciation and a picture of the previous highest coastline. The pictures were produced from SKB's Geographic Information System. /SKB, 1995/.*

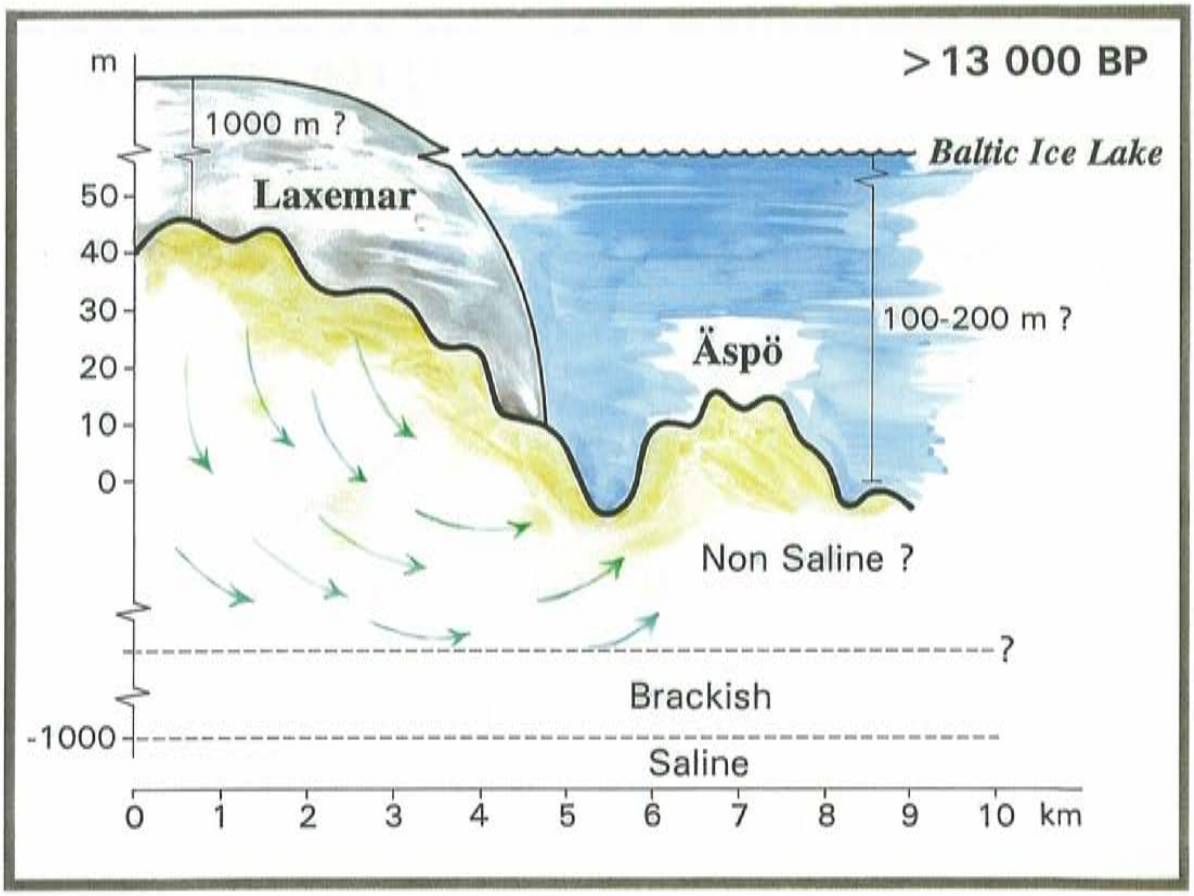

Figure 7-18. *A post-glacial scenario at Laxemar and Äspö. Possible flow lines, non-saline, brackish and saline water interfaces are shown. Injection of Glacial melt-water into the basement.*

When the continental ice was melting and retreating, glacial melt-water was injected in to the basement, *(Figure 7-18).* The depth to which the meltwater reached is largely unknown. Groundwater flow models suggest that under hydraulic gradients caused by a thick ice cover the meltwater could be pressed to a depths of more than 1000 m */Svensson, 1996/*. Whether or not this has been the case is beyond present knowledge. It is important to note that a deep saline groundwater with a relatively high density can act as a barrier which may prevent less dense shallow water from penetrating the deeper regions. It is also uncertain whether or not there has been a water pressure below the ice of such a magnitude as the thickness of the ice cap.

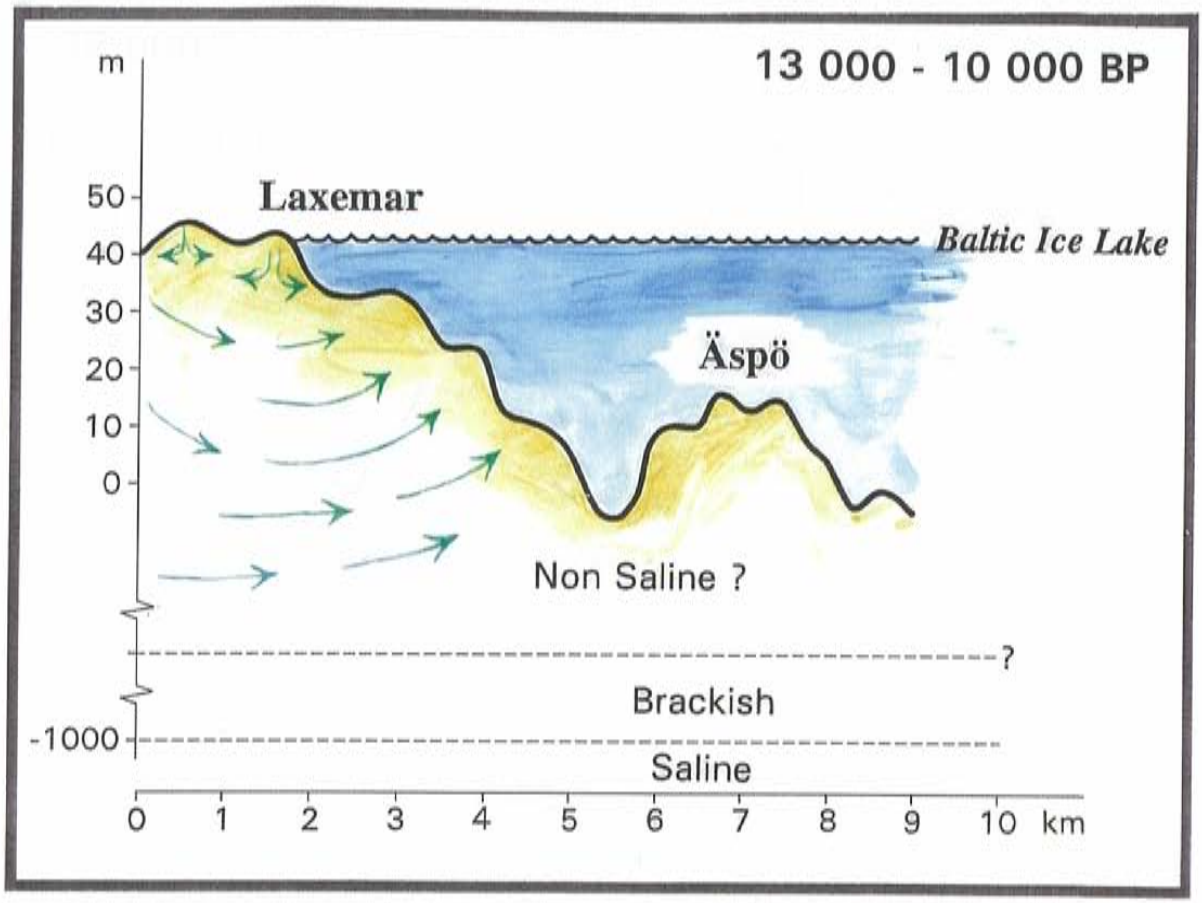

Figure 7-19. *A post-glacial scenario at Laxemar and Äspö. Possible flow lines, density-driven turnover, non-saline, brackish and saline water interfaces are shown. Baltic Ice Lake stage.*

The first stage of the Baltic Sea, known as the Baltic Ice Lake, started to form about 13 000 years ago. 10000 B P the Baltic Ice Lake still covered the Äspö area *(Figure 7-19)*. The fresh water probably did not affect the glacial water in the basement since there was no hydraulic hydraulic head difference when the island was under water. Far to the west the Laxemar area rose above the water level.

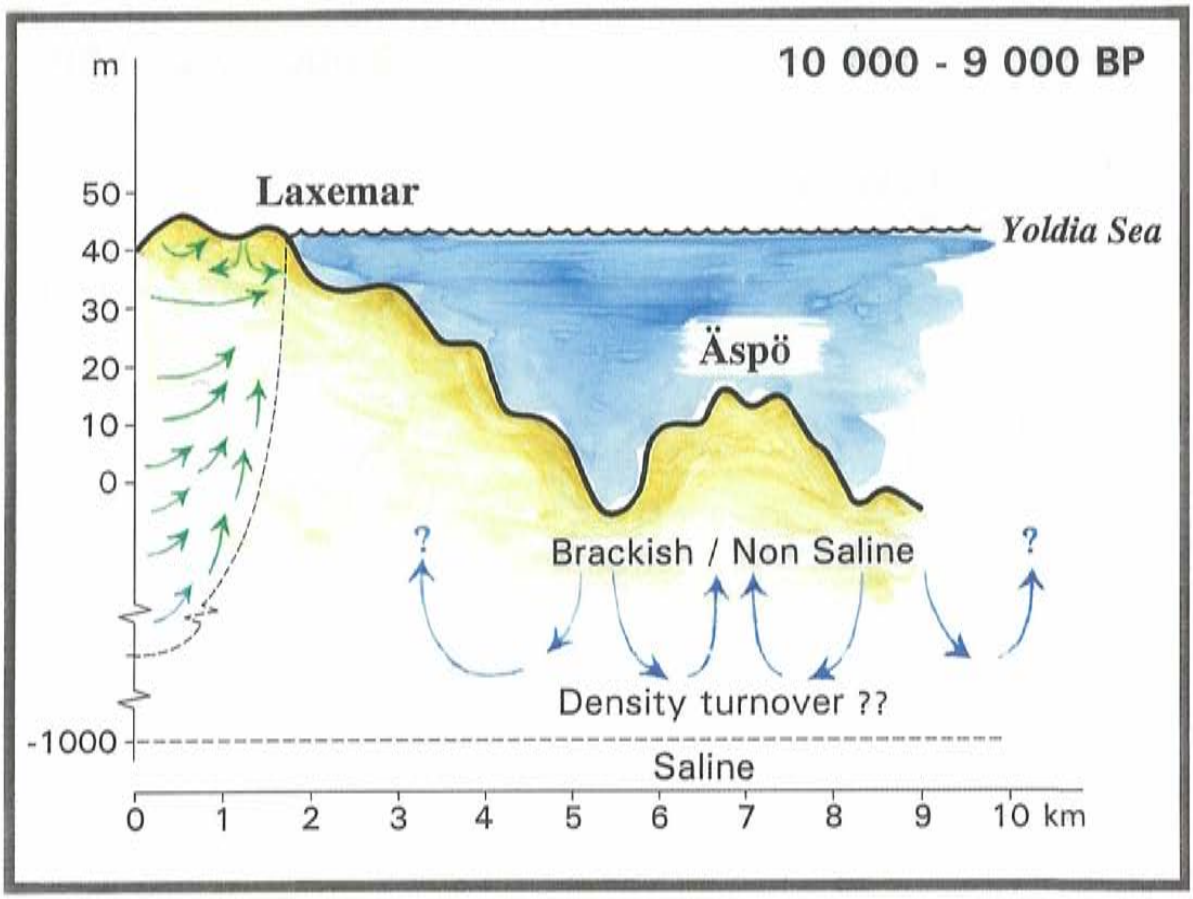

Figure 7-20. *A post-glacial scenario at Laxemar and Äspö. Possible flow lines, density-driven turnover, non-saline, brackish and saline water interfaces are shown. Yoldia Sea stage.*

During the next phase the Yoldia Sea (10000-9000 B P) covered the island. The brackish-marine water could have affected the more conductive upper parts of the basement to some extent by density-driven turnover (buoyancy flow), as shown in *Figure 7-20*. The Yoldia sea stage was short compared to the other stages and the influence on the groundwater system could have been insignificant. As implied in *Figure 7-19* any effect of the Yoldia stage would have differentiated the situation at Äspö from the situation at Laxemar, giving a fresh-saline water interface at the shoreline at Laxemar.

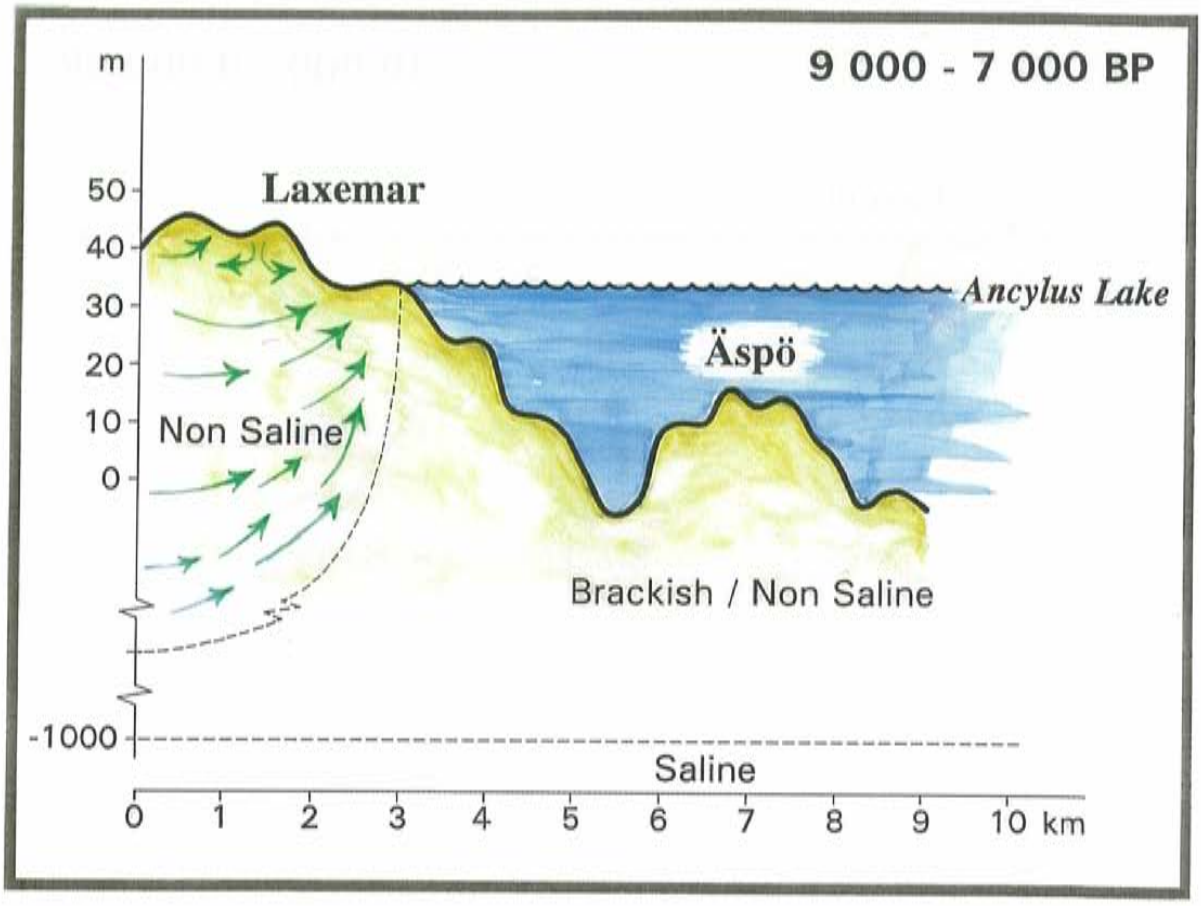

Figure 7-21. *A post-glacial scenario at Laxemar and Äspö. Possible flow lines, density-driven turnover, non-saline, brackish and saline water interfaces are shown. Ancylus Lake stage.*

The Ancylus Lake (9000-7000 B P), which was a freshwater lake, probably did not affect the water in the basement of Äspö. At Laxemar the recharge and discharge controlled by the topography affected the areas above the water level *(Figure 7-21).*

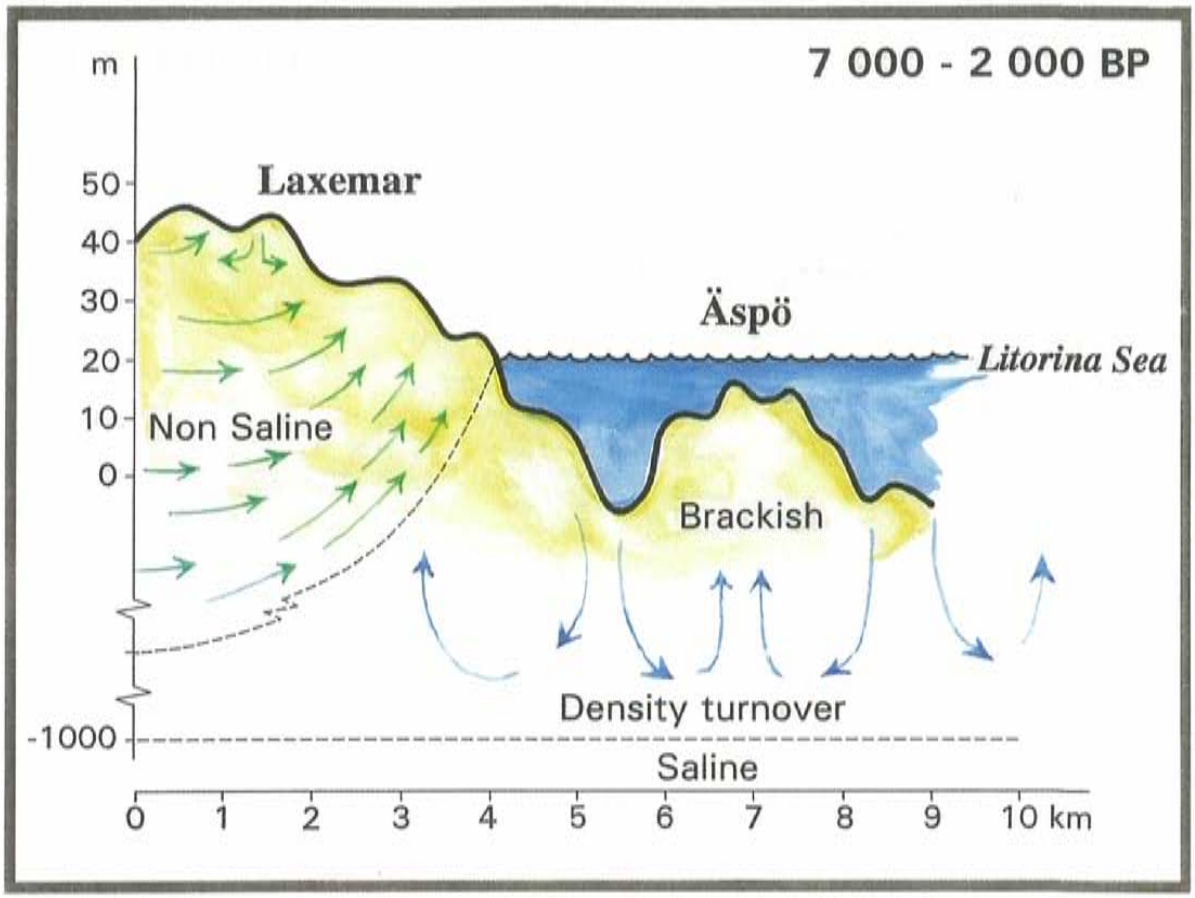

Figure 7-22. *A possible post-glacial scenario at Laxemar and Äspö. Possible flow lines, density-driven turnover, non-saline, brackish and saline water interfaces are shown. Litorina Sea stage.*

The next stage was the Litorina (7000-2000 B P) Sea which most likely provided saline waters which reached salt content expressed as Cl = 7 000 mg/l ($\delta^{18}O$ = -4.5‰, δD = -38‰) */pers. com. Tullborg, 1995 - calculation based on Kankainen, 1986/*. Density-driven turnover is believed to be an important process during this period. The glacial water was replaced and mixed with the sea water *(Figure 7-22)*. In the Baltic Shield area the highly saline coastal groundwaters are only found below the highest shoreline of the postglacial Litorina Sea since the density-driven turnover was probably an important process during this stage. Previous works */Frape and Fritz, 1987, Gascoyne, 1987, Nurmi et al, 1986, Fontes et al, 1989, Wallin, 1990/* showed that groundwater in the crystalline basement on the Canadian and Baltic shields may have been formed or affected by marine water intrusions.

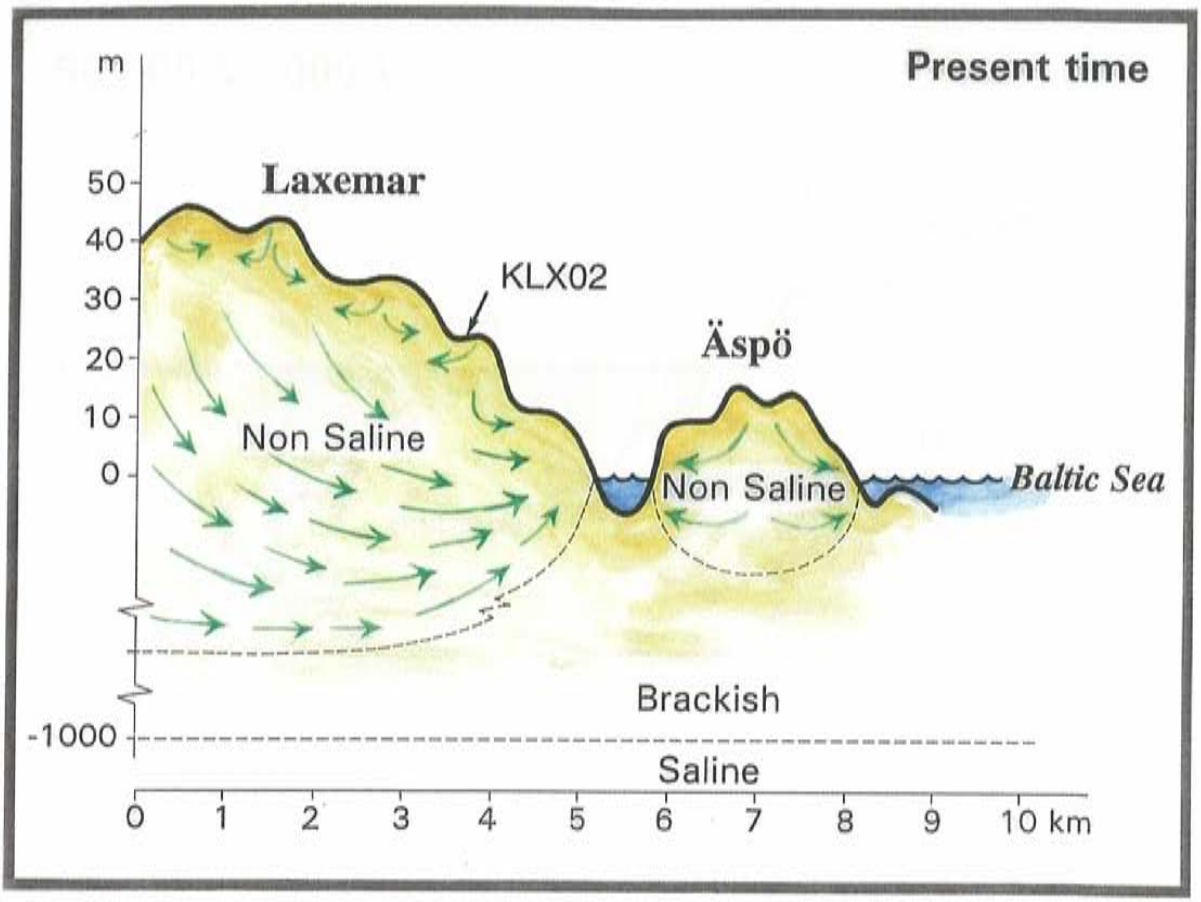

Figure 7-23. *A possible post-glacial scenario at Laxemar and Äspö. Possible flow lines, density-driven turnover, non-saline, brackish and saline water interfaces are shown. Present day situation. The approximate location of the deep borehole KLX02 is indicated by an arrow on this picture.*

The Äspö area rose above the sea level some 4000 B P). A meteoric water aquifer started to form which created hydraulic head differences and started to wash the sea water out of the more shallow parts of the basement *(Figure 7-23)*. Regional flow from the mainland could have started to affect the water composition. The saline waters at depth were probably not affected by the post-glacial events *(Figure 7-21)*. Traces of deglaciation in more shallow groundwaters should be detectable in the groundwater composition.

The isotopes, both radiogenic and stable, were used to evaluate the pre-history of the groundwater. Due to the scarcity of the data from pre-investigations it was not possible to predict the isotopic signatures of the groundwater. During the construction phase */Wallin and Peterman, 1994/* the knowledge of end-member signatures and background levels have increased. The combination of several isotopic methods has provided the means to tackle the history of the groundwater in a systematic way. So far the events occurring after the latest glaciation have been resolved and these data have been of the outmost importance for the identification of the end-members used to construct *Model 96.*

An illustration of the models based on the data from pre-investigations and the data from the tunnel construction phase are given in *Figure 7-24*. The corresponding salinity distribution is presented in *Figure 7-25* and *7-26*. The differences in salinity distribution are due to the effects caused by the tunnel drawdown. The biological and redox conditions are not presented since they are considered to be evenly distributed in the rock mass.

The *Model 96*, developed during the construction phase, is more developed and quantitative than *Model 90* from the pre-investigation phase. In *Figure 7-24* the presentation is made in such a way that the models can be compared, but it must be realized that the figure only illustrates parts of the models. *Model 90* groups the groundwater observations into four classes based on principal component analyses. The *Model 96* defines the end-members, reference waters and mixing proportions of the reference waters. In *Figure 7-24* the dominating reference waters are qualitatively related to the statistically defined classes of the previous model.

A consistent picture was obtained by ^{2}H, ^{3}H, ^{18}O, ^{13}C, ^{14}C, ^{87}Sr, ^{34}S and ^{36}Cl analyses which were made on different occasions during tunnel construction. There are a few additional isotopic methods, $^{36}Ar/^{40}Ar$ and ^{85}Kr which might be useful for differentiating between the effects of the latest and previous glaciations. So far these methods have not been employed on Äspö groundwater samples.

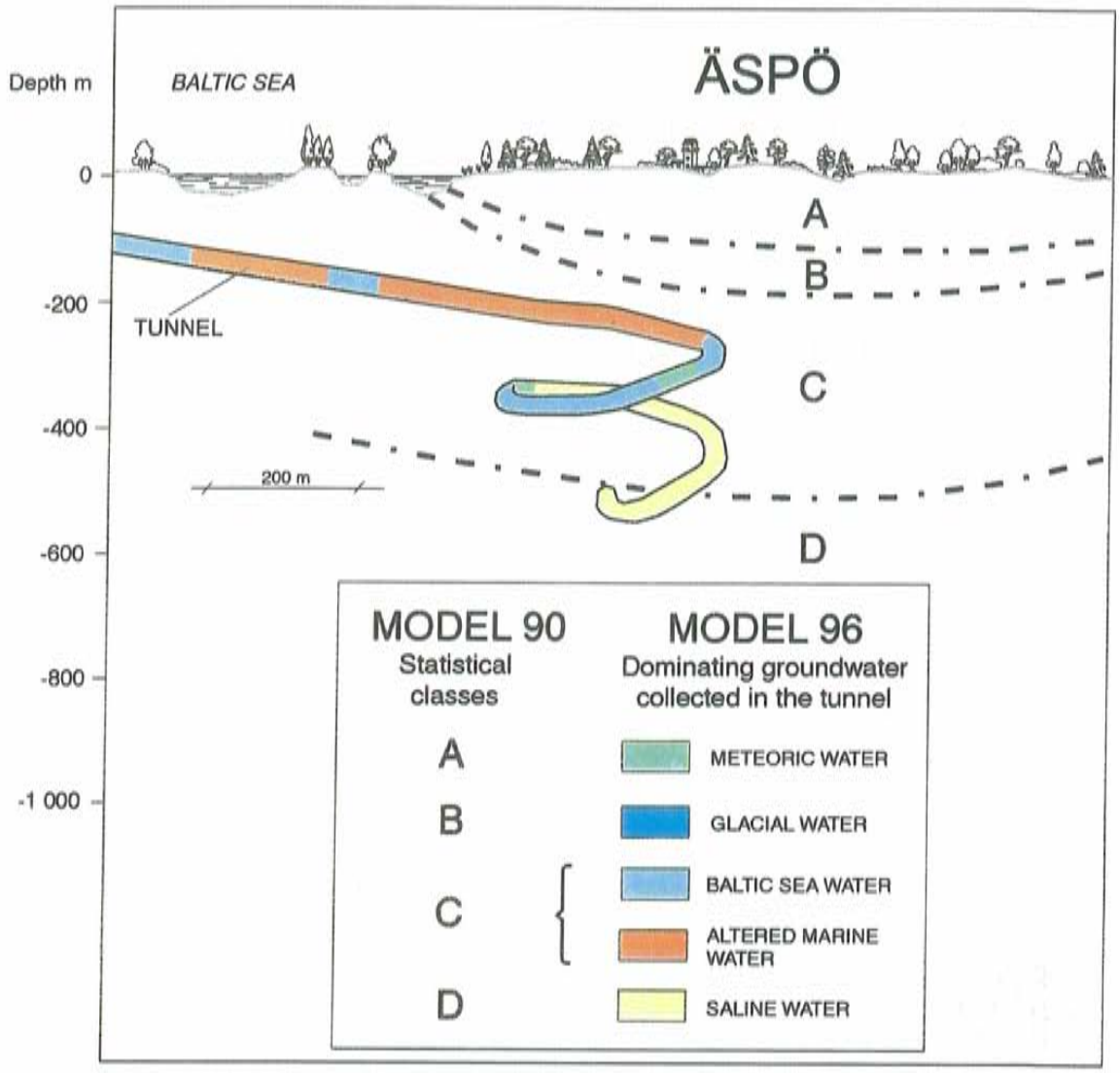

Figure 7-24. *Illustration of Model 90 based on data from the pre-investigations and Model 96 which also involves the data collected during the tunnel construction phase. Model 90 defines 4 four classes based on statistical treatment of the data, whereas Model 96 is based on identified end-members and selected reference waters and the mixing proportions of these waters (see Section 7.2.3).*

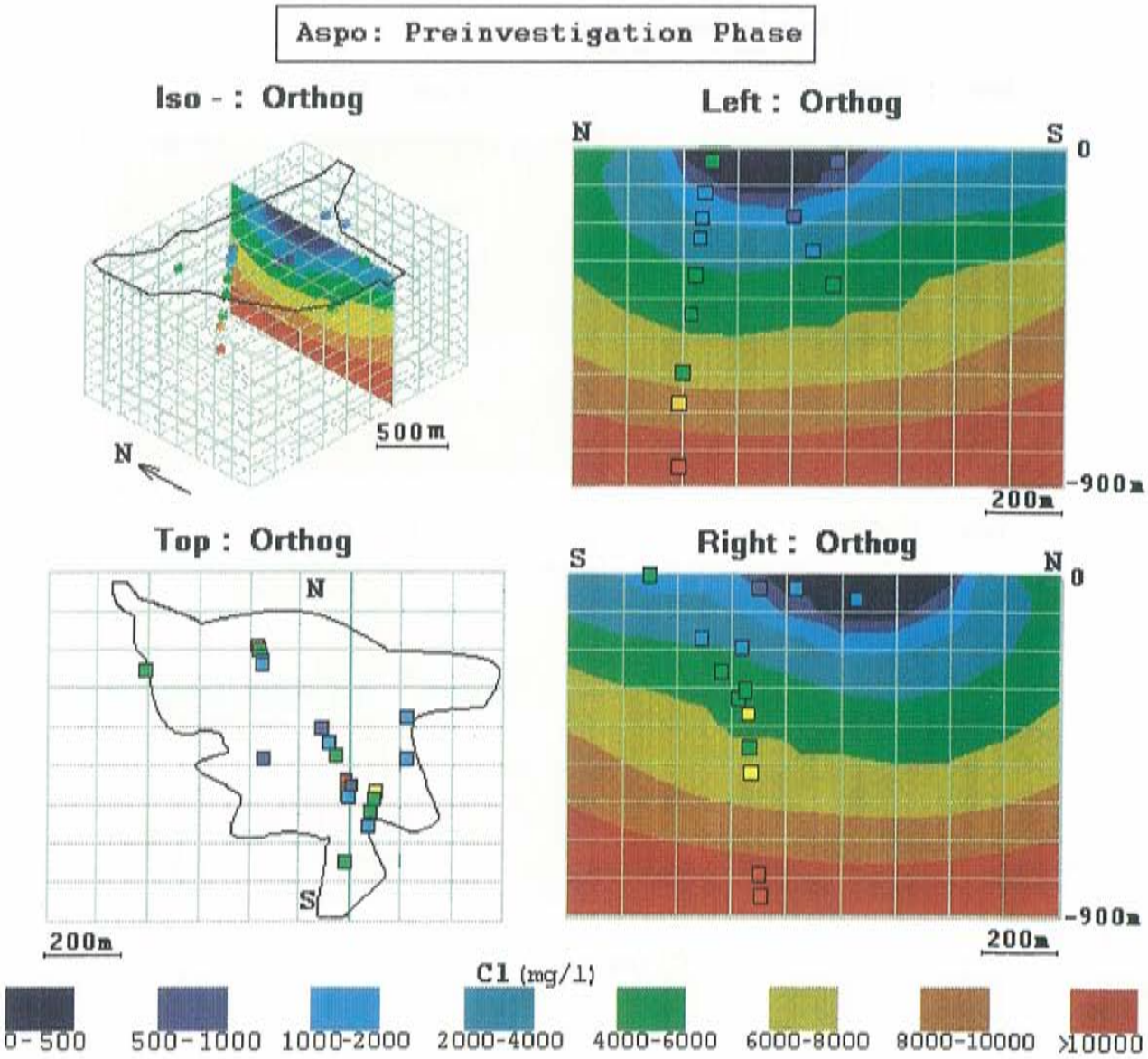

Figure 7-25. *The salinity distribution presented as the chloride concentration under the undisturbed conditions prior to excavation. The sampling locations are marked in the figure. (Total salinity = 1.7 times the chloride concentration).*

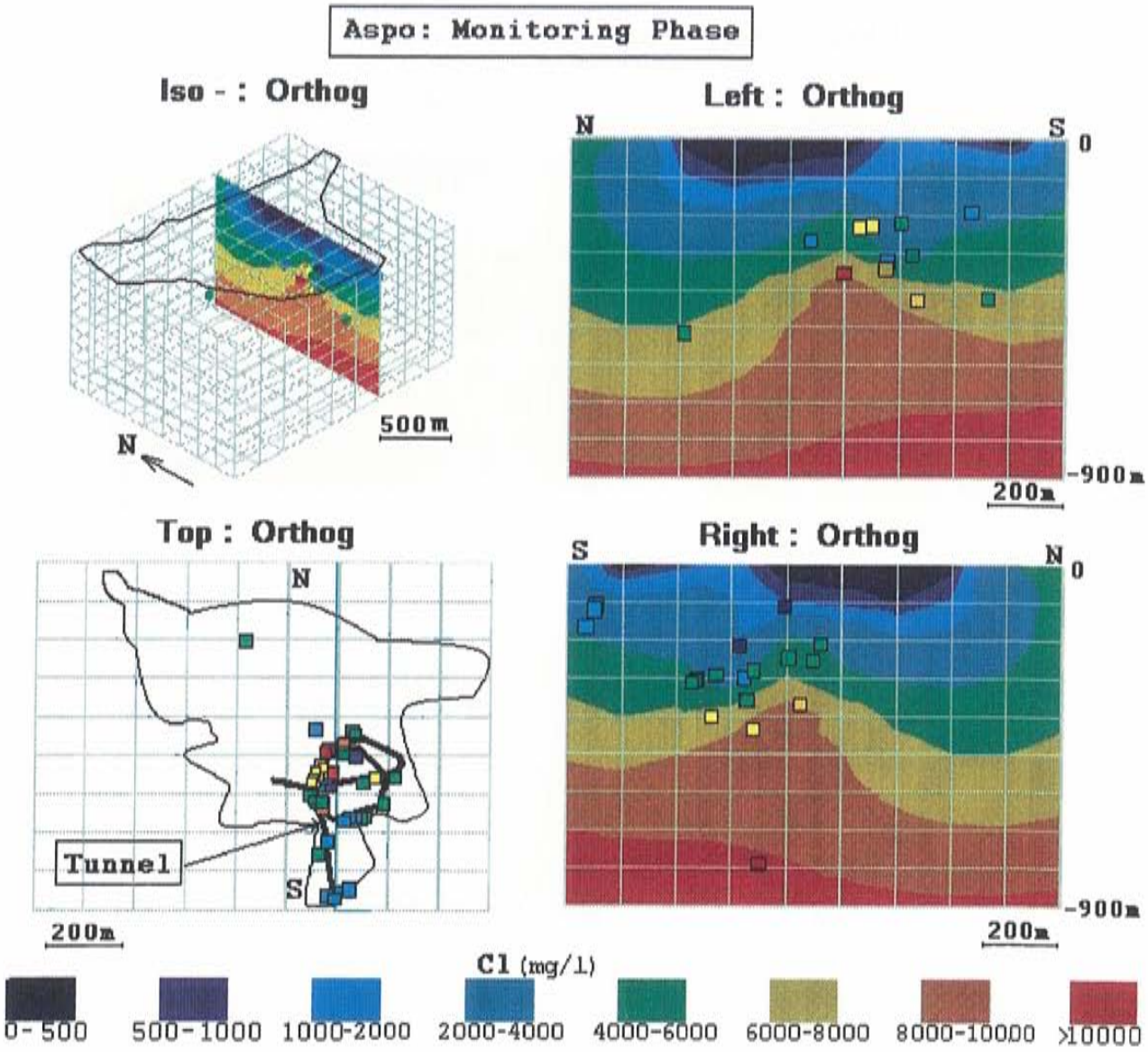

Figure 7-26. *The salinity distribution presented as the chloride concentration under the disturbed conditions after construction. The sampling locations are marked in the figure. (Total salinity = 1.7 times the chloride concentration).*

7.5 REDOX CONDITIONS

Redox conditions are important for the safety assessment of a nuclear waste repository */SKB, 1995/*. The observed redox potential (Eh) and the redox buffering constituents in the groundwater are extremely sensitive to disturbances caused by sampling and analyses. The redox buffer is to a large extent provided by the fracture filling minerals in contact with the groundwater and by the biological processes */Banwart (ed.), 1995/*.

Great efforts have been made to investigate and solve the issue of deep groundwater redox conditions */Grenthe et al, 1992/*. The present understanding is that the ferrous and ferric iron minerals generally govern the redox properties. This is also the case for data from the investigations at Äspö. However, occasionally other systems are thought to dominate, e.g. the uranium system in an Uranium mineralization */Ahonen et al, 1992/*. Regardless of which system controls the Eh it has been clearly demonstrated that the deep groundwaters in granitic rocks are generally reducing.

The redox-sensitive elements, for which analyses are normally made are iron (total and ferrous), manganese, sulphide, uranium and dissolved oxygen. As expected, there are normally no measurable concentrations of dissolved oxygen, but the sensor is needed to register any disturbances in the groundwater pumping and sampling procedure. A zero reading of the dissolved oxygen content indicates that the water is anoxic.

Eh measurements are made using three types of electrode, gold , platinum and glassy carbon. Only the sampling procedure denoted complete chemical characterization, see *Report 4 /Rhén et al, 1997/*, included the proper Eh measurements during the pre-investigations. The measurements were continued for a period of several days (weeks) until the readings levelled out at roughly the same value for all three electrodes. This is the reported Eh value. During sampling in the tunnel no Eh or dissolved oxygen contents were measured, except for those in the redox experiment */Banwart et al, 1995/*.

The enhanced water flow in the upper part of the rock, caused by the inflow to the tunnel, was expected to transport oxygenated water down into the fracture zones and enter the tunnel. This phenomenon was studied in a fracture zone at a depth of 70 m below ground level */Banwart et al, 1995/*. The predictions of oxygen breakthrough failed because the effects of biological oxygen consumption were not taken into account. The conclusion is that an enhanced groundwater inflow does not cause oxygenated water to reach any greater depths, as long as the amount of organic matter is larger than the amount of dissolved oxygen. These conditions could of course vary from place to place but as a starting point the situation at Äspö could also be expected at any other place. At the Stripa mine, for example, where the hydrology had been affected by the drawdown by the mine gallery for several decades, there was no oxygen in the infiltrating groundwater at a depth of 400 metres. Most evidence suggests that the penetration depth for oxygen is at maximum 100 m for undisturbed conditions and it is not expected to be significantly deeper under disturbed

conditions (drawdown in groundwater flow into tunnels of a facility). The effective oxygen consumption by bacteria strengthens the general opinion that anoxic (oxygen free) conditions could always be expected in the deep groundwater.

The Eh value is coupled to the pH value. An empirical relation is a decrease of 60 mV with an increase of one pH unit. At pH 7 the Eh values are mostly between -100 and -300 mV. Plots of the Eh-pH data from the pre-investigation phase and from a few observations in the tunnel are shown in *Figure 7-27.* At these low Eh-levels uranium exists in a reduced (+IV) form and is extremely insoluble.

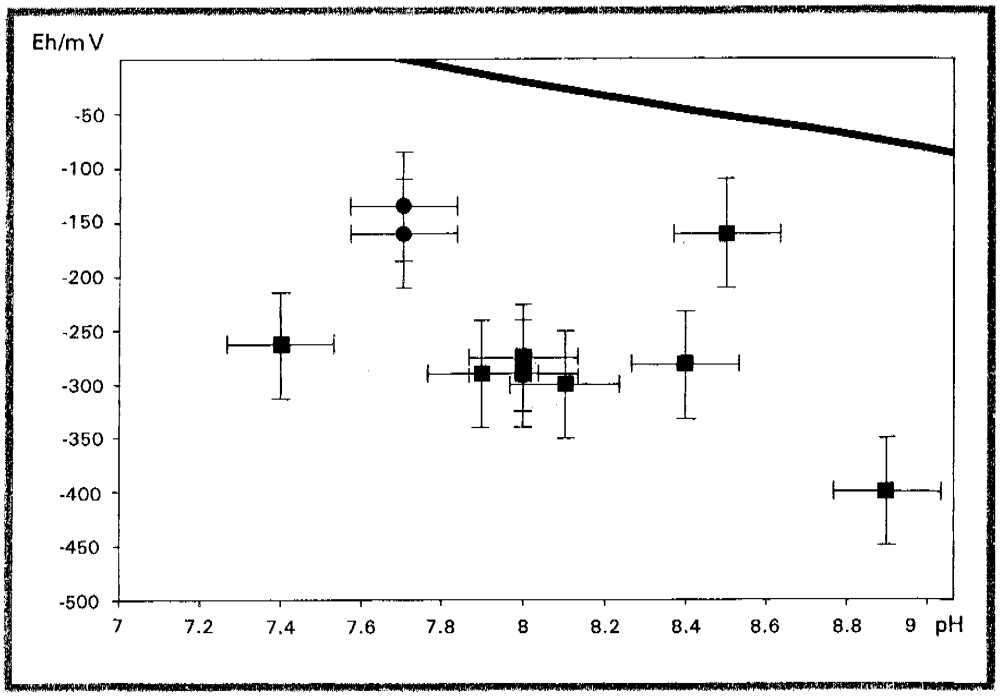

Figure 7-27. *Eh versus pH for the data obtained from the pre-investigation phase (squares) and from the construction phase (Circles). The uncertainty in Eh is estimated to be ±50 mV and the uncertainty in pH is ±0.1 pH unit. The figure includes the calculated Eh for the equilibrium between* UO_2 *and dissolved* UO_2^{2+} *at a concentration of 10 ppb.*

A practical approach for nuclear waste disposal safety assessment is therefore to define reducing conditions to be when uranium (plutonium, technetium and neptunium as well) exists in a reduced form, and oxidising conditions when uranium exists in the hexavalent (+VI) state. The usefulness of this approach is that it resembles well the conditions of the iron system. Under reducing conditions ferrous iron is present in the groundwater in measurable quantities, up to ppm levels. In this context it might also be worth mentioning that there is a large difference between reducing and anoxic conditions. Anoxic

conditions only mean that there is no measurable amount of dissolved oxygen in the water, whereas reducing means that the Eh value needs to be low enough to have uranium in a reduced form (concentrations at ppb levels). A reducing groundwater is always anoxic.

7.6 THE SALINE GROUNDWATERS OF THE ÄSPÖ-LAXEMAR AREA

7.6.1 General features of the saline groundwaters

Saline groundwaters, Cl >5000 mg/l, *(Figure 7-6)* are obtained from the deeper part of Laxemar (>1100 m), Äspö (>350 m) and the HRL tunnel (>100 m). Saline groundwaters have been described in detail by *Smellie and Laaksoharju /1992/, Laaksoharju et al /1995/, Laaksoharju and Skårman /1995/* and also *Louvat et al, Peterman and Wallin, Trotignon et al, Wallin and Peterman,* in *Laaksoharju and Wallin /1997/.*

The depth of the saline groundwaters is controlled by the prevailing hydrogeological conditions. The hydraulic head in combination with heterogenous spatial distribution of the conductive fractures determines the position of the interface between saline and brackish water. Laxemar, which is on the mainland, has a relatively high water table resulting in an interface at large depth (1100 m) between saline and brackish waters. On Äspö island, whose topography is flat, the water table is lower and the interface can exist at shallower depths (350 m). Under the Baltic Sea saline groundwater may be unaffected by any hydraulic forces since the Litorina Sea stage. Here the saline groundwater can exist at close to a 100 m depth. The depth at which the saline groundwater is encountered depends on the history of the groundwater, see *Section 7.4*, and on the topography and density.

The saline groundwater is characterized by a sodium chloride rich variety at depths of 100-600 m and a calcium chloride variety at depths greater than 600 m. At 100-600 m depths a complex mixing pattern includes several reference waters. Possible regional flow in combination with near stagnant conditions are believed to dominate at the deeper (>600 m) regimes.

7.6.2 Saline groundwaters with a brine component

Chemical composition

The deep (600-850 m) saline groundwaters at Äspö has a brine component. At 800 metres at Laxemar (KLX02), chlorinity increases dramatically by almost three orders of magnitude (to approximately 16,000 mg/l) over a distance of 250 m (depth of 1150 m). Chlorinity continues to increase with depth (to 47,200 mg/l) displaying inflection points at approximately 1350 m and 1000 m, see *Figure 7-30.* Hydraulic tests showed that the transmissivity decreased with depth at the Laxemar borehole. The working hypothesis is that the brine

water represents a hydraulically and geochemically isolated system such that highly saline groundwaters exist in a near-stagnant environment */Laaksoharju et al, 1995/*. These calcium chloride dominated brines represent deep regional groundwaters where long residence times and water/rock interactions have played a dominant role in creating their composition.

$^{40}Ar/^{36}Ar$

Evidence of water/rock interaction at great depth is suggested from $^{40}Ar/^{36}Ar$ ratio measurements. The isotope ^{40}Ar is enriched (from feldspar breakdown) by a factor of four (compared with atmospheric input) in the highly saline groundwaters */Smellie, 1996/*.

$\delta^{18}O$ and $\delta^{2}H$

The stable isotope data ($\delta^{18}O$ =-10.4 to -8.9‰ (SMOW); $\delta^{2}H$ = -60.2 to -44.9‰ (SMOW)) from the deep saline groundwaters show significant deviation from the meteoric water line. The trend towards increasing salinity can reflect a greater dependency on water/rock reactions in combination with minimal influence from past marine and glacial melt fluctuations at great depth. The long contact time with rock may have modified the ^{18}O values from the meteoric water line */Alley, 1993/* (*Figure 7-28*).

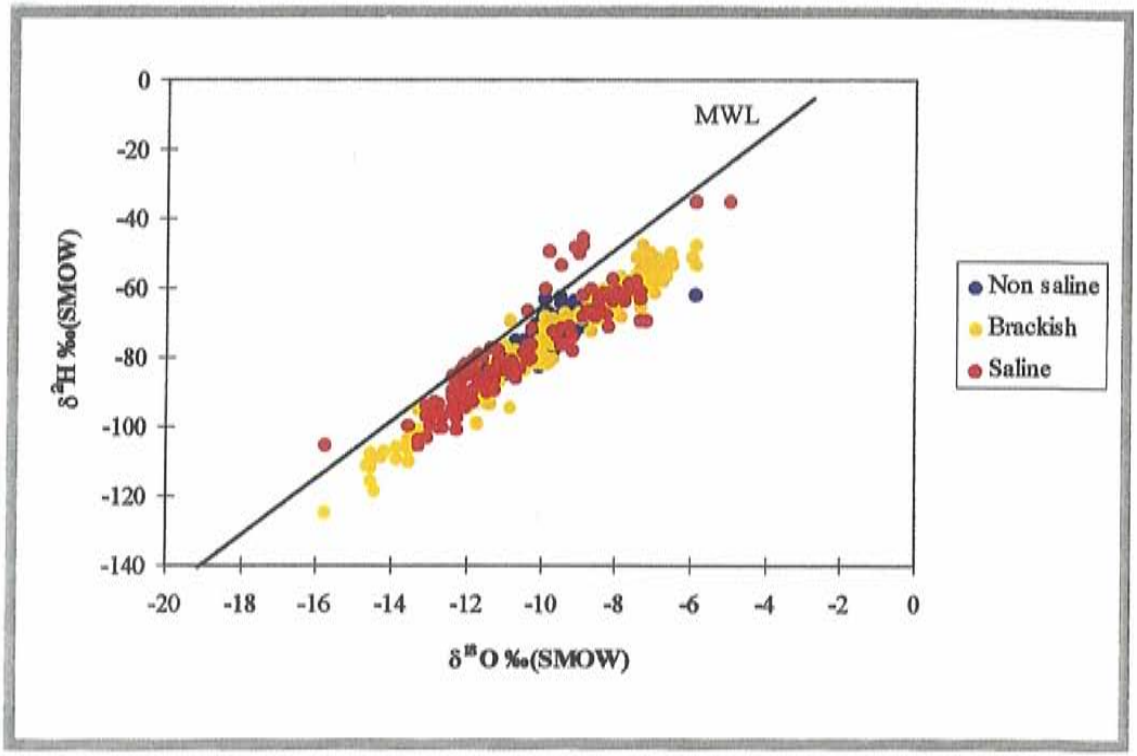

Figure 7-28. *$\delta^{18}O$ versus deuterium for the Äspö and Laxemar groundwaters. The long contact time with the rock may have shifted the ^{18}O-deuterium signature to above the meteoric water line. The data point below the meteoric water line indicates a cold climate recharge.*

^{36}Cl

The high apparent age is supported by the measured ^{36}Cl values which indicated the water has been isolated from the atmosphere for 1.5 M years */Louvat et al,* in *Laaksoharju and Wallin, 1997/*.

Cl^-/Br^-

By comparing the Äspö site groundwater Cl^-/Br^- ratio with marine and sedimentary ratios it was suggested that the brine correspond to an evoluted sea water which has been concentrated by evaporation to the precipitation stage of halite. The $\delta\,^{18}O$ signature *(Figure 7-29)* and chloride contents of the saline samples coming from the deepest intervals of the Laxemar boreholes, could then be explained by a sedimentary primary brine in the Äspö deep groundwater */Louvat et al, 1997/*. Preliminary noble gas analyses show that the deep groundwaters give an Xe signature which indicates a possible recharge temperature of 25°C which in turn suggests much warmer climatic conditions than the present-day ones */Smellie, 1996/*, which could support the sedimentary primary brine assumption.

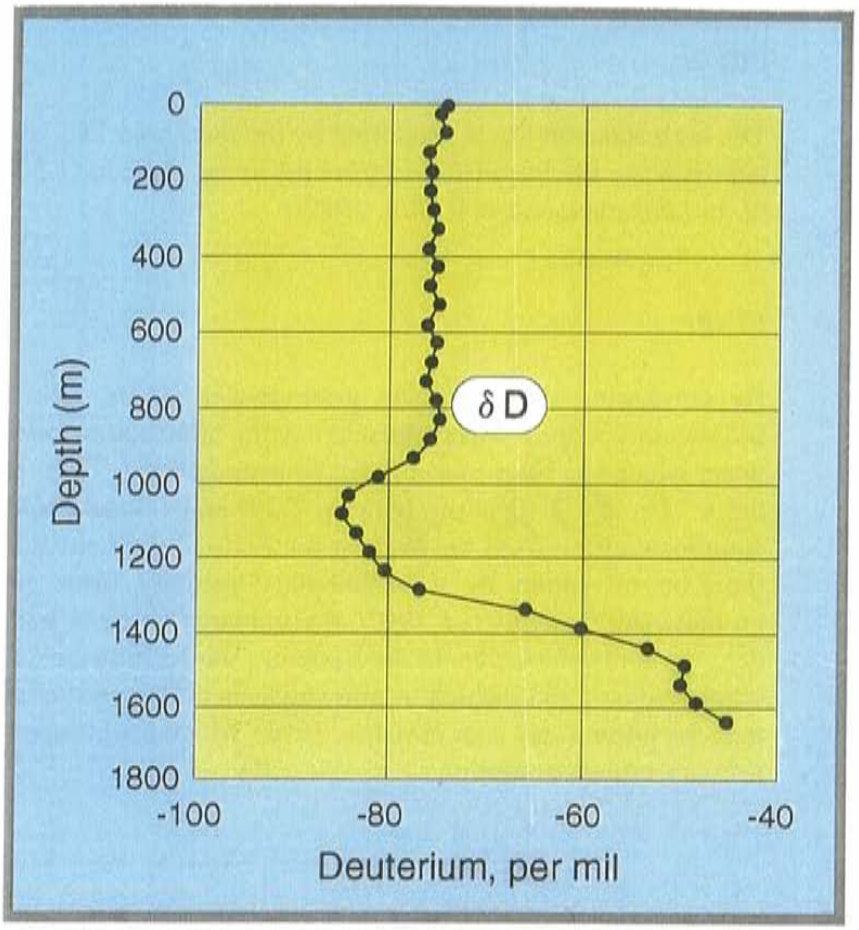

Figure 7-29. *The glacial component shows a distinctive negative deviation in δ^2H contents which culminates at a depth of 1100 m (± 200 m) at Laxemar. Borehole (KLX02).*

Sr and $\delta^{87}Sr$

Dissolved Sr (0.5 mg/L) in the fresh-water layer has a $\delta^{87}Sr$ value of +9.9‰ whereas a sample of saline water from the interval of 1420 to 1705 m contains 449 mg/L Sr with a $\delta^{87}Sr$ of +12.9‰. Throughout the deep Laxemar borehole the strontium concentration increases congruently with the chlorinity */Wallin and Peterman, 1997/* (see *Figure 7-30*). This is strongly indicating a long-term interaction between the water and clay minerals.

$\delta^{34}S$

The $\delta^{34}S$ isotopic composition of sulphur in dissolved sulphate also reflects the compositional stratification of this groundwater system with $\delta^{34}S$ values of +10‰ in the deep saline and +19‰ in the fresh layer.

Brine evolution: diffusion-mixing-processes

The age determination and the other isotope investigations indicate that the brine exists in a stagnant environment. This in turn implies that the brines are not affected to any large extent by advective flow and mixing, and in that case **diffusion** is the only process by which the salt could have been transported. The diffusion was calculated using Fick's second law, and the diffusivity of chloride in water. The assumption for initial conditions was that there was a sharp boundary between a saline and a fresh water. Cl diffusion calculations for 100Ka, 1Ma and 5Ma are shown in *Figure 7-31* together with the measured chlorine concentration at depths of 800-1600 m at KLX02. The figure shows that the 1 Ma model plot is relatively close to the measured chlorine concentration which is within relative agreement with the measure ^{36}Cl value of 1.5 Ma. The measured chlorine values show deviations from the diffusion line which may indicate disturbance by mixing.

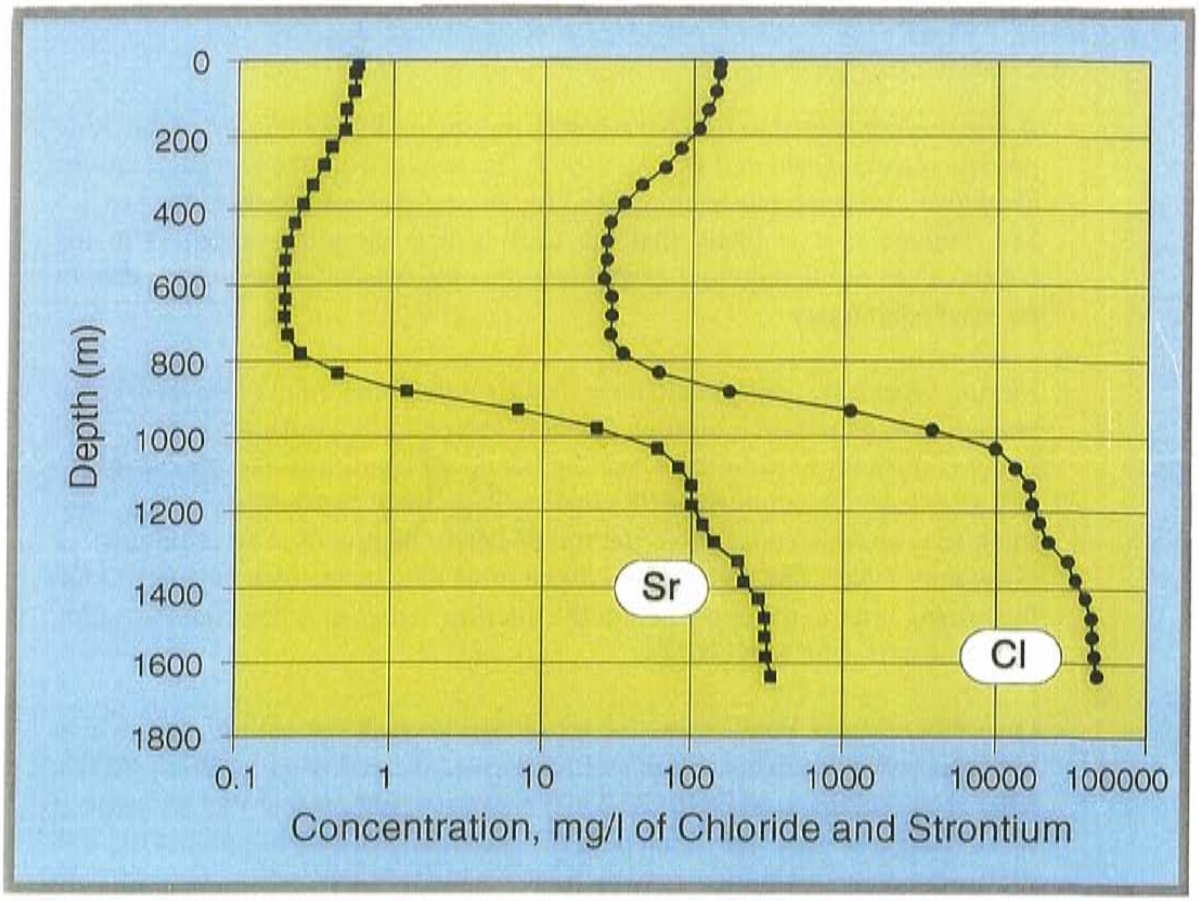

Figure 7-30. *Strontium and chloride concentrations in borehole KLX02.*

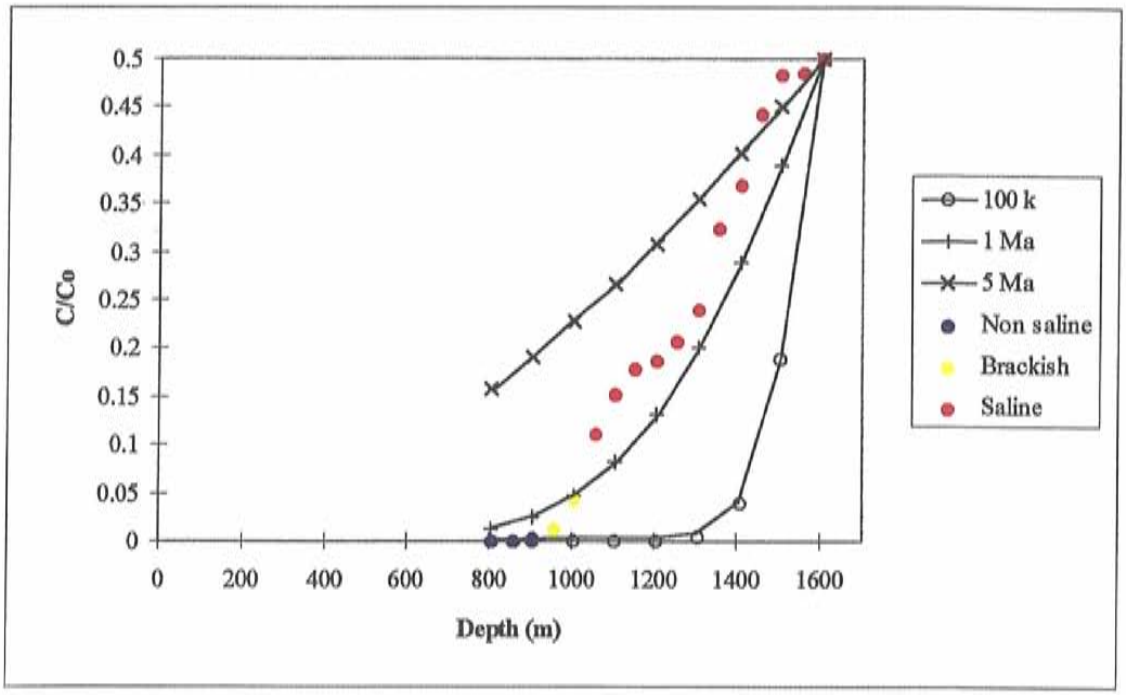

Figure 7-31. *Results from the diffusion modelling of the deep groundwater at Laxemar. Chlorine diffusion models for 100K, 1Ma and 5Ma are compared with the measured chlorine concentration in borehole KLX02.*

A test was conducted to find out whether mixing or diffusion is the dominating process */Laaksoharju and Wallin, 1997/*. The results from the two calculations show that diffusion has been masked by mixing processes during the last 1.5 Ma. However, it is likely that the drilling and sampling activities in the borehole has resulted in mixing. If this is the only reason for the mixing cannot be concluded today.

Mixing processes, which could have disturbed the brine, might also have taken place due to penetration of glacial water. The penetration depth of the glacial water is difficult to estimate, since the boundary conditions are impossible to define exactly. Assuming that the hydraulic gradient is established by a 3 km thick ice cap, this could drive the meltwater to depths of several kilometres */Svensson, 1996/*. The high density of the brine may in any case have restricted the mixing layer to the upper part of the interface between saline and non-saline groundwaters seen in KLX02.

Disturbance from borehole activities is also seen in the tritium data which indicates a significant content of surface derived water down to 1420 m. At this level (1420 m) the presence of 26 TU (i.e. in excess of present-day recharge at 22 TU) suggests that, after excluding the possibility of in-situ production, one of the mixing end-members may be "old" tritium rich meteoric waters infilling during the period 1958-1965. This water may have been drawn into the

borehole at various levels during drilling and other activities. The hydraulic testing and the 6 month maintenance pumping prior to groundwater sampling lowered the groundwater level by 4 m in borehole KLX01 situated almost one kilometre away */S Follin, 1996/*. Effects in the different sections of KLX02 are not known. However, it must be kept in mind that the water sampled from the borehole when it was newly drilled never exceeded 0.3 TU. Thus it is evident that the high tritium content is caused by borehole activities.

In conclusion it is most likely that the deep brine below 1100 m depth has been stable for a long time and can be considered stagnant in the time scale of a waste repository, 100 000 years. The origin of the brine can be either an evaporite or long-term leaching of the rock. Regardless of which, it has been isolated from meteoric input for more than 1 million years. Whether or not the brine is part of a slow regional transport system cannot be judged today.

7.6.3 Saline groundwaters with a glacial component

Regardless of the fact that the salinity increases by depth, there is a distinct influence of glacial (cold climate) groundwater at depths. The cold climate water might have been injected during the last glaciation but might also be a remnant from previous glaciations.

$\delta^{18}O$ and $\delta^{2}H$

The glacial component is shown as a distinctive negative deviation in the $\delta^{18}O$ and $\delta^{2}H$ contents of the groundwaters. Saline groundwaters, sampled from the deep (1705 m) borehole KLX02, contain a glacial component which culminates at a depth of 1100 m (±200 m) *(Figure 7-29)*. At Äspö the glacial component in the saline groundwater is found at variable depths (100-850 m).

Ca and SO_4

When the melting started dilute and possibly aggressive glacial melt-water could have oxidized the sulphide in the glacial soil debris. The M3 calculations show a sink for Ca *(Figure 7-32)* and a source for sulphate *(Figure 7-33)* which is believed to be associated with the influx of glacial water associated with calcite precipitation. Losses can also be due to ion-exchange reactions. However, the isotopic character of the sub-glacial water is such that it must be developed during the course of the latest glaciation or be a remnant of previous glaciations. It is not caused by the melting of the latest glaciation. This might indicate that there is a missing end-member with a high sulphate and low calcium concentration. Such a saline water could be resulting from repeated freezing and melting of a permafrost which created stagnant conditions with no groundwater flow below parts of the continental ice replaced by dynamic conditions.

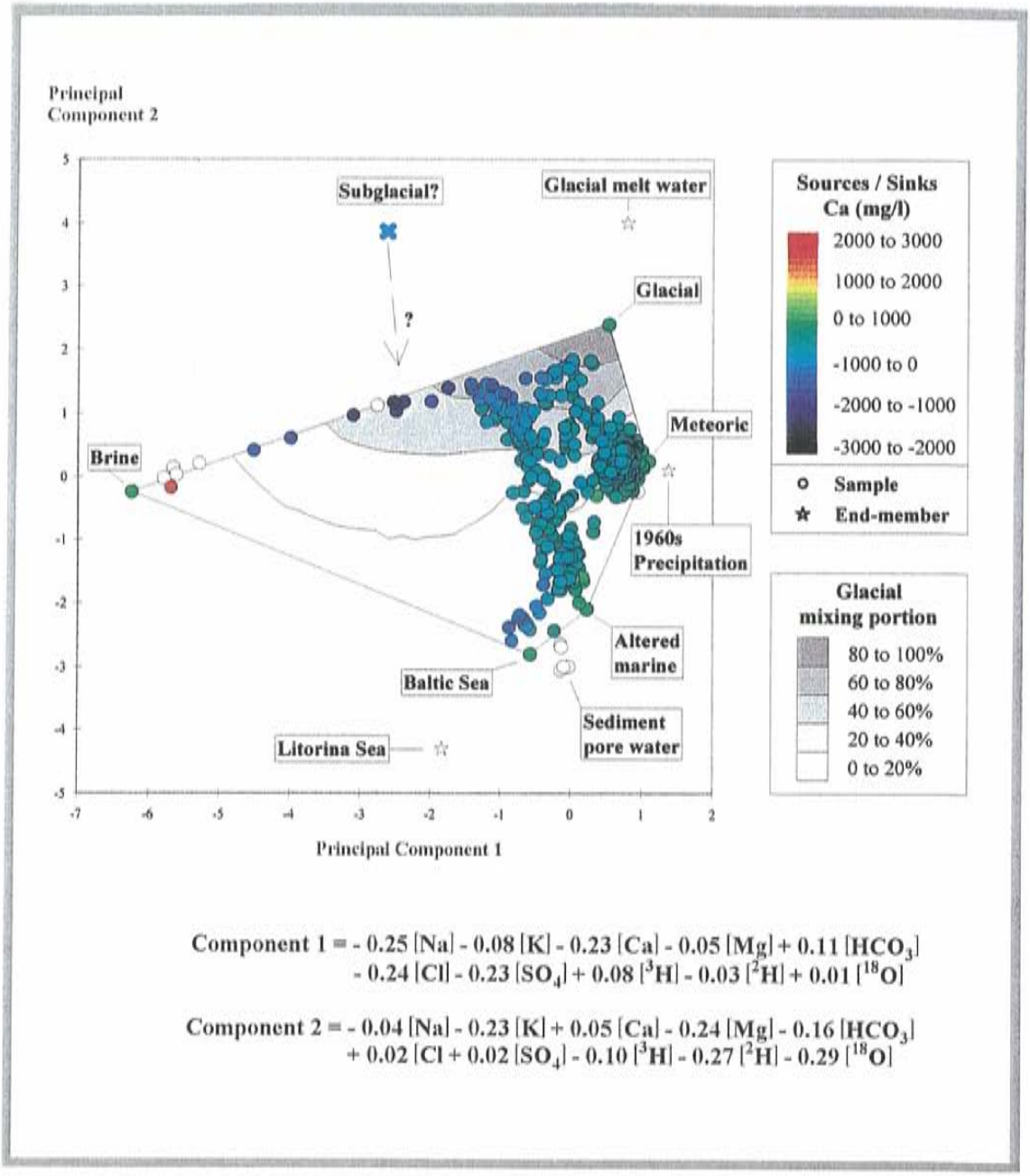

$$\text{Component 1} = -0.25\,[Na] - 0.08\,[K] - 0.23\,[Ca] - 0.05\,[Mg] + 0.11\,[HCO_3] - 0.24\,[Cl] - 0.23\,[SO_4] + 0.08\,[^3H] - 0.03\,[^2H] + 0.01\,[^{18}O]$$

$$\text{Component 2} = -0.04\,[Na] - 0.23\,[K] + 0.05\,[Ca] - 0.24\,[Mg] - 0.16\,[HCO_3] + 0.02\,[Cl + 0.02\,[SO_4] - 0.10\,[^3H] - 0.27\,[^2H] - 0.29\,[^{18}O]$$

Figure 7-32. *Principal Component plot used to illustrate the sinks of calcium which are believed to be associated with the mixing of glacial water. The mixing is shown progressively for 20%, 20-40%, 40-60%, 60-80% and 80-100%. The numerical values are normalized, see Section 7.2.2.*

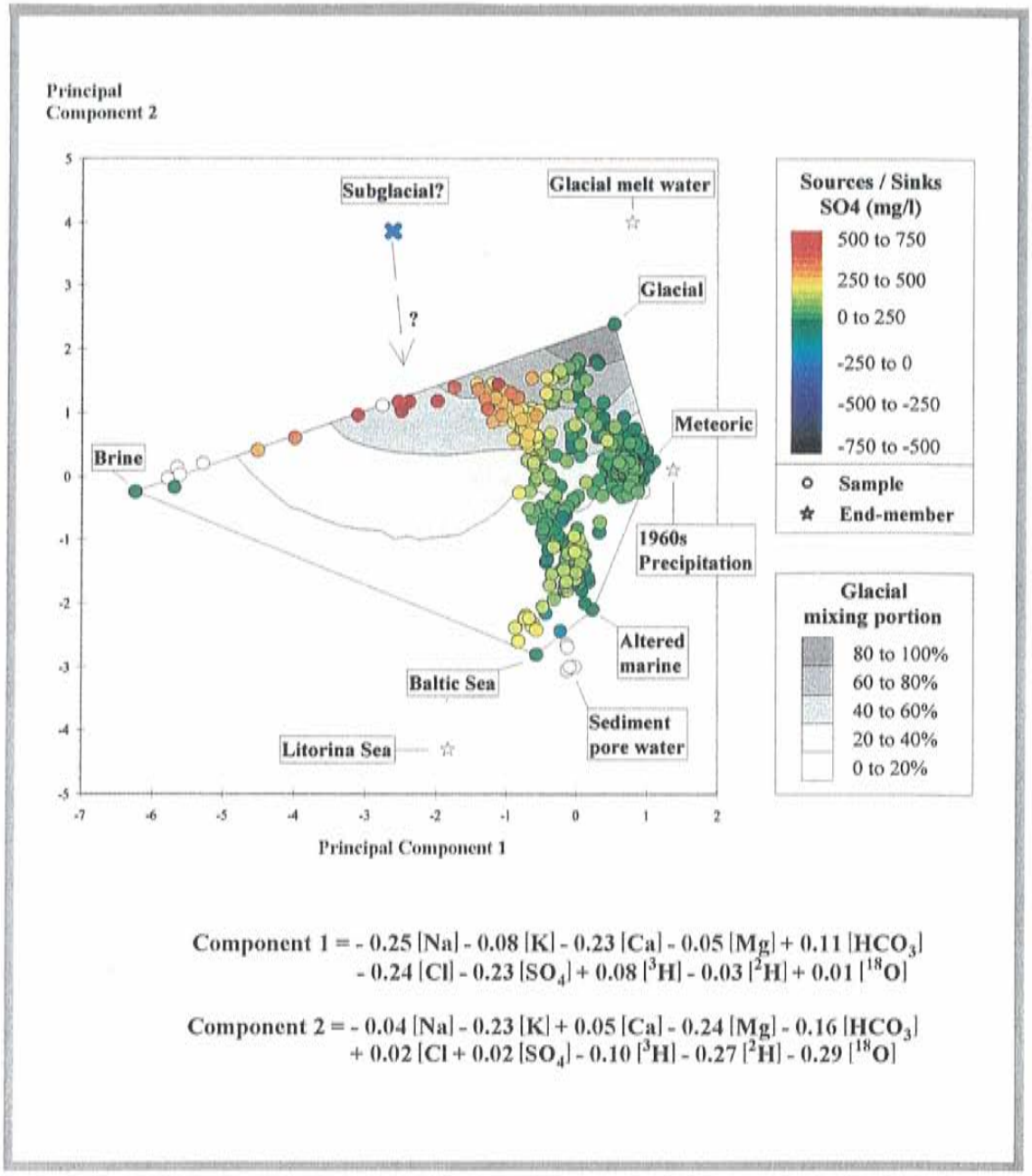

$$\text{Component 1} = -0.25\,[Na] - 0.08\,[K] - 0.23\,[Ca] - 0.05\,[Mg] + 0.11\,[HCO_3] - 0.24\,[Cl] - 0.23\,[SO_4] + 0.08\,[^3H] - 0.03\,[^2H] + 0.01\,[^{18}O]$$

$$\text{Component 2} = -0.04\,[Na] - 0.23\,[K] + 0.05\,[Ca] - 0.24\,[Mg] - 0.16\,[HCO_3] + 0.02\,[Cl + 0.02\,[SO_4] - 0.10\,[^3H] - 0.27\,[^2H] - 0.29\,[^{18}O]$$

Figure 7-33. *Principal Component plot used to illustrate the sources of SO_4 which are believed to be associated with the mixing of glacial water. The mixing is shown progressively for 0-20%, 20-40%, 40-60%, 60-80% and 80-100%. The numerical values are normalized, see Section 7.2.2.*

7.6.4 Saline groundwaters with a marine component

General Chemistry

The saline waters at Äspö (350 - 600 m) and during construction of the HRL tunnel (>100 m) were sampled from a hydrogeologically more dynamic system than the deeper Äspö and Laxemar (brine) systems. The dominating groundwater type is a sodium chloride water. The measured Cl concentration for these saline groundwaters is 5000-12300 mg/l. A general feature of the saline groundwaters sampled in the tunnel is that the location (i.e. under sea or under land) and depth determine the origin. Under the sea at a moderate depth influx of marine waters was observed. Observations at larger depths show that these are dominated more by older water types such as glacial and brine water */Laaksoharju and Skårman, 1995/.*

The results from the influx of a marine component on the saline groundwaters can be seen as a source for Mg *(Figure 7-34)*. The interpretation is that this may be a result of a Litorina Sea influx. The salinity of Litorina Sea water was a factor of two higher than modern Baltic Sea water. The Mg content correspond well to a Litorina origin. This was further supported by the chlorine content which is similar to the Litorina Sea water.

7.7 BRACKISH GROUNDWATER AT ÄSPÖ AND LAXEMAR

7.7.1 General features of the brackish groundwater

Brackish groundwaters *(Figure 7-6)* are obtained generally at a depth of 100-350 m at Äspö and along the HRL tunnel. At Laxemar the brackish water is found down to a depth of 1000 m. The difference in depth at which the brackish water is found is due to the prevailing hydraulic conditions.

The brackish groundwater is of Na-Ca, Cl-SO_4 type. The water is a result of a complex mixing pattern that includes all the reference waters in varying proportions. The brackish groundwaters represent a mixing regime where a regional and local flow system, long-term, slow chemical reactions (dissolution, precipitation, sorption, redox reactions, gas generation and consumption) and short-term, fast reactions (ion exchange, precipitation, dissolution, redox reactions and sorption) take place */Alley, 1993/.*

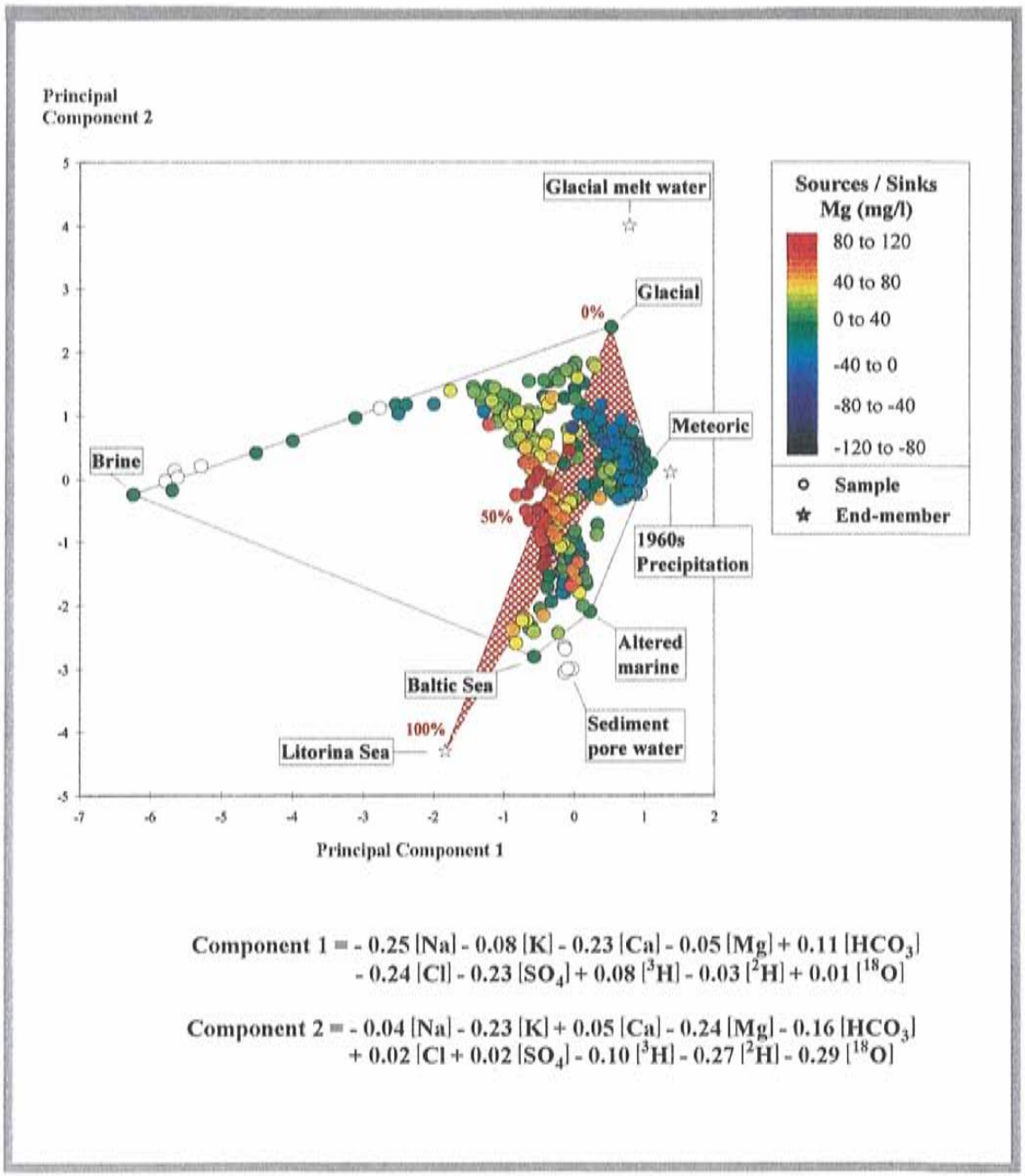

$$\text{Component 1} = -0.25\,[Na] - 0.08\,[K] - 0.23\,[Ca] - 0.05\,[Mg] + 0.11\,[HCO_3] - 0.24\,[Cl] - 0.23\,[SO_4] + 0.08\,[^3H] - 0.03\,[^2H] + 0.01\,[^{18}O]$$

$$\text{Component 2} = -0.04\,[Na] - 0.23\,[K] + 0.05\,[Ca] - 0.24\,[Mg] - 0.16\,[HCO_3] + 0.02\,[Cl + 0.02\,[SO_4] - 0.10\,[^3H] - 0.27\,[^2H] - 0.29\,[^{18}O]$$

Figure 7-34. *Principal Component plot used to illustrate the sources of Mg which are believed to be associated with the mixing of marine water possibly Litorina Sea water. The mixing of the Litorina Sea is shown as an area of influence which is based on the predicted ^{14}C age (see Figure 7-16) related to the Litorina stage. The possible influx percentages of the Litorina Sea are shown in steps of 100%, 50% and 0%. The numerical values are normalized, see Section 7.2.2.*

7.7.2 Multi-component mixing of brackish groundwater

Most of the brackish groundwaters were sampled from the HRL tunnel at tunnel chainage 0-1500 m (0-200 m below sea level). The emphasis in this section is therefore on the groundwaters sampled from the HRL tunnel.

The groundwater chemistry reflects the dynamics in the system which is driven by changing hydraulic heads due to the construction of the HRL tunnel. The groundwater observations were therefore sorted according to where and when the sampling was conducted. The data has been divided into experimental days, where day 0 (1990-10-14) indicates the start of the tunnel construction, day 150 represents 1991-03-13, day 350 (1991-09-29), day 550 (1992-04-16), day 750 (1992-11-02), day 950 (1993-05-21), day 1150 (1993-12-07) and day 1350 represents the date 1994-06-25. A sample collected closest to the actual experimental day (e.g. day 150) was selected to represent that experimental day. A comprehensive presentation of the results is made in *Laaksoharju and Skårman /1995/.*

On experimental days 150, 350, 550 and 750 of the HRL tunnel construction meteoric water and glacial water dominated the inflow to tunnel section below the sea. On day 950 altered marine water started to dominate at tunnel chainage 1200-1480 m, a tunnel section under land but in contact with the Baltic Sea through the NE-1a and EW-3a fracture zones. On day 1150 Baltic Sea water and altered marine water started to dominate at tunnel section 2110-2240 m which is located under the sea. On day 1350 this domination was replaced by meteoric water, although Baltic Sea water was still an important component. At greater depths (>300 m) and tunnel chainages (>2400 m) the dominating water type was a cold climate (glacial) water in combination with brine. A general feature of the tunnel water is that the location (i.e. under sea, under land) and depth determines the dominating water type and changes in the mixing proportions with time. Observations under the sea at a moderate depth (<300 m) show modern Baltic Sea water or altered marine water with time. Observations below land at a moderate depth show meteoric water. Observations at greater depths show that these are dominated more by older water types. These mixing calculations showed a general agreement with the hydrogeological modelling */Laaksoharju and Skårman, 1995/.*

Dominating water types in the HRL tunnel over time, viewed from the side, are shown in *(Figure 7-35).* It is important to note that in many tunnel sections the difference between the calculated mixing portions are small (i.e. 26% Baltic Sea water and 25% shallow water). Kriging was used to interpolate between the observation points. Greater accuracy was obtained close to the sampling point.

In *Figure 7-35* the reference waters has been changed compared to the references in previous PCA figures. The saline reference water is now represented by the most saline water of Äspö (KAS02 860 m) and the glacial reference water is the same as the glacial end member. The difference in the

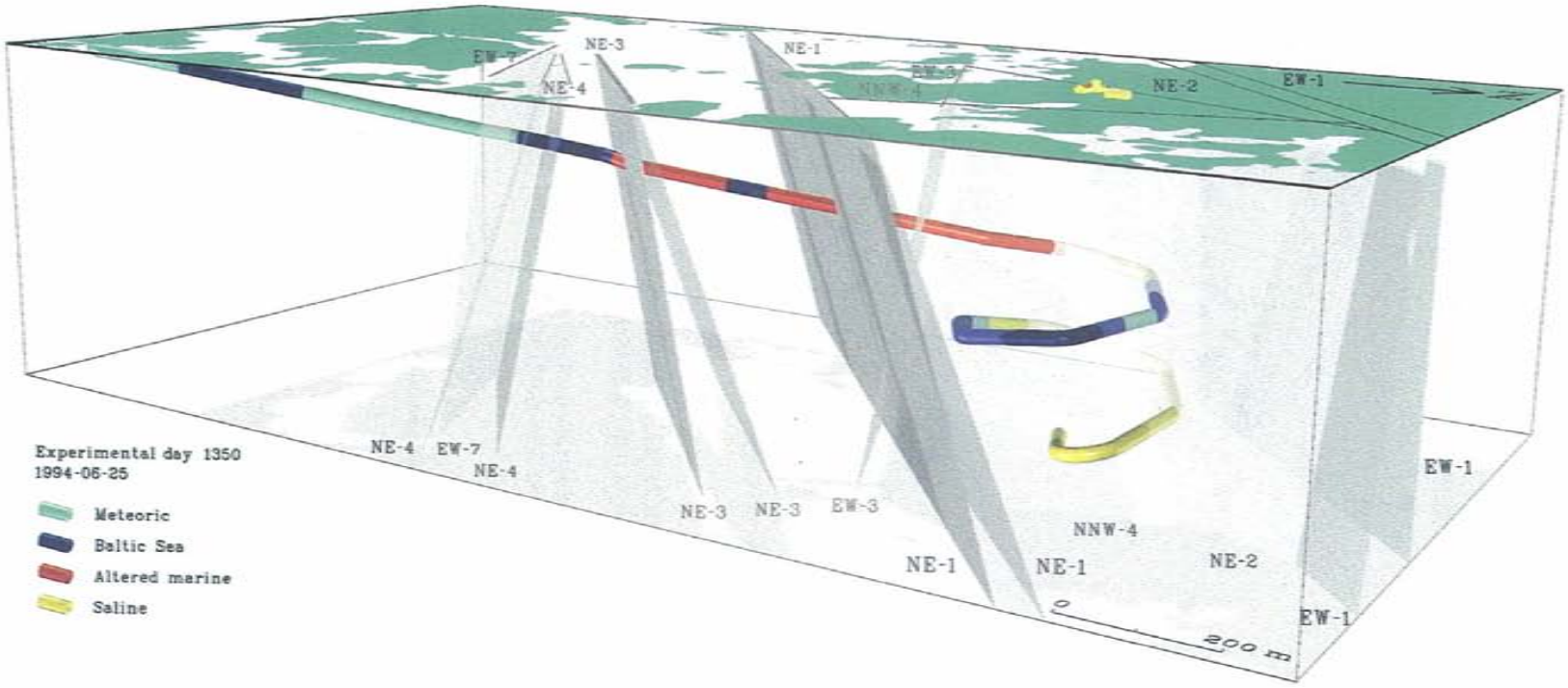

Figure 7-35. *Influx of the dominating water in the HRL tunnel seen from the side on day 1350 (1994-06-25) of the tunnel construction.*

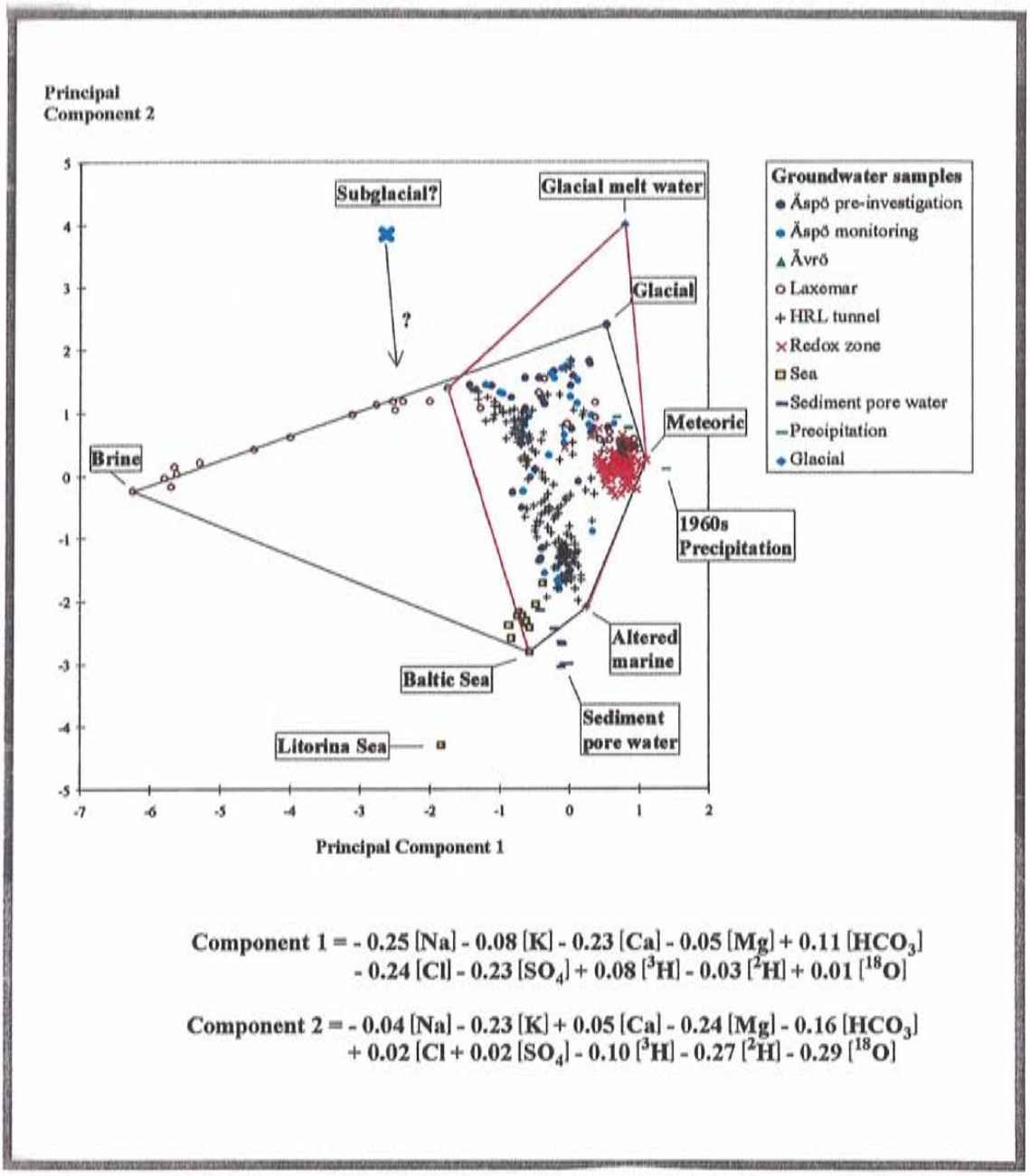

Figure 7-36. *PCA plot, cf. Figure 7-2, of the groundwater data of the Äspö-Laxemar area. Red line indicates the reference waters used to calculate the mixing proportions presented in Figure 7-35. These reference waters are also used to present the dominating groundwater in Figure 2-14.*

data treatment is seen in *Figure 7-36* where the new reference waters are connected with the red line.

The presentation above is thought to give a better view of the dominating water types along the tunnel than what is obtainer by the use of the reference waters from the PCA plots.

7.8 NON-SALINE GROUNDWATER AT ÄSPÖ

7.8.1 General features of the non-saline groundwaters

Non-saline groundwaters *(Figure 7-7)* are usually obtained at a depth of less than 100 m at Äspö and the HRL tunnel. At Laxemar the non-saline water is found down to a depth of 850 m. The difference in the depth location of the brackish water is due to different prevailing hydraulic conditions at Laxemar compared with Äspö, see *Section 7.6.2*.

The non-saline groundwater is characterised by a Na-HCO_3 or a Ca-HCO_3 rich groundwater. The water is a result of an influx of a meteoric water which is mixed in a complex pattern with brackish water. The non-saline groundwaters belong to the shallow bedrock where local flow systems exist and fast reactions (ion exchange, precipitation, dissolution, redox reactions and sorption) dominate */Alley, 1993/*.

Most of the data comes from the Redox Zone in the HRL tunnel */Banwart ed, 1995/*. The investigations were focussed on the redox conditions and how these were developing. On March 13, 1991 tunnel construction in the HRL tunnel intersected a sub-vertical, hydraulically-conductive fracture zone (Redox Zone) at tunnel section 513 metres and at a depth of 70 metres. This provided an opportunity to study geochemical changes resulting from non-saline water inflow into a crystalline bedrock aquifer as anticipated during construction and operation of a deep repository. For a period of three years the inflow to the tunnel and discharge from boreholes drilled into the fracture zone from the tunnel were monitored to observe if dissolved oxygen was transported from the surface into the groundwater under the intense hydraulic disturbance created by the tunnel construction work.

^3H, surface water break-through

As predicted by model calculations prior to the start of the experiment, dilute, non-saline (<10 mg/l, Cl) water from the surface displaced the native brackish (5000 mg/l, Cl) water of the fracture zone. A sharp dilution front, corresponding to 80% dilution of the native groundwater, indicated the arrival of non-saline groundwater to the tunnel after 3 weeks. Although a slight oxygen breakthrough was observed a few weeks after the non-saline water breakthrough, the fracture zone rapidly returned to anoxic conditions */Banwart et al, 1995/*. By using tritium and deuterium as conservative tracers the recharge of the Redox Zone was calculated to be 4050 m^3/year with a groundwater residence time of 8 months */Banwart (ed.), 1995/*. The influx of modern precipitation water is seen as a sink for the tritium content with respect to the reference water content in *(Figure 7-37)*. The meteoric reference water contains (59 TU) which reflects precipitation dating from the 1960s (100 TU). This fact gives a view of the residence time in the undisturbed conditions prevailing before tunnel construction. The effect of the influx of meteoric water affects both brackish and saline groundwaters. There is evidence of extensive

lateral flow between the recharge areas and the discharge point in the access tunnel.

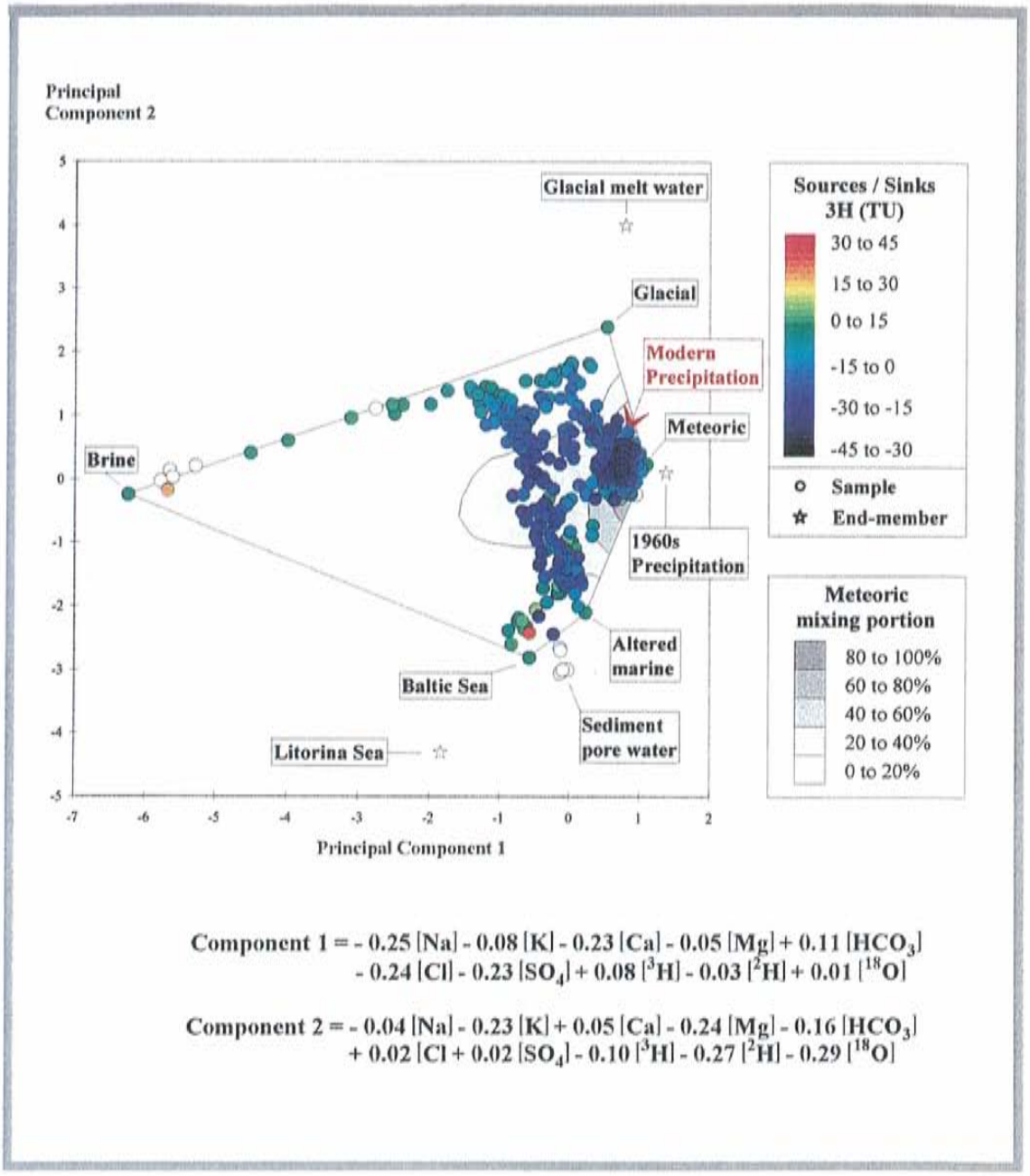

$$\text{Component 1} = -0.25\,[Na] - 0.08\,[K] - 0.23\,[Ca] - 0.05\,[Mg] + 0.11\,[HCO_3] - 0.24\,[Cl] - 0.23\,[SO_4] + 0.08\,[^3H] - 0.03\,[^2H] + 0.01\,[^{18}O]$$

$$\text{Component 2} = -0.04\,[Na] - 0.23\,[K] + 0.05\,[Ca] - 0.24\,[Mg] - 0.16\,[HCO_3] + 0.02\,[Cl] + 0.02\,[SO_4] - 0.10\,[^3H] - 0.27\,[^2H] - 0.29\,[^{18}O]$$

Figure 7-37. *Influx of modern precipitation water is seen as a source for the tritium content with respect to the reference water content. The effect of the mixing of meteoric water is shown in the background. The mixing is shown progressively for 0-20%, 20-40%, 40-60%, 60-80% and 80-100%. The weight for the different elements is shown in the equations for the first and second Principal Component respectively.*

HCO_3

Major element hydrochemistry and carbon and oxygen stable isotope data indicated large inputs of HCO_3 and biogenic CO_2 (g). Elevated CO_2 concentrations in the groundwater (6050 to 15037 ppm) exceed atmospheric concentrations by one or two orders of magnitude. High TOC values (up to 20 mg/L) and the $\delta^{13}C$ isotope values of the HCO_3 (-16 to -14‰ PDB) and CO_2 (-14 to -25‰) confirm a large uniform organic carbon source as one end-member for the carbon system. Methane (1030 to 4070 ppm) in the fracture zone and the shallow boreholes with $\delta^{13}C$ values between -39.8 and -50.8‰ strongly support a biogenic source for this gas. The build up of the bicarbonate reservoir most likely takes place in the lower saturated part of the shallow groundwater (below 30 m). The effect of this process is seen as a source of HCO_3 in *(Figure 7-38)*.

The input of organic carbon with shallow groundwater provides a possible energy and carbon source for anaerobic respiration. The accelerated input of organic carbon added a net reducing capacity to the groundwater which, in turn, prevented oxygen penetration. Reduction of iron (III) minerals to iron (II) in solution is an anaerobic process found to be the successor to the aerobic respiration of organic matter observed in the block scale redox experiment. The process takes place when the amount of organic matter is larger than the amount of dissolved oxygen. This is roughly the case at >10 mg/l total organic content. A detailed description of the iron reduction is given in the reporting of the redox project */Banwart et al, 1995/*. Inorganic oxygen reduction was expected, but biological consumption of oxygen was found. Other processes which can be a source for HCO_3 are calcite dissolution, iron and manganese and sulphate reduction. Sinks for HCO_3 are often associated with calcite precipitation.

SO_4

The sulphate concentration increased, possibly by desorption from fracture minerals or from an influx from a lateral flow including a glacial or marine component *(Figure 7-34)*. The possible release of sulphate may have been due to adsorption competition with the large amounts of bicarbonate that accumulated in the groundwater during anaerobic respiration. Proposed microbial processes during lateral flow include anaerobic respiration coupled with a reduction of iron hydroxide, methanogenesis, precipitation of calcite and secondary ferrous minerals */Banwart et al, 1995, Banwart (ed.) 1995/*.

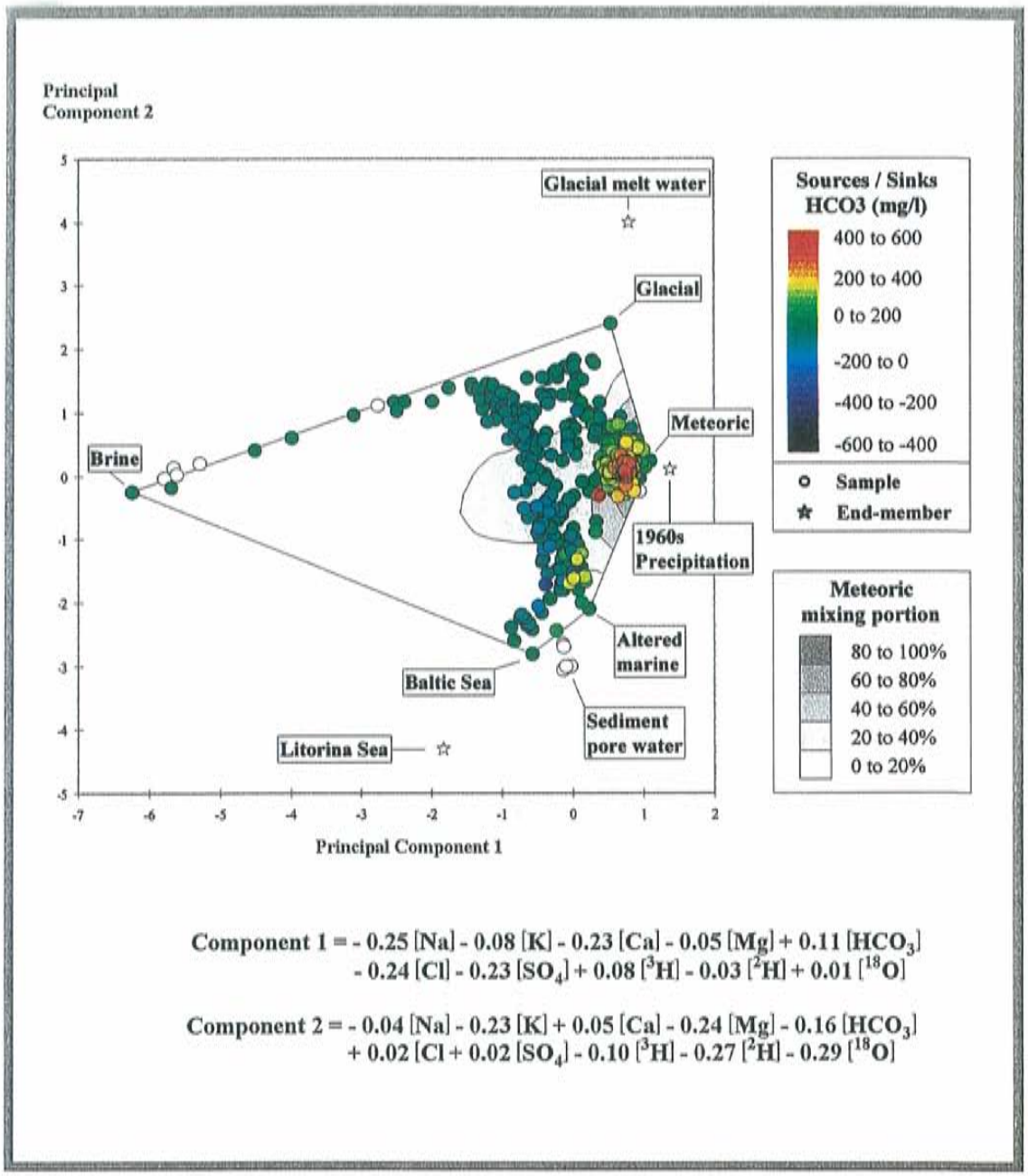

$$\text{Component 1} = -0.25\,[\text{Na}] - 0.08\,[\text{K}] - 0.23\,[\text{Ca}] - 0.05\,[\text{Mg}] + 0.11\,[\text{HCO}_3] - 0.24\,[\text{Cl}] - 0.23\,[\text{SO}_4] + 0.08\,[^3\text{H}] - 0.03\,[^2\text{H}] + 0.01\,[^{18}\text{O}]$$

$$\text{Component 2} = -0.04\,[\text{Na}] - 0.23\,[\text{K}] + 0.05\,[\text{Ca}] - 0.24\,[\text{Mg}] - 0.16\,[\text{HCO}_3] + 0.02\,[\text{Cl} + 0.02\,[\text{SO}_4] - 0.10\,[^3\text{H}] - 0.27\,[^2\text{H}] - 0.29\,[^{18}\text{O}]$$

Figure 7-38. *Anaerobic respiration coupled to organic decomposition is believed to be the major source of HCO_3. The effect of the mixing of meteoric water is shown in the background. The mixing is shown progressively for 0-20%, 20-40%, 40-60%, 60-80% and 80-100%. The weight for the different elements is shown in the equations for the first and second Principal Component respectively. The numerical values are normalized, see Section 7.2.2.*

Na and Ca

Associated Na-Ca ion-exchange was modelled in the Redox Zone */Viani and Bruton, 1994/*. This was supported by the M3 modelling which shows that a Na/Ca ion exchange may occur not only in the Redox zone but also at the Äspö site. The interpretation is that these processes occur in fracture systems containing clay minerals. The sinks and sources of anions and cations described above could be a result of surface complexation as suggested by */Bruton and Viani 1997/*.

Variably charged solids such as oxyhydroxides of Fe can serve as sources and sinks of anions and cations through surface complexation. Surface complexation reactions on hydrous ferric oxides involve sorption of both cations and anions. The masses of sorbent required to exert a significant impact on fluid chemistry through sorption/desorption reactions seem to be reasonable when compared with the occurrence of hydrous ferric oxides at Äspö. Thus, it is possible that small changes in fluid chemistry can cause significant releases of cations or anions into the fluid phase or, alternatively, result in an uptake of aqueous species onto hydrous ferric oxides surfaces.

$\delta^{34}S$

The $\delta^{34}S$ values from dissolved SO_4^{2-} in shallow groundwater are available from the Redox zone boreholes (KR0012B, KR0013B and KR0015B). The isotope signatures varied between +21 to +17‰, indicating a mixed sulphur source. One possibility is leaching of the Litorina-stage marine sediments by meteoric water. The water residing at the site at the beginning of the experiment had slightly higher chloride values (KA0483A = 4890 mg/l, Cl) than modern Baltic Sea water (2500-4000 mg/l, Cl) and may therefore have been older intrusions of saline waters such as Litorina Sea water *(Figure 7-39)*.

Sr

Several samples of precipitation were also analysed by means of $\delta^{87}Sr$, showing low concentrations of Sr in the range of 0.001 to 0.003 mg/L ($\delta^{87}Sr$ values +1.7 to +7.5). These values indicate the ion exchange model presented by *Viani and Bruton /1994/* is consistent with the concentration behaviour of $\delta^{87}Sr$ and Sr. They suggested that smectite may be the principal exchanger within this zone.

7.8.2 Calcite fracture fillings

Calcite fracture fillings exhibit a wide range in $\delta^{13}C$ of between -15 and -6‰ indicating a mixing of two different carbon sources. Oxygen isotope data from the calcite fracture fillings show a range between +10.6 and +23.5‰ and part

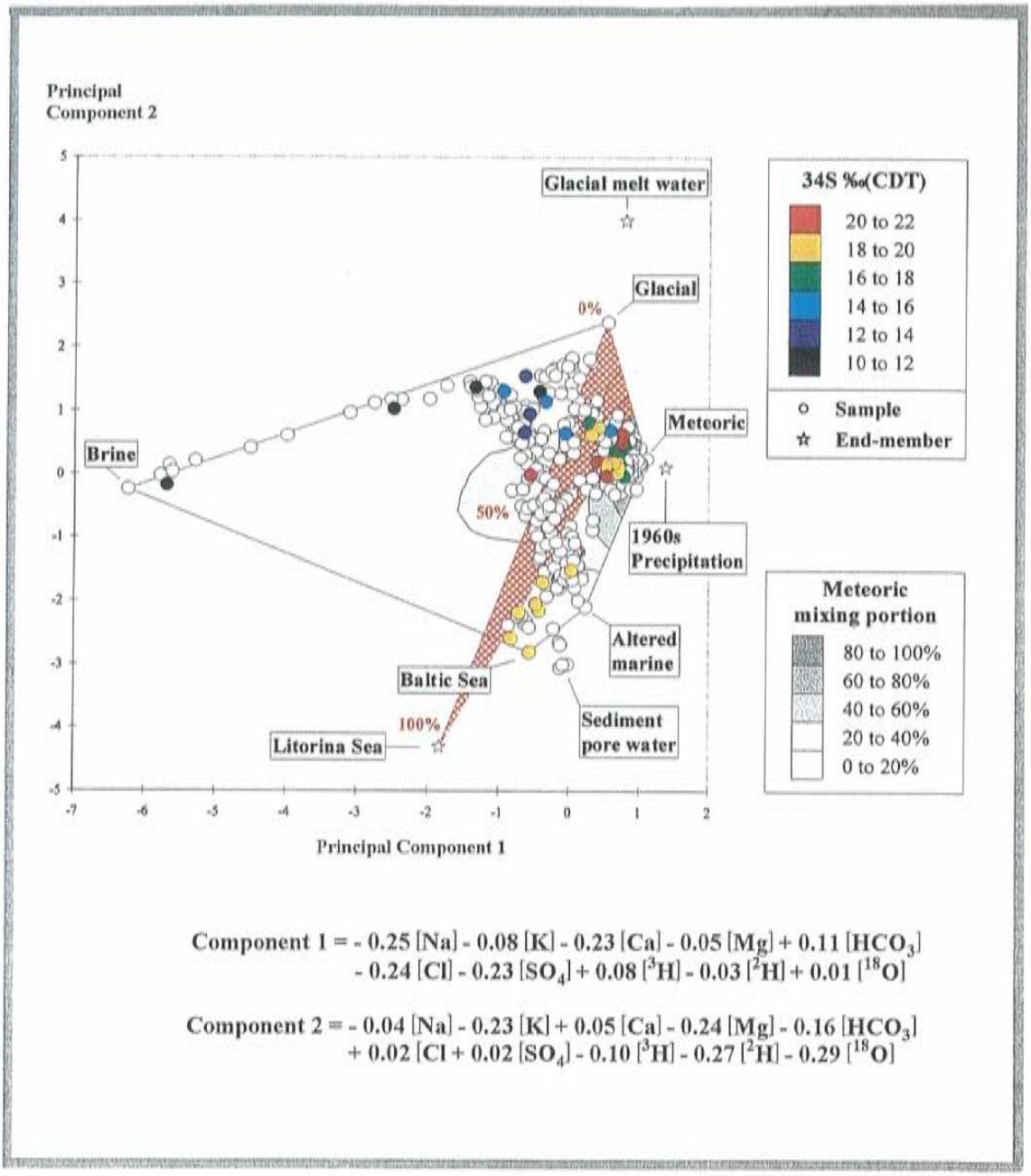

Figure 7-39. *Principal Component plot used to illustrate the measured $\delta^{34}S$ values from dissolved SO_4^{2-} in non-saline groundwater which may be associated with leaching of Litorina-stage marine sediments by meteoric water. The numerical values are normalized, see Section 7.2.2.*

of the calcite may be in equilibrium with the water observed today in the fracture zone. ^{14}C analyses on the HCO_3 show a variation of between 61.4 and 91.8 pmC (per cent modern carbon) and organic carbon (fulvic acids) range between 91.8 and 98.1 pmC. The average in-mixing of modern carbon in the bicarbonate observed in the fracture zone corresponds to a residence time of 550 years. This is in agreement with the estimated rate of organic matter degradation which is expected to be about 100 to 500 years in such a system. The lower percentage of modern carbon observed in the bicarbonate may

therefore be due to a dissolution of older calcite in the upper unsaturated zone of the groundwater with respect to calcite or a result of mixing of shallow waters with different ages */Wallin and Peterman, 1997/.*

7.9 HYDROCHEMISTRY OF MAJOR FRACTURE ZONES

The hydrochemistry of the major fracture zones has been carefully evaluated by *Laaksoharju and Skårman /1995/* for the entire tunnel construction phase. The evaluation was based on the results of the Principal Component Analyses, together with mixing and mass balance calculations (M3). The location of the fracture zones which have been evaluated are shown in *Figure 7-40*. All sampling points are shown in a vertical section along the tunnel in *Figure 7-41*. A summary of the results is presented in *Figures 7-42 to 7-48* where the dominating reference waters are visualized along the tunnel at different time intervals. The time intervals are 200 days. Observations which are 100 days off are included, e.g. samples collected between days 650 and 850 are included in the time step 750 days. *Appendix 3* shows the proportion of each reference water at the different time steps and the hydrochemistry in sampling points associated with the different fracture zones at the different time intervals as well as the proportions of the reference waters. Briefly the hard facts are:

Redox zone (KR0012)

Experimental days 150-1350: Cl = 695-1330-500 mg/L, HCO_3 = 198-245-325 (mg/L) and pH = 7.8-7.7-7.3 units. The chloride concentration increased initially from 675 to 1330 mg/l and decreased to 500 mg/l. At the same time steps the bicarbonate concentration went graduate from 198 to 245 to 325 mg/l and pH 7.8 - 7.7 - 7.3. For a detailed description see *Appendix 3*.
Dominating groundwater types are: [Cl-Na-HCO_3-Ca-SO_4-K]; [Cl-Na-Ca-HCO_3-SO_4-K]; [Cl-Na-HCO_3-SO_4-Ca-K] .

The dominating influx is from meteoric water (73-64-82%).

No indications of sulphate-reducing bacteria.

NE-4a, 4b (SA813B, SA850B)

Experimental days 350-1350: Cl = 5440-3450-3272 mg/L, HCO_3 = 170-481-302 (mg/L) and pH = 7.7-7.3-7.0 units.

Dominating groundwater types are: [Cl-Na-Ca-HCO_3-SO_4-K]; [Cl-Na-HCO_3-Ca-SO_4-K]; [Cl-Na-Ca-HCO_3-SO_4-K].

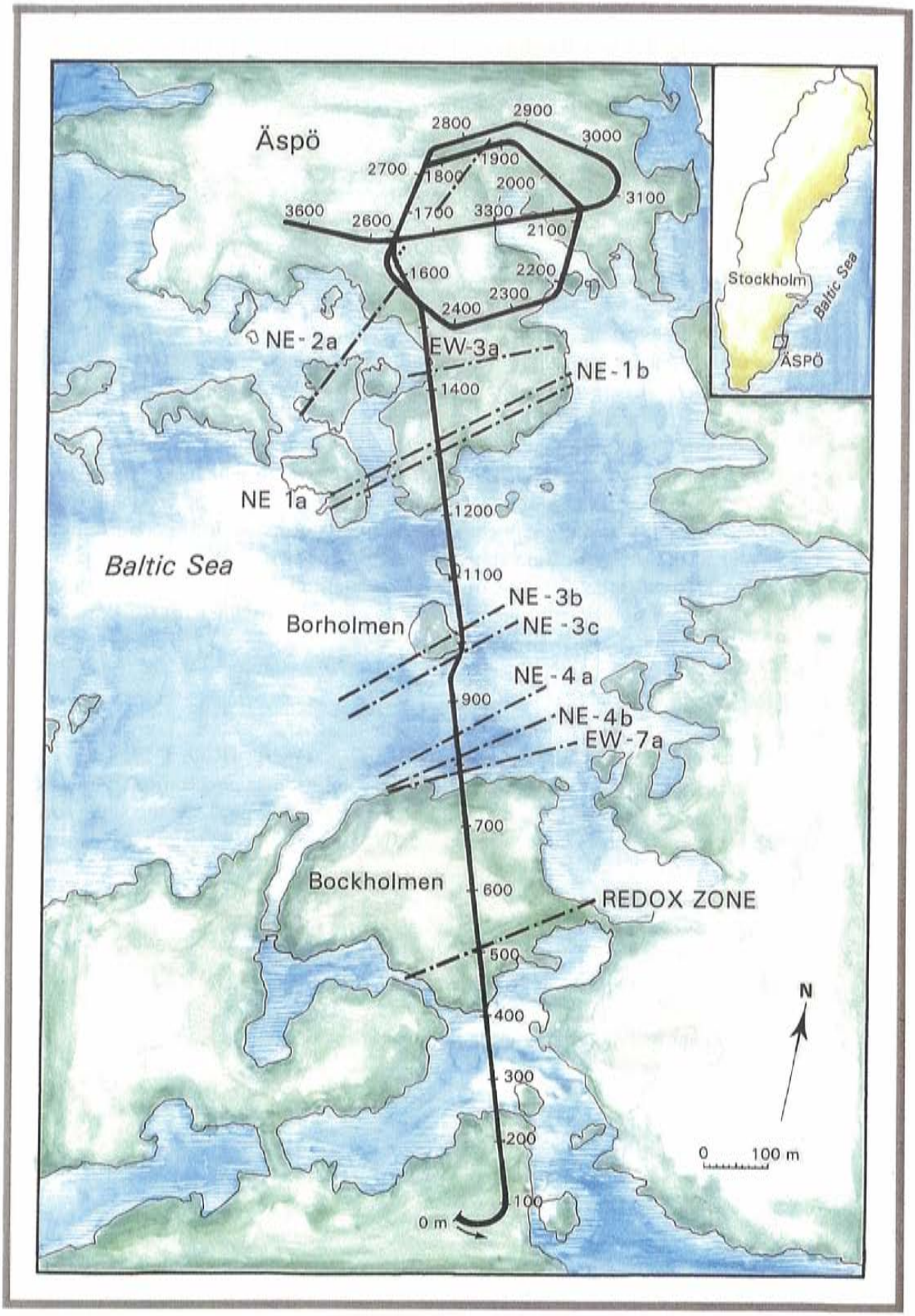

Figure 7-40. *Location of the hydrochemically evaluated fracture zones. The locations correspond to the intersections in the tunnel.*

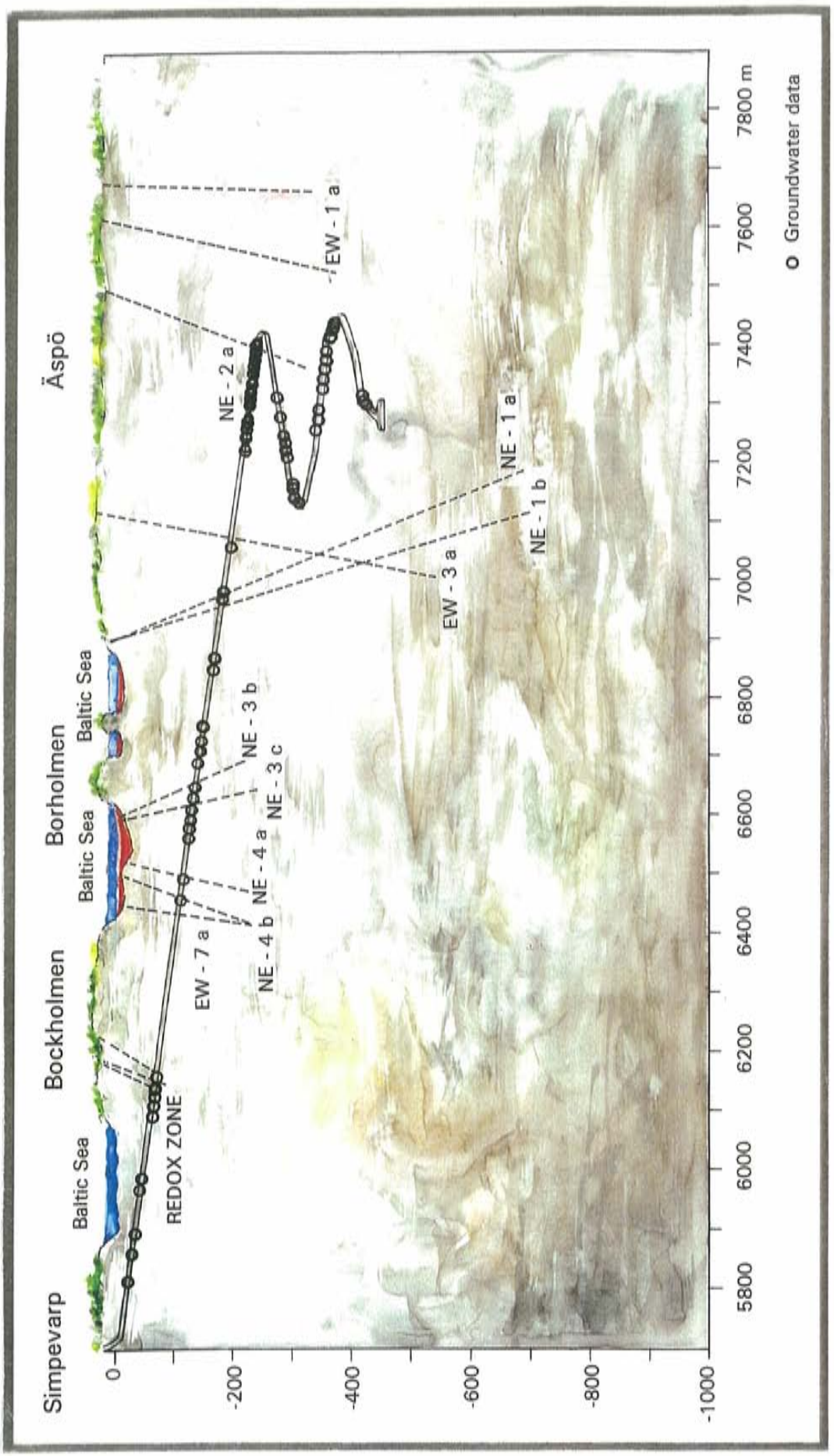

Figure 7-41. *Location of the hydrochemical sampling points on a vertical profile along the tunnel.*

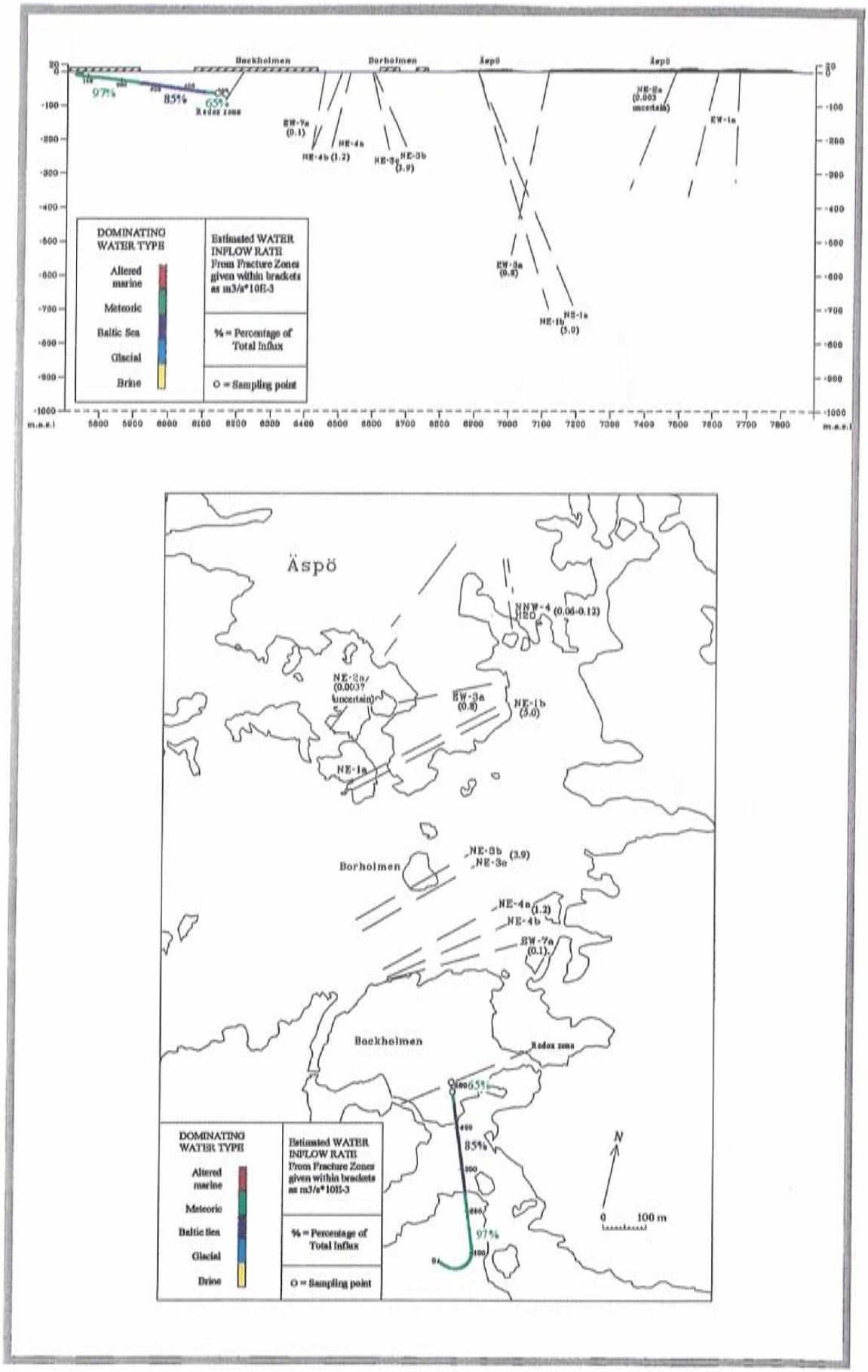

Figure 7-42. *Dominating influx to the tunnel 150 days after the start of tunnel excavation. 1991-03-13.*

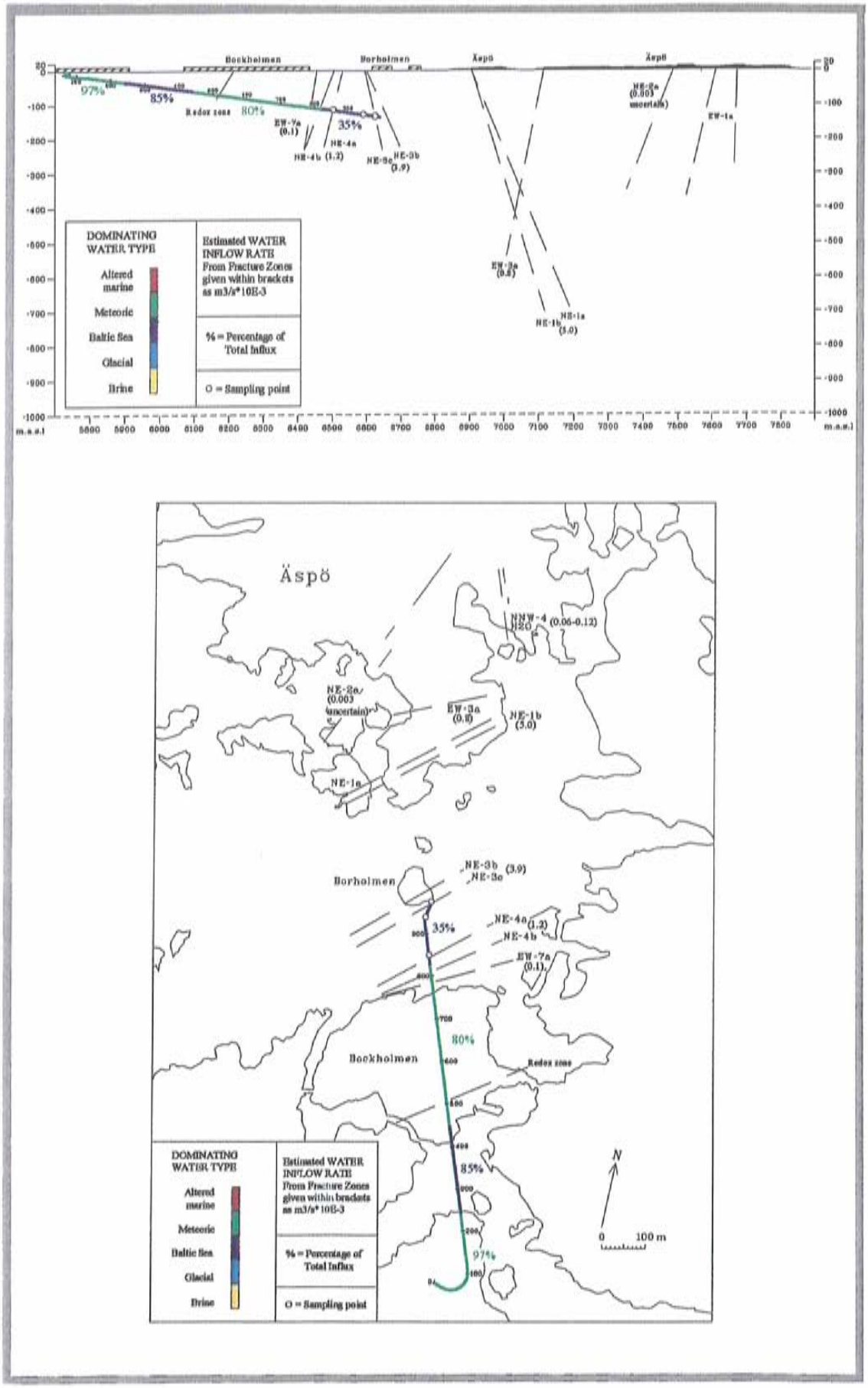

Figure 7-43. *Dominating influx to the tunnel 350 days after the start of tunnel excavation. 1991-09-29.*

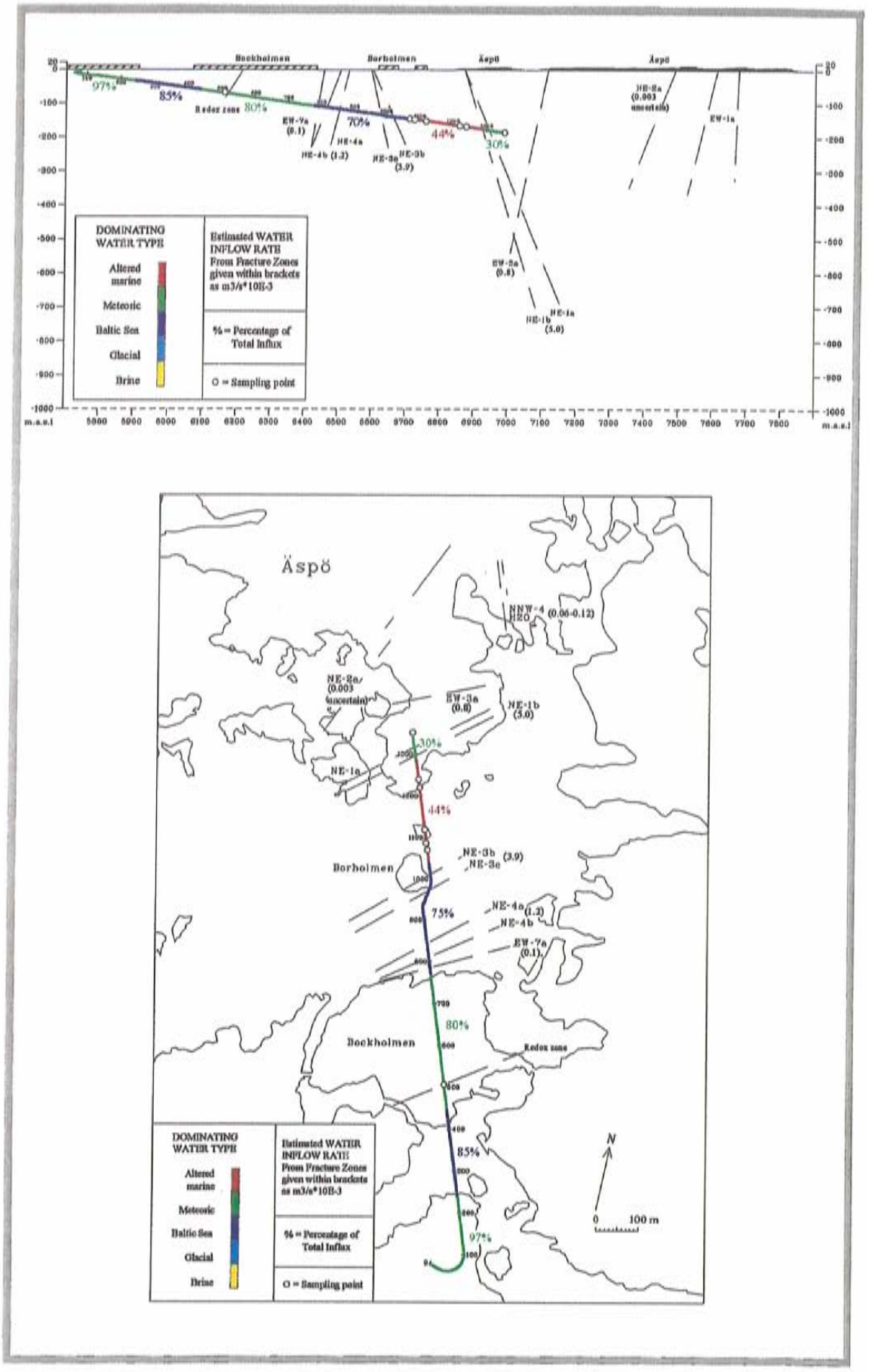

Figure 7-44. *Dominating influx to the tunnel 550 days after the start of tunnel excavation. 1992-04-16*

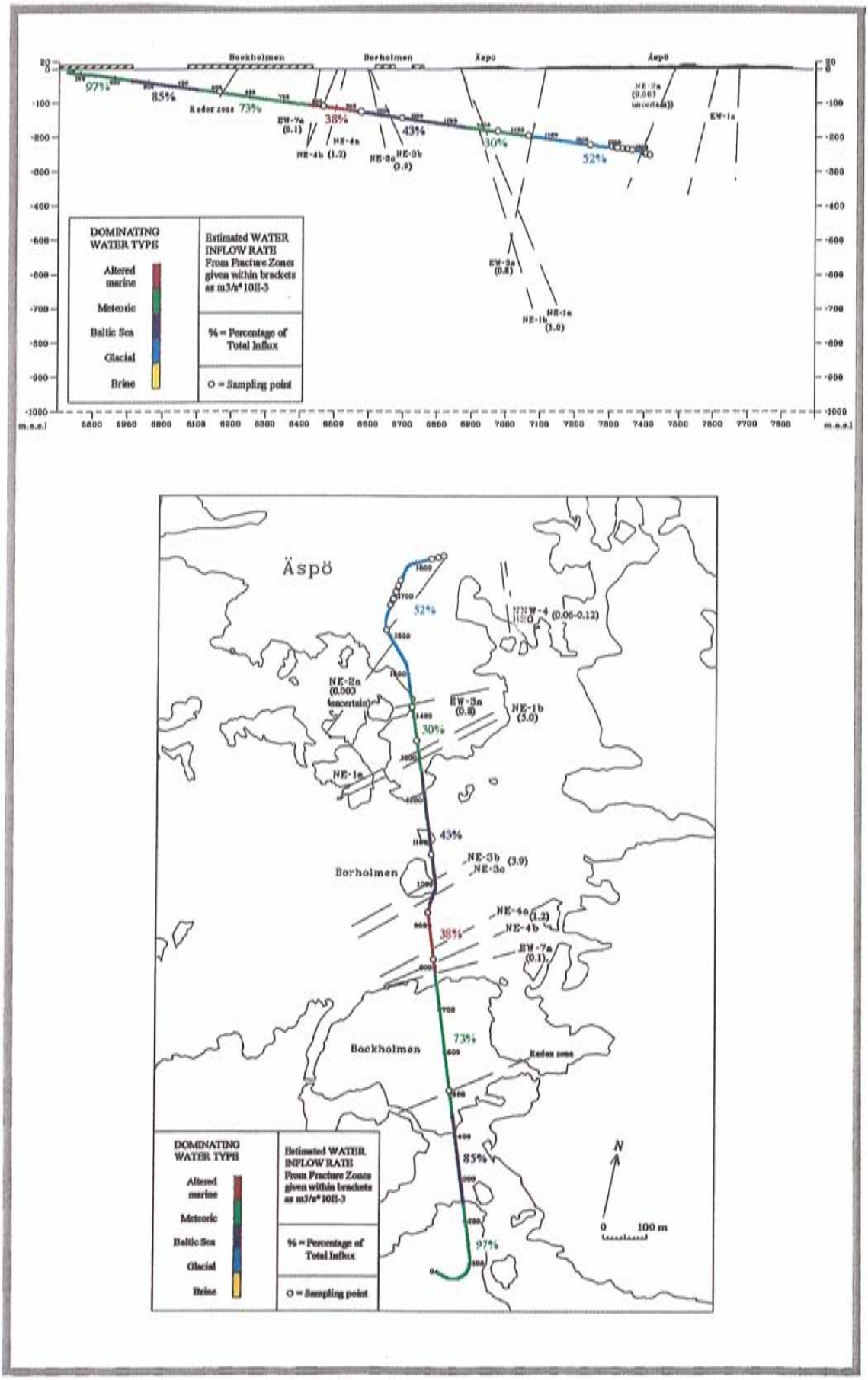

Figure 7-45. *Dominating influx to the tunnel 750 days after the start of tunnel excavation. 1992-11-02.*

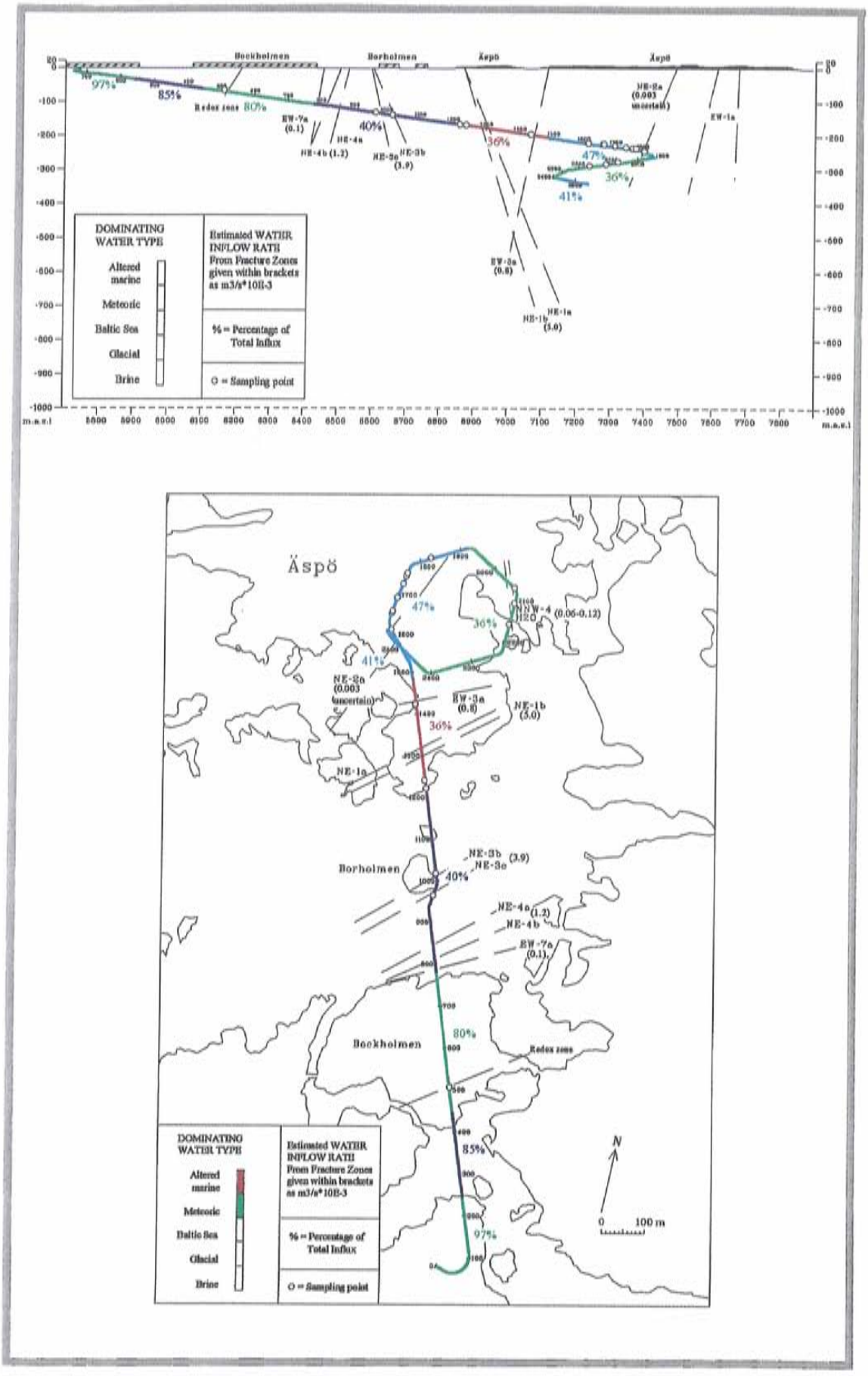

Figure 7-46. *Dominating influx to the tunnel 950 days after the start of tunnel excavation. 1993-05-21.*

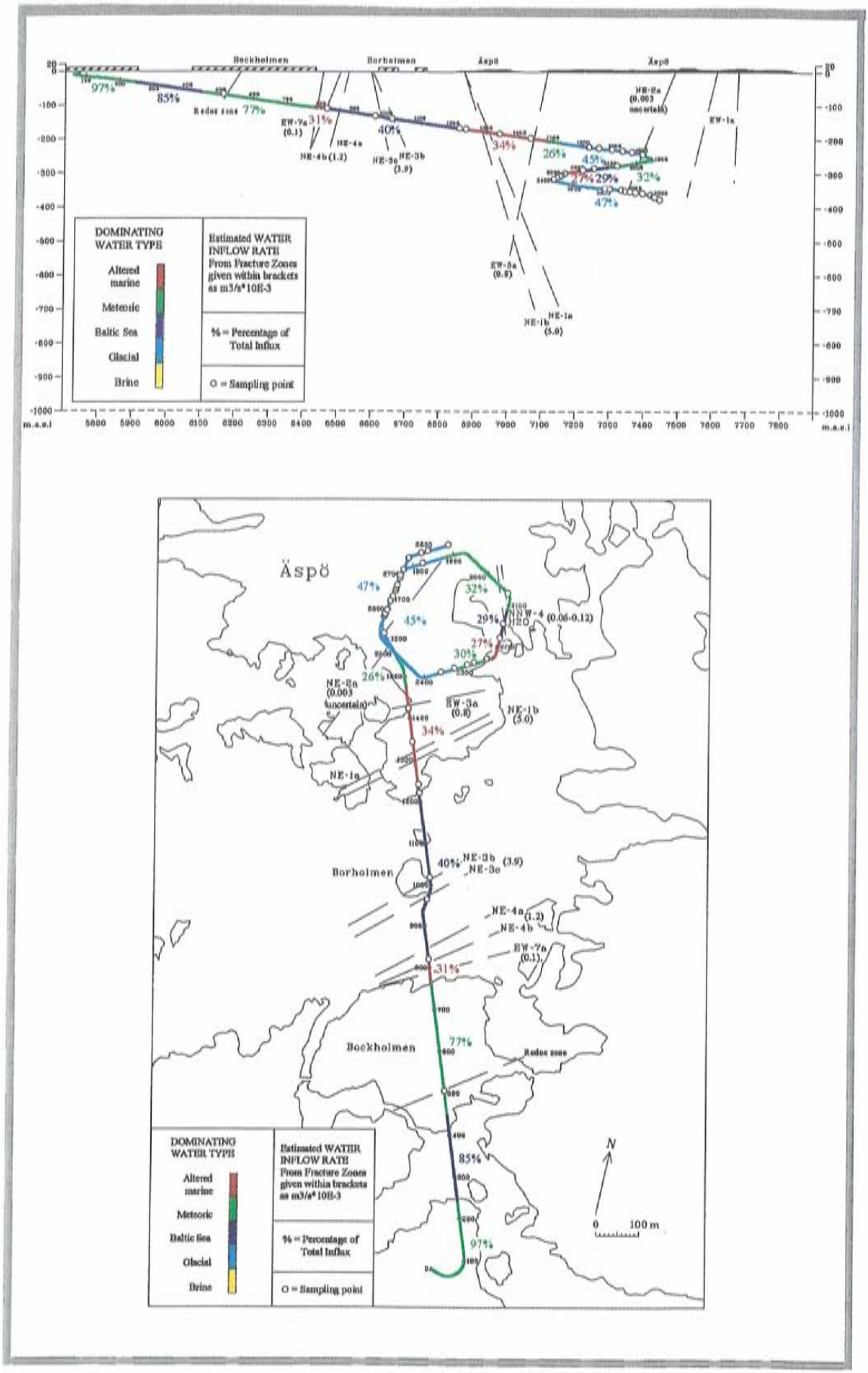

Figure 7-47. *Dominating influx to the tunnel 1150 days after the start of tunnel excavation. 1993-12-07.*

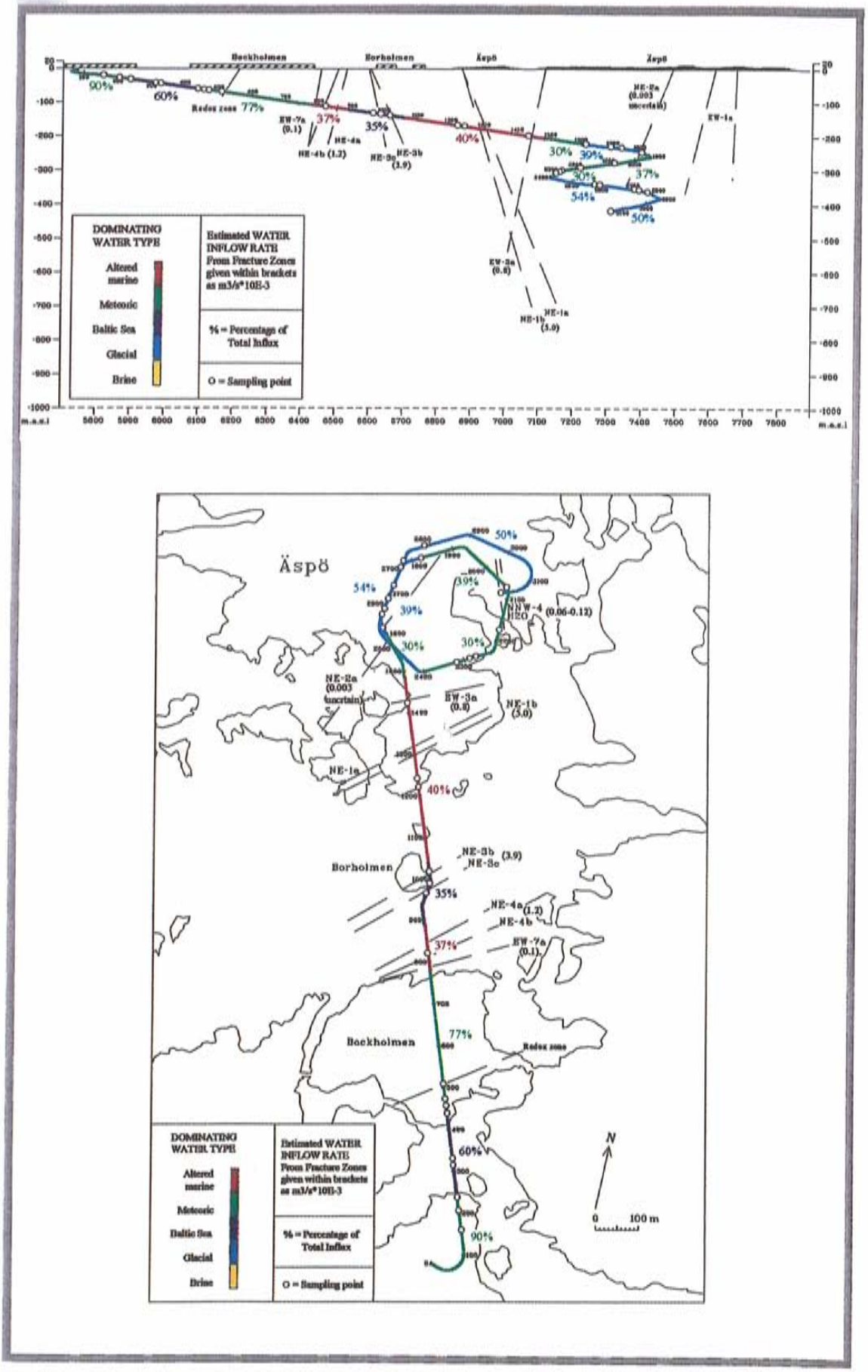

Figure 7-48. Dominating influx to the tunnel 1350 days after the start of tunnel excavation. 1994-06-24.

The dominating influx is from Altered marine water (23-42-46%).

Indication of sulphate-reducing bacteria.

NE-3b, 3c (SA0976B, SA1062B, SA958B)

Experimental days 350-1350: Cl = 5590-5320-3641 mg/L, HCO_3 = 500-531-274 (mg/L) and pH = 7.2-7.3-7.0 units.

Dominating groundwater types are: [Cl-Na-Ca-HCO_3-SO_4-K]; [Cl-Na-Ca-HCO_3-SO_4-K]; Cl-Na-Ca-SO_4-HCO_3-K].

The dominating influx is from Altered marine water (42-40-42%).

Indication of sulphate-reducing bacteria.

NE-1a, 1b (SA1342B, HA1327B, SA1229A)

Experimental days 550-1350: Cl = 4730-4211-3928 mg/L, HCO_3 = 170-426-336 (mg/L) and pH = 7.3-7.0-7.0 units.

Dominating groundwater types are: [Cl-Na-Ca-HCO_3-SO_4-K].

The dominating influx is from Altered marine water (23-44-44%).

Indication of sulphate-reducing bacteria.

EW-3a (SA1420A)

Experimental days 750-1350: Cl = 3930-3420-3053 mg/L, HCO3 = 170-215-206 (mg/L) and pH = 7.6-7.3-7.2 units.

Dominating groundwater types is: [Cl-Na-Ca-SO_4-HCO_3-K].

The dominating influx is from Altered marine water (20-39-43%).

No indication of sulphate reduction.

NE2a-1 (SA1614B)

Experimental days 750-1350: Cl = 5160-6207-5176 mg/L, HCO3 = 37-32-109 (mg/L) and pH = 7.4-7.6-7.2 units.

Dominating groundwater types is: [Cl-Na-Ca-SO_4-HCO_3-K].

The dominating influx is from Glacial water (65-51-30%).

No indication of sulphate reduction.

NE2a-2 (SA1828B)

Experimental days 750-1350: Cl = 5200-6010-5123 mg/L, HCO_3 = 43-48-111 (mg/L) and pH = 7.4-7.3-7.2 units.

Dominating groundwater types is: [Cl-Na-Ca-SO_4-HCO_3-K].

The dominating influx is from Glacial water (45-33-19%).

No indication of sulphate reduction.

NE2a-3 (SA2583A)

Experimental days 1150-1350: Cl = 6647-6896 mg/L, HCO3 = 13-44 (mg/L) and pH = 7.5-7.9 units.

Dominating groundwater types is: [Cl-Na-CaSO_4-HCO_3-K].

The dominating influx is from Glacial water (47-45%).

No indication of sulphate reduction.

NNW-4H_2O-1 (SA2074A)

Experimental days 950-1350: Cl = 5283-4276 mg/L, HCO_3 = 47-94 (mg/L) and pH = 7.0-7.3 units.

Dominating groundwater types is: [Cl-Na-Ca-SO_4-HCO_3-K].

The dominating influx is from Shallow water (30-30%).

No indication of sulphate reduction.

NNW-4H_2O-2 (SA2109B, SA2142A, SA2175B)

Experimental days 950-1350: Cl = 4480-3880-5442 mg/L, HCO_3 = 67-127-127 (mg/L) and pH = 8.1-7.4-7.8 units.

Dominating groundwater type is: [Cl-Na-Ca-SO_4-HCO_3-K].

The dominating influx is from Shallow water (38-27%).

No indication of sulphate reduction.

NNW-4H2O-3 (KA3191F)

Experimental day 1350: Cl = 7410 mg/L, HCO_3 = 29 (mg/L) and pH = 7.3 units.

Dominating groundwater type is: [Cl-Na-Ca-SO_4-HCO_3-K].

The dominating influx is from Glacial water (45%).

No indication of sulphate reduction.

7.10 HYDROCHEMISTRY IN A LOW CONDUCTIVITY-ROCK MASS

A pilot study was conducted to sample and analyse the water of low-conductivity rock. The samples were taken from boreholes KA1639A and KA1750A. In addition to the water samples core samples were also prepared and analysed. The entire pilot study is presented by *Wikström and Björklund /1994/*. The hydrochemical data from the study is shortly presented in *Table 7-2* and also reported in *Nilsson /1995/*.

The experiences are:

- The development and testing of equipment and methodology for sampling water with extremely low flow were successful. Minor changes in the procedure have been suggested.

- Only one of the tested analytical methods turned out to be practically (and economically) feasible for the trace element analyses. The high salinity caused serious problems for most of the methods. The successful technique was ICP-MS with a modified nebulizer. AAS and INAA methods failed.

- The results of analyses gave no clear indications of differences regarding rock type or hydraulic conductivity.

Table 7-2. The composition of groundwater in low-conductivity and highly-conductive rock masses of Äspö in both Äspö diorite and greenstone. Concentrations are given in mg/l or for element X(x)* in µg/l. A represents chloride interval 6200-6600 mg/l and B 3900-4300 mg/l. (Samples from boreholes KA1639A and KA1750A).

Constituent	Äspö diorite Highcond.	Äspö diorite Lowcond.	Green-stone Highly-cond.	Green-stone Low-cond.
flow ml/ min	600	30	11	2.5
Na (A)	2030	1990		2080
Na (B)	1720		1610	1640
Ca (A)	1700	1680		1720
Ca (B)	620		650	750
Mg (A)	77	72		68
Mg (B)	142		128	43
HCO_3 (A)	40	34		24
HCO_3 (B)	260		252	17
Cl (A)	6400	6200		6600
Cl (B)	4100		3920	4200
Br (A)	34	38		45
Br (B)	18		16	26
SO_4 (A)	435	444		450
SO_4 (B)	243		225	125
Sr (A)	26	27		30
Sr (B)	10		9	14
Fe (A)	0.44	0.32		0.05
Fe (B)	2.4		2.3	0.05
Mo (A)*	50	71		79
Mo (B)*	10		7	17
U (A)*	0.6	0.07		0.53
U (B)*	2		3	0.06
La (A)*	0.7	0.56		0.76
La (B)*	0.3		0.45	0.26

7.11 BIOLOGICAL PROCESSES

The microbes themselves do not create new reactions, but they catalyse reactions which would otherwise not take place, e.g. the reduction of sulphate to sulphide and dissolution and reduction of ferric iron minerals. At Äspö the biological processes turned out to be even more important than the chemical interaction between the groundwater and the minerals. The microbial processes always involve redox reactions. They mostly also produce (or consume) carbon dioxide and thus affect both the calcite and redox systems */Pedersen and Karlsson, 1995/*. Because of the unexpected effects of the biological processes the observed bicarbonate, sulphate and iron concentrations were different from those predicted. This was especially noticeable in the tunnel sections passing below the sea, where the water percolating through the seabed sediments transported large quantities of organic matter into the rock.

The biological processes which have affected the hydrochemistry of Äspö are:

- Sulphate reduction taking place most predominantly in the tunnel section passing below the sea, but also occasionally at depth in the tunnel spiral. A major effort to evaluate the conditions around the sulphate reduction has pointed towards the salinity interval of 4000-6000 mg/l as optimum for the process. Also a high content of organic material (>10 mg/l) seems to favour the biological sulphate reduction. It has in a few cases been observed to give bicarbonate concentrations of above 1000 mg/l with a corresponding decrease of sulphate from above 500 mg/l to less than 100 mg/l. No corresponding high concentrations of sulphide have been observed. The sulphate reduction is reported in detail by */Laaksoharju (ed), 1995/*.

- Reduction of iron(III) minerals to iron(II) in solution is an anaerobic process similar to the sulphate reduction. This process was found to be the successor to the aerobic respiration of organic matter which was observed in the redox zone. A detailed description of the iron reduction is given in the report on the redox project */Banwart et al, 1995/*.

- The block scale redox experiment focused on the reduction of dissolved oxygen in the infiltrating surface water to assess the risk for breakthrough of oxidizing surface water into a repository during construction and operation. Inorganic oxygen reduction was expected, but biological consumption was found. The process takes place when the amount of organic matter is larger than the amount of dissolved oxygen. This is roughly the case at > 10 mg/l total organic content. The conclusion is that oxidizing surface water should **not** be expected in a repository, regardless of the time of construction and operation */Banwart (ed), 1995/*.

8 GROUNDWATER FLOW AND TRANSPORT OF SOLUTES

8.1 INTRODUCTION

The flow field below Äspö has been modelled by SKB using the computer code PHOENICS */Spalding/*, and in *Section 8.2* an overview of the flow situation in the regional scale and below Äspö island is given based on simulations made 1997.

Up to 1995 only a few attempts have been made at the Äspö HRL to estimate transport properties in the rock mass. *Section 8.3* contains a brief presentation of these results together with some data from other sites compiled in *Andersson /1995/* in order to give possible values or ranges for some of the transport parameters.

The Äspö International Task Force on Modelling of Groundwater Flow and Transport of Solutes was formed in 1992. Besides SKB, modelling teams from ANDRA, CRIEPI, PNC, Posiva and Nirex have modelled a long-term pumping and tracer test (called LPT-2) and the drawdown caused by the Äspö HRL following somewhat different approaches. The major conclusion is that the general behaviour of the groundwater flow can be fairly well reproduced with all approaches based on the available data. However, the tasks have also illuminated needs for model developments and input data to the models.

The LPT2 test was performed on a large test scale, several 100 m, and several hydraulic conductor domains were tested. As a connectivity test it was useful but the evaluation of the transport properties was more difficult. A number of modelling groups used the data from the LPT2 test and tried to simulate the transport, but found it difficult to find a 'unique' solution concerning the transport parameters. The modelling work is summarized in *Gustafson and Ström /1995/* and reported in detail in *Rhén et al /1992/, Hautojärvi /1994/, Taivassalo et al /1994/, Billaux et al/ 1994/, Noyer and Fillion /1994/, Barthelemy et al /1994/, Holton and Milický /1996/, Gylling et al /1994/, Kobayashiet al /1994/, Igarashiet al /1994/ and Uchida et al /1994/.*

The simulations by others than SKB of the tunnel drawdown have up to autumn 1997 been presented in *Uchida et al /1997/, Holton and Milický /1997/, Mészáros /1996/, Tanaka et al /1996/.* The first simulations made by SKB of the tunnel drawdown are presented in *Svensson /1991/.* In *Löfman and Taivassalo /1995/* a few concepts were tested on how to model the pressure and salinity fields around Äspö Island the last 3000 years. One conclusion was that a dual-porosity approach seemed useful but there was no salinity data available that was considered to represent the matrix blocks and that could be used for consistency check.

8.2 FLOW FIELD BELOW AND AROUND ÄSPÖ ISLAND

8.2.1 Purpose with the flow modelling

The expected interface between the fresh water and the saline water is quite irregular due to the heterogeneity of the rock mass. This was shown in *Svensson /1988/* and is briefly presented in *Section 8.2.4*.

Late 1996 a regional groundwater flow model was set up based on *Model 96* and some of the results are presented in *Section 8.2.5*. The purpose was to make a 3D regional model useful for calculating the natural (undisturbed) groundwater flow and the groundwater flow with the Äspö HRL present. Density driven flow dependent of the salinity of the groundwater was to be included. The intension with the model was also that the regional model should be used for calculating the boundary conditions for a site model. The detailed results are presented in *Svensson /1997a/*.

The site model was made to get a better resolution of the flow field below Äspö that should be useful for the evaluation of the groundwater chemistry, modelling pressures and flows in the rock mass outside the tunnel for planning of future experiments and, finally, with the intention that the model should be used for calculating the boundary conditions for a local detailed laboratory model. The site model was finalized summer 1997 and the results were reported in *Svensson /1997b/*. Some of the results are presented in *Section 8.2.6*.

For all models a stochastic continuum approach was chosen and the code used was PHOENICS.

8.2.2 Concepts and data

Process description

The flow was based on the following equations:

- Continuity equation (mass balance equation).
- Equation of motions (Darcy's law including density driven flow).
- Transport equation.
- Equation of state (Salinity-density relationships).

The dispersion used was proportional to the local Darcy velocity. The simulations were steady state simulations. See *Chapter 3* for details of how the the relations above were treated in PHOENICS.

Geometric framework and parameters

Regional model

The model covers an area of 10·10 km^2 and down to a depth of 3 km. The model consists of 360 000 cells and the cells are 100 m cubes below a depth of 100 m. Above 100 m depth in the model the height of the cells decreases and the uppermost cells follow the topography on land as well as the topography of the sea bottom, see *Figure 8-1*. BFC (Body Fitted Coordinates) net is used. The regional hydraulic conductor domains and hydraulic rock mass domains are defined according to *Appendix 2* and *Chapter 6*.

Site scale model

The model covers an area of 1.8·1.8 km^2 and down to a depth of 1 km. The model consists of 445 500 cells and the cells are 20 m cubes below a depth of 100 m. Above 100 m depth in the model the height of the cells decreases and the uppermost cells follow the topography on land as well as the topography of the sea bottom, see *Figure 8-1*. BFC (Body Fitted Coordinates) net is used. The site scale hydraulic conductor domains and hydraulic rock mass domains are defined according to *Appendix 2* and *Chapter 6*.

Material properties

The material properties assigned to the bedrock before calibration has started are described in *Appendix 2* and *Chapter 6*. Transmissivities of the hydraulic conductor domains are constant for each domain and hydraulic rock mass domains are described as a stochastic continuum. The hydraulic conductor domains described in the site scale model in this report were simplified in the regional scale due to the large cells in the regional model.

Regional model

Properties for the hydraulic rock mass domains are based on the hydraulic tests in 100 m test scale as shown in *Appendix 2* and *Chapter 6*.

The uppermost four cells (down to about 15 m below ground surface) in the model are given constant hydraulic conductivities with higher values than the geometric mean hydraulic conductivity for the rest of the model. This is made in order to make the sub-program treating the unsaturated zone to work properly. It may be interpreted as if there is a higher hydraulic conductivity of the soil cover and the uppermost part of the bedrock, but also that a possible overland flow (in the uppermost cell) should be incorporated in the model in order to give a correct run-off for the modelled area.

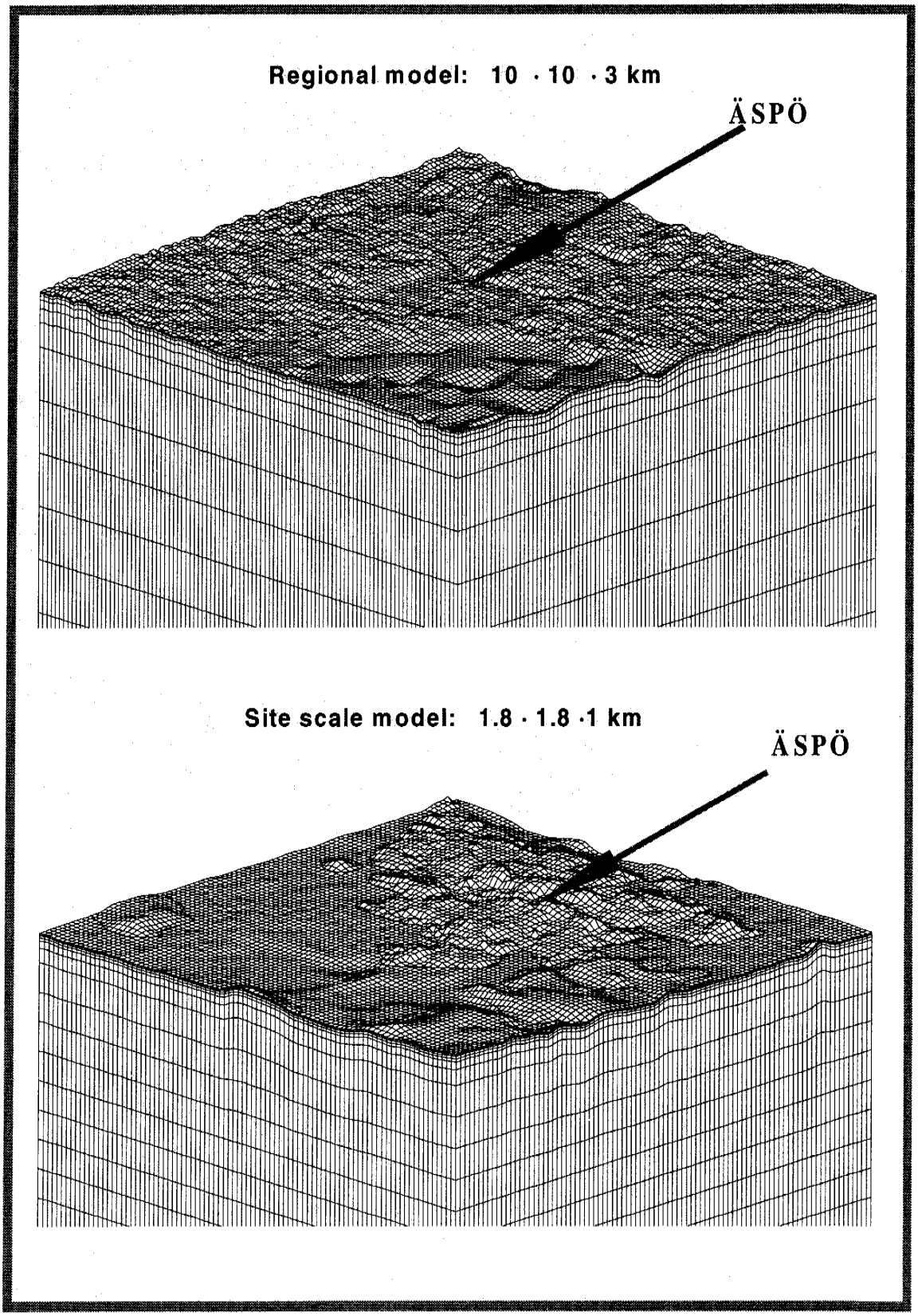

Figure 8-1. *Top: Finite-volume net close to surface for the regional model. View from south-east with Äspö in the centre. (Vertical scale is magnified about 15 times). /Svensson, 1997a/.*
Bottom: Finite-volume net close to surface for the site scale model. View from south-east with Äspö in the centre. (Vertical scale is magnified about 7 times). /Svensson, 1997b/.

Two of the main streams are also simulated by assigning high hydraulic conductivity (1 m/s) for the uppermost cells in the position where the streams are.

Site scale model

Properties for the hydraulic rock mass domains are based on the hydraulic tests in 3 m test scale, which are scaled to target scale 20 m. The model properties are shown in *Appendix 2* and *Chapter 6*. The uppermost five cells (down to about 10 m below ground surface) in the model are given constant hydraulic conductivities somewhat higher than the geometric mean hydraulic conductivity for the uppermost part of the domains. This is made in order to make the sub-program treating the unsaturated zone to work properly.

Below the Baltic a clay layer of a few metres thickness is normally found. This was modelled by placing a 3 m thick layer with a hydraulic conductivity of 10^{-9} m/s 5 m below the sea bed.

Spatial assignment method

Regional model

Zonation was chosen as the assignment method for the hydraulic rock mass domains, see *Appendix 2* and *Chapter 6* for details. No correlation between the hydraulic conductivities of the cells are assumed. Each hydraulic conductor domain was assigned a constant transmissivity. One realisation of the hydraulic conductivities is shown in *Figure 8-2.*

Site scale model

Zonation was chosen as the assignment method for the hydraulic rock mass domains, see *Appendix 2* and *Chapter 6* for details. No correlation between the hydraulic conductivities for the cells are assumed. Each hydraulic conductor domain was assigned a constant transmissivity.

Large drawdown and the algorithm for the unsaturated zone, see *Chapter 3*, were found to generate isolated water columns above cells with very low hydraulic conductivity. This was considered not realistic, and therefore a minimum vertical hydraulic conductivity of $5 \cdot 10^{-9}$ m/s was used for the cells above the tunnel spiral down to a depth of 140 m. One realisation of the hydraulic conductivities is shown in *Figure 8-3.*

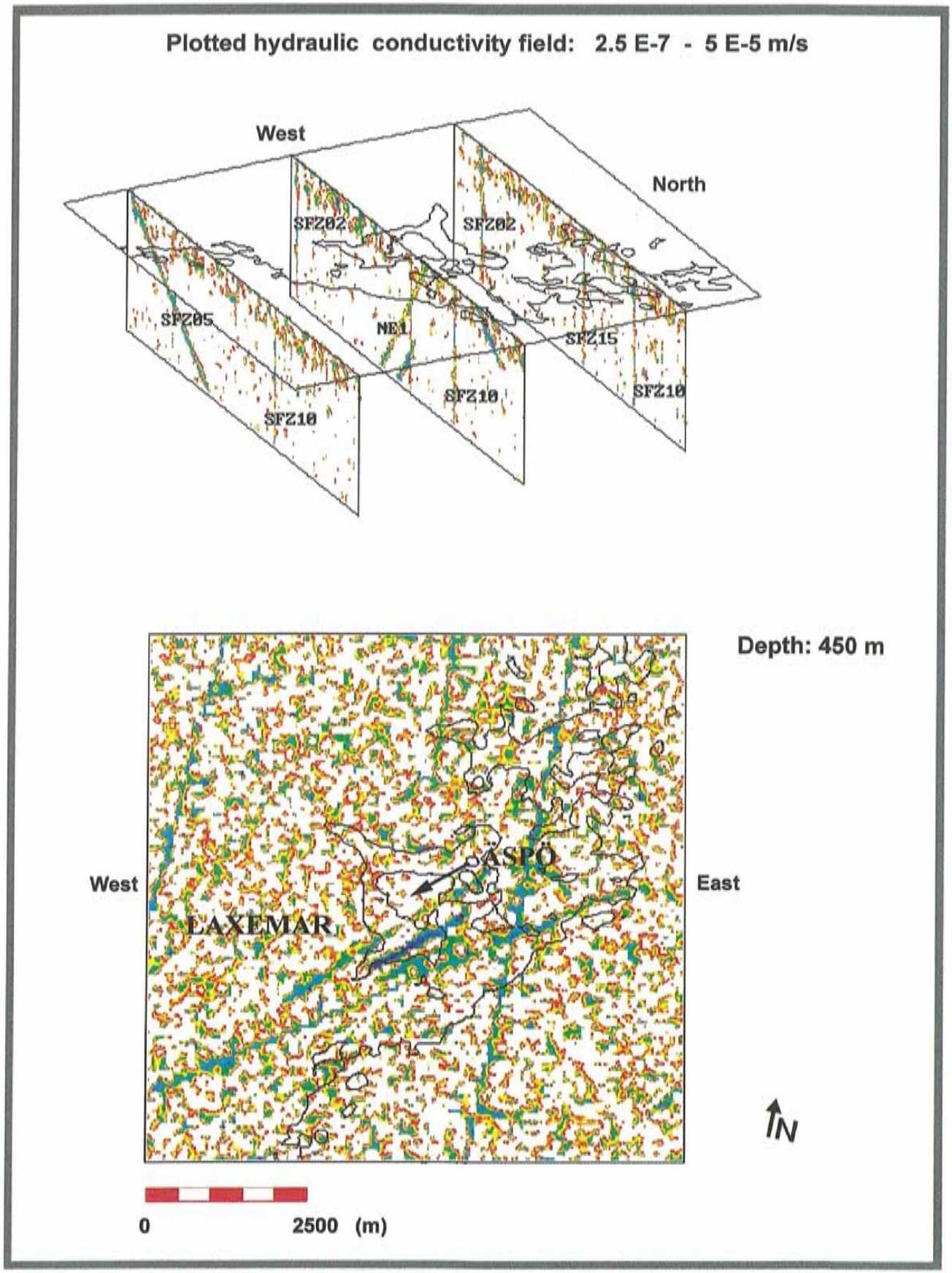

Figure 8-2. *Illustration of the hydraulic conductivity field for the regional model. Plotted hydraulic conductivity interval: $2.5 \cdot 10^{-7}$-$5.0 \cdot 10^{-5}$ m/s. /Svensson, 1997a/. Top: Perspective view. Bottom: Horizontal section at a depth of 450 m.*

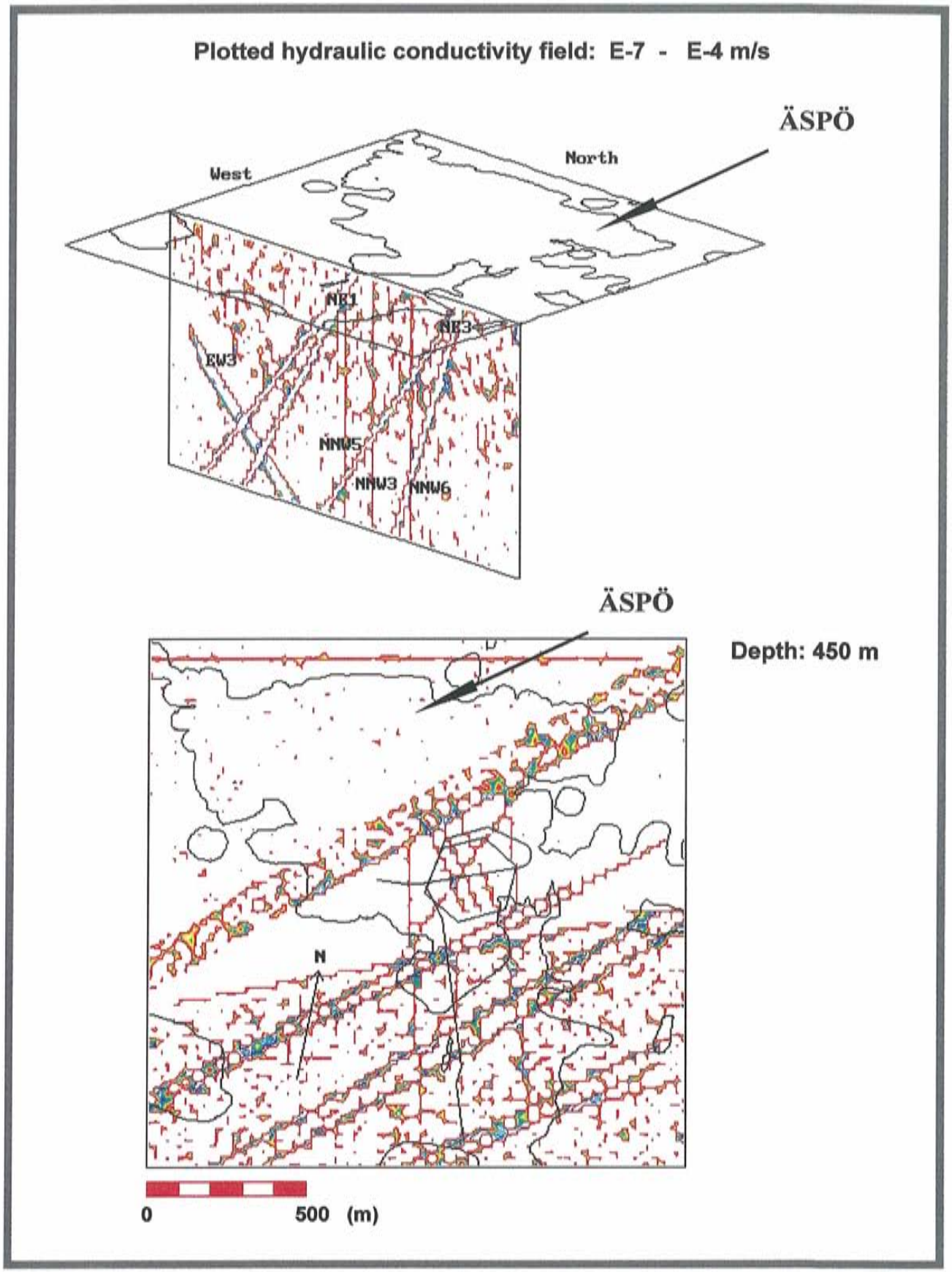

Figure 8-3. *Illustration of the hydraulic conductivity field for the site scale model. Plotted hydraulic conductivity interval: 10^{-7}-10^{-4} m/s. /Svensson, 1997b/. Top: Perspective view. Bottom: Horizontal section at a depth of 450 m.*

Boundary conditions

Upper boundary:

Net precipitation (P-E, P: Precipitation, E: Evapotranspiration) on the upper boundary was set 200 mm per year for the regional model and 100 for the mm per year for the site scale model for the upper surface not covered by the sea. Calculated net groundwater recharge locally depends on elevation of topography and the elevation of the water table, see the algorithm for the unsaturated zone presented in *Chapter 3*. 200 mm per year correspond approximatly to the mean run-off for the area around Äspö, as mentioned in *Chaper 6*. In the site scale model it was needed to decrease the (P-E) to 100 mm per year in order to get a fresh water lense to the depth during naural conditions that approximately corresponded to the measured values.

The sea surface was modelled as constant pressure. In the regional and site scale models the salinity of the Baltic Sea is assumed to be 0.6 %. Precipitation is assumed to have a salinity of 0 %.

Side boundary:

Regional model: Boundaries facing the Baltic (eastern and part of the southern boundary) are assigned hydrostatic pressure and two linear functions for the increase of salinity by depth, based on measurements of natural conditions at Laxemar and Äspö. Zero flux conditions for water and salinity for other boundaries.

Site model: Boundary conditions from regional model except for the uppermost 100 m in the model where zero flux conditions were used due to the difference in resolution of the regional and site scale computational nets .

Lower boundary:

Regional model: Zero flux conditions.

Site model: Boundary conditions from regional model.

Internal boundaries:

Tunnel: Flow rates into the tunnel assigned to hydraulic conductor domains intersecting the tunnel for two tunnel face positions; 2875 and 3600 m.

8.2.3 Calibration

Regional model

The four top cells were given the following hydraulic conductivities, uniformly applied on and sea, from surface downwards: $2 \cdot 10^{-3}$, $8 \cdot 10^{-4}$, $5 \cdot 10^{-6}$ and $1 \cdot 10^{-6}$ m/s. Local calibration of the hydraulic conductivity of the area around Äspö ($1.4 \cdot 1.2$ km^2) was applied in order to be able to approximately reproduce the drawdown by Äspö HRL. The top four layers were multiplied with 0.3 and the cells below these with 0.5. This is in line with the properties given for Äspö in relation to the regional model!

Site scale model

Four test cases were used: Natural (undisturbed) conditions, pumping test LPT2 (pumping of borehole KAS06) and the drawdown by the Äspö HRL when the tunnel was at chainage 2875 and 3600 m. The last case, "3600 m", was only used to test that the drawdowns would be approximately as for "2875 m". Calibration was made to match the measured piezometric levels for all cases and the salinity of the groundwater for natural conditions by adjusting the transmissivities and the arithmetic mean of $Log_{10}(K)$, (K: hydraulic conductivity) by trial and error approach.

Two major disagreements with the model presented in *Chapter 6* and *Appendix 2* were found. The transmissivity of NNW-7 and NE-2 should be more than 10 times more transmissive according to the calibration. The rock mass south of Äspö was too conductive and therefore the hydraulic conductivity of SRD4 was decreased. In *Tables 8-1* to *8-3* the calibration results are shown.

The measured salinity in 22 borehole sections were generally higher close to surface but lower below 500 m depth, compared to the calculated values in the calibrated model. The water table for the natural conditions and when the tunnel was at chainage 2875 m compares rather well with the measured as shown in *Figure 6-27* and *Figure 8-12*.

The correction of the hydraulic rock mass domains on Äspö is as expected, see *Chapter 6*. The correction of SRD4 is not surprisingly as the rock mass below the Baltic is highly fractured and some of the tests in the probeholes outside the wide hydraulic conductor domains may have been more representative for the conductor domain than the rock mass domain. There are also comparatively few tests along the part of the tunnel below the Baltic compared to the rest of the site.

Sensitivity tests for drawdown with the tunnel face at chainage 2875 m were made by multiplying the transmissivities for the hydraulic conductor domains with 0.5 and 2 and two other cases by multiplying the hydraulic conductivities for all the cells of the hydraulic rock mass domains with 0.5 and 2. Two other cases for the undisturbed conditions were made by multiplying the net precipitation 100 mm per year (P-E) with 0.5 and 2. The results indicate that

the mean error of the piezometric levels or depth of the fresh water lense (mean of (measured value-calculated value)) becomes larger for the cases above. However, one of the realisations for the calibrated model had an error that was slightly less than the 0.5 case for the hydraulic conductivity, see *Svensson /1997b/*. It was concluded in *Svensson /1997b/* that the depth of the fresh water lense and the undisturbed water table is sensitive to P-E.

Table 8-1. Modified properties by calibration of the site Scale hydraulic Conductor Domains (SCD). T =Transmissivity, Calibration = Modification according to *Svensson /1997b/, Model 96* =Values according to *Chapter 6* in this report.

Group of domains	T Calibration (m^2/s) $\cdot 10^{-5}$	T Model 96 (m^2/s) $\cdot 10^{-5}$
EW-3	1.2	1.7
NE-2	0.8	0.012
NE-1	30	22
NNW-1	3.0	0.86
NNW-2	1.0	2.4
NNW-7	8.0	0.75
NNW-8	0.1	0.8

8.2.4 Saline interface is irregular due to the heterogeneity of the rock

Svensson /1988/ made a generic study which shows the interaction between the fresh water recharge and the saline water in a coastal region. The only variable that is changed is the magnitude of the heterogeneity, that is the number of low and high values of hydraulic conductivity values changes but the mean value is the same. As can be seen in the *Figure 8-4*, the flow pattern becomes more channelized as the magnitude of the heterogeneity of increases. It is interesting to note that more saline water can be found above water of lower salinity, that is a heavier water can be found above a lighter water. It is therefore not surprising if the salinity varies considerably within a broad zone near a coast consisting of crystalline rock and with a saline sea.

Table 8-2. Modified properties by calibration of the Site scale hydraulic Rock mass Domain (SRD). K = Hydraulic conductivity, scale = target scale = cell size in numerical model, m = arithmetic mean of $Log_{10}(K)$, Calibration = Modification according to *Svensson /1997b/*, *Model 96* = Scaled values according to *Chapter 6* in this report.

Group of domains	Depth range (m)	Scale (m)	m(Log_{10}(K)) Calibration Log_{10}(m/s)	m(Log_{10}(K)) Model 96 Log_{10}(m/s)
SRD1	0-600	20	-7.8	-8.1
SRD2	0-600	20	-7.1	-7.18
SRD3	0-600	20	-8.7	-8.83
SRD4	0-600	20	-7.6	-6.36

Table 8-3. Modified properties by calibration of the uppermost cells in the numerical model. K = Hydraulic conductivity, scale = target scale = cell size in numerical model, m = arithmetic mean of $Log_{10}(K)$, Calibration= Modification according to *Svensson /1997b/*, *Model 96*= Scaled values according to *Chapter 6* in this report.

Depth below surface (m)	K Calibration (m/s)	K *Model 96* (m/s)
0 -0.5	$1 \cdot 10^{-3}$	see *Table 8-2*
0.5-1.5	$1 \cdot 10^{-3}$	see *Table 8-2*
1.5-3.0	$5 \cdot 10^{-4}$	see *Table 8-2*
3.0-5.0	$1 \cdot 10^{-5}$	see *Table 8-2*
5.0-10.0	$3 \cdot 10^{-7}$	see *Table 8-2*

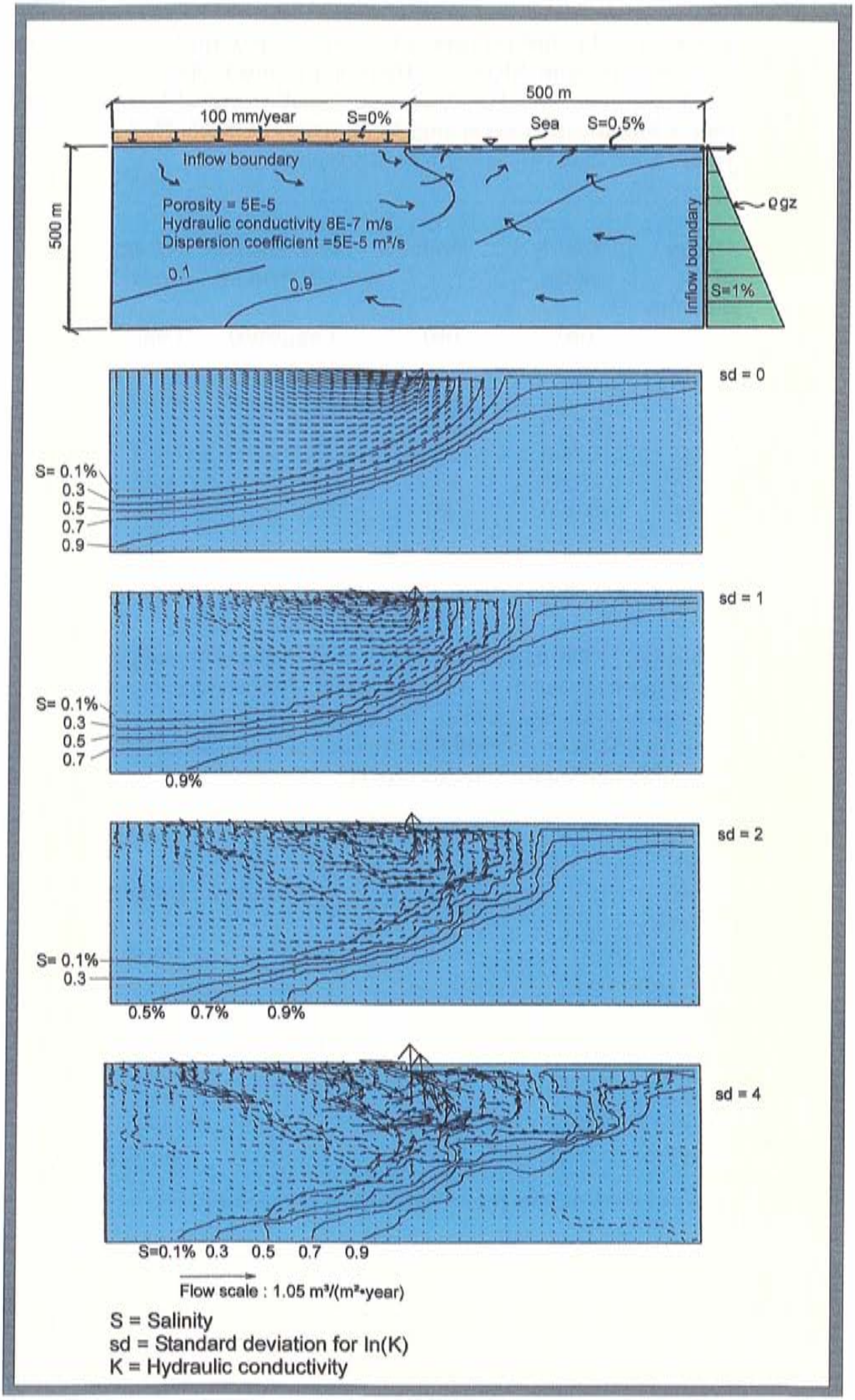

Figure 8-4. *Sensitivity of flow patterns and salinity distribution due to the magnitude of the heterogeneity of hydraulic conductivity. /After Svensson, 1988/.*

8.2.5 Regional model

Recharge- and discharge areas

The flow in the uppermost cells are shown in *Figure 8-5* and the two streams in the area can easily be seen in the figure. The water tables for natural conditions (undisturbed by tunnel) and with Äspö HRL is shown in *Figure 8-6*. The notable change of the elevation of the water table is on Äspö island.

The groundwater flow field close to the surface and at approximately 500 m depth is illustrated in *Figures 8-7* and *8-8*. The horizontal flow component is shown in *Figure 8-7* for depths 5 m and 450 m. The flow rate is considerably lower at 450 m depth compared to 5 m depth but the flow pattern has great similarities for the two depths on the mainland. A difference between 5 m and 450 m depth is that below the islands and peninsulas the flow rate is low compared to the mainland at 450 m depth. Some of the regional hydraulic conductor domains are indicated by higher flow rates in the figure for depth 450 m .

The recharge- and discharge pattern is also illustrated by the vertical flow component shown as isolines, for downwards and upwards flow, in *Figure 8-8* for depths 30 m and 500 m. As can be seen for depth 30 m, and in *Figure 6-2* showing the topography, the recharge areas are in the situated on the hills and the discharge areas are found in the valleys, as expected. The general pattern of downwards and upwards flow is also seen for depth of 500 m, but the flow rate is much smaller.

With the Äspö HRL present the flow pattern at 450 m depth changes considerably below Äspö island, see *Figure 8-9*.

Salinity distribution

East-west and north-south vertical sections through the model are shown in *Figures 8-10* and *8-11*. The sections intersects the centre of the tunnel spiral. As can be seen in the figures there is fresh water (0.1% salinity iso-line) down to about 850 to 950 m, where the boreholes KLX 02 is situated, and about 300 m below Äspö under natural conditions. One can also see that the water from the Laxemar area is discharging mainly close to the coastline.

The flow into the Äspö HRL tunnel changes the distribution of the salinity mainly below Äspö, see *Figures 8-10* and *8-11*. Upconing of saline water can be seen in the figures.

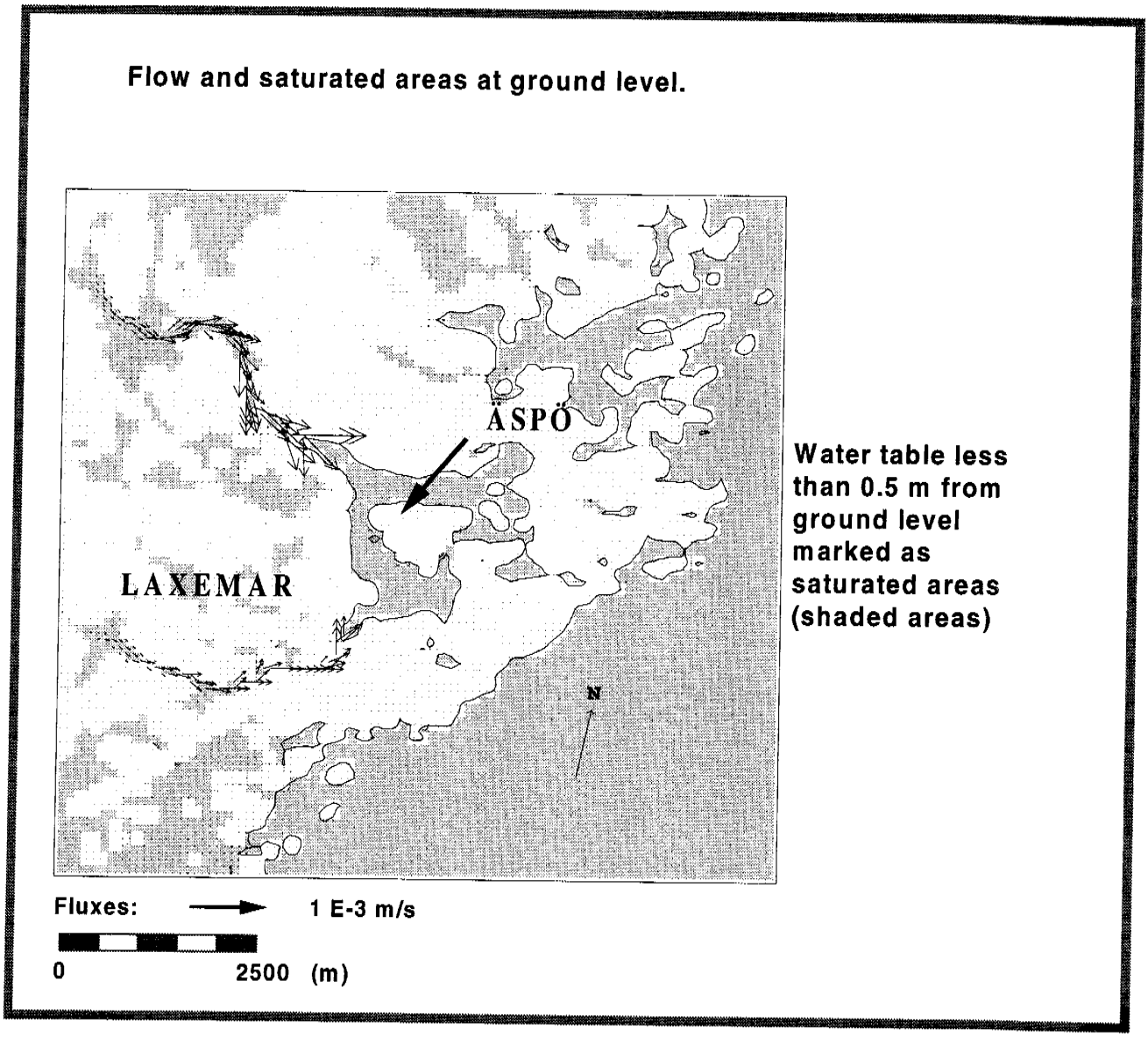

Figure 8-5. *Regional scale groundwater flow model. Natural conditions. Flow and saturated areas at ground level. Areas with the water table less than 0.5 m from ground surface are considered saturated and in the figure marked as shaded areas. The rivers in the area are were the Darcy velocities are the highest. Darcy velocity scale: Vector length 12 mm = 10^{-3} m/s. /Svensson, 1997a/.*

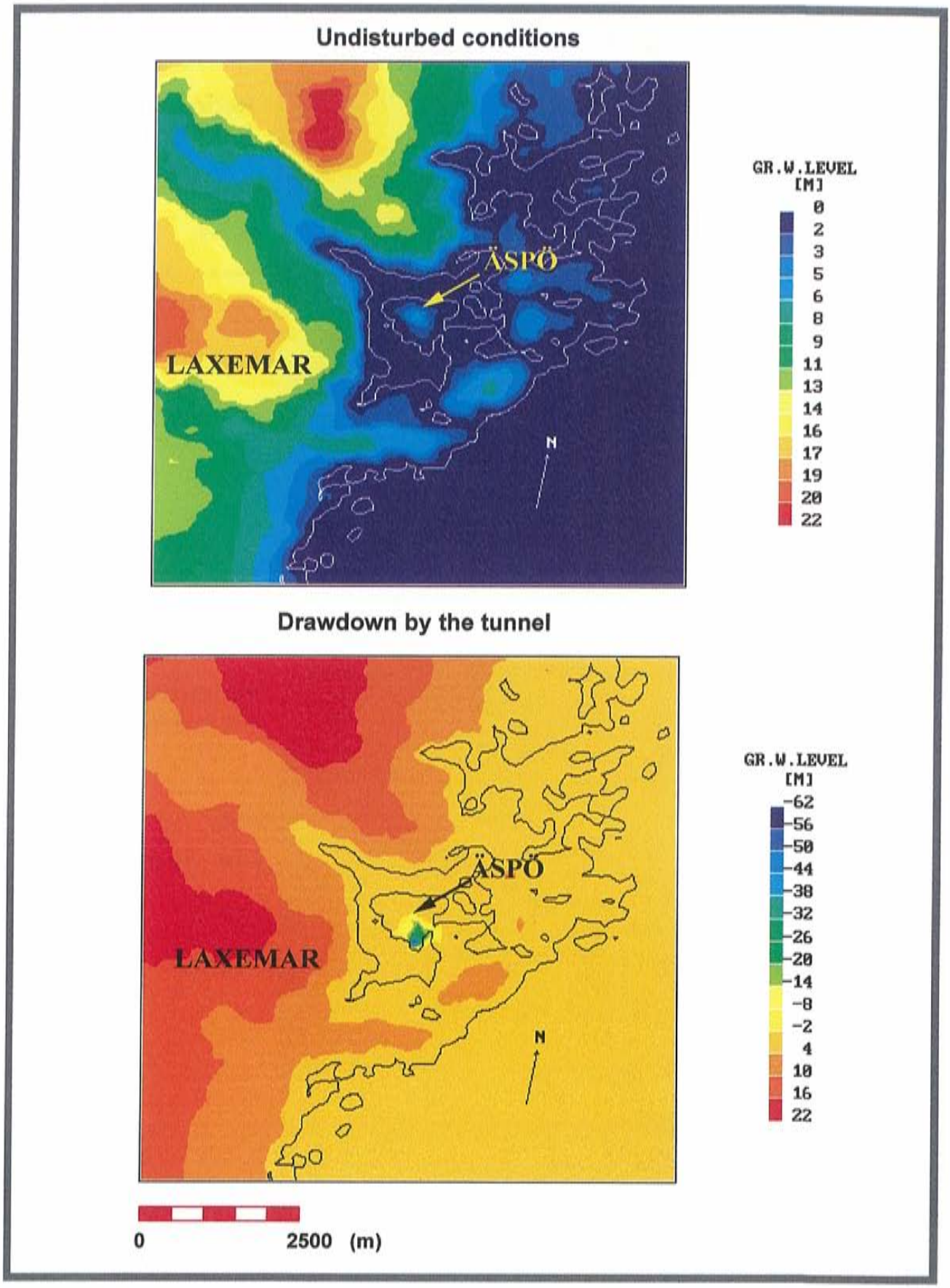

Figure 8-6. *Regional scale groundwater flow model. Water table (metre above mean sea level). /Svensson, 1997a/. Top: Natural conditions. Bottom: Drawdown due to inflow to Äspö HRL.*

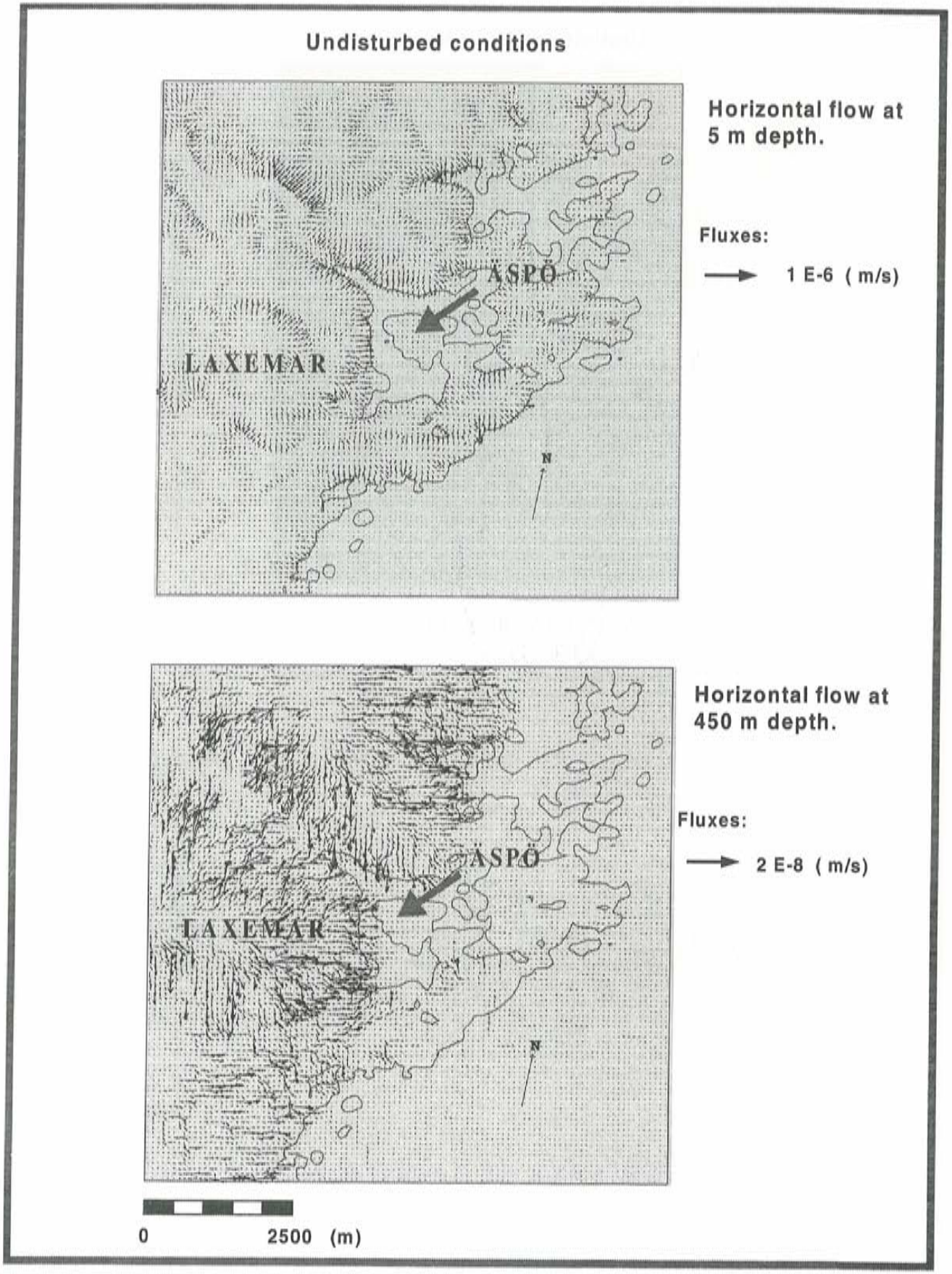

Figure 8-7. *Regional scale groundwater flow model. Natural conditions. /Svensson, 1997a/. Top: Horizontal flow at 5 m depth. Bottom: Horizontal flow at 450 m depth.*

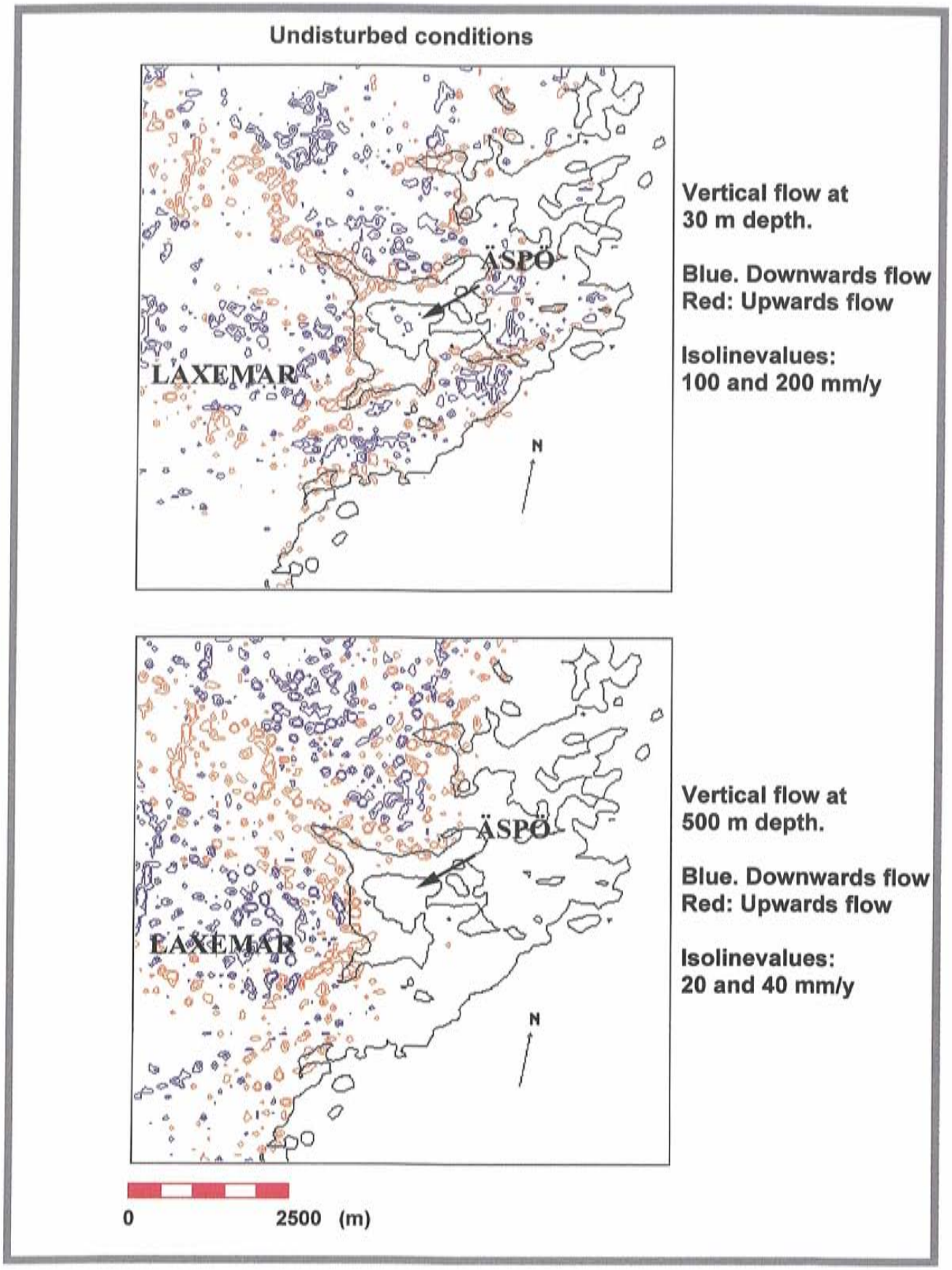

Figure 8-8. *Regional scale groundwater flow model. Natural conditions. Blue colour indicates downwards and red upwards flow /Svensson, 1997a/. Top: Vertical flow at 30 m depth. Bottom: Vertical flow at 500 m depth.*

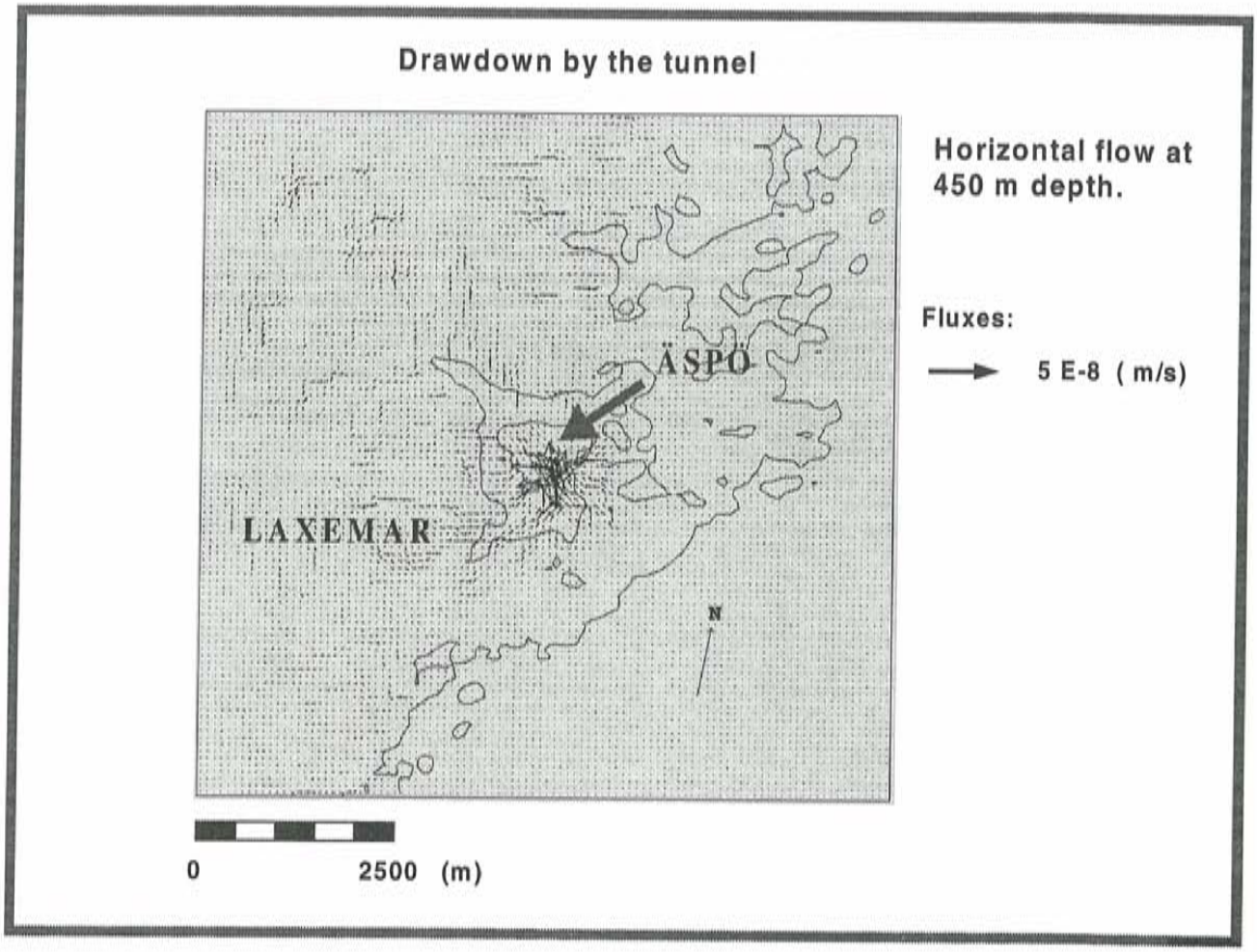

Figure 8-9. *Regional scale groundwater flow model. Drawdown due to inflow to Äspö HRL. /Svensson, 1997a/. Horizontal flow at 450 m depth.*

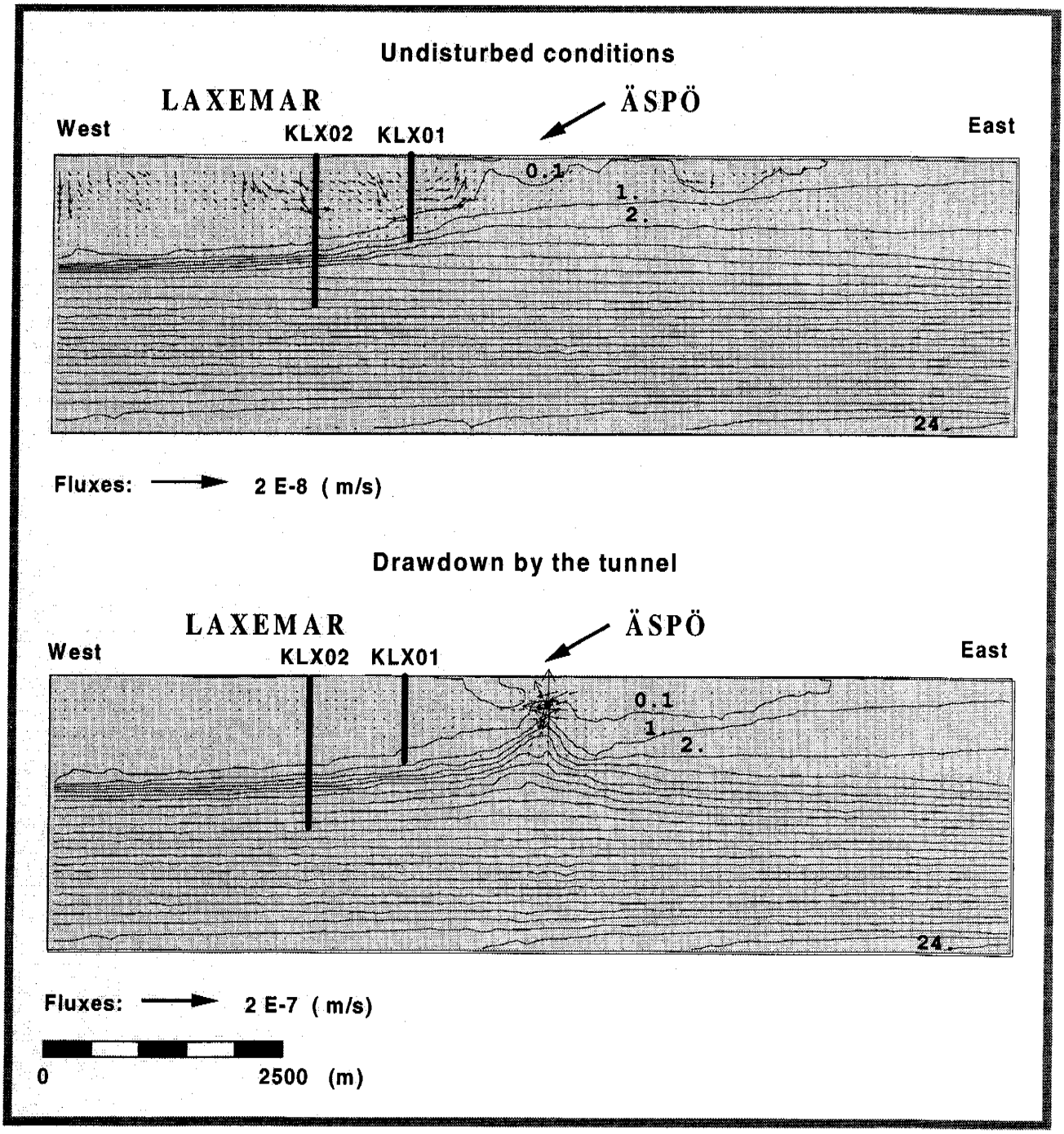

Figure 8-10. *Regional scale groundwater flow model. West-East vertical sections through Äspö HRL. Salinity fields in %. Top: Natural conditions. Bottom: Drawdown due to inflow to Äspö HRL. (Note: Flow field from surface down to 100 m depth is not shown). /Svensson, 1997a/.*

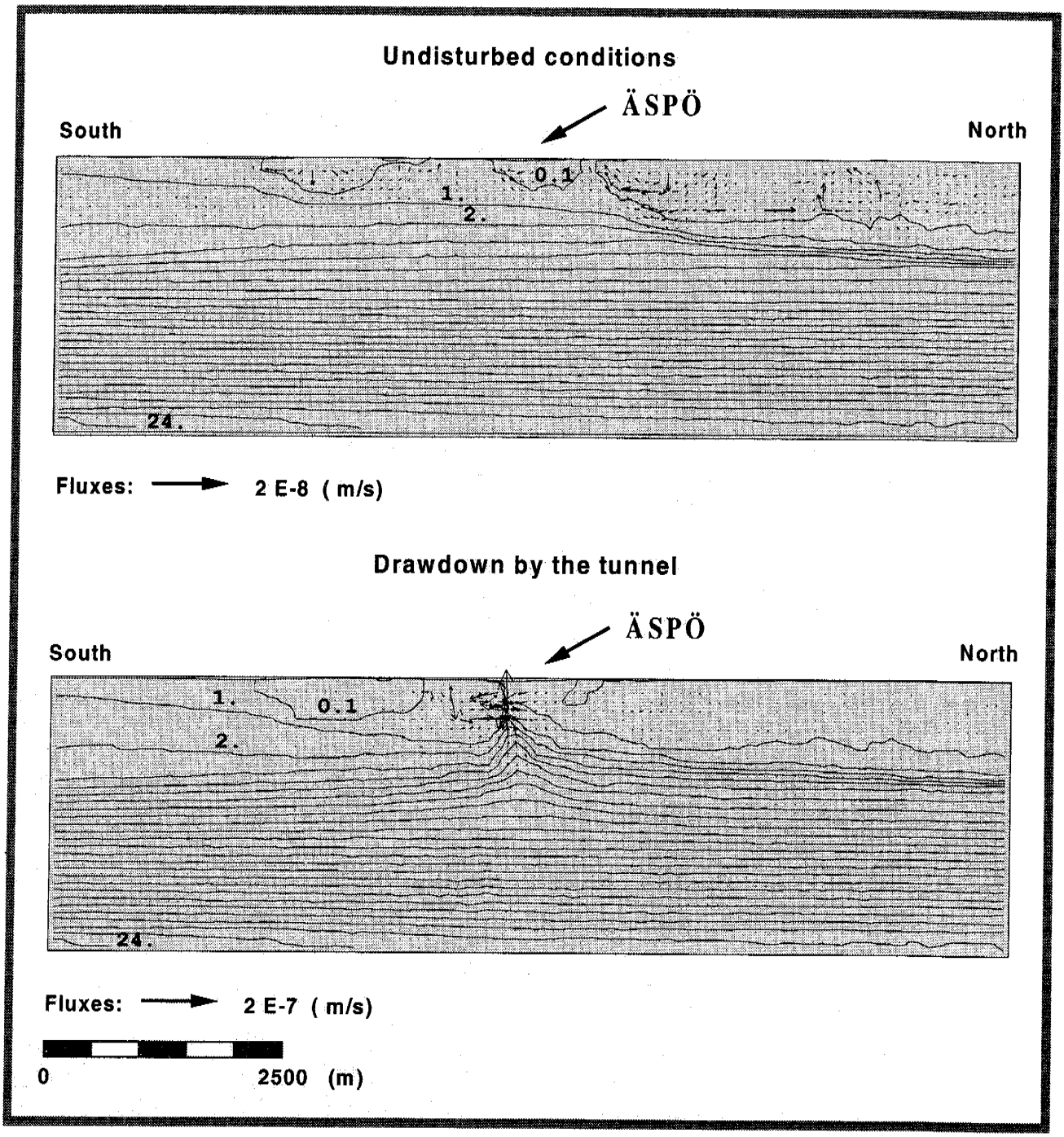

Figure 8-11. *Regional scale groundwater flow model. North-South vertical sections through Äspö HRL. Salinity fields in %. Top: Natural conditions. Bottom: Drawdown due to inflow to Äspö HRL. (Note: Flow field from surface down to 100 m depth is not shown). /Svensson, 1997a/.*

8.2.6 Site scale model

Recharge- and discharge pattern

The water tables for natural conditions (undisturbed by tunnel) and with Äspö HRL is shown in *Figure 8-12*. As can be seen in the figure the largest drawdown takes place in the hydraulic conductor domains, as expected.

The groundwater flow field close to the surface, at approximately 100 m and 450 m depth is illustrated in *Figures 8-13* to *8-15* for natural conditions and with Äspö HRL present in *Figures 8-16* to *8-18*. The horizontal flow component is shown in *Figure 8-13* for depths 4 m and 100 m. As can be seen in this figure, and also *Figure 8-15,* the flow rate decreases with depth. In the plot for 4 m depth one can see where the discharge to valleys and wet lands takes place and in the plot for 100 m depth the hydraulic conductor domains are indicated by somewhat larger flows.

The recharge- and discharge pattern is also illustrated by the vertical flow component shown as isolines, for downwards and upwards flow, in *Figures 8-14* and *8-15* for depths 30 m and 500. The recharge and discharge pattern is rather diffuse at 5 m depth but at 100 and 450 m depth much of the vertical flow takes place in the hydraulic conductor domains.

The flow pattern, mainly on southern Äspö, changes considerably with the Äspö HRL present, see *Figures 8-16* to *8-18*. Much of the flow is concentrated to the hydraulic conductor domains, except for close to the surface. The flow rates around the tunnel system is also larger than for the natural conditions.

Salinity distribution

East-west and north-south vertical sections through the model are shown in *Figures 8-19* and *8-20*. The sections intersects the centre of the tunnel spiral. As can be seen in the figures the maximum depth of the fresh water lense (0.1% salinity iso-line) is about 300 m below Äspö under natural conditions.

The flow into the Äspö HRL tunnel changes the distribution of the salinity mainly below Äspö. Upconing of saline water can be seen in the figures.

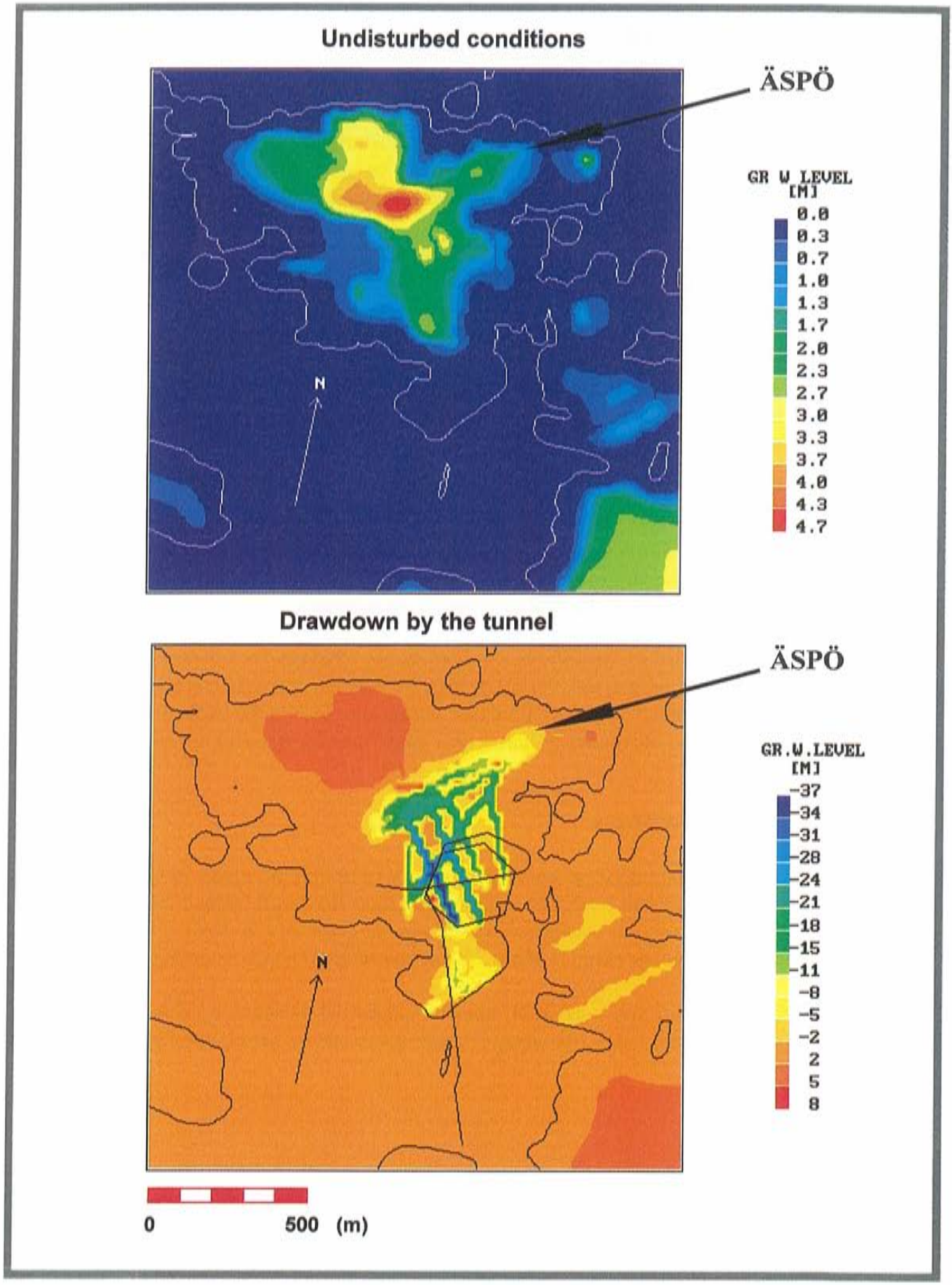

Figure 8-12. *Site scale groundwater flow model. Water table (metre above mean sea level). /Svensson,1997b/. Top: Natural conditions. Bottom: Drawdown due to inflow to Äspö HRL.*

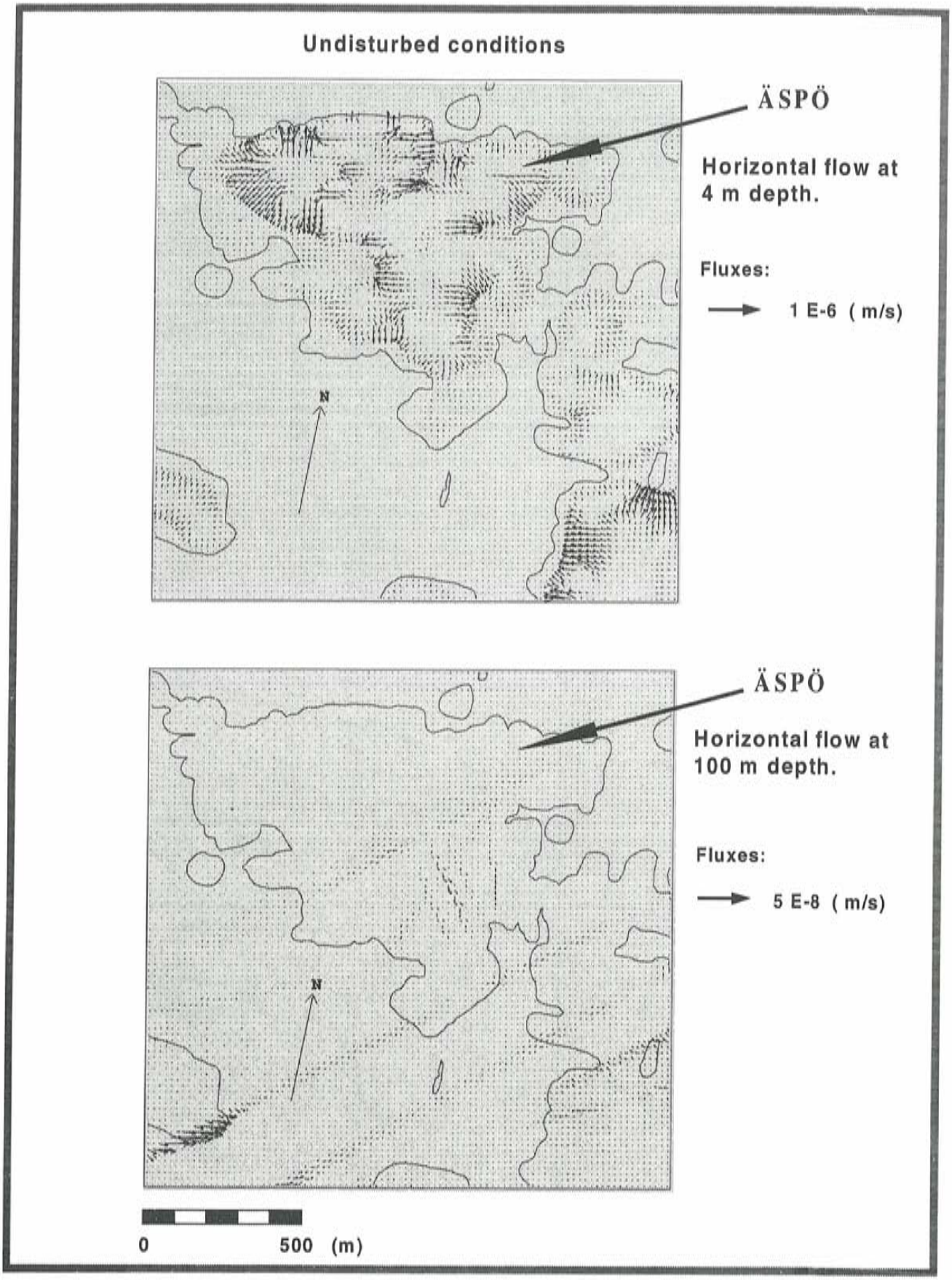

Figure 8-13. *Site scale groundwater flow model. Natural conditions. /Svensson, 1997b/. Top: Horizontal flow at 4 m depth. Bottom: Horizontal flow at 100 m depth. Darcy velocity scale: Vector length 10 mm = $5 \cdot 10^{-8}$ m/s.*

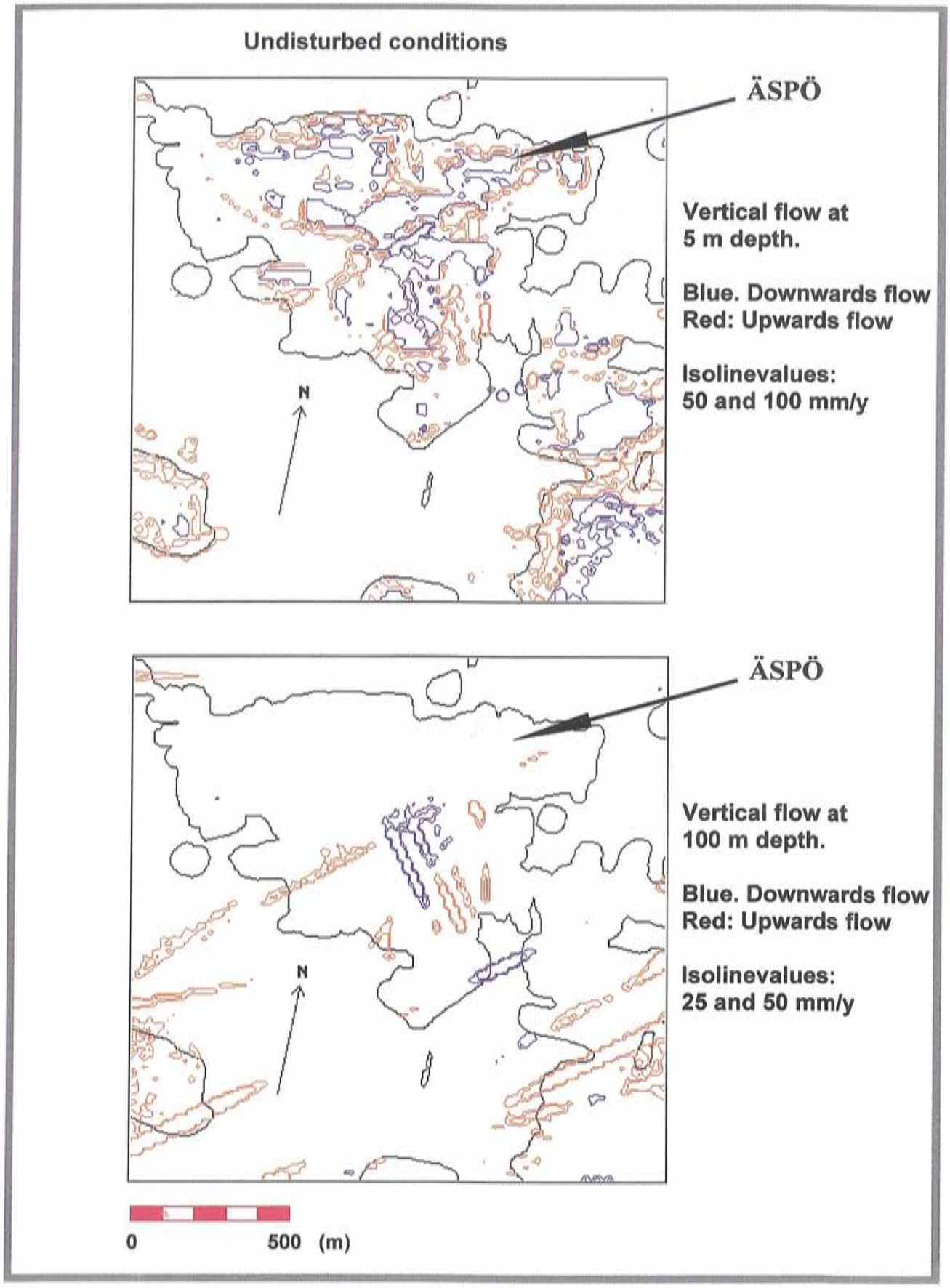

Figure 8-14. *Site scale groundwater flow model. Natural conditions. Blue colour indicates downwards and red upwards flow /Svensson, 1997b/. Top: Vertical flow at 5 m depth. Bottom: Vertical flow at 100 m depth.*

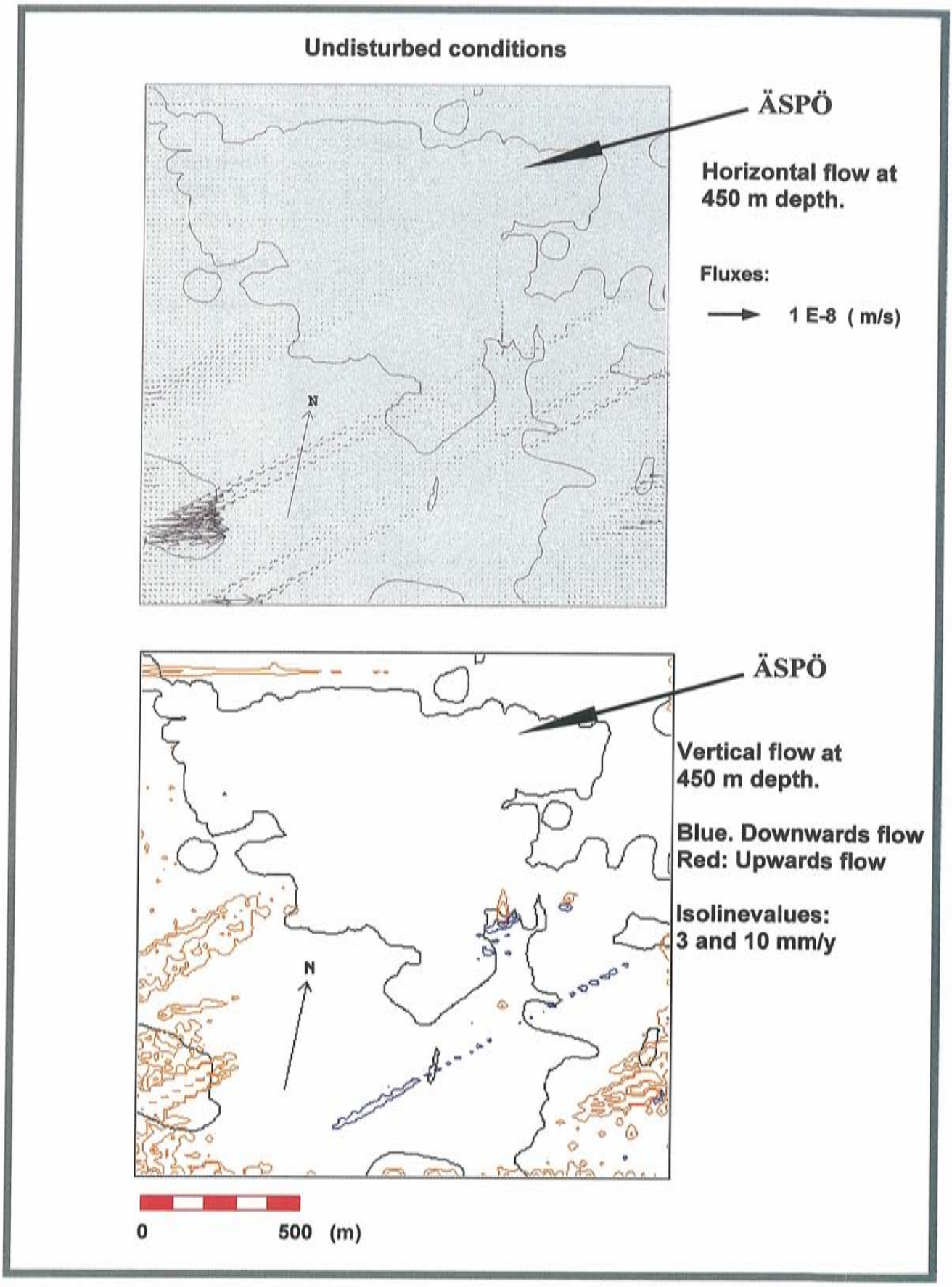

Figure 8-15. *Site scale groundwater flow model. Natural conditions. Blue colour indicates downwards and red upwards flow /Svensson, 1997b/. Top: Horizontal flow at 450 m depth. Bottom: Vertical flow at 450 m depth.*

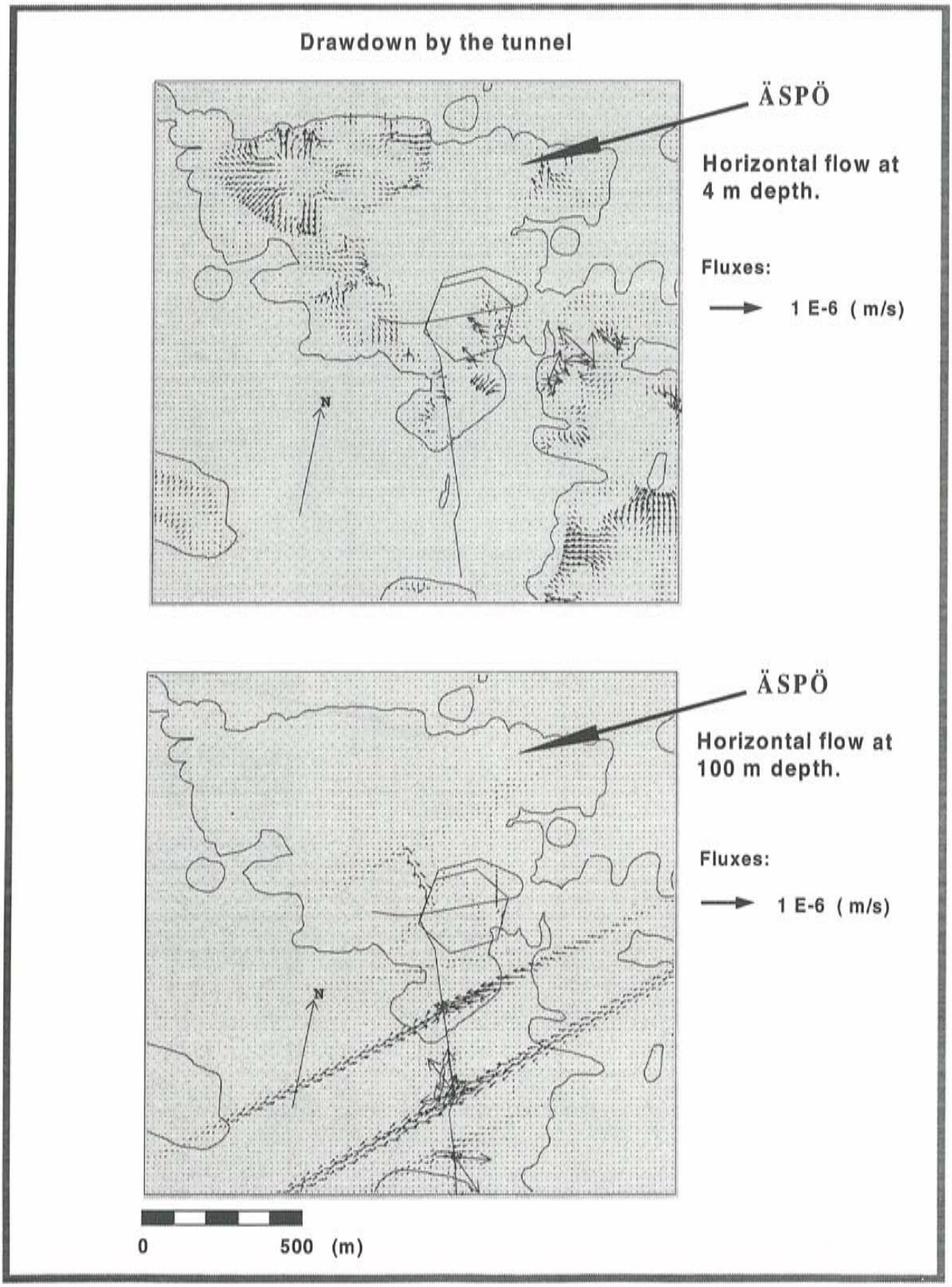

Figure 8-16. *Site scale groundwater flow model. Drawdown due to inflow to Äspö HRL. /Svensson, 1997b/. Top: Horizontal flow at 4 m depth. Bottom: Horizontal flow at 100 m depth.*

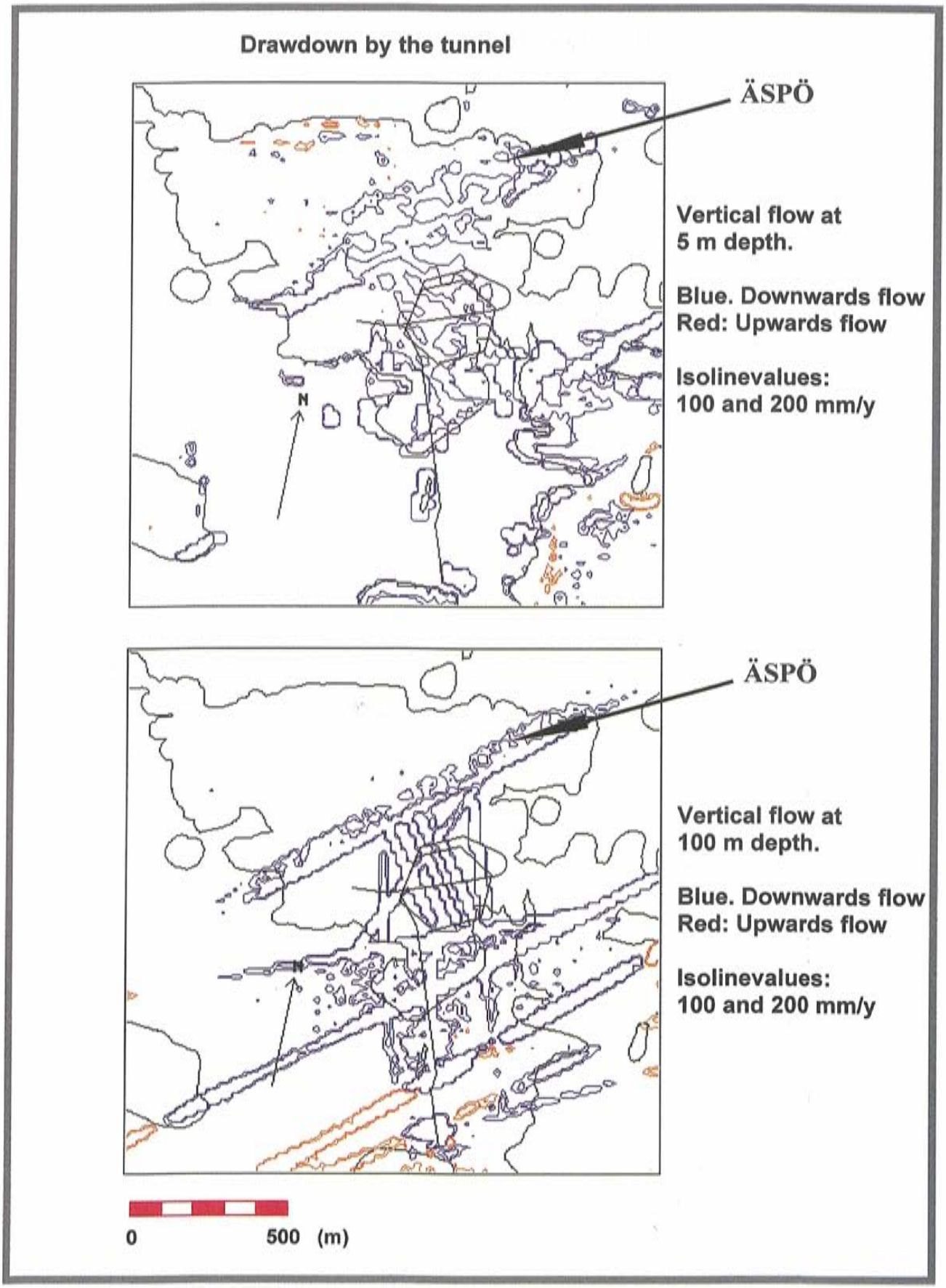

Figure 8-17. *Site scale groundwater flow model. Drawdown due to inflow to Äspö HRL. Blue colour indicates downwards and red upwards flow /Svensson, 1997b/. Top: Vertical flow at 5 m depth. Bottom: Vertical flow at 100 m depth.*

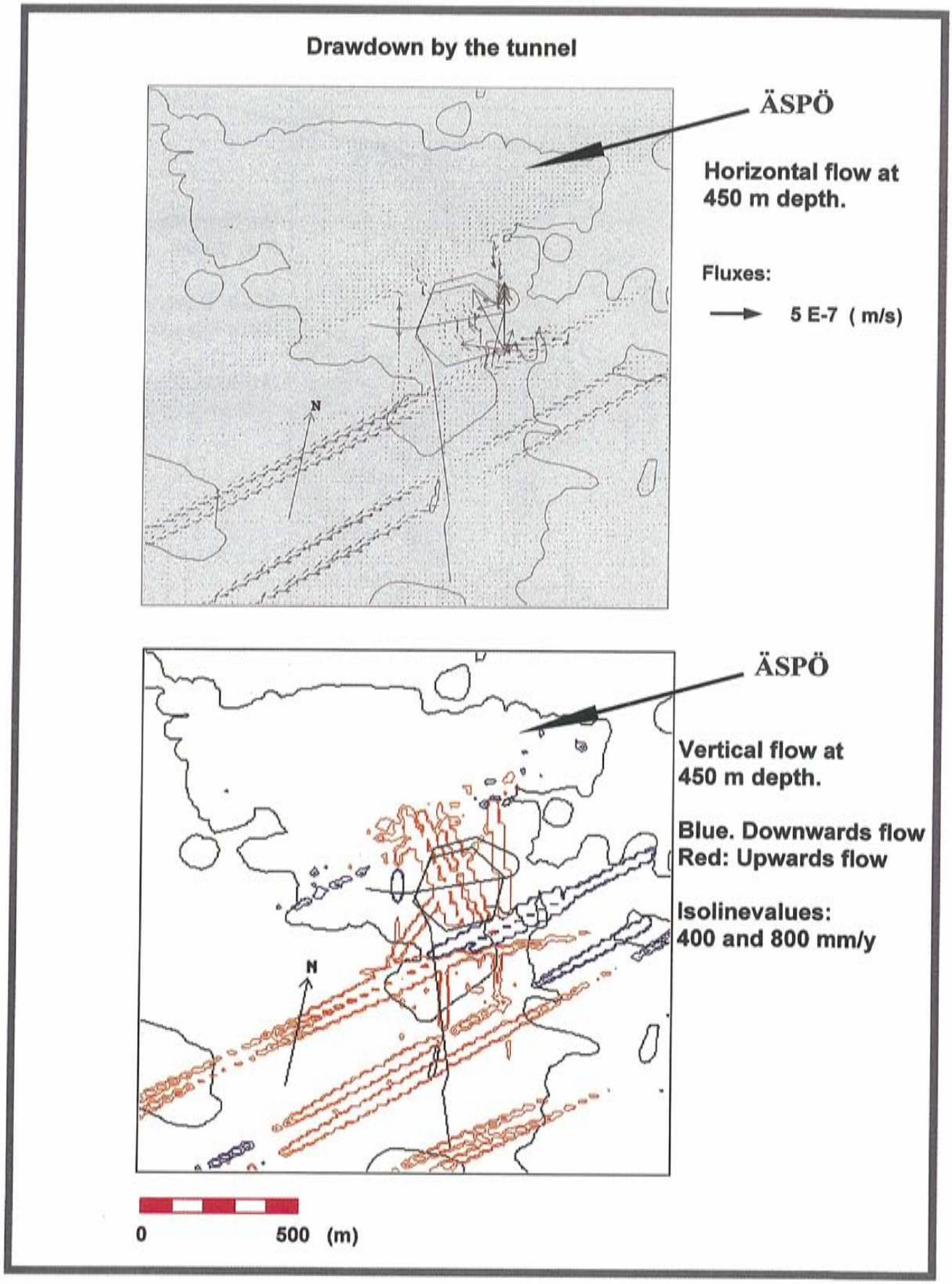

Figure 8-18. *Site scale groundwater flow model. Drawdown due to inflow to Äspö HRL. Blue colour indicates downwards and red upwards flow /Svensson, 1997b/. Top: Horizontal flow at 450 m depth. Bottom: Vertical flow at 400 m depth.*

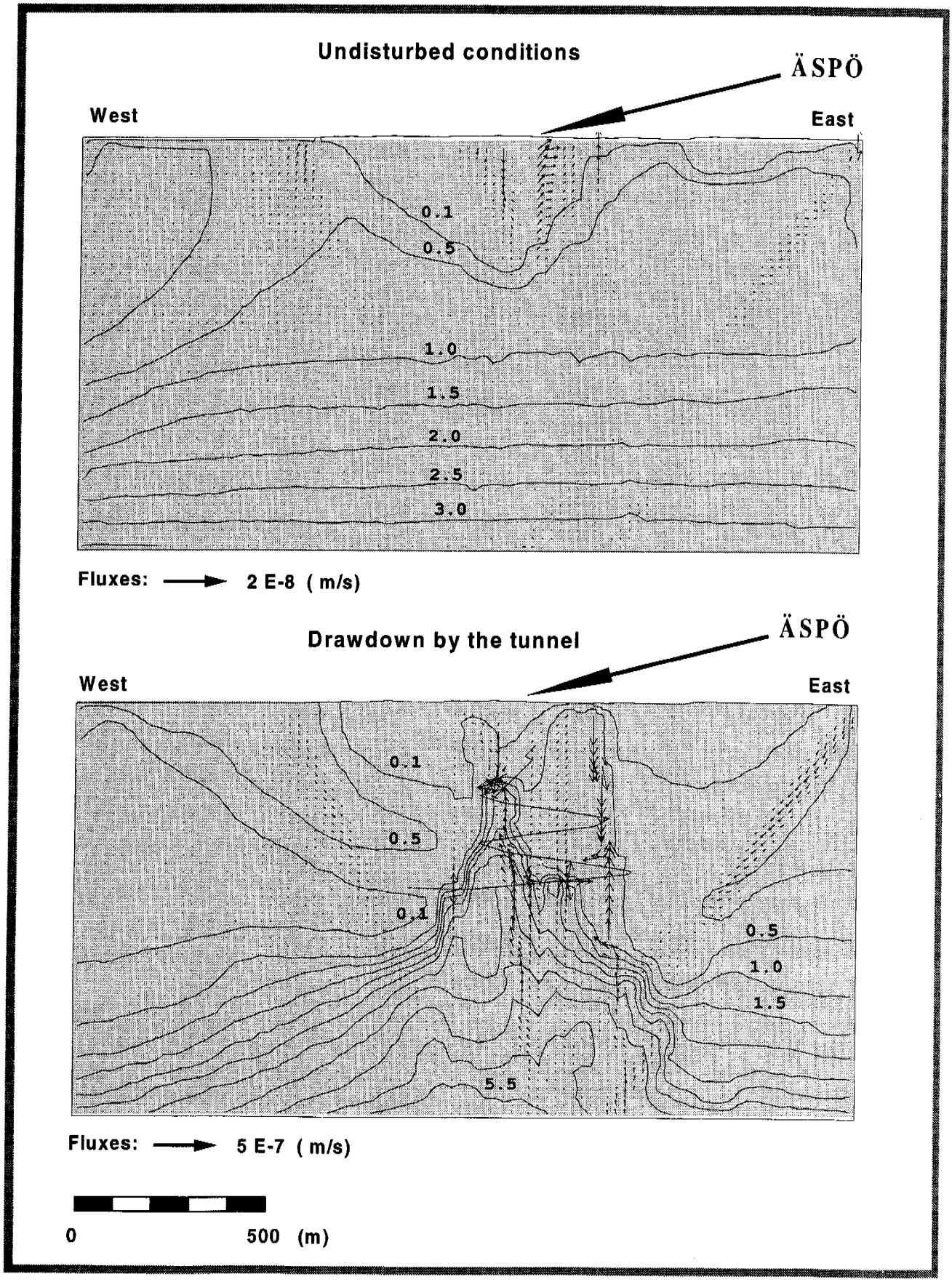

Figure 8-19. *Site scale groundwater flow model. West-East vertical sections through Äspö HRL.Salinity fields in %. Top: Natural conditions. Bottom: Drawdown due to inflow to Äspö HRL. (Note: Flow field from surface down to 20 m depth is not shown). /Svensson, 1997b/.*

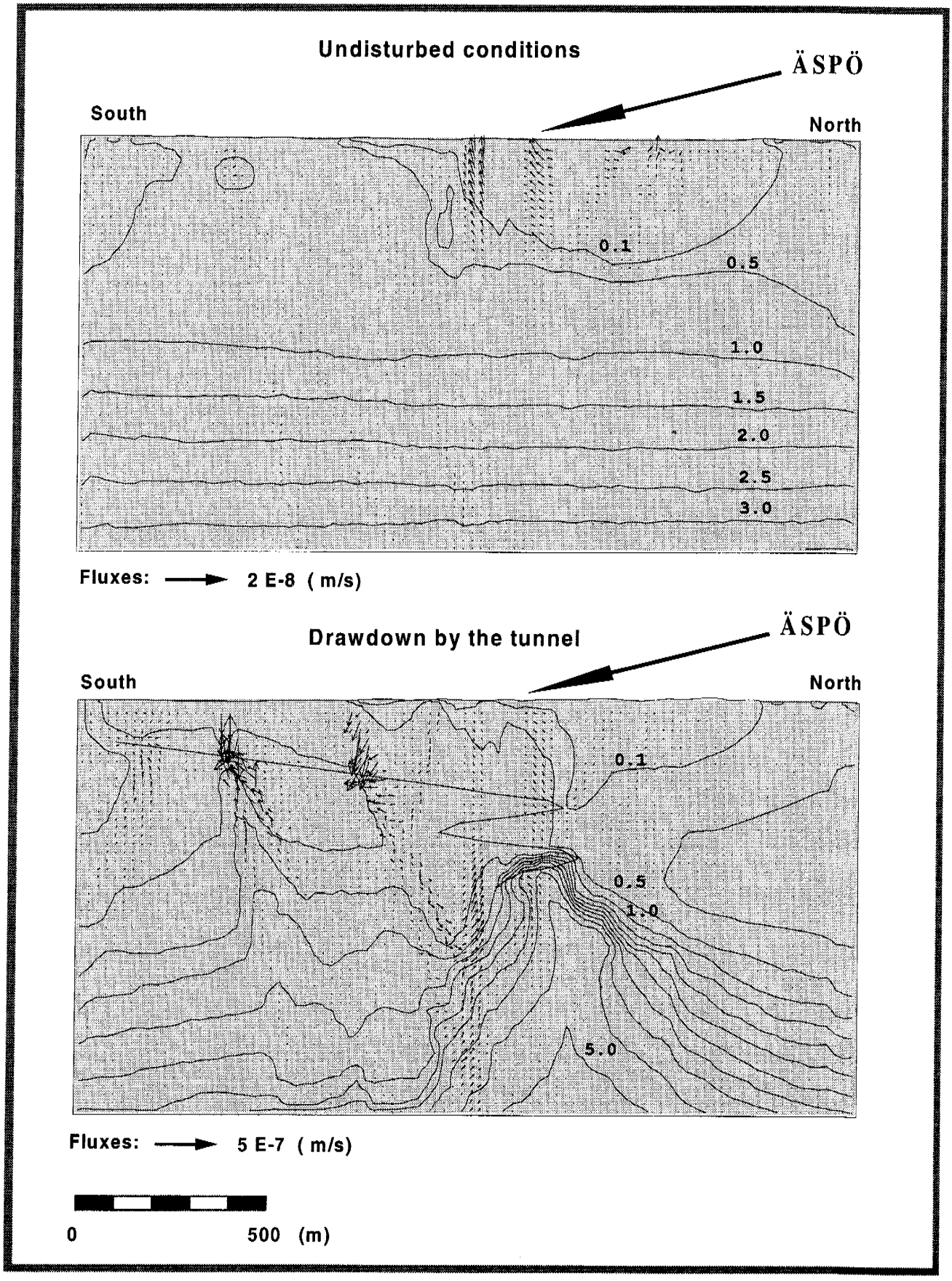

Figure 8-20. *Site scale groundwater flow model. North-South vertical sections through Äspö HRL. Salinity fields in %. Top: Natural conditions. Bottom: Drawdown due to inflow to Äspö HRL. (Note: Flow field from surface down to 20 m depth is not shown). /Svensson, 1997b/.*

Box analysis of the fluxes

In *Svensson /1997b/* the water and salinity fluxes over the boundaries of large control volume, more or less corresponding to the site model, and a smaller with dimension 600 · 400 · 400 m^3 were calculated. In *Table 8-4* the results for the smaller box is shown. The tables illustrates the magnitudes in the fluxes.

The fluxes and salinity distribution in the present site scale model is also illustrated for depth level 450 m in *Figures 8-21* to *8-23* and *Tables 8-5* to *8-6*. *Figures 8-21* and *8-22* show the fluxes through the cell walls for each computation cell and the magnitude or the flux-vector (called RES-Flux in the figures and tables) computed as the vector sum of the cell wall fluxes. The deterministic hydraulic conductor domains are indicated in the figures by higher fluxes. The absolute values of the fluxes in *Figures 8-21* and *8-22* are also illustrated in a probability distribution plot in *Figure 8-23* and some characteristic values for the fluxes are shown in *Table 8-5* and *8-6*.

According to the calculations the average salinity of the water flowing into the tunnel is 0.69 %, with a variation from 0.11% (NNW-1 crossing tunnel section 1745-1883 m) to 3.04% (NNW-1 crossing tunnel section 3179- 3426 m) for the different hydraulic conductor domains. The electrical conductivity of the water flowing into each tunnel section, limited by the dams in the tunnel, have been measured a few times */Rhén et al, 1995/*. Values from April and November 1995 showed a salinity of about 0.77 % for tunnel section 1745-1883 m, 0.6% (min value for the tunnel spiral) for tunnel section 2028-2178 m, 1.5% (max value along the entire tunnel) for tunnel section 2699-2840 m and 1.2% for tunnel section 3179-3411 m. The values indicate that the model can still be improved.

Table 8-4. Box analysis of the fluxes over the boundaries of a box with the Äspö coordinates X: 1840 to 2440 m, Y: 7100 to 7500 m and Z: -600 to -200 m. / *Svensson, 1997b/*. Positive flux: flux in the positive coordinate direction. "Flux" in the table is the sum of the cell fluxes over one of the sides in the box.
X: positive direction towards East in Äspö coordinate system.
Y: positive direction towards North in Äspö coordinate system.
Z: positive direction is upwards in Äspö coordinate system.

Boundary	Net flux (l/s)	Positive flux (l/s)	Negative flux (l/s)	Max Darcy velocity (m/s)	Min Darcy velocity (m/s)	Salt flux (g/s)
NATURAL CONDITIONS						
West	-4.0E-4	3.0E-3	3.4E-3	4E-10	-2E-9	0.19
East	6.9E-3	7.0E-3	1.0E-4	1E-9	-9E-11	0.47
South	9.0E-3	9.8E-3	8.0E-4	2E-9	-2E-10	0.69
North	-8.0E-4	6.0E-3	6.8E-3	8E-10	-2E-9	0.18
Bottom	-1.0E-3	1.0E-3	2.0E-3	2E-10	-4E-10	-0.15
Top	1.0E-3	2.0E-2	1.9E-2	3E-9	-1E-9	0.12
ÄSPÖ HRL						
West	0.69	0.69	0	9E-8	-2E-13	2.19
East	-1.71	0	1.71	7E-11	-1E-7	-7.98
South	1.26	1.39	0.13	2E-7	-6E-8	9.95
North	-1.77	0.15	1.92	6E-8	-2E-7	-14.08
Bottom	2.31	2.53	0.22	3E-7	-8E-8	76.71
Top	-2.87	0.13	3.0	8E-8	-1E-7	-14.75

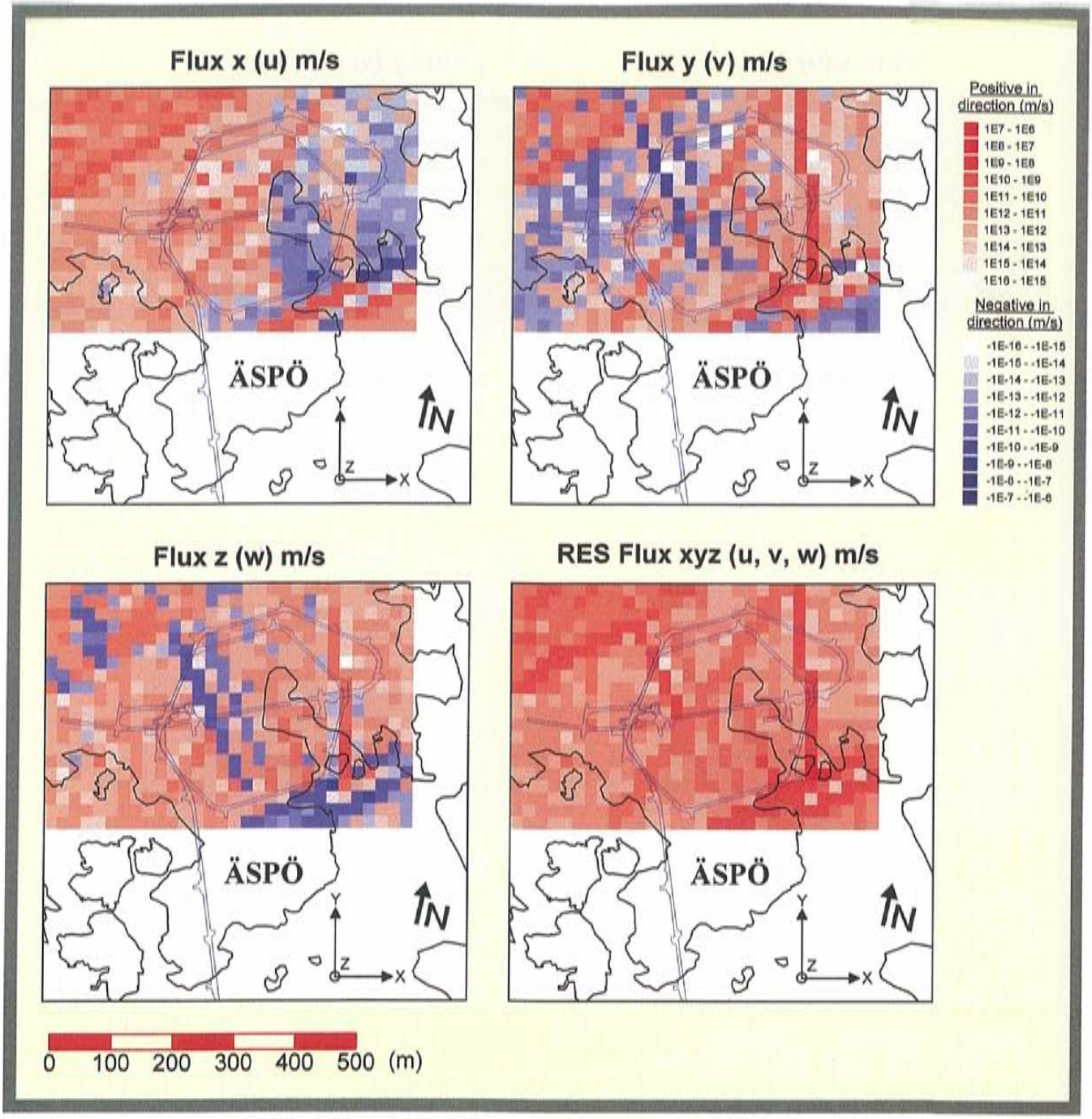

Figure 8-21. *Darcy fluxes at a depth of 450 m. Natural conditions. /Svensson, 1997b/.*

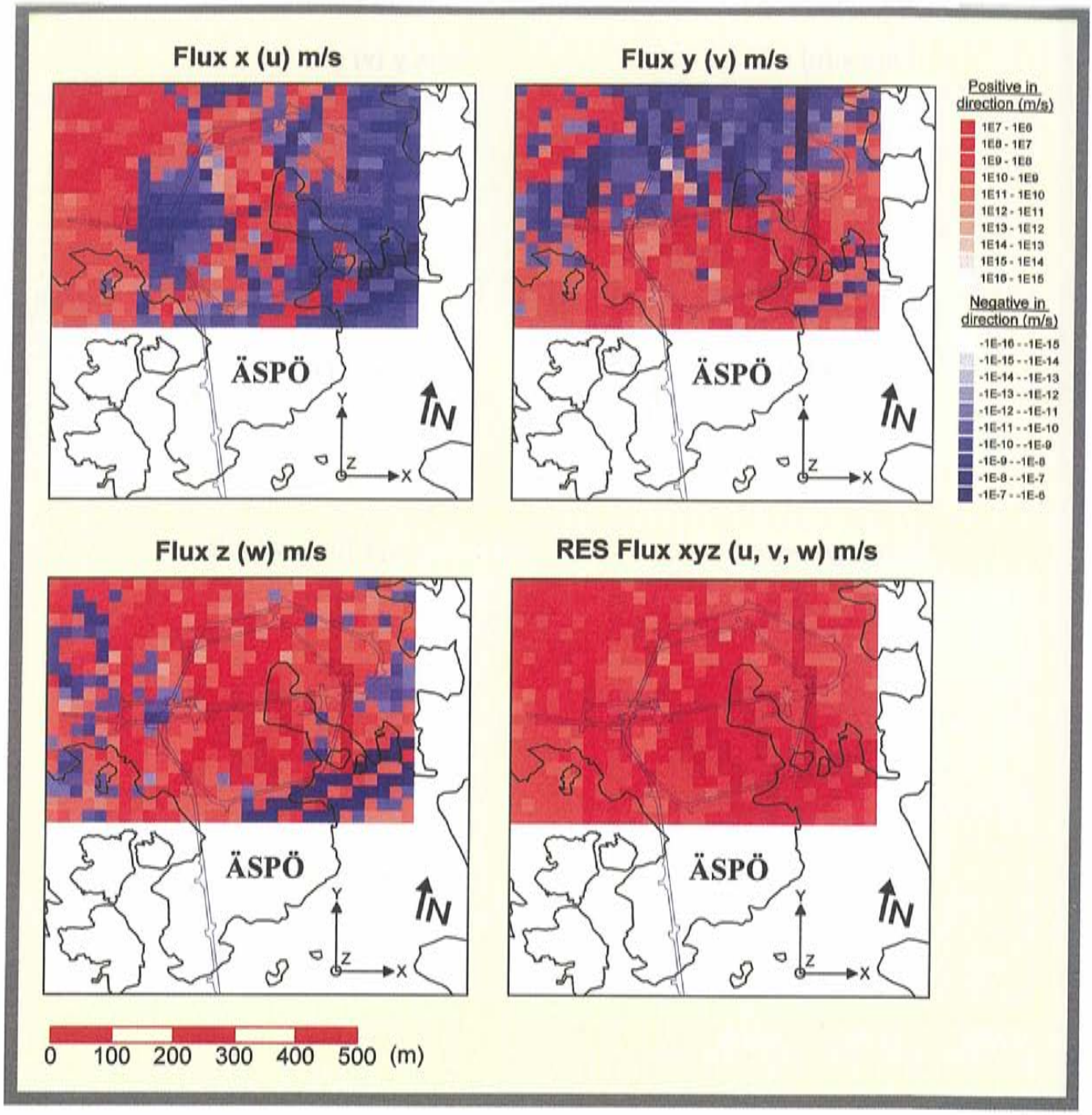

Figure 8-22. *Darcy fluxes at a depth of 450 m. Drawdown by the Äspö HRL-tunnel face at 3600 m. /Svensson, 1997b/.*

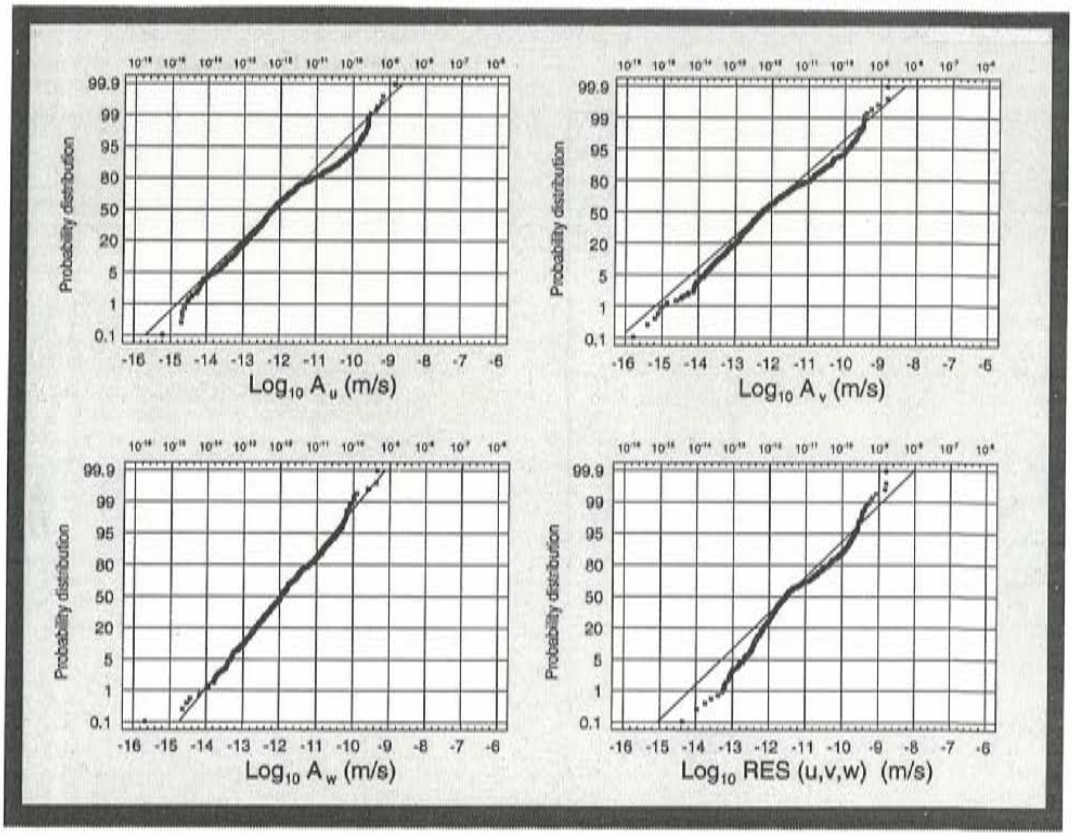

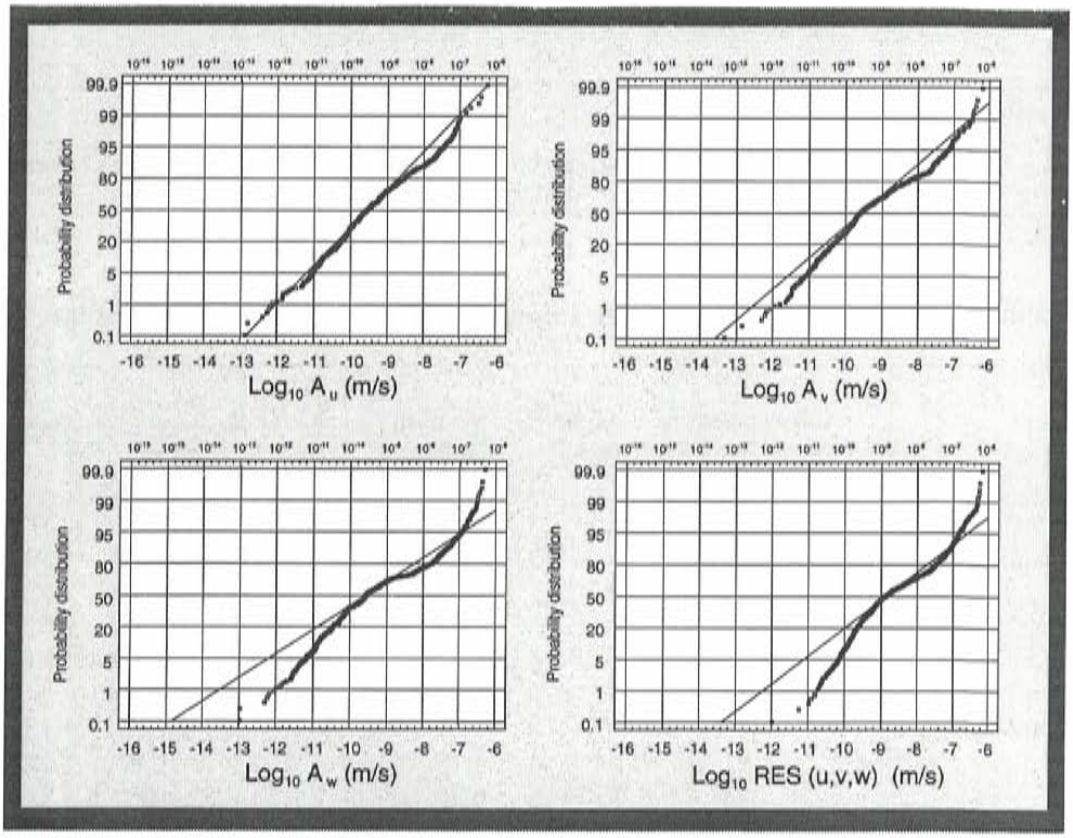

Figure 8-23. *Statistics of the absolute value of Darcy fluxes at a depth of 450 m, shown in Figures 8-21 and 8-22. Top: Natural conditions. Bottom: Drawdown by the Äspö HRL-tunnel face at 3600 m. /Svensson, 1997b/.*

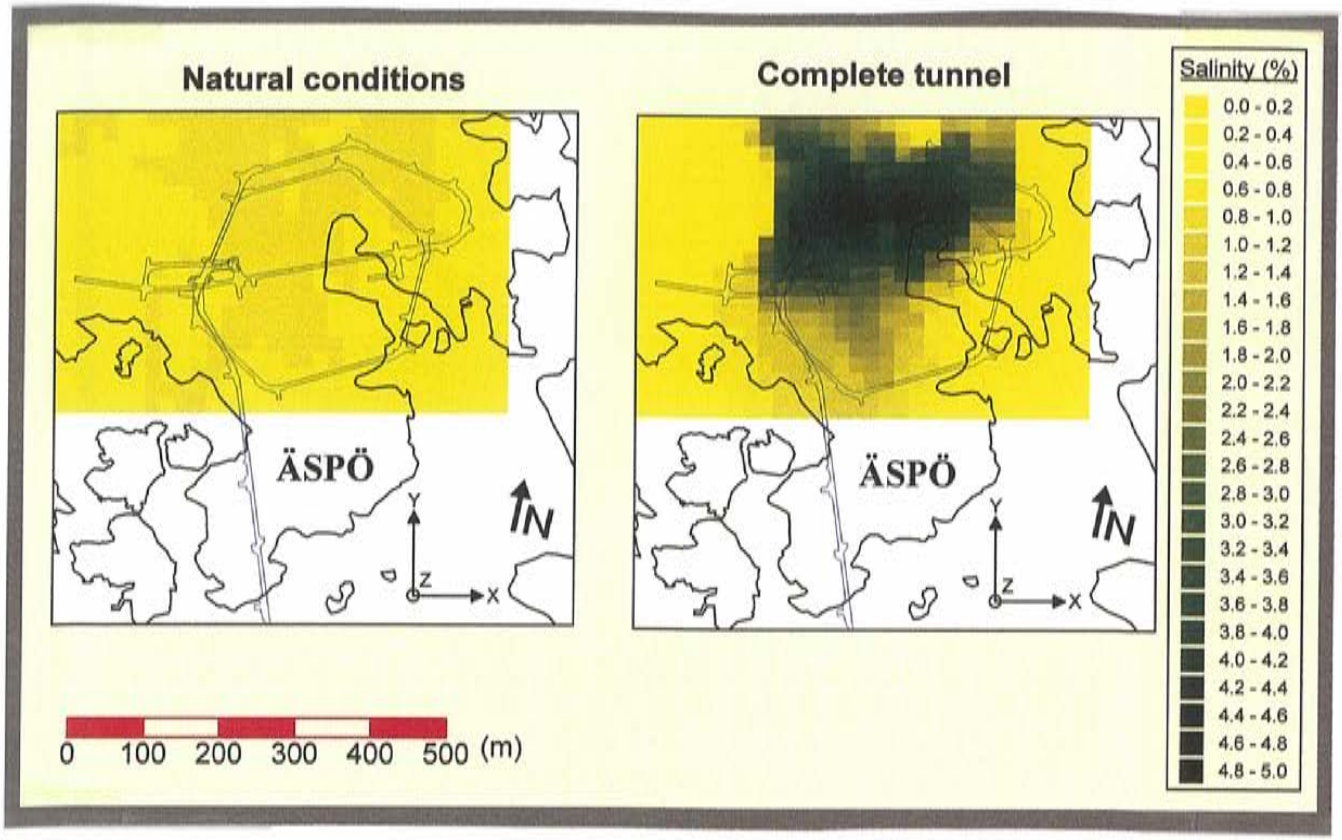

Figure 8-24. *Salinity distribution at a depth of 450 m for natural conditions and with complete tunnel. /Svensson, 1997b/.*

Table 8-5. Statistics of the absolute values of the fluxes at a depth of 450 m.

Case	Component (X)	Mean (X) (m/s)	Median (X) (m/s)	Min (X) (m/s)	Max (X) (m/s)	$sLog_{10}$ (X)
Natural conditions	A_u	9.7E-13	6.8E-13	6.2E-16	1.4E-09	1.19
	A_v	8.7E-13	5.8E-13	1.6E-16	1.5E-09	1.25
	A_w	1.2E-12	1.1E-12	2.1E-16	4.5E-10	0.92
	RES (u, v, w)	4.7E-12	2.9E-12	4.3E-15	1.6E-09	1.01
Complete tunnel	A_u	3.8E-10	2.8E-10	1.4E-13	5.8E-07	1.15
	A_v	4.6E-10	2.7E-10	4.8E-14	6.3E-07	1.27
	A_w	5.4E-10	2.8E-10	1.1E-13	5.0E-07	1.42
	RES (u, v, w)	2.3E-09	1.4E-09	1.1E-12	6.9E-07	1.15

Table 8-6. Statistics of salinity at a depth of 450 m.

Case	Component (X)	Mean (X) (%)	Median (X) (%)	Min (X) (%)	Max (X) (%)	$sLog_{10}$ (X)
Natural conditions	Salinity	0.78	0.78	0.66	0.85	0.04
Complete tunnel	Salinity	1.38	0.73	0.05	4.54	1.36

Transport

The transport time from deeper level up to surface is illustrated in *Figures 8-25* to *8-26*. Kinemetric porosity was assigned to elements according to *Section 8.3* and the particles were tracked for 100 years. As illustrated in the figures about 15 % of the particles will reach surface in 100 years if the particles are released at a depth of 450 m. If the particles are released at 550 m depth none will reach the surface in 100 years, while about 50 % will reach the surface if the particles are placed at a depth of 350 m. The sensitivity to the initial depth is mainly due to the density stratification.

The salinity and flow field is also illustrated for a few hydraulic conductor domains in *Svensson /1997b/*. Those figures illustrate that both the salinity and flux field can be rather complex. One example is shown in *Figure 8-27*.

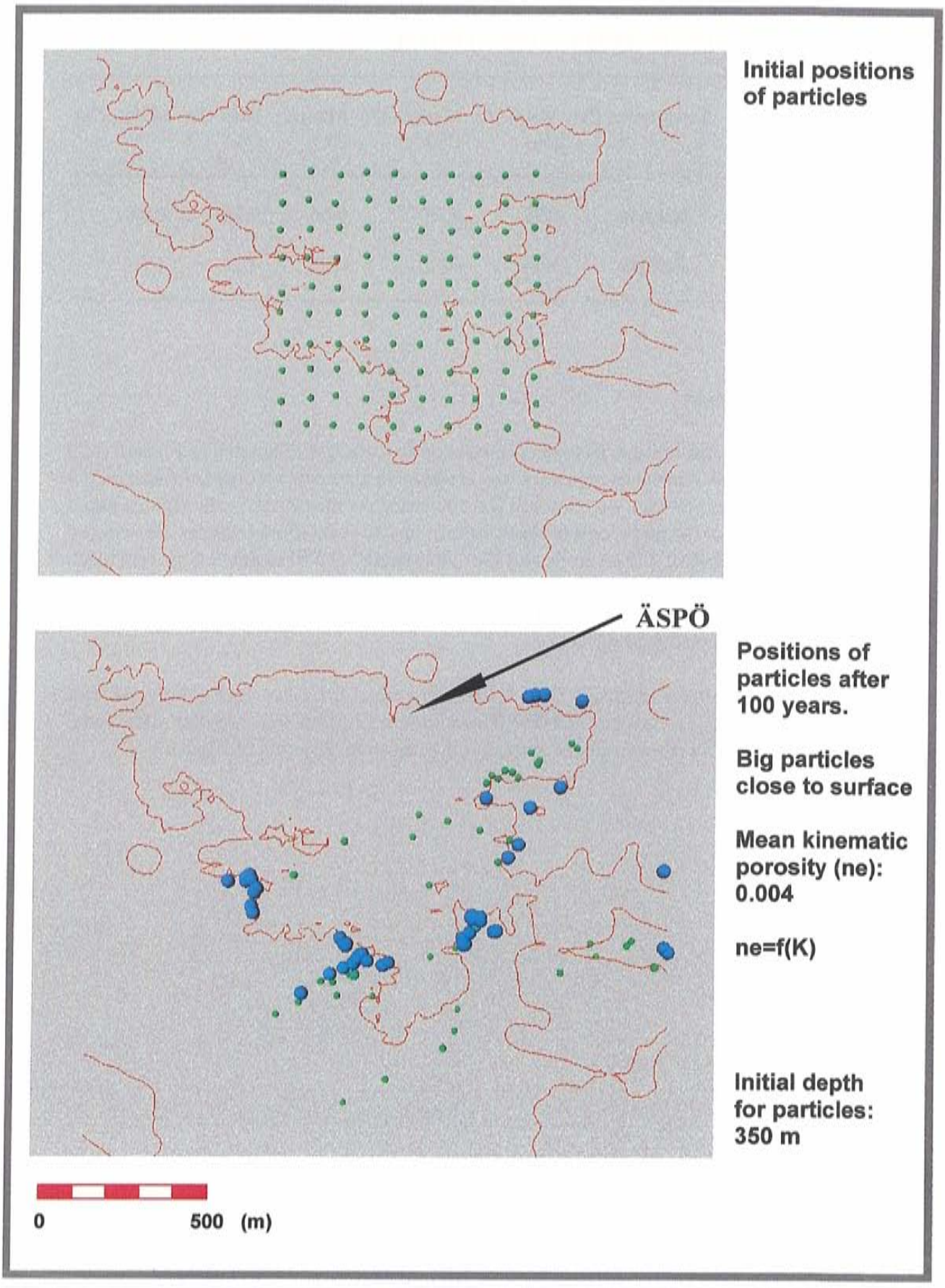

Figure 8-25. *Transport time. Big blue particles are close to ground surface, while smaller ones are at deeper levels. Top: Initial positions of particles. Bottom: Positions of particles after 100 years for an initial depth of 350 m. /Svensson, 1997b/.*

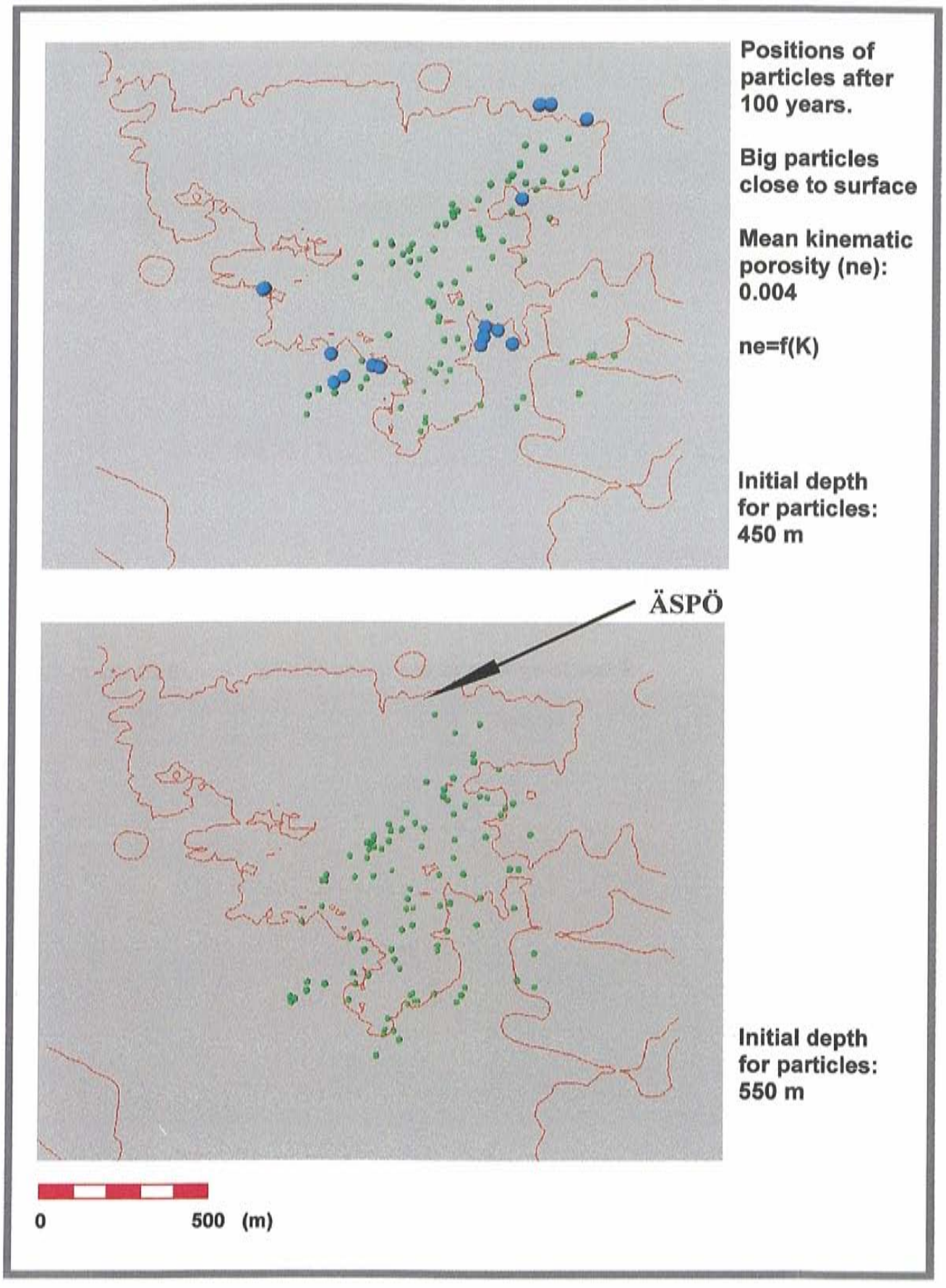

Figure 8-26. *Transport time. Big blue particles are close to ground surface, while smaller ones are at deeper levels. Top: Positions of particles after 100 years for an initial depth of 450 m. Bottom: Positions of particles after 100 years for an initial depth of 550 m. /Svensson, 1997b/.*

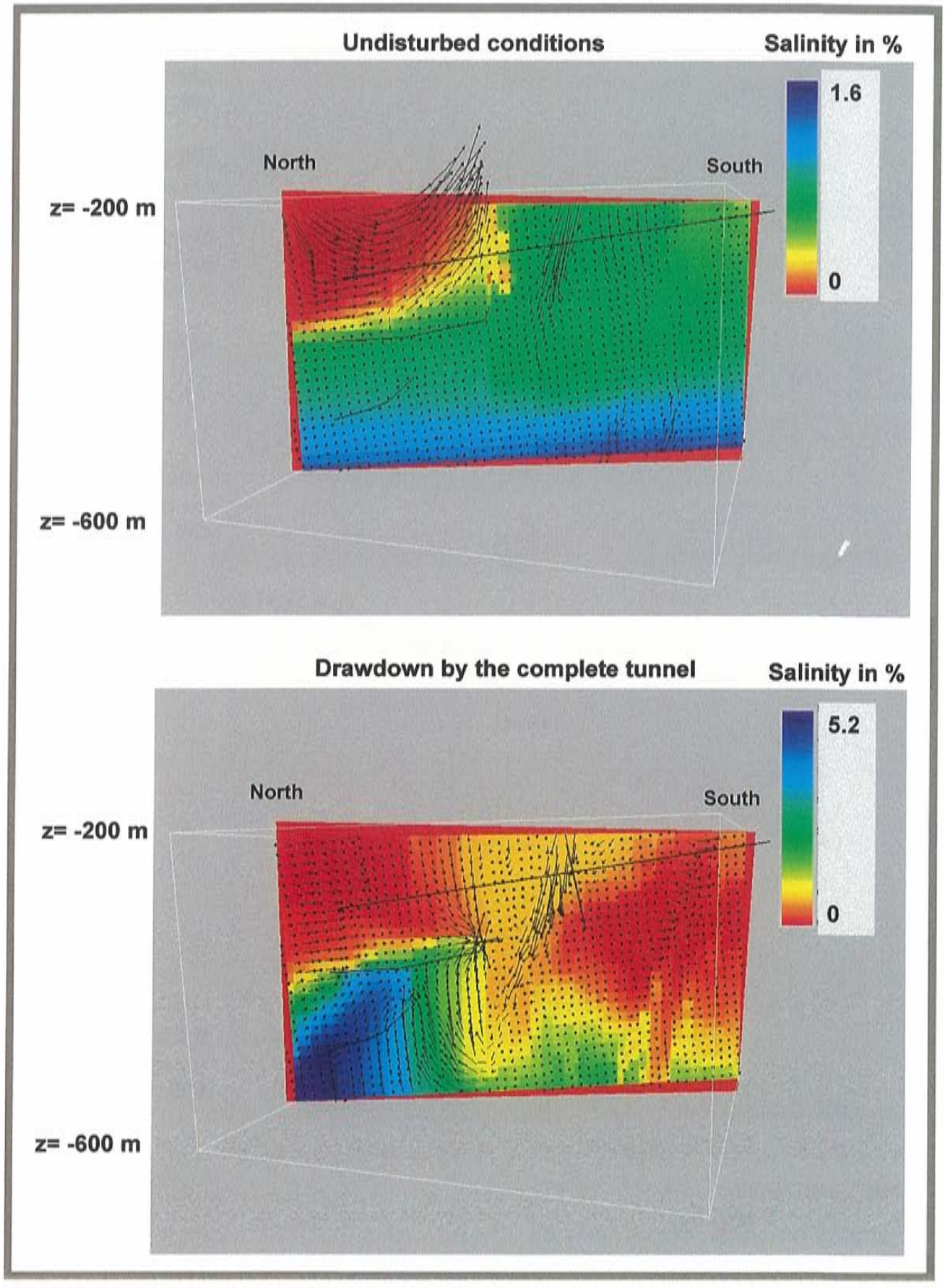

Figure 8-27. *Flow and salinity distribution in hydraulic conductor domain NNW-1 for depth interval -200 to -600 m. View from West. Salinity in %. (The red part of the domain outside the box only illustrates the plane). Top: Natural conditions. Bottom: Complete tunnel. /Svensson, 1997b/.*

8.3 TRANSPORT PARAMETERS

8.3.1 Background

A few tests have been performed at the Äspö HRL with the objective to estimate the transport properties of the rock. These tests are described below briefly.

At the Äspö HRL a Long-Term-Pumping test (called LPT2) was performed on the southern part of Äspö in 1990 */Rhén et al 1992/*. During this test tracers were injected into a number of boreholes with the main purpose of testing the connectivity of the conductive system. The dilution in the injection sections was monitored and the arrival of the tracers was monitored in the pumped borehole.

During the construction of the tunnel a simple tracer test was performed in hydraulic conductor NE-1 */Rhén and Stanfors 1993, Stanfors et al 1992/*. The purpose was to obtain some indications of the kinematic porosity before the tunnel penetrated the hydraulic conductor NE-1.

Extensive investigations were performed in a conductive structure intersecting the tunnel at approximately tunnel section 500 m, at about 70 m depth below Hålö */Gustafsson et al, 1994; Banwart et al 1995/*. As a part of these investigations, hydro tests and a tracer test were performed in the conductive structure.

A project called Tracer Understanding Experiment (TRUE) was started in 1995 and the first tracer test was performed in late 1995 */Winberg (ed), 1996/*. The tests were performed in a rock of fairly low conductivity.

The evaluations in the reports above were based on **analytical methods** assuming radial or linear flow. Some of the results presented in these reports have been plotted below. The **results** from the Äspö HRL **presented in the figures below are based on the radial flow assumption**, as it is considered to be somewhat more realistic concerning the flow field for these cases. The transport aperture and kinematic porosity were evaluated as below:

$$e_T = \frac{Q_w \cdot t_0}{\pi \cdot (r^2 - r_w^2)} \qquad (8\text{-}1)$$

e_T	=	Transport aperture	(m)
Q_w	=	Discharge from fracture zone	(m^3/s)
r	=	Distance to point of tracer injection	(m)
r_w	=	Radius of borehole	(m)
t_0	=	Mean travel time for the tracer	(s)

$$n_e = e_T / b_T \quad (8\text{-}2)$$

$$K = T / b_T \quad (8\text{-}3)$$

b_T	=	Approximate zone width assumed to be representative for evaluated T	(m)
K	=	Effective hydraulic conductivity	(m/s)
T	=	Transmissivity	(m^2/s)

To put the data from Äspö in a general perspective data from a compilation from the literature on tracer tests in fractured rocks presented by *Andersson /1995/* are shown. The evaluation methods used were analytical and/or numerical and the evaluated parameters are given as a single value or range for each parameter. In the figures below the range for evaluated parameters is shown as a rectangle or line and the arithmetic mean value of the range is shown as an open circle or open triangle. The tests presented in the figures below were performed in crystalline rock and are reported to have been performed in fracture zones, densely fractured rock or a single fracture (see *Figures 8-29, 8-30* and *8-31*).

As can be seen in the figures the variability is generally large. The reason is probably due to different conditions at different sites but probably also due to the evaluation methods used. The equations below should be considered as approximative relations that can be used for scoping calculations if no conditions specific to the site are known.

8.3.2 Kinematic porosity and transport aperture

Crystalline rock is generally fractured and the groundwater flows mainly in the larger fractures because of the low permeability of the matrix between the larger fractures. A strict distinction between fractures and matrix cannot be made as fractures down to micro fractures between or through the mineral grains can be found. However, as larger fractures are generally assumed to be the fractures that are hydraulically well-connected and also most transmissive, a useful concept for advective flow is to divide the rock mass into (large) fractures and matrix. For advective transport on the detailed scale (1-10 m) and larger it is the kinematic porosity of the fractures on these scales that is of interest.

As it is difficult to obtain site-specific values of the kinematic porosity (n_e) and the transport aperture (e_T) it is useful if these can be correlated to other parameters such as transmissivity (T) and hydraulic conductivity (K). The rationale for expressing n_e as a function of K and e_T as a function of T is the relationship between the fracture aperture and equivalent hydraulic conductivity for a system of parallel and continuous fractures, in which the hydraulic conductivity of the matrix (K_m) is neglected */Marsily, 1986/*:

$$K = \frac{e}{b_f} \cdot K_f \cdot \frac{F}{C_F} = \frac{1}{b_f} \cdot T_f \cdot \frac{F}{C_F} =$$

$$= \frac{e}{b_f} \cdot \frac{e^2 \rho g}{12 \mu} \cdot \frac{F}{C_F} \qquad (8\text{-}4)$$

b_f	=	Mean distance between fractures	(m)
C_F	=	Correction coefficient for flow regime	(-)
e	=	Fracture aperture	(m)
F	=	Open fracture surface area / total fracture surface area	(-)
g	=	Acceleration of gravity	(m^2/s)
K_f	=	Intrinsic fracture hydraulic conductivity	(m/s)
T_f	=	Fracture transmissivity	(m^2/s)
μ	=	The dynamic viscosity of the fluid	(Pa s)
ρ	=	Fluid density	(kg/m^3)

For laminar flow $C_F = 1$.

The kinematic porosity can be estimated using a simplified model of a fracture system consisting of matrix blocks of equal size shaped like plates or cubes (see *Figure 8-28*). It is assumed that the fracture aperture between the blocks and the block size are both constant The relationship between permeability (k) based on the cubic law, total fracture porosity (n), kinematic porosity (n_e), fracture width (e) and block size (b_f) is shown in *Table 8-8*. It is further assumed that fracture width is much smaller than the block size and that the flow direction is parallel to fracture planes for the plates or one of fracture planes separating the cubes. If the blocks are shaped like matches the values will be equal to or between the values for plates and cubes in *Table 8-8*.

Table 8-8. Permeability and porosity of simplified models of the fracture systems illustrated in *Figure 8-28*. Assumption: $e << b_f$.
b_f: distance between joints (m), e: fracture aperture (m), n: total porosity, n_e: kinematic porosity, k: permeability (m^2).

	n (-)	n_e (-)	k(n, e) (m^2)	k(n_e, e) (m^2)	k(n, b_f) (m^2)	k(n_e, b_f) (m^2)
plates	e/b_f	e/b_f	$e^2 \cdot n/12$	$e^2 \cdot n_e/12$	$n^3 \cdot b_f^2/12$	$n_e^3 \cdot b_f^2/12$
cubes	$3e/b_f$	$2e/b_f$	$e^2 \cdot n/18$	$e^2 \cdot n_e/12$	$n^3 \cdot b_f^2/162$	$n_e^3 \cdot b_f^2/48$

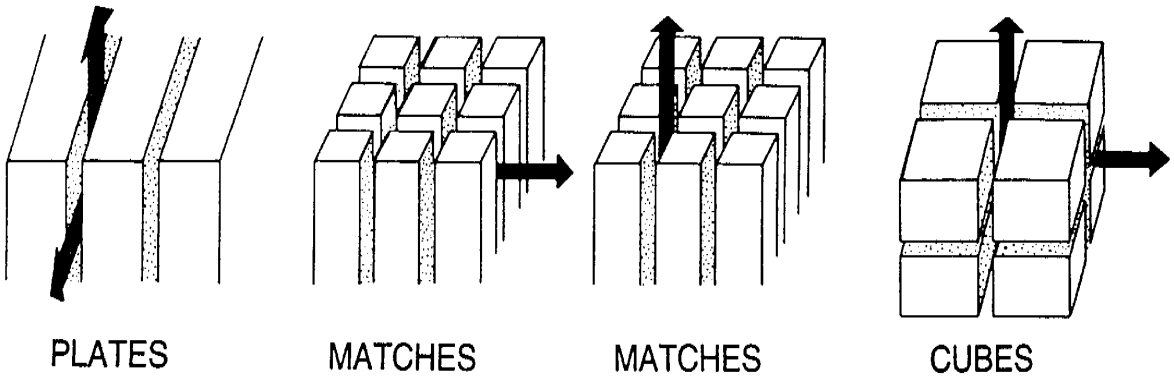

Figure 8-28. *A simplified model of a fracture system consisting of matrix blocks of equal size shaped either as plates, matches or cubes. /After van Golft-Racht 1982/.*

For a multi-fracture random distribution, the permeability can be expressed as */van Golft-Racht 1982/*:

$$k = n^3 / (29.9 \cdot (P_{21})^2) \quad (8\text{-}5)$$

From *Table 8-8* the relationship below can be set up:

$$n_e = (k)^{1/3} \cdot (1/b_f)^{2/3} \cdot C_1 \quad (8\text{-}6)$$

where the constant C_1 is about 2.3-3.6. If the hydraulic conductivity (K) is put into *Equation 8-6* instead of k the constant C_1 will become about 0.01-0.02,

assuming $F=C_F \approx 1$ and water temperature 10°C. It may be seen from *Equation 8-6* that if the permeability increases at the same time as the distances between the fractures decrease, the increase in the kinematic porosity relative to the permeability will be somewhat greater than $(k)^{1/3}$. For b_f = 20- 0.01 m $(1/ b_f)^{2/3}$ becomes about 0.1-22 and C_2 in *Equation 8-7* will be in the range:

b_f (m)	C_2 $(s/m)^{(1/3)}$
20	$1.6 \cdot 10^{-3}$ -$2.5 \cdot 10^{-3}$
10	$2.5 \cdot 10^{-3}$ - $4 \cdot 10^{-3}$
2	$7.4 \cdot 10^{-3}$-$1.2 \cdot 10^{-2}$
1	$1.2 \cdot 10^{-2}$ - $1.9 \cdot 10^{-2}$
0.1	$5.4 \cdot 10^{-2}$ - $8.6 \cdot 10^{-2}$
0.01	$2.5 \cdot 10^{-1}$ - $4 \cdot 10^{-1}$

$$n_e = (K)^{1/3} \cdot C_2 \qquad (8\text{-}7)$$

As shown in *Chapter 6,* b_f for the more or less intact rock mass can possibly be within the range 2-20 m (1/ P_{10} in *Table 6-25,* 100-10 % of the fractures conducting water), thereby putting C_2 in range 0.01-0.001. The values for n_e in *Winberg (ed) /1996/* indicate C_2 values around 0.01, which compares rather well with the b_f in the table above as the two features tested are considered to be one or a few fractures over a test length of a few metres. The evaluated kinematic porosity from the tests in NE-1, NNW-2 and the Redox zone indicate C_2 values around 0.1 to 0.6. NE-1 is a highly fractured zone about 30 m wide. The Redox zone is about one metre wide and highly fractured. NNW-2 is interpreted as being 10-30 m wide and with a higher fracture frequency compared with the surrounding rock.

The limited data above indicate that an increase in the hydraulic conductivity should be coupled to an increase in the fracture frequency. This seems reasonable. *Figure 8-29* shows a plot of the limited data from the Äspö HRL. In *Figure 8-29* the kinematic porosity (n_e) is plotted as a function of the hydraulic conductivity (K) and *Equation 8-8* shows the linear approximation between Log_{10} (K) and $Log_{10}(n_e)$.

$$n_e = 34.87 \cdot K^{0.753} \qquad (8\text{-}8)$$

Equation 8-8 was tested numerical site model presented in *Section 8.2.6.* The arithmetic mean kinematic porosity was calculated to 0.006. However, in some very conductive cells the kinematic porosity became large. Assuming that the kinematic porosity for a cell never can be larger than 0.05 gives a arithmetic mean kinematic porosity of 0.004 in the site model. (The hydraulic conductivity field was based on the implemented hydraulic conductor domains and the hydraulic rock mass domains).

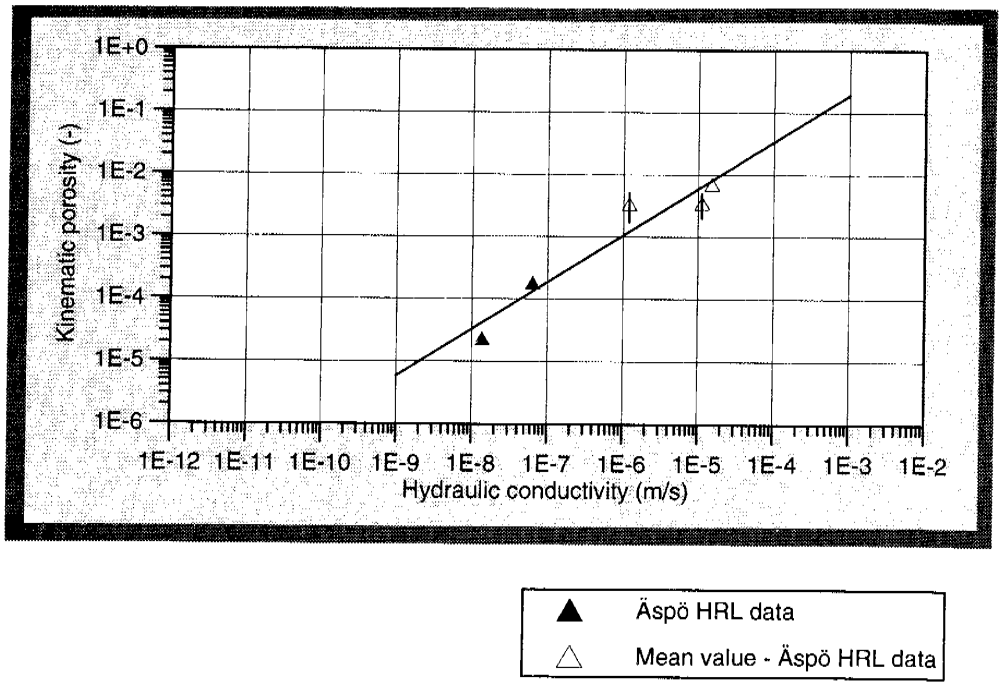

Figure 8-29. *Kinematic porosity versus hydraulic conductivity. Data from the Äspö HRL. In the figure the range for evaluated parameters is shown as a line and the arithmetic mean value of the range is shown as an open triangle. The tests presented in the figures below were performed in crystalline rock and are reported to have been performed in fracture zones, densely fractured rock or a single or a few fractures. The line is based on a least-square fit of the points indicated by circles and triangles. The highest value is based on the tests in NE-1, the two lowest values from the first tests in the TRUE project and the other two is related to the LPT2 test and the test in the Redox zone. The K value is estimated from a judged zone width and the evaluated transmissivity.*

The transport aperture (e_T) may be defined as the total width needed for the total flow, thus an effective value of the sum of a number of fracture apertures, see *Equation 8-1*. If it assumed that the flow takes place in a number of sub-parallel fractures (flow in two dimensions) the following relationships can be set up. If the flow takes place in a number of sub-parallel fractures (flow in two dimensions) the transmissivity can be estimated at */Earlougher R C, 1977 /*:

$$T = \sum_{n=1}^{i} T_{fi} \qquad (8\text{-}9)$$

T_{fi}	=	Transmissivity of fracture i	(m^2/s)
T	=	Transmissivity	(m^2/s)

Using *Equation 8-4, Equation 8-9* can be transformed into *Equation 8-10* in which C_3 is approximately $0.63 \cdot 10^6$ at a water temperature of 10°C:

$$T = \sum_{n=1}^{i} C_3 \cdot e_i^3 \qquad (8\text{-}10)$$

If n fractures dominating the flow have approximately the same apertures the transport aperture can be expressed as *Equation 8-11* in which C_4 is approximately $1.2 \cdot 10^{-2}$:

$$e_i = (T)^{1/3} \cdot (1/n)^{1/3} \cdot C_4 \qquad (8\text{-}11)$$

$$e_T = n \cdot e_i = (T)^{1/3} \cdot (n)^{2/3} \cdot C_4 \qquad (8\text{-}12)$$

e_T = Transport aperture (m)
n = Number of fractures

If the number of fractures increases with the transmissivity (T) the transport aperture increases by a factor of more than $(T)^{1/3}$ according to *Equation 8-12.* If the number of fractures increase from 1 with $T=10^{-10}$ m^2/s to 40 with $T=10^{-4}$ m^2/s the transport aperture will increase by approximately $(T)^{1/2}$ *:*

T (m^2/s)	n (-)	e_T (m)
10^{-10}	1	$5.6 \cdot 10^{-6}$
10^{-10}	10	$2.6 \cdot 10^{-5}$
10^{-4}	1	$5.6 \cdot 10^{-4}$
10^{-4}	10	$2.6 \cdot 10^{-3}$
10^{-4}	40	$6.5 \cdot 10^{-3}$
10^{-4}	100	$1.2 \cdot 10^{-2}$

By using the mean travel time for a non-sorbing tracer and an assumption of the flow dimension it is possible to estimate the mean total fracture width needed for the transport, here called the transport aperture (e_T), by considering the mass balance, see *Equation 8-1.*

In *Figure 8-29* the transport aperture (e_T) is plotted as a function of transmissivity (T). *Equation 8-13* shows the linear approximation between $Log_{10}(T)$ and $Log_{10}(e_T)$.

$$e_T = 1.428 \cdot T^{0.523} \qquad (8\text{-}13)$$

e_T = Transport aperture (m)
T = Transmissivity (m^2/s)

If the transmissivity and the transport aperture have been evaluated an approximate estimate of the number of dominating flowing fractures can be estimated from *Equation 8-12* and *8-13*.

Equation 8-12 and *8-13* give the approximate number of fractures for a given transmissivity.

$$N = 1300 \bullet (T^{0.523\text{-}1/3})^{3/2} \approx 1300 \bullet T^{0.28} \qquad (8\text{-}14)$$

The high transmissivity (T) values in *Figure 8-30* represent data for NE-1, a fracture zone at Finsjön in Sweden and URL in Canada. The fracture zone with T around $4 \cdot 10^{-6}$ m^2/s is situated at Finsjön and the fracture zones with T around $1 \cdot 10^{-6}$ m^2/s are situated at Stripa in Sweden and Chalk River in Canada. The range for the calculated transport aperture was very large for the Stripa case according to *Andersson /1995/*. The other Äspö zones are NNW-2, the Redox zone and the feature A and B in *Winberg (ed) /1996/*. As can be seen in *Figure 8-23* the transport aperture will increase by about $(T)^{1/2}$ indicating an increasing number of fractures as the transmissivity increases.

It should be remembered that values shown in *Figures 8-29* and *8-30* and *Equations 8-8*, *8-13* and *8-14* represent some mean values that should be associated with increasing volumes (scales) as K or T are increasing. Locally the transport aperture may be quite large. According to *Chapter 4* centimetre wide fractures in fracture zone NNW-4 were observed in the tunnel. The variability shown in these figures also indicates that the equation should be seen as approximate relations.

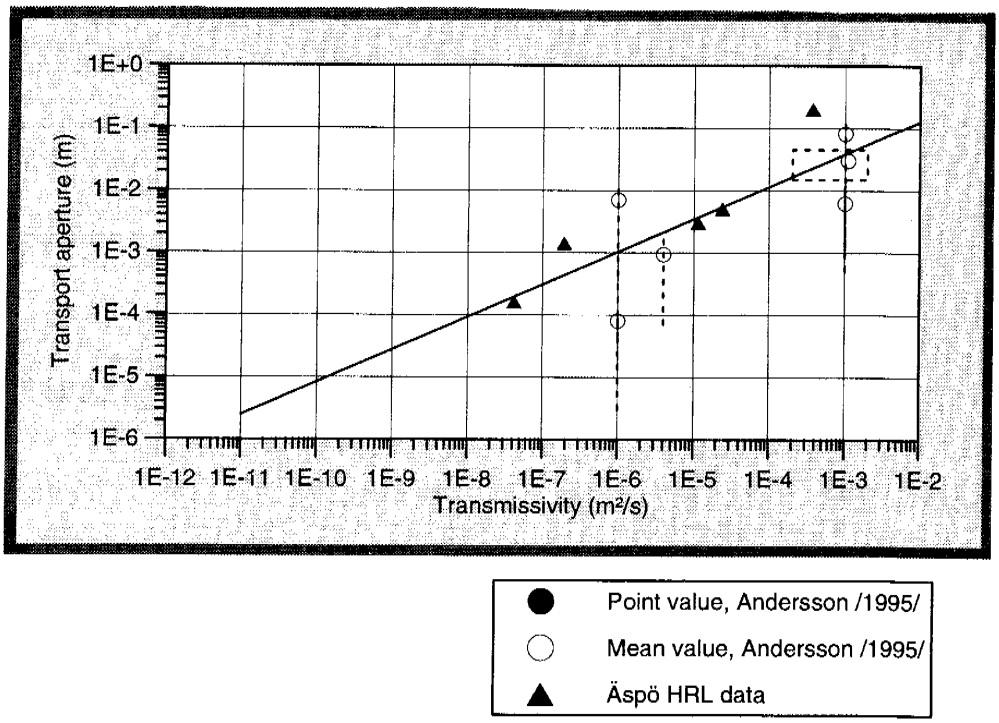

Figure 8-30. *Transport aperture versus transmissivity. Data from Andersson /1995/ and the Äspö HRL. In the figure the range for evaluated parameters is shown as a line and the arithmetic mean value of the range is shown as an open circle. The tests presented in the figures below were performed in crystalline rock and are reported to have been performed in fracture zones, densely fractured rock or a single or a few fractures. The line is based on a least-square fit of the points indicated by circles and triangles.*

8.3.3 Matrix porosity

The porosity of rock samples from the Äspö HRL has been determined using a number of different methods. Hg injection porosimetry, water saturation (imbibition) followed by drying the samples and, finally, He gas expansion technique. The results are compiled in *Mazurek et al /1996/.* A few results from the report are presented below.

Fresh and undeformed rocks

Fine-grained granite has the lowest porosity (averages: 0.23-0.27 % by volume), followed by Småland granite (0.17-0.38 % by volume) and Äspö diorite (0.40-0.45 % by volume).

Foliated rocks and mylonites

Three samples had approximately the same porosities as the fresh and undeformed rocks. However, analyses using some methods indicated low porosities (< 0.08 % by volume), and core impregnations show that the mylonites, due to their low grain-size and full recrystallization, have lower porosities than undeformed rocks.

Cataclasites

The porosity distribution in epidotic cataclasites is highly inhomogeneous (0.5-2.5 % by volume).

Hydrothermally altered rocks

The average porosity (0.43 % by volume) is slightly higher than that of fresh rock. Excluding a sample of weakly altered fine-grained granite the average porosity is 0.63 % by volume.

8.3.4 Dispersivity

As pointed out in *Chapter 3* dispersivity is a factor that takes into account the heterogeneity of the velocity field within a volume in which the hydraulic conductivity and effective porosity are assumed to be constant. In *Figure 8-31* the evaluated longitudinal dispersivity (α_L) is plotted as a function of the spatial scale (s). The spatial scale indicates the linear distance between the injection point and the sampling point. *Equation 8-15* shows the linear approximation between Log_{10} (s) and $Log_{10}(\alpha_L)$.

$$\alpha_L = 0.053 \cdot s^{1.210} \qquad (8\text{-}15)$$

α_L	=	Longitudinal dispersivity	(m)
s	=	Spatial scale	(m)

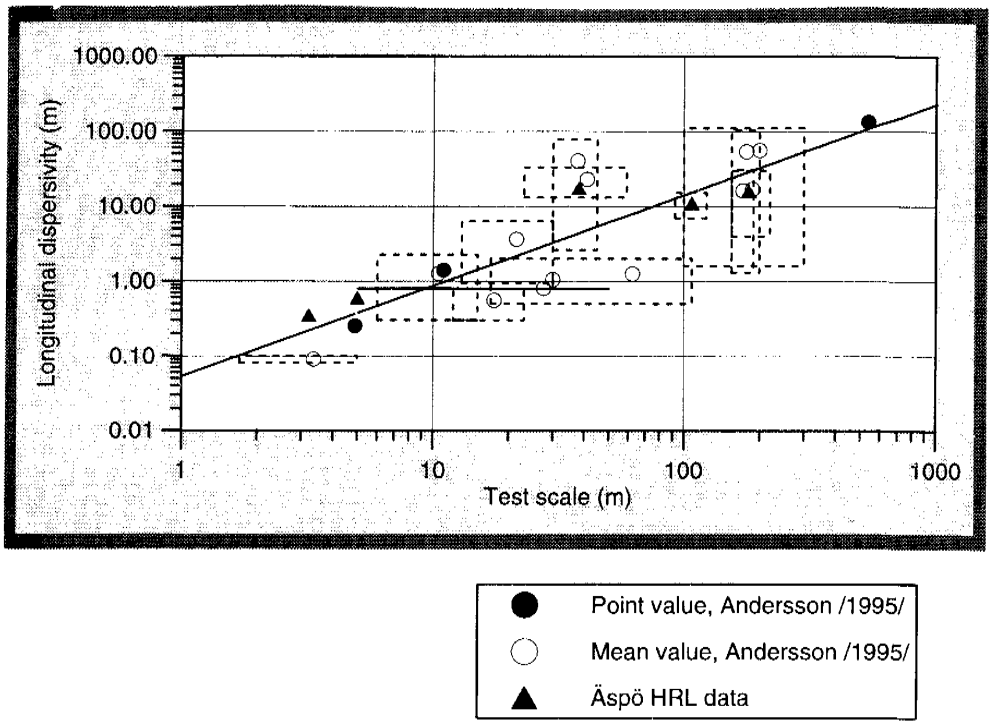

Figure 8-31. *Dispersivity versus test scale. Data from Andersson /1995/ and the Äspö HRL. In the figure the range of the evaluated parameters is shown as a line or a rectangle and the arithmetic mean value of the range is shown as an open circle. The tests presented in the figures below were performed in crystalline rock and are reported to have been performed in fracture zones, densely fractured rock or a single or a few fractures. The line is based on a least-square fit of the points indicated by circles and triangles.*

9 CONCLUDING REMARKS

General comments on the characterization of the rock mass

The contents of a model is always dependent on the intended use of the model. The areal extent, different types and the level of detail of investigations are thus closely linked to the objectives. However, the way the models are built up is also dependent on site specific conditions that are found during the investigations. Due to this the regional model is normally less detailed than the site scale model. Related to this are the "effective" properties considered important for a certain scale and how to estimate the "effective" properties in another scale. The transformation of "effective" properties from one scale to another is a problem which requires further attention.

It is important to clearly state the purpose of the model, the processes that are considered to be governing the situation that is to be studied and the concepts used. The conceptual model is the systematic description of the approaches and assumptions that are needed for models made for a certain scale. Having such description it will be easier to understand the limitations of the models and the data presented.

Integration between the different disciplines in both planning of investigations and evalution of main features is considered important for developing a consistent model and execution of investigations of good quality.

Below a few comments are outlined which are related to some of the possible future developments of the present models.

Characterization of the rock mass around Äspö HRL

The models in this report cover regional scale to detailed scale but the main focus in the report is the site scale models.

Geology

It is judged that the position and main orientation of the sub-vertical fracture zones near Äspö HRL are well known. The frequency and orientation of minor zones is partly known but their extent is less well known. The minor zones must be treated as a stochastic variable until detailed investigations from the tunnel can give a basis for describing some of them deterministically. The database of the small scale fracturing, the mapped fracture minerals and main fracture orientations is judged to be of good quality but less good regarding fracture spacing and fracture length. The discontinuity model can be improved if a better knowledge regarding the, possibly more or less continous spectrum,

of discontinuity spacing and discontinuity radius/extent can be achived. For example fracture frequency obsevations in boreholes and tunnels differ but to a large extent this is probably a matter of the scale of the observations.

Data on is how the properties within the rock change along a (major) fracture zone are limited. Better knowledge could improve the ability to localize tunnels.

Mechanical stability

The measured rock stress orientation is judged to be reliable. The stress levels presented in this report show great variability possibly due to a large natural variability. Work has already started to get a better understanding of the observed variability.

The evaluation of fracture surface properties involves major difficulties both in predicting and documenting the selected parameters. Fracture surface properties are, however, an important factor for the stability conditions in an underground construction.

Hydrogeology

It is important to perform tests on different scales systematically in the boreholes, both for scale relationships but also to gain flexibility in the interpretation of how to divide the rock mass into hydraulic conductor domains and hydraulic rock mass domains. It is also important to perform large-scale interference tests for modelling purposes, and to provide data for interpreting the hydraulic connectivity between the major fracture zones (or with the nomenclature in Chapter 6, hydraulic conductor domains).

The Äspö site is heterogenous and anisotropic on a large scale. That makes the investigations and evaluation work more extensive and difficult.

So far no spatial correlation model for hydraulic conductivity has been used in the groundwater flow simulations. Data has shown a large nugget effect in the variogram models and because of this a generated hydraulic conductivity field becomes essentially stochastic without any major correlation. However, there is probably some spatial correlation within the hydraulic rock mass domains due to the probable existence of a number of permeable features which are larger than the cell size in the present groundwater flow models.

A phenomenon related to the spatial correlation model is the fact that the arithmetic mean and standard deviation of Log_{10} (hydraulic conductivity) measured from a borehole section or entire borehole depends on the length of each test interval in the borehole and the test time. The evaluation made shows that the probability distributions of the (effective) hydraulic conductivity varies

with test scale. So far an empirical relationship has been used for transformation of the mean and the standard deviation between geometrical scales.

In conclusion, continued efforts should be made to try to find a methodology to define a reasonably good spatial correlation model for the hydraulic properties that can include the effects of anisotropy and scale dependency.

Hydrochemistry

The hydrochemical situation at Äspö suggests that a variety of groundwater regimes have been dominating for longer or shorter time periods since the latest glaciation due to land uplift and evolution of the Baltic sea. Glacial melt water, old and modern sea water and meteoric water, are mixed in different proportions with deep old saline water.

The evaluation of the hydrochemistry of Äspö resulted in a new development of a modelling tool called M3. The approach of M3 is to evaluate the effects of mixing as the dominating process behind the observed conditions. Chemical reactions and other processes affecting the chemical composition are considered to be of secondary importance. Further improvements of the tool is needed to further assess areas of its application.

The spatial variability of the groundwater composition is based on only a few points. The reason is that groundwater sampling normally is made in high transmissive borehole sections for technical and economical reasons. Attempts will be made to further develop and refine the sampling methodology and techniques as well as improving the understanding of differences between the low conductive and high conductive rock mass.

Redox conditions and also the general chemical conditions are important to define in a long term perspective. Currant work is starting from the fairly good understanding of the development of the conditions at Äspö since the latest glaciation and possibly also up to the next glaciation. Emphasis will be made to get a thorough understanding of the possible changes up to the next ten thousand years.

Microbial processes have been investigated and evaluated. For a thorough understanding of all aspects of relevance further work is needed.

Transport of solutes

Groundwater flow models for calculations of flow paths in the rock mass can be compared to the geochemical groundwater mixing and mass balance modelling to provide useful information on flow paths and transport times. However, there is still much work to be done to improve the integration between models on groundwater flow, groundwater chemistry and transport of solutes. A task related to this issue was 1997 initiated as part of the work that

is performed within the Äspö Task Force, with participants from several international organisations */Rhén et al, 1997/.*

Tracer tests are useful for checking the connectivity within and between hydraulic conductor domains. At a relatively small scale, about 50-100 m, it seems possible to get rough estimates of the flow porosity and dispersivity within a hydraulic conductor domain. At larger scales it is difficult to evaluate the transport properties but the tests can still be useful for defining hydraulic connectivity.

ACKNOWLEDGEMENTS

The listed reports in the foreword summarize the investigation and evaluation work carried out by a large number of skilled and enthusiastic people. A few of these have been involved throughout the entire project and made important contributions to the realization of the reports. We wish to mention especially:

Karl-Axel Kornfält and Hugo Wikman, Geological Survey of Sweden. (Bedrock investigations and petrographic analyses).

Håkan Stille, KTH, Stockholm, Pär Olsson, Skanska, Stockholm, Bengt Leijon, SKB, Stockholm and Bengt Stillborg, LTH, Luleå. (Rock stress measurement and Rock mechanics modelling).

Raymond Munier, Scandiaconsult, Stockholm and Jan Hermansson, Golder Associates, Stockholm. (Geological-structural field investigations and structural modelling).

Seje Carlsten and Per Askling, Geosigma, Uppsala. (Borehole radar investigations and CAD illustrations).

Mikael Erlström, Geological Survey of Sweden, and Ingemar Markström, Sydkraft Konsult, Malmö. (XRD analyses and CAD illustrations).

Peter Danielsson, Torbjörn Forsmark, Lars Nilsson, VBB Viak, Gothenburg. (Evaluation of hydraulic tests and data compilation for groundwater flow modelling and illustrations in the report).

Magnus Liedholm, VBB Viak, Gothenburg. (Analyses of hydrogeological data, accuracy and confidence of geological estimates).

Leif Stenberg, Kristian Annertz, Mats Olsson, Katinka Klingberg, SKB Äspö HRL, Robert Gass, Per Nilsson, VBB Viak, Bengt Gentzschein, Geosigma. (Tunnel data documentation).

Urban Svensson, CFE. (Numerical groundwater flow modelling).

Karl-Göran Nederfeldt, ÅF-IPK, Agne Bern, John Olausson, Kent Hansson, Lennart Ekman, Göran Nyberg, Stig Jönsson, Geosigma. (Field work, field support and groundwater monitoring).

Eva-Lena Tullborg, Terralogica. (Fracture mineralogy).

Marcus Laaksoharju, Intera KB, John Smellie, Conterra. (Hydrochemical modelling).

Bill Wallin, Geokema. (Isotope chemistry).

Ann-Chatrin Nilsson, KTH. (Hydro-chemical data quality control).

We are also grateful for the review of this report provided by peers at Posiva. We also like to acknowledge the review made by our colleagues at SKB. We are also grateful for Ingalill Gunnarsons and Eva Fritz's, VBB Viak, Göteborg, patience with our manuscripts. They have made most of the typing of this report and the reports 2-4.

REFERENCES

CHAPTER 1

Gustafson G, Liedholm M, Rhén I, Stanfors R, Wikberg P, 1991. Äspö Hard Rock Laboratory. Predictions prior to excavation and the process of their validation, SKB TR 91-23, Stockholm.

R&D-Programme 86, 1986, Parts I-III. Handling and final disposal of nuclear waste. Programme for research, development and other measures, SKB, Stockholm.

R&D-Programme 89, 1989, Parts I-II. Handling and final disposal of nuclear waste. Programme for research, development and other measures, SKB, Stockholm.

R&D-Programme 95, 1995, Parts I-II. Treatment and final disposal of nuclear waste. Programme for encapsulation, deep geological disposal and research, development and demonstration, SKB, Stockholm.

Rhén I (ed), Bäckblom (ed), Gustafson G, Stanfors R, Wikberg P, 1997a. Äspö HRL - Geoscientific evaluation 1997/2. Results from pre-investigations and detailed site characterization. Summary report. SKB TR 97-03.

Rhén I, Gustafson G, Wikberg P, 1997b. Äspö HRL - Geoscientific evaluation 1997/4. Results from pre-investigations and detailed site characterization. Comparison of predictions and observations. Geohydrology, Groundwater chemistry and Transport of solutes. SKB TR 97-05.

Stanfors R, Erlström M, Markström I, 1997a. Äspö HRL - Geoscientific evaluation 1997/1. Overview of site characterization 1986-1995. SKB TR 97-02.

Stanfors R, Olsson P, Stille H, 1997b. Äspö HRL - Geoscientific evaluation 1997/3. Results from pre-investigations and detailed site characterization. Comparison of predictions and observations. Geology and Mechanical stability. SKB TR 97-04.

CHAPTER 2

Almén K, Zellman O, 1991. Äspö Hard Rock Laboratory. Field investigation methodology and instruments used in the pre-investigation phase, 1986-1990. SKB TR 91-21.

Gustafson G, Stanfors R, Wikberg P, 1988. Swedish Hard Rock Laboratory. First evaluation of pre-investigations 1986-87 and target area characterization. SKB TR 88-16.

Gustafson G, Stanfors R, Wikberg P, 1989. Swedish Hard Rock Laboratory. Evaluation of 1988 year pre-investigations and description of the target area, the island of Äspö. SKB TR 89-16.

Gustafson G, Liedholm M, Rhén I, Stanfors R, Wikberg P, 1991. Äspö Hard Rock Laboratory. Predictions prior to excavation and the process of their validation. SKB TR 91-23.

Smellie J, Laaksoharju M, 1992. The Äspö Hard Rock Laboratory. Final evaluation of the hydrogeochemical pre-investigations in relation to existing geologic and hydraulic conditions. SKB TR 92-31.

Stanfors R, Erlström M, Markström I, 1991. Äspö Hard Rock Laboratory. Overview of the investigations 1986-1990. SKB TR 91-20.

Wikberg P (ed), Gustafson G, Rhén I, Stanfors R, 1991. Äspö Hard Rock Laboratory. Evaluation and conceptual modelling based on the pre-investigations. SKB TR 91-22.

CHAPTER 3

Axelsson C L, 1987. Generic modelling of the SKB rock laboratory. SKB PR 25-87-12.

Axelsson C, Jonsson E-K, Geier J, Dershowitz W, 1990. Discrete fracture modelling. SKB PR 25-89-21.

BRAINMAKER PROFESSIONAL for Windows, 1993. Simulated biological intelligence by California Scientific Software. Nevada City, California, USA.

Bäckblom G, 1989. Guide-Lines for use of nomenclature on fractures, fracture zones and other topics. SKB PR HRL-96-18.

Bäckblom G, Gustafson G, Stanfors R, Wikberg P, 1990. A synopsis of predictions before the construction of the Äspö Hard Rock Laboratory and the process of their validation. SKB PR 25-90-14.

Carlsson L, Gustafson G, 1984. Provpumpning som geohydrologisk undersökningsmetodik, (Byggforskingsrådet), R41:1984, Stockholm.

Chatfield and Collins, 1989. Introduction to multivariate analysis. Chapman and Hall.

Clark I and Fritz P, 1997. Environmental Isotopes in Hydrology. Lewis Publishers, New York, 328 p.

Cooper H H, Jacop C E, 1946. A generalized graphical method for evaluating formation constants and summarizing well field history. Am. Geophysical Union Trans. Vol. 27, pp 526-534.

Davis S N, 1964. The Chemistry of Saline Waters by R A Krieger - Discussion, Groundwater 2 (1), 51.

Domenico P A, Schwartz F W, 1990. Physical and Chemical Hydrogeology, (John Wiley & Sons), New York.

Earlougher R C, 1977. Advances in well test analysis. SPE monograph Volume 5 of Henry L. Doherty Series

Forina M, Leardi R, Armanino C and Lanteri S, 1988. PARVUS. Elsevier Science Publisher B.V., Amsterdam.

Grenthe I, Stumm W, Laaksoharju M, Nilsson A-C and Wikberg P, 1992. Redox potentials and redox reactions in deep groundwater systems. Chemical Geology, 98, 131.

Grundfelt B, Lindbom B, Liedholm M, Rhén I, 1990. Predictive Groundwater Flow Modelling of a Long-term Pumping Test (LPT 1) at Äspö. SKB PR 25-90-04.

Hecht-Nielsen R, 1991. Neurocomputing. Addison-Wesley Publishing Company, Reading, Massachusetts.

Hemström B, Svensson U, 1988. The penetration of sea water into a fresh-water aquifer. A numerical study. SKB PR 25-88-02.

Hermanson J, 1995. Structural geology of water-bearing fractures. SKB PR 25-95-23.

Hertz J, Krogh A and Palmer R G, 1991. Introduction to the theory of neural computation. Addison-Wesley Publishing Company, Reading, Massachusetts.

Hoek E, Brown E T, 1980. Underground excavation in rock. Institute of mining and metallurgy, IMM, London.

Ittner T, Gustafsson E, 1995. Groundwater chemical composition and transport of solutes. Evaluation of the fracture zones NE-1, NE-2 and NNW-4 during pre-investigation and tunnel construction. SKB PR HRL-96-03.

IUGS SUBCOMISSION ON THE SYSTEMATICS OF IGNEOUS ROCKS 1973. Classification and Nomenclature of Plutonic Rocks. Recommendations. N. Jb. Miner. Mh. 1973, H4, 149-164.

IUGS SUBCOMISSION ON THE SYSTEMATICS OF IGNEOUS ROCKS 1980. Classification and Nomenclature of Volcanic Rocks, Lamprophyres, Carbonatites and Melilitic Rocks. Geol. Rundschau 69, 194-207.

Kuylenstierna H-O, Svensson U, 1994. On the numerical generation of fracture aperture distributions. SKB PR 25-94-18.

Laaksoharju M, 1990. Measured and predicted groundwater chemistry at Äspö. SKB PR 25-90-13.

Laaksoharju M, Skårman C, 1995. Groundwater sampling and chemical characterization of the Äspö HRL tunnel in Sweden. SKB PR 25-95-29.

Laaksoharju M, Nilsson A-C, 1989. Models of groundwater composition and of hydraulic conditions based on chemometrical and chemical analyses of deep groundwater at Äspö and Laxemar. SKB PR 25-89-04.

Lawrence J, 1992. Introduction to neural networks and expert systems. California Scientific Software, Nevada City.

Marsily G de, 1986. Quantitative hydrogeology. Groundwater hydrology for engineers, Academic Press, Inc., New York.

La Point P R, Wallman P, Follin S, 1995. Estimation of effective block conductivities based on discrete network analysis using data from the Äspö site. SKB TR 95-15.

Olsson O, Bäckblom G, Gustafson G, Rhén I, Stanfors R, Wikberg P, 1994. The structure of conceptual models with application to the Äspö HRL Project. SKB TR 94-08.

Pedersen K, Karlsson F, 1995. Investigation of sub terrain micro-organisms. Their importance for performance assessment of radio-active waste disposal. SKB TR 95-10.

Rhén I, Gustafson G, Wikberg P, 1997. Äspö HRL - Geoscientific evaluation 1997/4. Results from pre-investigations and detailed site characterization. Comparison of predictions and observations. Geohydrology, Hydrochemistry and Transport of solutes. SKB TR 97-05.

Smellie J A T, Laaksoharju M, 1992. The Äspö Hard Rock Laboratory. Final evaluation of the hydrogeochemical pre-investigations in relation to existing geologic and hydraulic conditions. SKB TR 92-31.

Spalding D B, 1981. A general-purpose computer program for multi-dimensional one-two-phase flow. Math. and Comp. in Simulation, XIII, pp 267-276.

STATGRAPHICS PLUS for Windows, 1994. Statistical graphics system by Manugistics, Inc. Rockville, Maryland, USA.

STATISTICA for Windows, 1994. Complete Statistical System by StatSoft, Inc. Tulsa, USA.

SURFER for Windows, 1994. Contouring and 3D Surface Mapping by Golden Software, Inc. Golden, Colorado, USA.

Svensson U, 1988. Numerical simulations of seawater intrusion in fractured porous media. SKB PR 25-88-09.

Svensson U, 1990a. The island of Äspö. Numerical calculations of natural and forced Groundwater circulation. SKB PR 25-90-03.

Svensson U, 1990b. Numerical predictions of tracer trajectories during a pump test. SKB PR 25-90-10.

Svensson U, 1990c. Preliminary calculation of ambient and disturbed groundwater flow at Äspö including calculations of test case 2 HYDROCOIN, Level 1. SKB PR 25-90-11.

Svensson U, 1991a. Groundwater flow at Äspö and changes due to the excavation of the laboratory. SKB PR 25-91-03.

Svensson U, 1991b. Predictions of flow trajectories for the LPT2 pump test. SKB PR 25-91-17.

Svensson U, 1992a. Modelling tracer transport in fractured porous media. - An evaluation of concepts and methods using the LPT2 field experiment. SKB PR 25-92-12.

Svensson U, 1992b. Refinements of the numerical model of the Äspö Hard Rock Laboratory. SKB PR 25-92-13.

Svensson U, 1994a. Flow, pressure and salinity distributions around planned experimental sites at the Äspö Hard Rock Laboratory. SKB PR 25-94-11.

Svensson U, 1994b. Refined modelling of flow and transport in the numerical model of the Äspö Hard Rock Laboratory. - Refined modelling of fracture zones in the Äspö HRL numerical model. - An evaluation of the properties of the particle tracking routine developed for the Äspö HRL Project. - Visualization of data from the Äspö HRL model. SKB PR 25-94-12.

Svensson U, 1994c. Calculation of pressure, flow and salinity fields using measured inflow to the tunnel. SKB PR 25-94-27.

Svensson U, 1995a. Visualization techniques for computational fluid dynamics - a way to see the unseen. SKB PR 25-95-10.

Svensson U, 1995b. Modelling the unsaturated zone at Äspö under natural conditions and with the tunnel front at 2874 metres. SKB PR 25-95-24.

Svensson U, 1995c. Calculation of pressure, flow and salinity fields, with tunnel front at 2874 metres. SKB PR 25-95-25.

Svensson U, 1997a. A regional analysis of groundwater flow and salinity distribution in the Äspö area. SKB TR 97-09.

Svensson U, 1997b. A site scale analysis of groundwater flow and salinity distribution in the Äspö area. SKB TR 97-17.

Streckeisen A L, 1967. Classification and Nomenclature of Igneous Rocks. N. Jb. Miner. Abh. 107, 144-240.

Streckeisen A L, 1976. To each plutonic rock its proper name. Earth Sci Rev. 12.

CHAPTER 4

Andersson O, 1994. Deep drilling KLX02. Drilling and documentation of a 1700 m deep borehole at Laxemar, Sweden, SKB TR 94-19.

Brown E T, 1981 (ed). Rock characterization. Testing and Monitoring. ISRM suggested Methods. Pergamon Press.

Bäckblom G, 1989. Guide-lines for use of nomenclature on fractures, fracture zones and other topics, SKB HRL-96-18.

Bäckblom ed, 1989. Interdisciplinary study of Post-glacial faulting in the Lansjärv area northern Sweden 1986-1988. SKB TR 89-31.

Carlsten S, 1990. Borehole radar measurements at Äspö boreholes KAS09, KAS10, KAS11, KAS12, KAS13 and KAS14.

Carlsten S, 1993. Supplementary investigations of fracture zones in the tunnel, core mapping data and radar measurements. Compilation of technical notes. SKB PR 25-94-01.

Cosma C, Heikkinen P, Keskinen J, Kormonen R, 1990. VSP-survey including 3-D interpretation in Äspö, Sweden. Borehole KAS07. SKB PR 25-90-07.

Eliasson T, 1993. Mineralogy, geochemistry and petrophysics of red-coloured granite adjacent to fractures. SKB TR 93-06.

Ericsson L-O, 1987. Fracture mapping on outcrops. SKB PR 25-87-05.

Ericsson L O, 1988. Fracture mapping study on Äspö island. Findings of directional data. SKB PR 25-88-10.

Gaal G, Gorbatschev R, 1987. An outline of the Precambrian evaluation of the Baltic Shield. Precambrian Research 35.

Gentzschein B, Nilsson G and Stenberg L, 1987. Preliminary Investigations of Fracture Zones at Ävrö - Results of Investigations performed July 1986 - May 1987. SKB PR 25-87-16.

Hermanson J, 1995. Structural geology of water-bearing fractures. SKB PR 25-95-23.

IUGS SUBCOMISSION ON THE SYSTEMATICS OF IGNEOUS ROCKS 1973. Classification and Nomenclature of Plutonic Rocks. Recommendations. N. Jb. Miner. Mh. 1973, H4, 149-164.

IUGS SUBCOMISSION ON THE SYSTEMATICS OF IGNEOUS ROCKS 1980. Classification and Nomenclature of Volcanic Rocks. Lamprophyres, Carbonatites and Melilitic Rocks. Geol. Rundschau 69, 194-207.

Kickmaier W, 1995. Definition and characterisation of the N-S fracture system - tunnel sections 1/600m to 2/400m. Relationships to grouted sections - some remarks. SKB ICR 95-02.

Kornfält K-A, Wikman H, 1987. Description to the map (No 4) of solid Rocks of 3 small areas around Simpevarp. SKB PR 25-87-02a.

Kornfält K-A, Wikman H, 1987. Description to the map of solid Rocks around Simpevarp. SKB PR 25-87-02.

Kornfält K-A, Wikman H, 1988. The rocks of the Äspö island. Description to the detailed maps of solid rocks including maps of 3 uncovered trenches. SKB PR 25-88-12.

Larsson S Å, Tullborg E-L, 1993. Tectonic regimes in the Baltic Shield during the last 1200 Ma - A review. SKB TR 94-05.

La Pointe P R, Wallman P and Follin S, 1995. Estimation of effective block conductivities based on discett network analyses using data from the Äspö site. SKB TR 95-15.

Maddock R H, Hailwood E A, Rhodes E J, Muir Wood R, 1993. Direct fault dating trials at the Äspö Hard Rock Laboratory. SKB TR 93-24

Mansfeld J, 1991. U-Pb age determination of Småland-Värmland granitoids in Småland, Southeastern Sweden. GFF 113. Stockholm.

Markström I, Erlström M, 1996. Overview of documentation of tunnel, nisches and cored boreholes. SKB PR HRL-96-19.

Markström I, 1997. Updated overview of documentation of side tunnels and niches. Documentation updated after supplementary excavations performed during 1996 and 1997. SKB PR HRL-97-20.

Mazurek M, Bossart P, Eliasson T, 1996. Classification and characterization of waterconducting features at Äspö: Results of Investigations on the outcrop scale. SKB ICR 97-01.

Milnes A G, Gee D G, 1992. Bedrock stability in the southeastern Sweden - Evidence from fracturing in the ordovician limestones of northern Öland. SKB Technical Report, TR 92-23, Stockholm.

Munier R, Riad I, Tullborg E-L, Wikman H, Kornfält K-A, 1988. Detailed investigation of the drill-cores KAS02, KAS03 and KAS04 on Äspö island and KLX01 at Laxemar. SKB PR 25-88-11.

Munier R, 1989. Brittle tectonics on Äspö, SE Sweden. SKB PR 25-89-15.

Munier R, 1992. Update of structural models for the Äspö area; Emphasis on brittle deformation. SKB Progress Report PR 25-92-07. Stockholm.

Munier R, 1993b. Updated analysis of fracture arrays in the HRL tunnel. Section 700-1400 m. SKB Progress Report, in press, Stockholm.

Munier R, 1993c. Segmentation, Fragmentation and Jostling of the Baltic Shield with Time. Uppsala Dissertations of the Faculty of Science, vol 37. Almquist & Wiksell International, Sweden.

Munier R and Hermansson J, 1994. Updating of geological-structural model Compilation of technical notes. SKB PR 25-94-05.

Munier R, 1995. Studies of geological structures at Äspö. Comprehensive summary of results. SKB PR 25-95-21.

Mörner N-A, 1989. Postglacial faults and fractures on Äspö. SKB PR 25-89-24.

Nisca D, 1987. Aerogeophysical interpretation. SKB PR 25-87-04.

Olsson O et al, 1993. Localization of experimental sites and layout of turn 2. Compilation of Technical Notes. SKB PR 25-94-03.

Ploug C, Klitten K, 1989. Shallow reflection seismic profiles from Äspö, Sweden. SKB PR 25-89-02.

Poteri A, 1995. Analysis of bedrock fracturing of Äspö. SKB ICR 96-01.

Rhén I, Stanfors R, 1993. Evaluation of Investigation in Fracture Zones NE-1, EW-7 and NE-3. SKB PR 25-92-18.

Rhén I, Stanfors R, 1995. Supplementary investigations of fracture zones in Äspö tunnel. SKB PR 25-95-20.

Rosén L, Gustafson G, 1993. Possible Strategies for Geoscientific Classification for High-Level Waste Repository Site Selection. SKB TR 93-12.

Rosén L, Gustafson G, 1995. Suitable near field design. Stage 2. Provisional positioning index (PPI) predictions with respect to lithology, hydraulic conductivity and rock designation index along the TBM-tunnel. SKB PR 25-95-19.

Slunga R, Norrman P and Glans A-C, 1984. Baltic shield seismicity, the results of a regional network. Geophys. Res. Lett., 11, 1247-1250.

Stanfors R, Erlström M, Markström I, 1991. Äspö Hard Rock Laboratory. Overview of the investigations 1986-1990. SKB TR 91-20.

Stanfors R et al, 1992. PASSAGE THROUGH WATER-BEARING FRACTURE ZONES. Compilation of technical notes.
SKB PR 25-92-18 A. Investigation during passage of fracture zone EW-7 and NE-3.
SKB PR 25-92-18 B. Passage through fracture zone NE-1 Geology and geophysics.
SKB PR 25-92-18 C. Passage through fracture zone NE-1. Hydrogeology and groundwater chemistry.
SKB PR 25-92-18 D. Construction and grouting.

Stanfors R, Liedholm M, Munier R, Olsson P, 1993a. Geological-Structural evaluation of the data from tunnel section 700-1475 m. SKB PR 25-93-05.

Stanfors R, Liedholm M, Munier R, Olsson P, Stille H, 1993b. Geological-structural and Rock mechanical evaluation of data from tunnel section 1475-2265 m. SKB PR 25-93-10.

Stanfors R, Rhén I, 1993. Evaluation of Investigation in Fracture Zones NE-1, EW-7 and NE-3. SKB PR 25-92-18.

Stanfors R, Liedholm M, Munier R, Olsson P, Stille H, 1994a. Geological-structural and rock mechanical evaluation of data from tunnel section 2265-2874 m. SKB PR 25-94-19.

Stanfors R, Rhén I, Forsmark T, Wikberg P, 1994b. Evaluation of the fracture zone EW-1, based on core boreholes KA1755A, KA1751, KA1754A and KAS04. SKB PR 25-94-39.

Stråhle A, 1989. Drillcore investigation in the Simpevarp area, Boreholes KAS02, KAS03, KAS04 and KLX01. SKB PR 25-88-07.

Talbot C, Riad L, 1987. Natural fractures in the Simpevarp area. SKB PR 25-87-03.

Talbot C, Munier R, 1989. Faults and fracture zones in Äspö. SKB PR 25-89-11.

Talbot C, 1990. Some clarification of the tectonics of Äspö and its surroundings. SKB PR 25-90-15.

Talbot C, 1991. Preliminary structural geology underground in the Äspö Hard Rock Laboratory. SKB PR 25-92-03.

Tirén S, Beckholmen M, 1987. Structural analysis of contoured maps. Äspö and Ävrö, South-eastern Sweden. SKB PR 25-87-22.

Tirén S, Beckholmen M, Isaksson H, 1987. Structural analysis of digital terrain models, Simpevarp area, South-eastern Sweden. Method study EBBA II. SKB PR 25-87-21.

Tirén S, Beckholmen M, 1988. Structural analysis of the Simpevarp sea area. Southeastern Sweden. Linaments and rock blocks. SKB PR 25-88-01.

Tullborg E-L, 1989. Fracture fillings in the drillcores KAS05-KAS08 from Äspö, Southeastern Sweden. SKB, PR 25-89-16.

Wahlström R, 1990. A catalogue of earthquakes in Sweden in 1375-1890. Geol. Fören. Stockholm Förh. 112, 215-225.

Wikman H, Kornfält K-A, 1995. Updating of a lithological model of the bedrock of the Äspö area. SKB PR 25-95-04.

Wikberg P (ed), Gustafson G, Rhén I, Stanfors R, 1991. Äspö Hard Rock Laboratory. Evaluation and conceptual modelling based on the pre-investigations. SKB TR 91-22.

Wikström A, 1989. General geological-tectonic study of the Simpevarp area with special attention to the Äspö island. SKB PR 25-89-06.

Winberg A, Andersson P, Hermanson J, Stenberg L, 1996. Results of the Select project. Investigation programme for selection of experimental sites for the operational phase. SKB PR HRL-96-01.

CHAPTER 5

Delin P, Olsson P, Stille H, 1993. Field and laboratory testing of rocks 700-1475 m. SKB PR 25-93-02

Gustafson G, Stille H, 1996. Prediction of groutability from grout properties and hydrogeological data. Tunnelling and Underground Space Vol. 11, No 3, 325-332.

Lee M, Bridges M, Stillborg B, 1992 and 1993. Äspö virgin stress measurement results in sections 1050, 1190 and 1620 m of the access ramp. SKB PR 25-93-02.

Leijon B, 1995. Summary of rock stress data from Äspö. SKB PR 25-95-15.

Rhén I, Stanfors R, 1995. Supplementary investigations of fracture zones in Äspö tunnel. SKB PR 25-95-20.

Stille H, Olsson P, 1990. Evaluation of Rock Mechanics. SKB PR 25-90-08.

Stille H, Gustafson G, Håkansson U, Olsson P, 1993. Experiences from the grouting of the section 1-1400 m of the tunnel. SKB PR 25-92-19.

Stille H, Jansson T, Olsson P, 1994. Experiences from the grouting of the section 1340-2565 m of the tunnel. SKB PR 25-94-13.

Stille H, Olsson P, 1996. Summary of rock mechanical experiences from the construction of Äspö Hard Rock Laboratory. SKB PR HRL-96-07.

CHAPTER 6

Ahlbom K, Andersson J-E, Nordqvist R, Ljunggren C, Tirén S, Voss C, 1991a. Gideå study site, Scope of activities and main results. SKB TR 91-51.

Ahlbom K, Andersson J-E, Nordqvist R, Ljunggren C, Tirén S, Voss C, 1991b. Fjällveden study site. Scope of activities and main results. SKB TR 91-52.

Ahlbom K, Andersson J-E, Andersson P, Ittner T, Ljunggren C, Tirén S, 1992a. Klipperås study site. Scope of activities and main results, SKB TR 92-22.

Ahlbom K, Andersson J-E, Andersson P, Ittner T, Ljunggren C, Tirén S, 1992b. Kamlunge study site. Scope of activities and main results. SKB TR 92-15.

Ahlbom K, Olsson O, Sehlstedt S, 1995. Temperature conditions in the SKB study sites. SKB TR 95-16.

Almén K-E, Olsson P, Rhén I, Stanfors R, Wikberg P, 1994. Äspö Hard Rock Laboratory - Feasibility and usefulness of site investigation methods. Experiences from the pre-investigation phase. SKB TR 94-24.

Björck S, Svensson N-O, 1992. Climate changes and uplift patterns - past, present and future. SKB TR 92-38.

Carlsson L, Gustafson G, 1984. Provpumpning som geohydrologisk undersökningsmetodik. (Byggforskningsrådet), R41:1984, Stockholm.

Dershowitz W, Thomas A, Busse R, 1996. Discrete fracture analysis in support of the Äspö tracer retention understanding experiment (TRUE-1). SKB, (in press).

Domenico P A, Schwartz F W, 1990. Physical and Chemical Hydrogeology. (John Wiley & Sons), New York.

Earlougher R C, 1977. Advances in well test analysis. SPE monograph Volume 5 of Henry L. Doherty Series.

Eriksson B, 1980. The water balance of Sweden. Annual mean values (1931-60) of precipitation, evaporation and run-off (in Swedish). SMHI Nr RMK 18 and Nr RHO 21 (1980), SMHI, Norrköping.

Forsmark T, 1992. Hydraulic tests at Äspö in KAS16. SKB PR 25-92-15.

Forsmark T, Stenberg L, 1993. Supplementary investigations of fracture zones in the tunnel. Hydrogeology. Measurements performed during construction of chainage 1475-2265 m. Compilation of Technical Notes. SKB PR 25-94-06.

Gottschalk L, 1982. Hydrologi. Hydrology compendium (in Swedish), Lund.

Hermanson J, 1995. Structural geology of water-bearing fractures. SKB PR 25-95-23.

Hermanson J, 1996. Visualization of the fracture network in rock blocks along the Äspö HRL tunnel using a DFN model approach. SKB PR HRL 96-08.

Jibao He, 1992. Lined underground openings. Rock mechanical effects on high internal pressure. Doctoral Thesis. Chalmers University of Technology.

Johansson J, Stille H, Sturk R, 1995. Dept. of Geotechnical Engineering, Gothenburg, Sweden.

Johansson J, Stille H, Sturk R, 1995. Pilotanläggning för inklädda gaslager i Grängesberg. Fördjupad analys av försöksresultaten. Kungliga Tekniska Högskolan. Inst för anläggning och miljö. Avd för jord och bergmekanik. ISRN KTH/ AMI/REPORT-3004-SE (Pilot plant for lined gas installations in Grängesberg. Deep analyses of test results. School of Civil engineering and the environment - in Swedish) ISRN KTH/ AMI/REPORT-3004-SE. Stockholm, Sweden.

Kickmaier W, 1993. Definition and characterisation of the N-S fracture system - tunnel sections 1/600m to 2/400m. Relationships to grouted sections - some remarks. SKB ICR 95-02.

La Pointe P R, 1994. Evaluation of stationary and non-stationary geostatistical models for inferring hydraulic conductivity values at Äspö. SKB TR 94-22.

La Point P R, Wallman P, Follin S, 1995. Estimation of effective block conductivities based on discrete network analysis using data from the Äspö site. SKB TR 95-15.

Liedholm M, 1987a. Regional Well Data Analysis. SKB PR 25-87-07.

Liedholm M, 1987b. Regional Well Water Chemistry. SKB PR 25-87-08.

Liedholm M (ed), 1991 a. Conceptual Modelling of Äspö. Technical Notes 1-17. General geological, hydrogeological and hydrochemical information. SKB PR 25-90-16 a.

Liedholm M (ed), 1991 b. Conceptual Modelling of Äspö. Technical Notes 18-31. General geological, hydrogeological and hydrochemical information. SKB PR 25-90-16 b.

Liedholm M, 1992. The hydraulic properties of different greenstone areas. A comparative study. SKB PR LOK 92-07.

Niemi A, 1995. Modelling of Äspö hydraulic conductivity data at different scales by means of 3-dimensional Monte Carlo simulations. SKB ICR 95-08.

Nyberg G, Jönsson S, Ekman L, 1996. Hydro Monitoring System. Report for 1995. SKB HRL-96-17.

Olsson O, Stanfors R, Ramqvist G, Rhén I, 1994. Localization of experimental sites and layout of turn 2. Results of investigations. SKB PR 25-94-14.

Olsson O (ed), 1994. Localization of experimental sites and layout of turn 2. Results from core mapping, radar and hydraulic investigations. Compilation of Technical Notes 2. SKB PR 25-94-15.

Olsson O, Emsley S, Bauer C, Falls S, Stenberg L, 1996. Zedex, a study of the zone of excavation disturbance for blasted and bored tunnels. SKB ICR 96-03.

Poteri A, 1996. Analysis of bedrock fracturing at Äspö. SKB ICR 96-01.

Priest S D, 1985. Hemispherical projection methods in rock mechanics. George Allen and Unwin, London.

Påsse T, 1996. A mathematical model of the shore level displacement in Fennoscandia. SKB TR 96-24.

Rhén I, 1988. Transient interference tests on Äspö 1988. Evaluation. SKB PR 25-88-13.

Rhén I, 1990. Transient interference tests on Äspö 1989 in KAS06, HAS13 and KAS07. Evaluation. SKB PR 25-90-09.

Rhén I, Gustafson G, 1990. DDP evaluation of hydrogeological data, Report U(G) 1990/59. Vattenfall, Vällingby.

Rhén I, Forsmark T, Nilsson L, 1991. Hydraulic tests on Äspö, Bockholmen and Laxemar 1990 in KAS09, KAS11-14, HAS18-20, KBH01-02 and KLX01. Evaluation. SKB PR 25-91-01.

Rhén I, Svensson U, Andersson J-E, Andersson P, Eriksson C-O, Gustafsson E, Ittner T, Nordqvist R, 1992. Äspö Hard Rock Laboratory. Evaluation of the combined long-term pumping and tracer test (LPT2) in borehole KAS06. SKB TR 92-32.

Rhén I, Danielson P, Forsmark T, Gustafson G, Liedholm M, 1993a. Geohydrological evaluation of the data from section 700-1475 m. SKB PR 25-93-06.

Rhén I, Danielsson P, Forsmark T, Gustafson G, Liedholm M, 1993b. Geohydrological evaluation of the data from section 1475 - 2265 m. SKB PR 25-93-11.

Rhén I, Danielsson P, Forsmark T, Gustafson G, Liedholm M, 1994a. Geohydrological evaluation of the data from section 2265-2874 m. SKB PR 25-94-20.

Rhén I, Forsmark T, Danielsson P, 1994b. Piezometric levels. Evaluation of the data from section 2265-2874 m. SKB PR 25-94-22.

Rhén I, Stanfors R, 1995. Supplementary investigations of fracture zones in Äspö tunnel. SKB PR 25-95-20.

Rhén I (ed), 1995. Documentation of tunnel and shaft data, tunnel section 2874 - 3600 m, hoist and ventilation shafts 0 - 450 m. SKB PR 25-95-28.

Rhén I (ed), Bäckblom (ed), Gustafson G, Stanfors R, Wikberg P, 1997a. HRL - Geoscientific evaluation 1997/2. Results from pre-investigations and detailed site characterization. Summary report. SKB TR 97-03.

Rhén I, Gustafson G, Wikberg P, 1997b. Äspö HRL - Geoscientific evaluation 1997/4. Results from pre-investigations and detailed site characterization. Comparison of predictions and observations. Geohydrology, Groundwater chemistry and Transport of solutes. SKB TR 97-05.

Sander P, 1996. Remote Sensing and GIS for Groundwater Assessment in Hard Rock Areas. Applications to Water Well Siting in Ghana and Botswana. Department of Geology, Chalmers University of Technology, Publ. A 80, Göteborg, Sweden.

Scherneck H-G, 1991. A parametrized solid earth tide model and ocean tide loading effects for global geodetic baseline measurements. Geophys. J. Int., 106, 677-694.

Serafin J L, Pereira J P, 1983. Consideration on the geomechanical classification of Bieniawski, Proc.Int. Symp. On Engr. Geology and Underground Construction, Lisbon, vol. 1.

Stanfors R, Rhén I, Forsmark T, Wikberg P, 1994. Evaluation of the fracture zone EW-1, based on the cored boreholes KA1755A, KA1751, KA1754A and KAS04. SKB PR 25-94-39.

Stille H, Olsson P, 1996. Summary of rock mechanical experiences from the construction of Äspö Hard Rock Laboratory. SKB PR HRL 96-07.

Sundberg J, 1991. Thermal properties of the rocks on Äspö island. Thermal conductivity, heat capacity, geothermal gradient and heat flow. SKB PR 25-91-09.

Sundblad B, Mathiasson L, Holby O, Landström O, Lampe S, 1991. Chemistry of soil and sediments, hydrology and natural exposure rate measurements at the Äspö Hard Rock Laboratory. SKB PR 25-91-08.

Svensson T, 1987. Hydrological conditions in the Simpevarp area. SKB PR 25-87-09.

Svensson U, 1995. Modelling the unsaturated zone at Äspö under natural conditions and with the tunnel front at 2874 metres. SKB PR 25-95-24.

Svensson U, 1997. A site scale analysis of groundwater flow and salinity distribution in the Äspö area. SKB TR 97-17.

Uchida M, Doe T, Dershowitz W, Thomas A, Wallmann P, Sawada A, 1994. Discrete-fracture modelling of the Äspö LPT-2, large-scale pumping and tracer test. SKB ICR 94-09.

Winberg A, 1989. PROJECT -90. Analysis of the spatial variability of hydraulic conductivity data in the SKB data base GEOTAB, SKI TR 89:12.

Wladis D, 1995. Assessing Hydraulic Properties of Rock using Remote Sensing. Chalmers University of Technology, Department of Geology, Publ A 78, Göteborg, Sweden.

Äspö HRL, 1996. Äspö Hard Rock Laboratory. 10 years of research. SKB, Stockholm.

Öhberg A, Saksa P, Ahokas H, Routsalainen P, Snellman M, 1994. Summary report of the experiences from TVO's site investigations. SKB TR 94-17.

CHAPTER 7

Ahonen L, Ervanne H, Ruskeeniemi T, Jaakkola T and Blomqvist R, 1992. Uranium Mineral - Groundwater Equilibration at the Palmottu Natural Analogue Study Site, Finland. Scientific Basis for Nuclear Waste Management XVI, 294, 1992.

Alley W M, 1993. Regional groundwater quality. ISBN 0-442-00937-2. Van Nostrand Reinhold, New York, USA.

Andersson P, Ittner T, Gustafsson E, 1992. Groundwater flow measurements in selected sections at Äspö before tunnel passage of fracture zone NE-1. SKB PR 25-92-05.

Andrews J N, Ford D J, Hussain N, Trivedi D, Youngman J, 1989. Natural radioelement solution by circulating groundwaters in the Stripa granite. Geochim. et Cosmochim. Acta, 53.

Andrews, J N and Wilson G B, 1987. The composition of dissolved gases in deep groundwaters and groundwater degassing. In: Fritz, P. and Frape, S. K., Saline water and gases in crystalline rocks. *Geol. Assoc. of Canada Spec. Pap.*, 33:245-252.

Banwart S, 1994. Proceedings of The Äspö International Geochemistry Workshop, June 2-3, 1994, Äspö Hard Rock Laboratory. SKB ICR 94-13.

Banwart S (ed.), 1995. The Äspö redox investigations in block scale. Project summary and implications for repository performance assessment. SKB TR 95-26.

Banwart S, Laaksoharju M, Nilsson A-C, Tullborg E-L, Wallin B, 1992. The large scale redox experiment. Initial characterization of the fracture zone. SKB PR 25-92-04.

Banwart S, Gustafsson E, Laaksoharju M, Nilsson A-C, Tullborg E-L, Wallin B, 1993. The large scale Redox experiment: Redox processes in a Granitic coastal aquifer. SKB Progress Report PR 25-93-03, Stockholm, Sweden.

Banwart S (ed), Laaksoharju M, Skårman C, Gustafsson E, Pitkänen P, Snellman M, Landström O, Aggeryd I, Mathiasson L, Sundblad B, Tullborg E-L, Wallin B, Pettersson C, Pedersen K, Arlinger J, Jahromi N, Ekendahl S, Hallbeck L, Degueldre C, Malmström M, 1995. The Redox experiment in block scale. Final reporting of results from the Three Year Project. SKB PR 25-95-06.

Blomqvist R, Suksi J, Ruskeeniemi T, Ahonen L, Niini H, Vuorinen U, Jakobsson K, 1995. The Palmottu natural analogue project. Summary report 1992-1994. Geological survey of Finland Report YST-88. ISBN 951-690-580-3, ISSN 0783-3555.

Bruton C and Viani B, 1997. Ion sorption onto hydrous Ferric oxides in Laaksoharju and Wallin 1997.

Chatfield C, Collins A J, 1989. Introduction to multivariate analysis. Chapman and Hall.

Ehlers J, 1996. Quaternary and glacial geology. John Wiley & Sons, England, 578 pages.

Follin S, 1997. (Personal communication).

Fontes J-Ch, Fritz P, Louvat D, Michelot J-L, 1989. Aqueous sulphates from the Stripa groundwater system. Geochim. et Cosmochim. Acta, 53.

Fortner B, 1992. The Data Handbook. Spyglass Inc. Champaign, Illinois, USA.

Frape S K, Fritz P, 1987. Geochemical trends for groundwaters from the Canadian shield. In: Fritz P and Frape S K, Saline water and gases in crystalline rocks. Geol. Assoc. of Canada Spec. Pap., 33:19-38.

Gascoyne M, Davison C C, Ross J D, Pearson R, 1987. Saline groundwaters and brines in plutons in the Canadian shield. In: Fritz, P. and Frape, S. K., Saline water and gases in crystalline rocks. Geol. Assoc. of Canada Spec. Pap., 33.

Grenthe I, Stumm W, Laaksoharju M, Nilsson A-C and Wikberg P, 1992. Redox potentials and redox reactions in deep groundwater systems. Chemical Geology, 98, 131.

Gustafson G, Stanfors R, Wikberg P, 1988. Swedish Hard Rock Laboratory. First evaluation of pre-investigations 1986-87 and target area characterization. SKB TR 88-16.

Gustafson G, Stanfors R, Wikberg P, 1989. Swedish Hard Rock Laboratory. Evaluation of 1988 year pre-investigations and description of the target area, the island of Äspö. SKB TR 89-16.

Gustafson G, Liedholm M, Rhén I, Stanfors R, Wikberg P, 1991. Äspö Hard Rock Laboratory. Predictions prior to excavation and the process of their validation. SKB TR 91-23.

Henley S, 1981. Nonparametric geostatistics. Elsevier Applied Science Publishers Ltd, Essex, England.

Ittner T, 1992. Groundwater flow measurements (TP2) in selected sections at Äspö after tunnel passage of fracture zone NE-1. SKB PR 25-92-17.

Ittner T, 1994. Äspö Hard Rock Laboratory. Groundwater Flow Measurements during Tunnel Construction Phase. Dilution measurements (TP4) at tunnel length 3168 m. SKB PR 25-94-26.

Ittner T, Gustafsson E, 1994. Groundwater chemistry and transport of solutes. Presentation of surface borehole data during pre-investigation and tunnel construction. SKB PR 25-94-38.

Ittner T, Gustafsson E, Andersson P, Eriksson C-O, 1991. Groundwater flow measurements at Äspö with the dilution method. SKB PR 25-91-18.

Kankainen T, 1986. Loviisa power station final disposal of reactor waste. On the age and origin of groundwater from the rapakivi granite on the island of Hästholmen. Nuclear Waste Commission of Finnish power Companies. Report YJT-86-29.

Laaksoharju M, 1988. Shallow groundwater chemistry at Laxemar, Äspö and Ävrö. SKB PR 25-88-04.

Laaksoharju M, 1990. Measured and predicted groundwater chemistry at Äspö. SKB PR 25-90-13.

Laaksoharju M (ed), 1995. Sulphate reduction in the Äspö HRL tunnel. SKB TR 95-25.

Laaksoharju M, Nilsson A-C, 1989. Models of groundwater composition and of hydraulic conditions based on chemometrical and chemical analyses of deep groundwater at Äspö and Laxemar. SKB PR 25-89-04.

Laaksoharju M, Skårman C, 1995. Groundwater sampling and chemical characterization of the Äspö HRL tunnel in Sweden. SKB PR 25-95-29.

Laaksoharju M, Wallin B, 1997. Evolution of the groundwater chemistry at the Äspö Hard Rock Laboratory. Proceedings of the second Äspö International Geochemistry Workshop, June 6-7, 1995. SKB ICR 97-04.

Laaksoharju M, Smellie J, Nilsson A-C, Skårman C, 1995. Groundwater sampling and chemical characterization of the Laxemar deep borehole KLX02. SKB Technical Report TR 95-05, Stockholm, Sweden.

Landström O, Tullborg E-L, 1993. Results from a geochemical study of zone NE-1, based on samples from the Äspö tunnel and drillcore KAS 16 (395 m to 451 m). SKB PR 25-93-01.

Landström O, Aggeryd I, Marthiasson L, Sundblad B, 1994. Chemical composition of sediments from the Äspö area and interaction between the biosphere and geosphere. SKB Status Report AR 94-03, Stockholm, Sweden.

Landström O, Tullborg E-L, 1995. Interactions of trace elements with fracture filling minerals from the Äspö Hard Rock Laboratory. SKB TR 95-13.

Liedholm M, 1987. Regional Well Water Chemistry. SKB PR 25-87-08.

Louvat D, Michelot J L, Aranyossy J F, 1997. Salinity origin and residence time of the Äspö groundwater system in Laaksojarju and Wallin, 1997. SKB ICR 97-04.

Nilsson A-C, 1989. Chemical characterization of deep groundwater on Äspö. 1989. SKB PR 25-89-14.

Nilsson A-C, 1991. Groundwater chemistry monitoring at Äspö during 1990. SKB PR 25-91-04.

Nilsson A-C, 1995. Compilation of groundwater chemistry data from Äspö 1990-1994. SKB PR 25-95-02.

Nurmi P A, Kukkonen I T, 1986. A new technique for sampling water and gas from deep drill holes. Canadian Journal of Eart Sciences. Volume 23, Number 9, 1986.

Pearson K, 1901. On lines and planes of closest fit to a system of points in space. Philosophical Magazine 2, 557-72.

Pedersen K, Karlsson F, 1995. Investigation of sub terrain micro-organisms. Their importance for performance assessment of radio-active waste disposal. SKB TR 95-10.

Peterman Z E, Wallin B, 1997. A Summary of strontium isotope systematics in groundwater at Äspö in Laaksojarju and Wallin, 1997. SKB ICR 97-04.

Pitkänen P, Snellman M, Banwart S, Laaksoharju M, Leino-Forsman H, 1994. The Äspö Redox Experiment in Block Scale: testing end-members for mixing models. In: Banwart S (ed). Proceedings of the Äspö International Geochemistry Workshop, June 2-3 1994, Äspö Hard Rock Laboratory. SKB International Co-operation Report 94-13.

Plummer L N, Prestemon E C, Parkhurst D L, 1991. An interactive code (NETPATH) for modelling NET geochemical reactions along a flow path. US Geological Survey, Water-Resources Investigation Report 91-4078.

Rhén I, Gustafson G, Wikberg P. Äspö HRL - Geoscientific evaluation 1997/4. Results from pre-investigations and detailed site characterization. Comparison of predictions and observations. Geohydrology, Groundwater chemistry and Transport of solutes. SKB TR 97-05.

Smellie J A T, 1996. Very deep hole concept. Geoscientific appraisal to conditions at large depths - Hydrochemistry. SKB PR U-96-17.

Smellie J A T, Laaksoharju M, 1992. The Äspö Hard Rock Laboratory. Final evaluation of the hydrogeochemical pre-investigations in relation to existing geologic and hydraulic conditions. SKB TR 92-31.

Stanfors R, Gustafson G, Munier R, Olsson P, Rhén I, Stille H, Wikberg P, 1992. Evaluation of geological predictions in the access ramp 0-0/700 metres. SKB PR 25-92-02.

Svensson U, 1996. Regional groundwater flow due to an advancing and retreating glacier. Scoping calculations. SKB PR (in preparation).

Toulhoat P, Beaucaire C, Michard G, Ouzounian G, 1992. Chemical Evolution of Deep Groundwater in Granites, Information Acquired from Natural Systems. Paleohydrogeological Methods and their Applications. Proceedings from an NEA workshop 9-10 November 1992.

Trotignon L, Beaucaire C, Louvat D, Aranyossy J F, 1997. Equilibrium geochemical modelling of Äspö groundwaters in Laaksoharju and Wallin, 1997.

Tullborg E-L, 1989. Fracture fillings in the drillcores KAS05 - KAS08 from Äspö, Southeastern Sweden. SKB PR 25-89-16.

Tullborg E-L, 1995. Mineralogical and chemical data on rocks and fracture minerals from Äspö. Written communications.

Tullborg E-L, Larson S, 1984. $\delta^{18}O$ and $\delta^{13}C$ for limestones, calcite fissure infillings and calcite precipitates from Sweden. Geologiska Föreningens in Stockholm Förhandlingar, Vol. 106, Pt. 2, Stockholm, Sweden.

Tullborg E-L, Wallin B, Landström O, 1991. Hydrogeochemical studies of fracture minerals from water conducting fractures and deep groundwaters at Äspö. SKB PR 25-90-01.

Wallin B, 1990. Carbon, Oxygen and Sulfur isotope signatures for groundwater classification at Laxemar, southeastern Sweden. SKB PR 25-90-12.

Wallin B, 1992. Sulphur and oxygen isotope evidence from dissolved sulphates in groundwater and sulphide sulphur in fissure fillings at Äspö, southeastern Sweden. SKB PR 25-92-08.

Wallin B, Peterman Z, 1994. SKB/DOE Hard Rock Laboratory Studies Task 3. Geochemical investigations using stable and radiogenic isotopic methods. SKB. SKB ICR 94-06.

Wallin B, Peterman Z E, 1997a. Calcite fracture fillings as indicators of paleohydrology at the Äspö Hard Rock Laboratory, Sweden. Laaksojarju and Wallin, 1997, SKB ICR 97-04.

Wallin B, Peterman Z E, 1997b. Isotopic systematics of saline waters at Äspö and Laxemar, Sweden. Laaksoharju and Wallin, 1997, SKB ICR 97-04.

Viani B and Bruton C, 1994. Effect of cation excange on major cation chemistry in the large scale Redox Experiment at Äspö. SKB International Cooperation Report ICR, 94-13.

Wikberg P, Gustafsson E, 1993. Groundwater chemistry and transport of solutes. Evaluation of the data from tunnel section 700-1475 m. SKB PR 25-93-07.

Wikberg P (ed), Gustafson G, Rhén in, Stanfors R, 1991. Äspö Hard Rock Laboratory. Evaluation and conceptual modelling based on the pre-investigations. SKB TR 91-22.

Wikberg P, Skårman C, Laaksoharju M, Ittner T, 1993. Groundwater chemistry and transport of solutes. Evaluation of the data from tunnel section 1475 - 2265 m. SKB PR 25-93-12.

Wikberg P, Skårman C, Laaksoharju M, Ittner T, 1994. Groundwater chemistry and transport of solutes. Evaluation of the data from tunnel section 2265-2874 m. SKB PR 25-94-21.

Wikström L, Björklund A, 1994. Trace elements in waters of low-conductivity rocks in the Äspö Hard Rock Laboratory. SKB PR 25-94-28.

Winn K, Werner F, Erlenkeuser H, 1988. Hydrography of the Kiel Bay, Western Baltic during the Litorina Transgression. Meyniana, 40.

CHAPTER 8

Andersson P, 1995. Compilation of tracer tests in fractured rock. SKB PR 25-95-05.

Banwart S (ed), Laaksoharju M, Skårman C, Gustafsson E, Pitkänen P, Snellman M, Landström O, Aggeryd I, Mathiasson L, Sundblad B, Tullborg E-L, Wallin B, Pettersson C, Pedersen K, Arlinger J, Jahromi N, Ekendahl S, Hallbeck L, Degueldre C, Malmström M, 1995. The Redox experiment in block scale. Final reporting of results from the Three-Year Project. SKB PR 25-95-06.

Barthelemy Y, Schwartz J, Sebti K, 1994. Hydrodynamic modelling of the original steady state and LPT2 experiments. MARTHE and SESAME codes. SKB ICR 94-16.

Billaux D, Guérin F, Wendling J, 1994. Hydrodynamic modelling of the Äspö HRL. Discrete fracture model. SKB ICR 94-14.

Earlougher R C, 1977. Advances in well test analysis. SPE monograph Volume 5 of Henry L. Doherty Series

Gustafsson E, Andersson-Ludvigson J E, Gentzschein B, Hautojärvi A, Koskinen L, Löfman J, 1994. Hydraulic modelling and tracer tests on the Redox experiment in the Äspö Hard Rock Laboratory tunnel. SKB PR 25-94-37.

Gustafson G, Ström A, 1995. The Äspö Task Force on Modelling of Groundwater Flow and Transport of Solutes. Evaluation report on Task No 1, the LPT2 large scale field experiments. SKB ICR 95-05.

Gylling B, Moreno L, Neretnieks I, Birgersson L, 1994. Analysis of LPT2 using the Channel Network model. SKB ICR 94-05.

Hautojärvi A, 1994. Data analysis and modelling of the LPT2 Pumping and Tracer Transport Test at Äspö. Tracer experiment. SKB ICR 94-11.

Holton D, Milický M, 1997. Simulating the LPT2 and tunnel drawdown experiment at Äspö using a coupled continuum-fracture network approach. SKB ICR 97-05.

Igarashi T, Tanaka Y, Kawanishi M, 1994. Application of three-dimensional smeared fracture model to the groundwater flow and the solute migration of LPT-2 experiment. SKB ICR 94-08.

Kobayashi A, Yamashita R, Chijimatsu M, Nishiyama H, Ohnishi Y, 1994. Analyses of LPT2 in the Äspö HRL with continuous anisotropic heterogeneous model. SKB ICR 94-07.

Löfman J, Taivassalo V, 1995. Simulations of pressure and salinity fields at Äspö. SKB ICR 95-01.

Marsily G de, 1986. Quantitative hydrogeology. Groundwater hydrology for engineers, Academic Press, Inc., New York

Mazurek M, Bossart P, Eliasson T, 1996. Classification and characterization of water-conducting features at Äspö: Results of investigations on the outcrop scale. SKB ICR97-01.

Mészáros F, 1996. Simulation of the transient hydraulic effect of the access tunnel at Äspö. SKB ICR 96-06.

Noyer M L, Fillion E, 1994. Hydrodynamic modelling of the Äspö Hard Rock Laboratory. ROCKFLOW code. SKB. ICR 94-15.

Rhén I, Stanfors R, 1993. Evaluation of Investigation in Fracture Zones NE-1, EW-7 and NE-3. SKB PR 25-92-18.

Rhén I, Svensson U, Andersson J-E, Andersson P, Eriksson C-O, Gustafsson E, Ittner T, Nordqvist R, 1992. Äspö Hard Rock Laboratory. Evaluation of the combined long-term pumping and tracer test (LPT2) in borehole KAS06. SKB TR 92-32.

Rhén I (ed), 1995. Documentation of tunnel and shaft data, tunnel section 2874 - 3600 m, hoist and ventilation shafts 0 450 m. SKB PR 25-95-28.

Spalding D B, 1981. A general-purpose computer program for multi-dimensional one- two-phase flow. Math. and Comp. in Simulation, XIII, pp 267-276.

Stanfors R et al, 1992. PASSAGE THROUGH WATER-BEARING FRACTURE ZONES. Compilation of technical notes. SKB PR 25-92-18 C Passage through fracture zone NE-1. Hydrogeology and groundwater chemistry.

Svensson U, 1988. Numerical simulations of seawater intrusion in fractured porous media. SKB PR 25-88-09.

Svensson U, 1991. Groundwater flow at Äspö and changes due to the excavation of the laboratory. SKB PR 25-91-03.

Svensson U, 1997a. A regional analysis of groundwater flow and salinity distribution in the Äspö area. SKB TR 97-09.

Svensson U, 1997b. A site scale analysis of groundwater flow and salinity distribution in the Äspö area. SKB TR 97-17.

Taivassalo V, Koskinen L, Laitinen M, Löfman J, Mészáros F, 1994. Modelling the LPT2 Pumping and Tracer Test at Äspö. Pumping test. SKB ICR 94-12.

Tanaka Y, Miyakawa K, Igarashi T, Shigeno Y, 1996. Application of three-dimensional smeared fracture model to the hydraulic impact of the Äspö tunnel. SKB ICR 96-07.

Uchida M, Doe T, Dershowitz W, Thomas A, Wallman P, Sawada A, 1994. Discrete-fracture modelling of the Äspö LPT-2, large-scale pumping and tracer test. SKB ICR 94-09.

Uchida M, Dershowitz W, Sawada A, Wallman P, Thomas A, 1997. Fracman discrete fracture modelling for the Äspö tunnel drawdown experiment. SKB ICR 97-03.

Van Golft-Racht, 1982. Fundamentals of fractured reservoir engineering. (Elsevier). Amsterdam.

Winberg A (ed), 1996. Descriptive Structural-hydraulic Models on Block and Detailed Scales of the TRUE-1 Site. SKB ICR 96-04.

CHAPTER 9

Rhén I (ed), Bäckblom (ed), Gustafson G, Stanfors R, Wikberg P, 1997. Äspö HRL - Geoscientific evaluation 1997/2. Results from pre-investigations and detailed site characterization. Summary report. SKB TR 97-03.

APPENDIX 1

Bäckblom G, 1989. Guide-lines for use of nomenclature on fractures, fracture zones and other topics. SKB PR HRL-96-18.

Hermanson J, 1995. Structural geology of water-bearing fractures. SKB PR 25-95-23.

Wikberg P (ed), Gustafson G, Rhén I, Stanfors R, 1991. Äspö Hard Rock Laboratory. Evaluation and conceptual modelling based on the pre-investigations. SKB TR 91-22.

This report is based on the following text files:

005mk0ir.wpd:	Summary, Chapter 1
005mk2rs.wpd:	Chapter 2
005mk3ir.wpd:	Chapter 3
005mk4rs.wpd:	Chapter 4
005mk5rs.wpd:	Chapter 5
005mk6ir.wpd:	Chapter 6
005mk7pw.wpd:	Chapter 7
005mk8ir.wpd:	Chapters 8 and 9
005ref.wpd:	References
005ma1rs.wpd:	Appendix 1
005ma2ir.wpd:	Appendix 2
005ma3pw.wpd:	Appendix 3